# Coronary blood flow quantification from X-ray angiography

**Sethumadhavan Vijayan**

Submitted in accordance with the requirements for the degree of

Doctor of Medicine (MD)

The University of Leeds

Division of Cardiovascular and Diabetes Research

Leeds Institute of Cardiovascular and Metabolic Medicine

School of Medicine

October 2020

*I wish to dedicate this thesis to the memory of*

*Professor Mohan Sivananthan,*

*who remains a constant source of inspiration and guidance.*

# Intellectual Property and Publication Statements

The candidate confirms that the work submitted is his own, except where work has been done collaboratively with others. The contribution of other colleagues to this work has been explicitly indicated below. The candidate confirms that appropriate credit has been given within the thesis where reference has been made to the work of others.



**Contributions to this work by others**

Professor Sivananthan and Dr Andrew Davies - Original idea to study coronary blood flow measurement from X-ray angiography.

Professor Sivananthan- original ethical approval for the study.

Dr Andrew Davies – Development of software that was used in this research, assistance during data collection.

Dr Andrew Davies and Dr David Barmby – preliminary bench work, initial design of the human validation study and recruitment of first three patients (data not included in this thesis) and worked collaboratively to develop and perform bench studies in this thesis.

Dr Pankaj Garg – acquisition and analysis of cardiac MRI data.

**Publications**

Chapter 1 - Assessing coronary blood flow physiology in the cardiac catheterisation laboratory. Vijayan S, Barmby DS, Pearson IR, Davies AG, Wheatcroft SB, Sivananthan M. Curr Cardiol Rev. 2017;13(3):232-243

**SV**- conception, drafting and revision of manuscript; **DSB, IRP, AGD, SBW, MS** – revision of manuscript.

Chapter 5 - Coronary blood flow quantification from X-ray angiography

S Vijayan, A Davies, D Barmby, S Wheatcroft, M Sivananthan -

Oral presentation at EuroPCR, 2019

**SV**- data collection, analysis, drafting and presentation of abstract; **DB, AD, MS** – conception, revision of abstract; **SW** – revision of abstract.

# Table of contents

## Figures and tables

## Acknowledgements

Professor Mohan Sivananthan was my supervisor and guided me throughout this research project. His untimely demise left a huge vacuum that I find impossible to fill. I am indebted to Mohan for his guidance during the conduct of the research and for teaching me coronary intervention.

I am very grateful to my academic supervisor Professor Stephen Wheatcroft for his encouragement and unwavering support from the start of this project to the completion of the thesis. This project would not have been possible without my supervisor Dr Andrew Davies, who wrote the software used in this research and provided all the technical support and troubleshooting often at short notice. I am very grateful to Andy for his support and guidance. Dr David Barmby worked on setting this project up by writing the initial protocol and gaining ethical approval. He also recruited the first three patients to the study which helped in optimising the protocol. I am grateful for his work and his continued support during the bench experiments.

I am extremely grateful to the Leeds Charitable Trustees for funding me. I remember with gratitude Dr Jim Mclenachan, the Clinical Director of Cardiology at Leeds General Infirmary for his support and help with completion of this project during difficulties. I would like to thank Professor Sven Plein and Dr Pankaj Garg of CMR research group for their collaboration and help with Cardiac MRI scans and reporting. I am grateful to Professor Hadj Benkreira and Mr Matt Palmer of University of Bradford for their help with the bench work.

I am very grateful to all the interventional cardiologists at LGI (Professor Sivananthan, Professor Stephen Wheatcroft, Dr Chris Malkin, Dr Jim Mclenachan, Dr Vivek Kodoth, Dr Ian Pearson, Dr Jon Blaxill,

Dr Dan Blackman, Dr Jeremy Butts, Dr Nigel Durham, Dr Basel Hanbali and Dr Dwayne Conway) who allowed me to recruit their patients to this study. I remember with special gratitude the words of encouragement from Dr Vivek Kodoth and Dr Ian Pearson during difficult periods. I am also grateful to the wonderful staff at the cardiac catheterisation laboratories at LGI, the nurses who cared for the patients, the radiographers who patiently performed the X-ray research protocol and the cardiac physiologists who supported the physiological assessments. I would also like to acknowledge the support from Phillips Health care and St Jude Medical in the conduct of this research.

I am very thankful to my long-suffering wife Lekshmy and daughter Janaki for their understanding and support.

Lastly, but most importantly, I would like to thank every single patient who took part in the study, selflessly dedicating so much of their time towards clinical research.

## Abstract

Coronary angiography provides anatomical information about the epicardial coronary arteries but is poor at evaluating coronary microcirculation. Coronary blood flow (CBF) measurements would be a superior tool for evaluation of coronary circulation but are difficult to perform in cardiac catheterisation laboratory in real time. A workflow for quantification of CBF using X-ray signal intensity analysis of coronary angiogram images was developed at the University of Leeds using a custom-built computer software – herein referred to as the 'X-ray Blood Flow' (XBF) method.

A bench study and two human pilot studies were conducted to test the feasibility of quantification of CBF using the XBF method. The bench study utilised a cardiac phantom that simulated CBF. The first human validation study compared XBF flow to CBF measured by continuous thermodilution technique. The second human study in ST elevation myocardial infarction (STEMI) patients study sought to establish the safety and utility of the XBF method by correlating the XBF flow and resistance measurements after primary percutaneous intervention to infarct parameters from cardiovascular magnetic resonance (CMR) imaging.

The key finding from the bench study was that flow quantification is possible by XBF method in a cardiac phantom, with excellent correlation between XBF flow and actual flow. The human validation study showed that XBF flow measurements correlated and agreed with the thermodilution CBF in right coronary arteries but did not correlate in left coronary arteries. The STEMI study showed that XBF flow measurements can be performed safely in patients presenting with STEMI. There was good correlation between the XBF

measured myocardial resistance and the index of microcirculatory resistance (IMR). There was weak correlation between the XBF flow and myocardial resistance and CMR derived infarct parameters.

The results from the bench study and the human pilot studies are encouraging and open the possibility of assessment of coronary blood flow and myocardial resistance from X-ray angiography alone. The XBF method needs further optimisation and larger studies are needed to establish its clinical utility.

## Glossary

| | |
|---|---|
| 3TSTEMI | Three tesla ST elevation myocardial infarction |
| AAR | Area at risk |
| ACS | Acute coronary syndrome |
| ACT | Activated clotting time |
| AD | Andrew Davies |
| ADC | Automatic dose control |
| AGC | Automatic gain control |
| AR | Aortic regurgitation |
| AV node | Atrio-ventricular node |
| BMF | Blood mimicking fluid |
| bSSFP | Balanced steady state free precession |
| CABG | Coronary artery bypass grafting |
| CAD | Coronary artery disease |
| CBF | Coronary blood flow |
| CFD | Computational flow dynamics |
| CFVR | Coronary flow velocity reserve |
| CMR | Cardiovascular magnetic resonance |
| CT | Computed tomography |
| CTP | myocardial computed tomography perfusion |
| DB | Dr David Barmby |
| DICOM | Digital Imaging and Communications in Medicine |
| dPR | Diastolic pressure ratio |
| ECG | Electrocardiogram |
| EDM | End diastolic mass |

| | |
|---|---|
| EDV | End diastolic volume |
| EF | Ejection fraction |
| eGFR | Estimated glomerular filtration rate |
| FFR | Fractional Flow Reserve |
| Fr | French |
| FWHM | Full width at half maximum |
| HLA | Horizontal long axis |
| HMR | Hyperaemic microvascular resistance |
| HSR | Hyperaemic Stenosis Resistance |
| iFR | Instantaneous wave-free ratio |
| IMR | Index of microcirculatory resistance |
| IRA | Infarct related artery |
| IV | Intravenous |
| LAD | Left anterior descending artery |
| LCA | Left coronary artery |
| LCx | Left circumflex artery |
| LGI | Leeds General Infirmary |
| LMS | Left main stem |
| LV | Left ventricle |
| LVEDP | Left ventricular end diastolic pressure |
| LVEDV | Left ventricular end diastolic volume |
| LVSV | Left ventricular stroke volume |
| MACE | Major adverse cardiac events |
| mAs | Milli amperes second |
| MBF | Myocardial blood flow |

| | |
|---|---|
| MCE | Myocardial contrast echocardiography |
| MI | Myocardial infarction |
| MINOCA | Myocardial infarction with no obstructive coronary arteries |
| MPR | Myocardial perfusion reserve |
| MRI | Magnetic resonance imaging |
| MSI | Myocardial salvage index |
| MVO | Microvascular obstruction |
| MVR | Microvascular resistance |
| NICOR | National Institute for Cardiovascular Outcomes Research |
| NSTEMI | Non-ST segment elevation myocardial infarction |
| OMT | Optimal medical therapy |
| Pa | Aortic pressure |
| PCI | Percutaneous coronary intervention |
| Pd | Pressure distal |
| Pw | Coronary wedge pressure |
| PET | Positron emission tomography |
| PG | Dr Pankaj Garg |
| PPCI | Primary percutaneous coronary intervention |
| QCA | Quantitative coronary angiography |
| RCA | Right coronary artery |
| RCT | Randomised controlled trial |
| RFR | Resting full-cycle ratio |
| ROI | Region of interest |
| RWMA | Regional wall motion abnormalities |
| SAX | Short axis |

| | |
|---|---|
| SD | Standard deviation |
| SPECT | Single-photon emission computed tomography |
| SPIR | Spectral Presaturation with Inversion Recovery |
| STEMI | ST segment elevation myocardial infarction |
| SV | Stroke volume |
| T2W | T2 weighted |
| TFT | Two-dimensional thin-film transistor |
| TIC | Time intensity curve |
| TIMI | Thrombolysis in myocardial infarction |
| TMPG | Thrombolysis in myocardial infarction myocardial perfusion grade |
| TT | Transit time |
| UMS | Professor U M Sivananthan |
| VLA | Vertical long axis |
| XBF | X-ray blood flow |

# Chapter 1 Introduction

Coronary artery disease (CAD) is a major cause of mortality world-wide, despite significant advances in management over the past three decades (Go et al., 2014; Townsend N and M, 2012; Moran et al., 2014). Currently, treatment of CAD is focussed on treatment of epicardial coronary stenosis simply because coronary angiography, which is widely available and used for diagnosing CAD is only good at demonstrating luminal narrowing in the major epicardial coronary arteries. Coronary angiography is not reliable in assessing the functional significance of lesions (White et al., 1984). This is especially relevant when trying to assess lesions of intermediate severity as determined by percent diameter stenosis.

Clinicians use functional ischaemia tests such as myocardial perfusion studies employing nuclear medicine techniques, stress echocardiography or more recently stress MRI studies to non-invasively assess for ischaemia. However, these techniques are not suitable to be used widely in the setting of a catheterisation laboratory where immediate decisions need to be made on the appropriateness of revascularisation during the procedure.

Coronary angiography is not good at evaluating coronary microcirculation, simply because these vessels are too small to be visualised, not just by X-ray angiography, but any imaging currently in clinical use.

Measuring myocardial blood flow and resistance in the catheter laboratory would be the obvious solution to these problems and researchers have attempted this with varying success rates. Measuring the hyperaemic blood flow normalised to the associated myocardial mass or vascular volume would be the ultimate functional test. There are no methods currently in wide use

that can be employed easily to reliably measure absolute myocardial blood flow or resistance in the catheterisation laboratory. Clinicians have therefore resorted to using pressure-based indices to make clinical decisions especially in situations of coronary artery stenosis of intermediate severity. Fractional Flow Reserve (FFR) has been established as the index with the largest evidence base for this. However, it is not helpful in evaluating coronary microcirculation. There are also indices developed for assessing the microcirculation. There are discussed in more detail later in this chapter. The most widely used one of these, the index of microcirculatory resistance (IMR) relies on mean transit time of fluid as a surrogate and is not really a measure of flow or resistance. By measuring coronary blood flow and combining it with pressure measurements, we can calculate the resistance to blood flow. Understanding the contribution of lesion resistance and myocardial resistance can help in more accurate decision-making regarding treatment of lesions in epicardial coronary arteries. Therefore, coronary blood flow measurements when combined with pressure-based indices would be helpful in evaluating the flow dynamics and physiology through the entire coronary circulatory tree.

## 1.1 Coronary blood flow physiology and regulation

The coronary arteries are the first branches of the aorta, and they branch like a tree into small arteries and arterioles with diameter less than 400 micrometres (μm). The coronary arterial system can be divided into three compartments with different functions (Camici and Crea, 2007). These are depicted in figure 1.1.

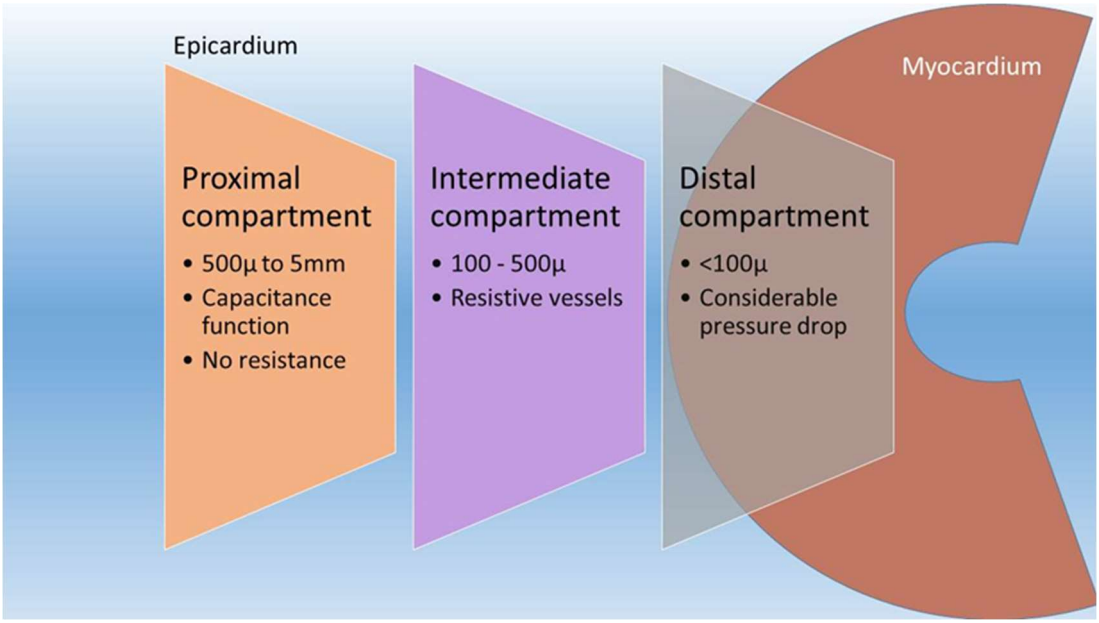


**Figure 1.1: Compartments of coronary circulation**

The anatomical borders of these compartments cannot be clearly defined. The proximal compartment includes the epicardial coronary arteries, (500 µm – 5 mm diameter) which have a capacitance function and offer little resistance to coronary blood flow. The intermediate compartment includes the pre-arterioles (100-500 µm diameter), which are characterised by a measurable pressure drop along their length. They are extra-myocardial and are not under direct vasomotor control by diffusible myocardial metabolites. Their specific function is to maintain pressure at the origin of arterioles within a narrow range when coronary perfusion pressure or flow changes. The more distal compartment is represented by intramural arterioles, (diameter <100 µm) which are characterised by a considerable drop in pressure along their path. Their function is the matching of myocardial blood supply and oxygen consumption.

It has been shown that in normal coronary arteries of cats, resistance to coronary blood flow (CBF) is minimal in arteries larger than 400µm in diameter

(Chilian et al., 1989). The arteries smaller than 400 μm are called resistive vessels and can vasodilate to modulate CBF according to physiological needs or in response to stress. CBF is kept constant over a large range of perfusion pressure by adjusting coronary microvascular resistance to changing perfusion pressures. The microvasculature is complex in structure and accounts for more than 90% of the vascular volume (Pries and Reglin, 2017). Coronary blood flow is also unique in that the flow is impeded during left ventricular systole because of the contracting myocardial fibres, unlike the systemic circulation. In the coronary circulation, pressure is generated from both the proximal and distal end of the artery – the aortic pressure and the pressure generated due to the effect of contraction and relaxation of the myocardium on the microvasculature (Sen et al., 2014). Because the increase in oxygen demand of the left ventricle is largely met by increasing the CBF, it is very closely regulated. During contraction of the left ventricle, the wall tension increases and compresses the intra-myocardial micro-vessels impeding the coronary arterial inflow. On the contrary, the venous outflow is increased. Due to the differential distribution of the transmural gradient, there is re-distribution of blood from sub-endocardial to sub-epicardial layers. Conversely, during diastole coronary arterial inflow increases and the transmural gradient favours perfusion of sub-endocardial layers (Hoffman and Spaan, 1990; Duncker et al., 2015).

The two major determinants of coronary flow are coronary arterial pressure and myocardial resistance determined by myocardial oxygen consumption. At constant oxygen consumption, coronary flow is relatively independent of arterial pressure which is referred to as coronary autoregulation. Under normal

autoregulation and over a wide range of arterial pressures, the CBF is independent of arterial pressure. At a given coronary arterial pressure, coronary flow increases with oxygen consumption, which is defined as metabolic adaptation (van de Hoef et al., 2012). This is achieved by modulating the resistance to blood flow. It is the distal compartment that is the primary site of blood flow regulation. The arteriolar tone is sensitive to chemicals produced during myocardial metabolism (Camici et al., 2012).

Atherosclerotic CAD causes increase in resistance in the epicardial arteries or micro-circulation or both. Coronary arterioles vasodilate and compensate for the increase in resistance to maintain the myocardial perfusion, but once the vasodilatory capacity has been exhausted, myocardial ischaemia sets in.

## 1.2 Microvascular dysfunction

In the absence of epicardial coronary stenosis, microvascular dysfunction can lead to angina symptoms and more importantly adverse clinical outcomes (van de Hoef et al., 2013a; Jespersen et al., 2012). Our understanding of microvascular dysfunction is limited by the difficulties in measuring coronary flow and microvascular resistance. Microvascular dysfunction may occur without significant epicardial coronary artery stenosis or in combination with it. When epicardial coronary artery stenosis occurs in combination with microvascular dysfunction, it can pose significant challenges in understanding the relative contribution of each to the symptoms and in clinical decision making (Corcoran et al., 2018b). Angina without epicardial CAD is observed in up to a third of patients undergoing elective coronary angiography (Patel, M.R. et al., 2010).

Several mechanisms contribute to the pathogenesis of coronary microvascular dysfunction. They include endothelial dysfunction, smooth muscle dysfunction and microvascular remodelling where there is medial wall thickening due to increased smooth muscle hypertrophy and collagen deposition (Camici et al., 2015). In addition, in the presence of myocardial diseases, factors such as extramural compression, vascular wall infiltration, reduced diastolic filling time, increased intra-myocardial pressure and tissue oedema, vascular rarefaction and perivascular fibrosis are implicated in microvascular dysfunction. Luminal obstruction by micro-emboli and autonomic dysfunction are the main mechanisms in patients with CAD and in those undergoing coronary interventional procedures (Camici et al., 2015).

The presence of microvascular dysfunction, alone or in combination with epicardial CAD, is a marker of poor prognosis (Corcoran et al., 2018b; Murthy, V. L. et al., 2011; Gulati et al., 2009). Patients with microvascular disease have similar risk profile to those with epicardial CAD. Smoking has been noted to impact the microvasculature and myocardial blood flow regulation, through its pro-oxidant effect (Kaufmann et al., 2000). Hyperlipidaemia and hypertension have been shown to increase the risk of microvascular dysfunction (Dayanikli et al., 1994; Yokoyama et al., 1996; Brush et al., 1988). Diabetes Mellitus has also been shown to increase the risk of microvascular dysfunction (Nitenberg et al., 1993; Pitkänen et al., 1998; Yokoyama et al., 1997). Chronic inflammatory conditions such as systemic lupus erythematosus and rheumatoid arthritis have similarly been associated with microvascular dysfunction (Amigues et al., 2019; Recio-Mayoral et al., 2009). Microvascular dysfunction is also associated with aortic stenosis and increases the severity

of adverse ventricular remodelling (Zhou et al., 2019). Microvascular dysfunction often complicates acute coronary syndromes, especially in the setting of ST elevation myocardial infarction (STEMI), in which it may be implicated in the initial pathogenesis or it may arise as a consequence of treatment for epicardial atherothrombosis (Lerman et al., 2007).

The human coronary microcirculation cannot be directly visualised *in vivo* requiring surrogate measures to be employed in its assessment. Camici and Crea classified microvascular dysfunction into four categories (table 1.1) (Camici and Crea, 2007).

**Table 1.1: Types of microvascular dysfunction**

| Type | Description |
|---|---|
| 1 | Coronary microvascular dysfunction in the absence of obstructive CAD and myocardial diseases. The traditional cardiovascular risk factors of smoking, dyslipidaemia and diabetes mellitus have been linked to this type. |
| 2 | Coronary microvascular dysfunction in the presence of myocardial diseases. This is thought to be due to adverse remodelling of intramural coronary arterioles. |
| 3 | Coronary microvascular dysfunction in the presence of obstructive CAD which may be in the context of stable CAD or acute coronary syndromes. |
| 4 | Iatrogenic coronary microvascular dysfunction. This includes vasoconstriction and distal embolisation during procedures |

Microvascular dysfunction is associated with poor long term clinical outcomes and increased mortality in the context of both acute MI and stable CAD (van de Hoef et al., 2013a; van de Hoef et al., 2013b).

Pharmacological treatment of microvascular dysfunction is challenging and there is currently a paucity of good quality evidence that drug therapies improve clinical outcomes. Limited evidence indicates that angiotensin converting enzyme inhibitors (ACE inhibitors), ranolazine, beta-blockers, calcium channel blockers, nicorandil and statins improve microvascular dysfunction (Turgeon et al., 2018).

## 1.3 Current methods of assessing coronary physiology.

### 1.3.1 Coronary flow reserve

Coronary flow reserve (CFR) is defined as the ratio of maximal flow in a coronary artery to the flow at rest at the same perfusion pressure. Coronary blood flow, as explained previously, is regulated largely by the distal compartment of the coronary arterial system. To achieve maximum coronary blood flow, a state of minimum myocardial resistance and maximum vasodilatation, also known as state of hyperaemia, needs to be achieved. Intra-venous administration of endothelium-independent vasodilators (e.g., adenosine, dipyridamole, regadenoson) can abolish the vasomotor tone and cause near maximal vasodilatation to achieve hyperaemic state. In clinical practice, cross-sectional peak velocity is measured rather than volume flow, yielding Coronary Flow Velocity Reserve (CFVR). CFVR was one of the earliest flow based techniques employed to ascertain the functional significance of coronary stenosis (Gould and Lipscomb, 1974). CFVR is

determined as the ratio of the mean flow velocity during hyperaemia (maximal flow) to the mean flow velocity during baseline (normal flow) conditions. There are several ways of assessing CFR, of which two invasive methods are more widely used – using a Doppler wire and using thermodilution method. The Doppler method involves passing a Doppler wire into the coronary artery and manipulating the wire until satisfactory velocity doppler signals are obtained. This is dependent on the skills and experience of the operator (Doucette et al., 1992; Barbato et al., 2004). The process is then repeated to measure the flow velocity during hyperaemia induced by adenosine. The ratio of the hyperaemic velocity to resting velocity gives the CFVR:

$$CFVR = APV_{hyperaemia}/APV_{baseline}$$

$APV_{baseline}$ and $APV_{hyperaemia}$ are the averaged peak velocity at rest and during hyperaemia, respectively.

The thermodilution method of assessing CFR uses a coronary guide wire with a temperature and pressure sensitive transducer near its tip. This wire is placed in the coronary artery. Boluses of room-temperature saline are injected briskly into the guide catheter to deliver it at the origin of the coronary artery; the temperature drop is measured as the blood mixed with the colder saline reaches the transducer and a thermodilution curve is obtained. The process is repeated after induction of hyperaemia (e.g., with intravenous infusion of adenosine). The mean transit times during baseline and hyperaemia are calculated from the thermodilution curves. The ratio of the baseline mean transit time to the hyperaemic mean transit time gives the CFR (Barbato et al., 2004).

$$CFR = \frac{Q_M}{Q_R} = \frac{V/T_{mn,hyperaemi}}{V/T_{mn,baseline}} = \frac{T_{mn,baseline}}{T_{mn,hyperaemic}}$$

where $Q_M$ and $Q_R$ are the maximal and resting flow, $V$ is the blood volume, and $T_{mn,}$ is the mean transit time at rest and stress.

Stress echocardiographic techniques can non-invasively assess CFVR and there is evidence to show that it adds prognostic information (Rigo et al., 2008). However, this technique has many limitations and has not gained wide use outside research setting.

CFVR has been shown to be prognostically valuable in several clinical scenarios, such as predicting left ventricular function recovery and peri-procedural outcomes after PCI, predicting major adverse cardiac events (MACE) in women with risk factors and in patients with chest pain and microvascular disease (Beleslin et al., 2008; Pepine et al., 2010; Albertal et al., 2002; Marks et al., 2004).

While an approximate threshold for recognition of inducible ischaemia has been established (CFVR<2.0), the technique is inherently dependent on hemodynamic conditions that affect both baseline as well as hyperaemic state measurements (Hoffman, 2000). Factors that influence baseline flow (e.g. workload, heart rate, gender) and age were identified as major determinants of CFVR, whereas coronary risk factors or cardiomyopathies affecting the functional capacity of the small resistance vessels tend to reduce CFVR by impairing maximal flow (Rossen and Winniford, 1993; Antony et al., 1993; Czernin et al., 1993; Marcus et al., 1982). To minimise these baseline flow influences, relative CFVR has been proposed which is the ratio of CFVR in a target vessel to another (ideally healthy) vessel (Baumgart et al., 1998). However, in patients with known atherosclerosis, flow in angiographically healthy contralateral arteries is abnormal, and for this reason, relative CFVR

has not had widespread adoption (De Bruyne, B. et al., 2001). CFVR interrogates the flow status of both the epicardial artery and the microcirculation but does not allow discrimination between these two components (Ng, M.K.C. et al., 2006). In addition, the technique of using Doppler wire to measure the velocity is considered relatively difficult to perform accurately by all but the experienced operators and for these reasons it has currently been superseded in routine clinical practice by pressure-based physiological measurements.

### 1.3.2 Fractional flow reserve

Fractional flow reserve (FFR) was developed using a simplified model of the hyperaemic coronary pressure–flow relationship. Pijls *et al* defined FFR of the coronary artery as the ratio of maximum possible flow in the artery in the presence of a stenosis ($Q_S$) to the maximum flow expected in the same artery in the absence of that stenosis ($Q_N$) (Pijls, N.H. et al., 1993), and hence

$$FFR = \frac{Q_S}{Q_N}$$

A direct relationship between coronary pressure and flow or flow reserve can be assumed only if coronary microcirculatory resistances remain constant and minimal. In a state of constant and minimal microvascular resistance, pressure measurements alone can be used to predict blood flow in the artery segment of interest. Letting $P_d$, $P_a$ and $P_v$ be the blood pressure in the distal coronary artery (beyond the stenosis), in the aorta, and in the venous system respectively, then

$$FFR = \frac{(P_d - P_v)/R_s}{(P_a - P_v)/R_N}$$

where $R_s$ and $R_N$ are the resistance of the myocardium in the presence of the stenosis, and in myocardium if the vessel were normal. When hyperaemia is induced, the resistance is assumed to be the same and negligible (i.e., $R_s = R_N$) and $P_v$ is also assumed to be negligible. So, the FFR equation is simplified to

$$FFR \approx \frac{P_d}{P_a}$$

Originally FFR was classed as myocardial FFR ($FFR_{myo}$) and coronary FFR ($FFR_{cor}$). This was to take into consideration the collateral flow by measuring the coronary wedge pressure (Pw). However, in practice this is rarely performed (Kern et al., 2006).

The functional significance of a lesion in an epicardial coronary artery can be assessed invasively by measuring the FFR (Pijls, N.H. et al., 1996). In clinical practice, this is performed by using a pressure sensitive coronary guide wire advanced into the coronary artery beyond the lesion in question. The pressure distal to the lesion and the aortic pressure are measured after the induction of hyperaemia, with adenosine or similar pharmacological agents. The ratio of $P_d/P_a$ during hyperaemia is the FFR. An FFR cut-off value of 0.75 was used in earlier studies, but more recent studies have used 0.80 as the cut-off value for attributing haemodynamic significance to a lesion. An FFR of 0.75-0.80 is considered the ‘grey zone’. Over the past decade, an increasing and substantial body of evidence showing that FFR guided PCI improves outcomes has served to cement FFR as the gold standard index for assessing coronary physiology in the catheterisation laboratory, most notably through the DEFER, FAME and FAME 2 trials, which are summarized in table 1.2 (Tonino et al., 2009; De Bruyne, B. et al., 2014; Pijls, N.H.J. et al., 2007).

**Table 1.2 : Landmark trials that established FFR as the most widely used invasive physiologic test**

| **Trial** | **DEFER** (Bech et al., 2001; Zimmermann et al., 2015) | **FAME** (Tonino et al., 2009) | **FAME 2** (De Bruyne, B. et al., 2014; Xaplanteris, Panagiotis et al., 2018) |
|---|---|---|---|
| **Design** | RCT, multi-centric | RCT, multi-centric | RCT, multi-centric |
| **Number of patients** | 325 | 1005 | 1220 |
| **Clinical syndrome** | Stable CAD | Stable multi-vessel CAD | Stable CAD |
| **Primary endpoint** | Absence of all-cause mortality, MI, CABG, PCI, and any procedure-related complication necessitating major intervention or prolonged hospital stay at 2 years | Death, nonfatal MI, and repeat revascularisation at 1 year | Death from any cause, nonfatal MI, unplanned hospitalisation leading to urgent revascularisation during the first 2 years |
| **Key finding** | Deferring PCI in lesions with FFR >0.75 is safe | FFR-guided PCI outperformed angiography guided PCI | FFR-guided PCI plus optimal medical therapy outperformed medical therapy alone |

RCT- Randomised controlled trial, CAD- coronary artery disease, MI- Myocardial infarction, CABG- coronary artery bypass grafting, PCI- Percutaneous coronary intervention, FFR- Fractional flow reserve

#### 1.3.2.1 Pitfalls of FFR

FFR has a high degree of reproducibility and low variability and it is relatively straightforward to perform in the cardiac catheterisation laboratory (de Bruyne, B. et al., 1996). Backed by the evidence in decision making in intermediate coronary artery stenoses, it has become the most widely performed coronary physiologic assessment in the catheterisation laboratory and has achieved an almost ‘gold standard’ status. However, it must be borne in mind that FFR is

not a measure of flow, but a surrogate measure of relative flow reduction in the presence of flow-limiting lesions. During resting conditions, no relationship exists between coronary pressure and blood flow as the blood flow is closely autoregulated.

FFR measurement using pressure wire requires several assumptions about coronary physiology that coronary pressure is linearly proportional to coronary flow when coronary resistance is minimal and constant. However, the relationship between coronary pressure and flow has a non-zero pressure intercept (i.e. coronary blood flow ceases at a perfusion pressure of about 20 mmHg) and is incremental linear in the physiological range of perfusion pressures, the slope of which is variable (van de Hoef et al., 2013c; van de Hoef et al., 2015b; Siebes et al., 2002).

Ideally, right atrial pressure ($P_v$) should be measured as patients may have a variety of conditions that cause this to be high. However, almost always in practice, additional catheterisation to measure the $P_v$ is not performed, and it is assumed to be negligible. In theory, this can lead to error in the calculation of FFR (Perera et al., 2004), as $P_v$ may not be negligible in individual patients. However, a recent study by Toth *et al* found that the impact of the $P_v$ is in fact negligible even in patients with high venous pressure (Toth et al., 2016). The coronary wedge pressure (Pw) is also not measured in clinical practice and nor are other potential sources of error, including collateral flow and venous flow routinely considered.

The accuracy of FFR depends on induction of steady state hyperaemia. There are several clinical scenarios where this may not be achieved and FFR assessment may therefore underestimate the significance of a lesion. These

range from errors in constitution of the drug and drug delivery to drug interactions (e.g., the effects of adenosine may be blunted by ingestion of caffeine). Fluctuations in degree of hyperaemia have been noted due to variability of adenosine metabolism (Jeremias et al., 2017) and adenosine alone may not abolish the vasomotor tone completely (Heusch, 2010).

In up to 30-40% of patients in clinical practice, FFR and CFR are discordant (van de Hoef et al., 2015a). A low coronary flow state can co-exist with a normal FFR and vice versa. Echavarria-Pinto *et al* demonstrated that more than half of the coronary arteries with intermediate stenoses and normal FFR can have abnormal haemodynamics if CFR and Index of microcirculatory resistance (IMR) are taken into account (Echavarria-Pinto et al., 2013). Patients with normal FFR but an abnormal CFR have been noted to be exposed to a significantly increased risk of major adverse cardiac event rates during long-term follow-up as opposed to those with abnormal FFR and normal CFVR (van de Hoef et al., 2014). The reason behind this discordance may be that FFR does not interrogate microvasculature whereas CFVR does. Johnson *et al* argues that the discordance must not be seen as a failure of FFR or CFR, but as reflecting different pathophysiological processes at play (Johnson et al., 2012).

FFR assumes that microvascular resistance is the same in association with stenosed and healthy vessels, but there is evidence to suggest that this is not the case (van de Hoef et al., 2013c). If microvascular resistance is high, FFR could be falsely elevated or normalised. Despite good evidence for improved clinical outcomes from PCI guided by FFR in general, the evidence for using cut-off values of FFR to guide the treatment in truly intermediate lesions is still

limited (van de Hoef et al., 2015a). This may be because the beneficial effects from PCI in landmark trials were driven by intervention to lesions that were causing more severe degrees of ischaemia (FFR<0.65) (Johnson et al., 2014). In clinical practice, an FFR value of 0.80 is widely used as the cut off above which no intervention is advocated. But this cut off is arbitrary and FFR is in fact a continuum with lower values representing lesions causing more ischaemia (Johnson et al., 2014). In the early clinical validation studies comparing exercise ECG with invasive FFR, an FFR value of 0.66 had the highest diagnostic accuracy at predicting an abnormal exercise ECG (De Bruyne, B. et al., 1995). The sensitivity and specificity of exercise ECG can vary widely, and this could be a limitation of this study (Gianrossi et al., 1989). FFR measurements as described already, are influenced by conditions that increase microvascular resistance. Acute myocardial infarction is such a situation where FFR measurements are unreliable and could be misinterpreted. In patients with Diabetes Mellitus, deferring revascularisation based on an FFR above 0.80 led to higher rates of target lesion failure as compared to non-diabetic patients (Kennedy et al., 2016). Age and gender also have influence on FFR measurements with older age and female gender associated with higher FFR values (Lim et al., 2014; Kang, S.J. et al., 2013). Recently, Hamaya, Kanaji *et al* published their work on elective PCI patients by measuring the absolute coronary blood flow using thermodilution method (described in detail in  1.5.3) and FFR before and after PCI (Kanaji et al., 2017; Hamaya et al., 2019). Although they found significant increase in FFR and absolute blood flow after PCI, there was no significant relationship between the individual changes in FFR and absolute blood flow. The

difference is believed to be due to changes in microcirculatory resistance after PCI and more importantly suggests that increases in FFR do not necessarily reflect increases in blood flow.

### 1.3.3 Instantaneous wave-free ratio

The instantaneous wave-free ratio (iFR) was proposed as a surrogate for FFR removing the need to induce hyperaemia, saving time, cost, and reducing side effects related to adenosine and other pharmacological agents (Sen et al., 2012). The index iFR uses a ‘wave-free period’ during diastole identified from coronary wave intensity analysis, during which resistance is considered to be minimal and stable, within which time pressures distal and proximal to a stenosis are recorded. The diastolic resting myocardial resistance is assumed to be equal to mean hyperaemic resistance. Measuring iFR also requires passage of a pressure sensitive wire connected to a recording unit with analysis software capable of identifying the wave free period (Philips Volcano). In a core-laboratory based analysis, iFR showed an overall accuracy of 80% compared with FFR, with the potential to avoid hyperaemia in 65% of cases (Sen et al., 2013). Results of comparative studies to FFR had been mixed, showing that the two indices were well matched for extreme values of FFR, but produced poor correspondence for the clinically important intermediate range (Johnson et al., 2013; Berry et al., 2013).

The publication of two large studies have been game changers for iFR as a clinical tool. In the Functional Lesion Assessment of Intermediate Stenosis to Guide Revascularisation (DEFINE-FLAIR) study published in March 2017, 2492 patients undergoing PCI for stable CAD or ACS were randomized to undergo evaluation of all stenosis of questionable severity by iFR or FFR. The

one year outcomes revealed that iFR was non-inferior to revascularisation guided by FFR with respect to the risk of major adverse cardiac events (Davies et al., 2017). Unsurprisingly, the incidence of adverse events associated with adenosine such as bronchospasm, arrhythmias, dyspnoea, and chest pain were all significantly lower in the iFR group as iFR assessment does not require induction of hyperaemia.

These results are similar to the findings of the Instantaneous Wave-free Ratio versus Fractional Flow Reserve in Patients with Stable Angina Pectoris or Acute Coronary Syndrome (iFR-SWEDEHEART) study also published in the same journal issue (Gotberg et al., 2017). In this trial, 2037 patients with stable CAD or NSTEMI were enrolled and randomized into FFR guided revascularisation and iFR guided revascularisation groups. The study found that an iFR-guided revascularisation strategy was non-inferior to an FFR-guided revascularisation strategy with respect to the rate of major adverse cardiac events at 12 months, and a low reports of adenosine related side effects in the iFR group. Both these studies used an iFR cut-off at 0.89 below which the lesion was considered significant and classed as needing revascularisation.

The avoidance of adenosine may have other advantages by reducing the cost and duration of the procedure. It remains to be seen whether iFR will replace FFR as the standard of care in PCI. This may well happen as longer-term results from these trials become available and more and more physicians get used to the technique. However, just as there are pitfalls with FFR, iFR and other non-hyperaemic indices suffer from many of the disadvantages of FFR, because of iFR being a surrogate measure rather than a measure of flow itself.

### 1.3.4 Other non-hyperaemic indices

Several non-hyperaemic indices have been proposed by various groups. These have been compared by van't Veer *et al* in an unselected population (van't Veer et al., 2017). The different indices are summarised in the table 1.3.

**Table 1.3: Non-hyperaemic indices similar to iFR**

| | |
|---|---|
| Diastolic pressure ratio (dPR) | average Pd/Pa over the entire diastole |
| $dPR_{25–75}$ | average Pd/Pa from 25% to 75% into diastole |
| $dPR_{mid}$ | Pd/Pa at the single point in time at mid-diastole |
| $iFR_{matlab}$ | average Pd/Pa from 25% into diastole until 5ms before end of diastole calculated using mathematical methods |
| $iFR_{-50ms}$ | average Pd/Pa from 25% into diastole until 50ms before end of diastole |
| $iFR_{-100ms}$ | average Pd/Pa from 25% into diastole until 100ms before end of diastole. |

They found that all these diastolic indices were numerically identical compared to iFR. These indices also agreed with FFR in an identical way to iFR (van't Veer et al., 2017).

Resting full-cycle ratio (RFR) is an index that makes used of maximal relative pressure difference over the entire cardiac cycle. In the Validate RFR study, this index was shown to be equivalent to iFR(Svanerud et al., 2018).

The non-hyperaemic indices have been validated in patient cohorts with lesions in the intermediate severity (Gotberg et al., 2017; Davies et al., 2017). So the validity of these indices in more severely stenotic lesions is not known (Michail et al., 2020). Kobayashi et al. showed that iFR and Pd/Pa when compared to FFR as a standard, the non-hyperaemic indices were less

accurate for lesions in left main stem and proximal LAD (Kobayashi et al., 2016). This discordance between iFR and FFR occurs in about 15-20% of the lesions (Kobayashi et al., 2016; Hennigan et al., 2016). The discordance has been noted to be higher in female patients (Arashi et al., 2019). Lee et al. found that FFR and non-hyperaemic indices are both equally good for predicting long term outcomes of cardiac death, vessel-related myocardial infarction, and ischemia-driven revascularisation at 5 years (Lee et al., 2020). However larger long-term data is still awaited for iFR and other non-hyperaemic indices and until that is available there will be debate between proponents of these and those of FFR. Non-hyperaemic indices are gaining popularity due to the advantage of obtaining the result rapidly without the cost and side-effects associated with adenosine.

### 1.3.5 Index of microcirculatory resistance

Fearon *et al* first described this measure of assessing the microcirculatory resistance (Fearon et al., 2003). Index of microcirculatory resistance (IMR) is defined as the distal coronary pressure divided by the inverse of the hyperaemic mean transit time (Fearon et al., 2003). It employs a thermodilution based technique and assumes that at peak hyperaemia the variability of resting vascular tone will be eliminated, and the minimum microvascular resistance will be achieved. The method employs the use of a temperature and pressure sensitive guide wire (Pressure wire$^{TM}$, St Jude Medical, Minnesota, US) within the coronary artery. A small bolus (usually 3 ml) of sterile normal saline at room temperature is then injected through the guiding catheter to obtain an indicator-dilution curve. From this, the mean transit time ($T_{mn}$) can be calculated which is inversely proportional to the flow.

$$Resistance = \Delta P/Q$$

ΔP is the pressure difference across the myocardium, i.e., $P_d$ - $P_v$, and Q the blood flow. *Q* is related to the mean transit time as $Q = V/T_{mn}$. V is the vessel volume. IMR uses the reciprocal of the mean transit time as an index of flow.

IMR can be calculated as follows

$$IMR = \frac{P_d - P_V}{1/T_{mn}} = (P_d - P_V)T_{mn}$$

Assuming $P_v << P_d$

$$IMR \approx P_d T_{mn}$$

IMR in practice, is therefore the product of the distal pressure and mean transit time of saline bolus in the coronary artery, during maximum hyperaemia measured using a temperature and pressure sensitive guide wire.

IMR has also been found to be more reproducible and less dependent on haemodynamics in comparison to CFVR (Ng, M.K.C. et al., 2006). IMR measured at the time of primary PCI was found to predict adverse outcomes including death and repeat hospitalizations in patients with STEMI (Fearon, William F. et al., 2013). It has also been shown to predict adverse features assessed by cardiac MRI (McGeoch et al., 2010; Payne et al., 2012; Yoo et al., 2012; Carrick et al., 2016a). An IMR greater than 40 has been associated with poorer outcomes post myocardial infarction, independently of infarct size (Carrick et al., 2016a).

Although some groups have noted an association of IMR to the presence and degree of microvascular obstruction (MVO) (Payne et al., 2012; McAlindon et al., 2018), other studies found no relationship or discordant relationships (De Maria et al., 2019; Patel, N. et al., 2015).

Measuring IMR requires instrumenting the coronary arteries with a coronary guide wire. Although it is largely independent of epicardial coronary stenosis it is affected by the presence of collateral flow (Aarnoudse et al., 2004a; Aarnoudse et al., 2004b). To accurately calculate IMR, collateral blood flow must be considered by incorporating coronary wedge pressure into the equation.

$$IMR = P_a T_{mn} \left[\frac{P_d - P_w}{P_a - P_w}\right]$$

where $P_w$ is the coronary wedge pressure. Pw is calculated by inflating a balloon passed over the pressure wire to occlude the coronary artery. The residual pressure (Pw) recorded represents collateral blood flow.

### 1.3.6 Hyperaemic stenosis resistance and Hyperaemic microvascular resistance

Independent measurement of the resistances of a stenotic lesion and the myocardium can be achieved by calculating the ratio of the pressure difference across the stenosis or myocardium to the blood flow. However, in practice, as a reliable *in vivo* measure of flow is unavailable, indices of resistances are used. Hyperaemic Stenosis Resistance index (HSR) is defined as the ratio of hyperaemic stenosis pressure gradient and hyperaemic average peak flow velocity (APV), obtained by means of a Doppler wire (Meuwissen, M. et al., 2002).

$$HSR = (P_a - P_d)/APV$$

where APV is the average peak flow velocity.

Hyperaemic microvascular resistance index (HMR) is measured as the ratio of mean distal coronary pressure to mean distal coronary flow velocity (Nolte et al., 2014; Meuwissen, Martijn et al., 2001).

$$HMR = P_d / APV$$

This derivation again assumes that $P_v$ is negligible.

Both these indices use a Doppler wire and therefore suffer from lack of reproducibility and operator dependence. Although incorporating such indices could provide a better understanding of coronary physiology, there are no large studies to support their routine clinical use. It must be borne in mind that velocity is different to flow, where velocity is dependent on size of the vessel.

## 1.4 Non- invasive methods of myocardial blood flow quantification

### 1.4.1 Myocardial contrast echocardiography

Myocardial contrast echocardiography (MCE) can quantify coronary blood volume. When gas containing (perfluoropropane or sulphur hexafluoride) microbubbles are injected intravenously myocardium can be opacified under echocardiographic imaging. These microbubbles resonate and can be destroyed when exposed to ultrasound. Analysis of the acoustic emissions from the destroyed microbubbles and their reappearance rates can provide measures of myocardial bubble velocity. Microvascular cross-sectional area can be inferred from microbubble concentration in the myocardium. From these myocardial blood flow can be calculated (Wei et al., 1998). In animal models, this was found to correlate well with coronary flow. This method was

also tested in humans and found to correlate well with myocardial blood flow from positron emission tomography (Vogel et al., 2005).

This method has the advantage of not needing ionising radiation. However, echocardiography is operator dependent which is one of its key drawbacks. The image quality can be suboptimal in many patients which is another problem. This method has not gained widespread popularity in clinical use.

### 1.4.2 Positron emission tomography (PET)

Positron emission tomographic (PET) assessment of regional myocardial blood flow involves the dynamic acquisition of images during the intravenous injection of a positron-emitting perfusion tracer, such as 13N-ammonia, $^{15}$O-water, $^{82}$Rubidium etc. (Schindler et al., 2010). The tracer passing through the central circulatory system and its extraction and retention in the myocardium is imaged. Tracer kinetic models are then used to quantify myocardial blood flow (MBF) after correction for errors. PET can yield regional MBF per unit of myocardial mass. This has been shown to be highly correlated with MBF measured by microspheres in animal models over a wide range of flows (Kuhle et al., 1992). $^{15}$O-water is considered as the most accurate PET flow tracer, because of its free diffusibility across capillary and cell membranes and 100% extraction, independent of flow (Klein et al., 2010). The ratio of MBF at stress to MBF at rest can be calculated which is called myocardial perfusion reserve (MPR). Abnormal MPR has been shown to be a marker of adverse cardiac risk (Murthy, V. L. et al., 2011). PET quantification of MBF and MPR, although a promising technique, is limited by several factors such as lack of wide availability of PET scanning, need for ionising radiation exposure, need for an on-site cyclotron to generate tracers and the high costs involved.

Furthermore, the results are not available in real time to enable clinical decision making in the catheterisation laboratory.

### 1.4.3 Cardiovascular magnetic resonance imaging (CMR)

Improvements in magnetic resonance scanners, techniques and image analysis software have enabled CMR imaging to assess myocardial blood flow (Kellman and Arai, 2007; Radjenovic et al., 2010; Christian et al., 2004). It uses gadolinium-based contrast media as an indicator to assess myocardial perfusion. CMR has the advantage of avoiding use of ionising radiation. CMR quantification of myocardial blood flow, however, involves non-volumetric ventricular coverage and relatively complex post-processing steps which are known disadvantages (Waller et al., 2014). CMR can be used to estimate MBF from time–intensity curves (TIC) for the LV tissue and LV cavity using extraction fraction models (Tomiyama et al., 2015; Morton et al., 2012).

Recently, a CMR stress T1 mapping technique was found to detect microvascular dysfunction as defined by abnormal IMR at cardiac catheterisation (Liu et al., 2018). CMR studies may be contraindicated in patients with claustrophobia and certain pacemakers or other metal implants. However, recently many implantable devices (e.g., pacemaker and implantable cardioverter defibrillators) have become available which are CMR-compatible.

### 1.4.4 Computed tomography imaging

Computed tomography (CT) coronary angiography is gaining popularity as a non-invasive anatomic test of choice, due to its ability to provide information on coronary anatomy relatively quickly and with limited radiation exposure

(Beigel et al., 2009). Dual-source CT imaging protocols have been developed to assess myocardial perfusion along with anatomic assessment (Blankstein et al., 2009). The ability to non-invasively and simultaneously assess coronary anatomy and myocardial perfusion using the same modality is certainly an interesting concept. Dynamic CT myocardial perfusion imaging produces serial datasets that allow the evaluation of contrast kinetics in the myocardium. This allows for absolute MBF quantification, at the expense of increased radiation exposure (Waller et al., 2014; Ho et al., 2010). Dynamic CT scanning is performed after injecting contrast agent with prospective ECG triggering of each scan, at every or alternate heartbeat for a few seconds and after contrast administration to recover the first pass of the contrast medium. The myocardial and arterial input time activity curves can be generated and mathematical modelling applied to produce estimates of absolute myocardial flow (Feher and Sinusas, 2017). Dynamic CT MBF has been shown to have excellent correlation with $^{15}O$-$H_2O$ PET MBF (Kikuchi et al., 2014). Dynamic CT acquisition techniques may allow for the identification of more subtle perfusion changes produced by moderate coronary stenosis (Schwarz et al., 2013).

Computational flow dynamics (CFD) have been employed to calculate FFR from CT coronary angiogram images ($FFR_{CT}$). $FFR_{CT}$ has been shown to be good at stratifying lesions to those producing ischaemia and those that do not. (Koo et al., 2011; Wu, W. et al., 2016). A three-dimensional patient specific anatomic model of coronary artery is first constructed from the CT coronary angiogram data. Boundary conditions are set after estimating the resistances. A mathematical model of hyperaemic condition is derived and CFD analysis performed (Hwang et al., 2016). $FFR_{CT}$ has been shown to detect significant

CAD with invasive FFR as the reference standard in clinical trial setting (Nørgaard et al., 2014).

## 1.5 Invasive methods of coronary flow measurement

### 1.5.1 TIMI myocardial perfusion grade

The TIMI myocardial perfusion grade (TMPG) is not a true measure of coronary or myocardial blood flow. Nevertheless, it is a useful qualitative clinical tool. It describes the “blush,” or intensity, of the radio-opacity of the myocardium achieved with an intra coronary injection of contrast medium, and the time taken for the blush to clear. The more intense the myocardial blush of the contrast medium and the faster its clearance, the better the microvascular perfusion; the TIMI myocardial perfusion grade (TMPG) is scored on a scale of 0 to 3, (table 1.4) with higher scores indicating better perfusion (Gibson et al., 2000; Gibson et al., 2002). Higher TIMI perfusion grades have been noted to have better outcomes. Although TMPG is most commonly employed in STEMI patients, there is emerging evidence that assessing the blush grade may have prognostic utility in NSTEMI patients as well (Ng, V.G. et al., 2016). However, TMPG is a visual estimate and may be subjective.

**Table 1.4: TIMI myocardial perfusion grade**

| TMPG | |
|---|---|
| 0 | No apparent tissue level perfusion or no blush |
| 1 | Blush present but no clearance from microvasculature |
| 2 | Blush clears slowly (blush is strongly persistent and diminishes minimally or not at all during 3 cardiac cycles of the washout phase |
| 3 | Blush begins to clear during washout (blush is minimally persistent after 3 cardiac cycles of washout |

TMPG- Thrombolysis in myocardial infarction myocardial perfusion grading

### 1.5.2 Doppler wire method of coronary flow calculation

Doucette *et al* used a Doppler tipped guide wire to assess coronary haemodynamics (Doucette et al., 1992) and described a method of quantitative flow calculation. A Doppler transducer tipped guidewire is advanced to the proximal segment of the coronary artery and Doppler signals obtained. A time-averaged parabolic velocity profile was assumed across the vessel with a mean velocity calculated as 0.5 times average peak velocity (APV) measured by the Doppler wire. Flow is calculated as follows

$$Q_{D=\pi\frac{D^2}{4}(0.5\times APV)}$$

$Q_D$ stands for Doppler derived time-average flow, D for vessel diameter, and APV for average peak velocity calculated from the Doppler traces. The vessel diameter was measured by quantitative coronary angiography (QCA) 5 mm distal to the wire tip. This technique has not been widely adopted in clinical use due to several limitations. The assumption that coronary flow has a parabolic velocity profile is not correct (Jenni et al., 1998a; Jenni et al., 1998b). The technique of obtaining good Doppler signals from the coronary arteries is

dependent on the operator's experience. QCA is also prone to errors, not least since any disease will often mean the arterial lumen is not circular in cross section.

### 1.5.3 Thermodilution method of volumetric coronary flow measurement

Aarnoudse *et al* described a method for measuring direct volumetric blood flow in coronary arteries during cardiac catheterisation by using the principles of thermodilution method first described by Ganz *et al* in 1971 (Aarnoudse et al., 2007; Ganz et al., 1971). The method relied on the continuous infusion of saline at room temperature through a 2.8 Fr infusion catheter, advanced over a pressure and temperature sensitive coronary guidewire. This technique is different to the assessment of CFVR by thermodilution described earlier.

Theoretically, during steady-state hyperaemia, the absolute coronary blood flow during saline infusion ($Q_b$) can be calculated as follows:

$$Q_b = 1.08 \times Q_i \left[\frac{T_b - T_i}{T_b - T}\right]$$

where $Q_i$ is the volumetric infusion rate of the saline, $T_b$ is the temperature of the blood before the start of saline infusion, $T_i$ is the temperature of the saline infusate at the tip of the infusion catheter, and $T$ is the temperature at the sensor in the distal coronary artery during steady-state infusion (i.e., the temperature of the blood after complete mixing with the infused saline). A correction factor 1.08 is applied to compensate for the difference in specific heat between saline and blood.

When $T_b$ is set to zero and $T_i$ and $T$ are expressed as the deviation of the respective temperatures from T*b*, the equation can be rewritten as:

$$Q_b = 1.08 \times Q_i(T_i/T)$$

The technique has been validated in an animal model and human patients (Aarnoudse et al., 2007; Xaplanteris, P. et al., 2018). In the animal study, excellent correlation was seen between the blood flow measured using thermodilution method and directly measured flow using a perivascular ring-mounted volumetric flow meter surgically placed around the coronary artery. In the human model, the validation was indirect by comparing the improvement in coronary flow measured by thermodilution to the ratio of coronary FFR before and after stenting. The main advantage of measuring the flow using this method is that the FFR and distal coronary pressure data are also simultaneously obtained from which coronary artery resistance can be calculated using an absolute measure of flow rather than the indices used in HSR and HMR.

This method, although promising, is not used widely in clinical practice, most likely due to practical reasons. The setup and methodology are cumbersome requiring additional specially designed infusion catheter and infusion lines for saline. Further, absolute coronary blood flow cannot be interpreted without knowledge of the mass of myocardium the coronary artery supplies. For this reason, there are no normal values of volumetric coronary blood flow available yet. In the human validation study, only arteries that satisfied a criterion of a 3cm segment without major side branches being present were included. It is therefore not applicable to all patients. It is not surprising that the human validation study had 31 RCAs studied whereas only 11 LCA (LAD and LCx combined) were studied (Aarnoudse et al., 2007).

### 1.5.4 X-ray based techniques.

Invasive X-ray coronary angiography is widely used to visualise coronary artery anatomy. If the same technique could be used to quantify coronary flow without the need for additional instrumentation of the coronary arteries, it would be of great benefit as it has the potential to be widely employed with very little additional risk and cost. Coronary blood flow quantification could be valuable in a variety of clinical conditions which is discussed in detail in section 1.6.

#### 1.5.4.1 Basics of X-ray physics

Professor Roentgen in 1896 discovered that human body partially allowed the passage of X-rays. X-rays are high energy photons produced by bombarding a metallic anode (positive electrode) with electrons in an evacuated tube. An X-ray generator produces the electrical supply to the X-ray tube. Electrons are produced by heating a filament by passing a current, causing electron emission. The electrons are accelerated towards a metal target anode by the application of a potential difference: typically, 60 – 120 kV for cardiac imaging. Interaction between the electrons and the anode produces Bremsstrahlung radiation and characteristic radiation (X-rays). Bremsstrahlung in German means “breaking radiation” and it is produced by a sudden slowing or deflection of electrons caused by interaction with a positively charged atomic nucleus. The loss of kinetic energy is converted to electromagnetic radiation. The bombarding electrons can eject electrons from inner shells of atoms followed by a quick filling of those vacancies by electrons dropping from higher levels to give rise to sharply defined characteristic X-rays, whose energies are

determined by the differences in the binding energies for the electron shells of the anode material.

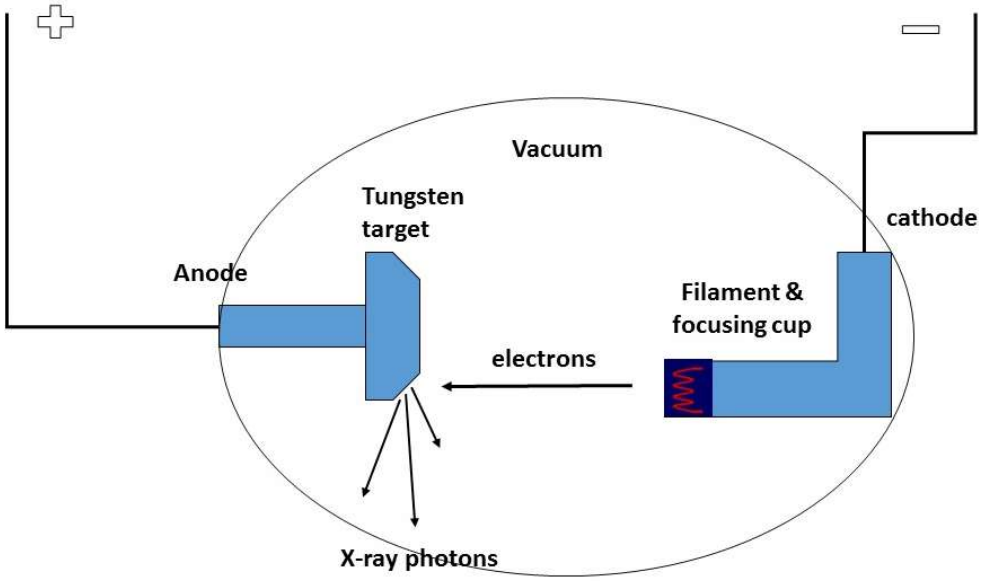


**Figure 1.2: X-ray production. The schematic diagram represents X-ray tube.** Electrons are produced by heating a cathode filament usually made from tungsten by passing a current, causing electron emission. The focusing cup which is negatively charged focus the electrons on the anode. A potential difference is applied between the anode and the cathode accelerating the electrons which when strikes the Tungsten target at the anode produces X-rays.

Each photon has a certain amount of energy, commonly expressed in units of electron volt, eV. As the X-ray beam passes through the tissue, some of the photons are absorbed (attenuation) or scattered. The differential attenuation of X-rays on interacting with the human body forms the basis of its application in medical imaging (Seibert, 2004). There are two ways of attenuation - photoelectric effect and Compton scattering. In photoelectric effect, the high energy photons of the X-ray beam lose all their energy and there is no scatter of photons. The photon strikes the atom of the tissue and uses its energy to eject an electron. There is difference in the X-ray attenuation between different

tissues. The probability of photoelectric absorption is proportional to the atomic number (Z) of the tissue atom and inversely proportional to the photon energy (E) cubed.

$$\text{Chance of photoelectric effect} \propto (Z/E)^3$$

Compton scatter or incoherent scatter happens when the high energy photons hit the atoms in the tissue but do not lose all their energy in ejecting the electrons. Instead, the photons are scattered in different directions with reduced energy.

The energy needed to eject an innermost or most strongly bound electron (K-shell electron) from an atom is called the K-edge. The photoelectric effect is highly accentuated at the K-edge of a material. The X-ray photons used in diagnostic radiology have energies between 10 and 150 keV. The K-edge of iodine atoms are in the region of 33.2 keV, which falls in the middle of the X-ray beam energy spectrum.

When an X-ray beam passes through the body, the beam is attenuated depending on the ability of that beam to penetrate and the characteristics of the tissue that it encounters (McKetty, 1998). Several factors affect attenuation including beam energy, density and atomic number of the material and thickness of the material.

The linear attenuation coefficient is a measure of the quantity of radiation absorbed by a given thickness of an absorbing material. It characterises how easily a volume of material can be penetrated. It increases as the atomic number of the absorber increases and decreases with the energy of the X-rays.

### 1.5.4.2 Iodinated contrast media

In cardiovascular imaging blood and soft tissue have nearly identical attenuation characteristics. Therefore, to visualise the lumen of vascular structures a contrast medium is used. Contrast media have a markedly different attenuation from blood or soft tissue, and they work by altering the photon attenuating characteristics. Positive contrast agents increase the attenuation and negative contrast agents decrease it. The common types of negative contrast agents used include barium compounds and iodinated compounds. Barium compounds are commonly used in gastrointestinal tract imaging. Barium is not suitable for use as intravascular contrast as it is not water soluble and will block the blood flow. Iodinated contrast agents are water-soluble agents based on iodinated benzene rings. They can be classified according to whether the agent dissociates in solution (ionic versus non-ionic) and structure (monomer versus dimer). In general, the potential for adverse reactions increases with the osmolality of the contrast agent. Solutions containing ionic agents have higher osmolality due to an increased number of particles in solution when compared with non-ionic agents. Solutions containing dimeric agents have more iodine atoms per molecule, and therefore have lower osmolalities relative to their monomeric counterparts. Ionic monomers are termed high osmolality contrast media and monomeric non-ionic compounds and dimeric ionic agents have been called low-osmolality contrast agents. Non-ionic dimers which are iso-osmolar contrast media have also been developed (Stacul, 2001).

### 1.5.4.3 X-ray equipment in cardiac catheterisation laboratory

The cardiac catheter laboratory is equipped with fluoroscopic equipment, which consists of a large 'C-arm', X-ray tube, image detector (mostly flat panel detectors), generator and operating console (figure 1.3). The C-arm has the X-ray tube and the image detector fixed to opposite ends. The X-ray tube has an evacuated metal or glass chamber with a circular anode (positive electrode) and a cathode (negative electrode) with one or more filaments (Bhatt, 2015).

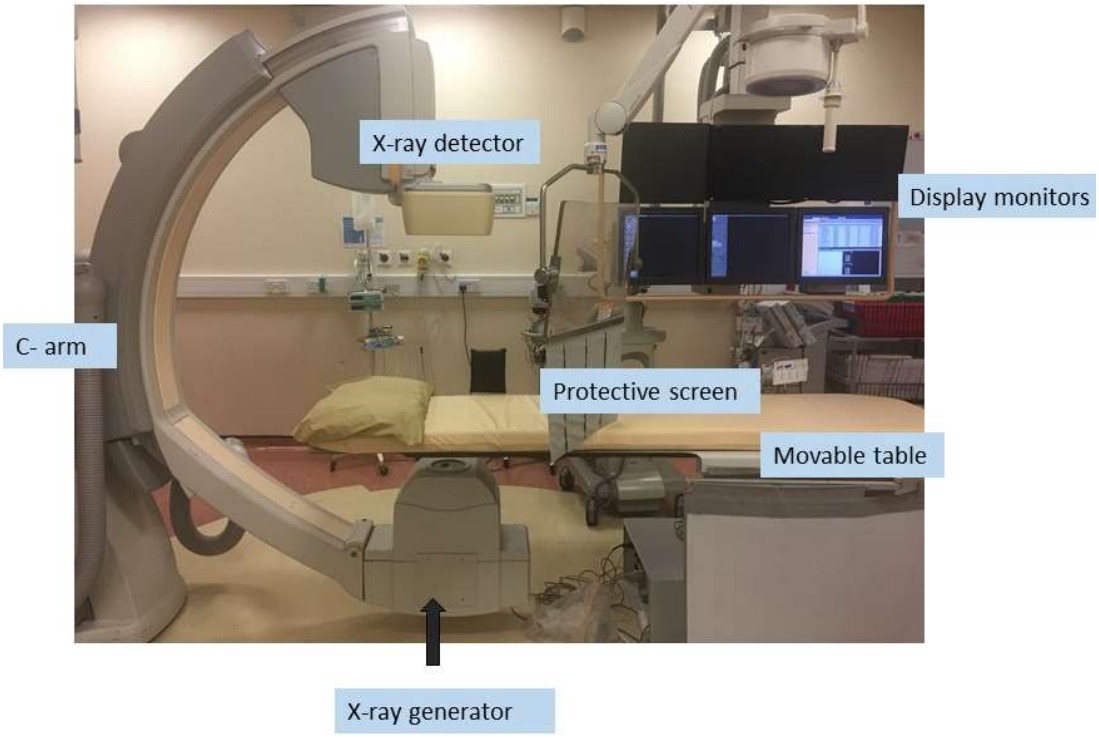


**Figure 1.3: Catheter lab 6 at Leeds General Infirmary where majority of the research work was carried out.** The X-ray generator and detector are mounted on a C shaped arm (C-arm) which moves around the patient lying on a movable table. Lead protection screens are used to protect the operator from radiation exposure. The X-ray images are displayed on ceiling mounted display monitors.

The parameters of the X-ray tube that affect the X-ray output include the following.

- Tube current: Milli amperes (mA): this is proportional to the number of electrons travelling across the anode-cathode gap per second. The X-ray output is linearly proportional to the tube current.
- Pulse duration: The duration of time during which X-rays are emitted to create a single fluoroscopic image. The X-ray output is directly proportional to the pulse duration. The pulse duration or width is colloquially referred to as milliseconds (ms). For cardiac procedures, this is usually 6-10ms.
- Tube voltage (Peak kilovoltage, kVp): This is the potential difference between the anode and cathode. This determines the photon energy distribution within the X-ray beam. The kVp has a complex relationship to the X-ray output, with a doubling of peak kilo voltage producing a quadrupling of X-ray output.
- Focal spot: This is a well-defined region on the anode where the accelerated electrons are focussed to produce X-rays.
- X-ray filtration: The X-ray beam passes through several materials, including the tube and the housing as well as added metallic filters (aluminium and copper) before reaching the patient. This is generally to reduce the number of lower energy X-ray photons.

The image detectors are mostly flat panel detectors, using an amorphous silicon detector coupled with a two-dimensional thin-film transistor (TFT) array. Most image detectors convert the X-ray energy into light, which is then converted to electrical signals via photodiodes. This information is amplified, sampled, digitised, and sent to a workstation where it undergoes image

processing prior to display. The detector also acts as a component of a feedback loop that regulates the X-ray output called automatic dose rate control (ADC). These systems are proprietary to the X-ray equipment manufacturer and the images available for review by clinicians are post processed and enhanced for optimal diagnostic performance while keeping the X-ray dose exposure to patient and staff low.

Cardiac catheterisation laboratory X-ray system can operate in two modes - fluoroscopy and digital acquisition (also called “cine”). Fluoroscopy is a low radiation dose mode which is used primarily to help with interventional equipment positioning. Digital acquisition uses higher dose (often up to 10 times) and gives high fidelity images better suited for clinical diagnosis and treatment (Gislason-Lee et al., 2013).

The typical temporal resolution is 15×5 ms pulses per second (15 frames/second) although higher resolution of 25 or 30 frames/second is possible.

#### 1.5.4.4 Assessing coronary blood flow from X-ray angiography

There have been several methods studied to assess coronary blood flow from X-ray angiography. Most of these techniques have been based on the analysis of the propagation of contrast following an injection of contrast material into the circulation. The contrast pass curve data in the coronary arteries or myocardium is used to calculate the flow or contrast transit time. Video-densitometric methods have been employed in the early seventies in attempts to quantify coronary blood flow (Smith et al., 1973; Rutishauser et al., 1970). These methods suffered from the need for high frame rates and the need to

know the arterial dimensions accurately to calculate the volume of distribution of the contrast.

Pijls *et al* described the concept of maximal flow ratio using video-densitometric assessment of the contrast agent in the myocardium and proved that improvement in myocardial flow is related to functional improvement on exercise testing (Pijls, N.H. et al., 1991; Pijls, N.H. et al., 1990).

Molloi *et al* attempted to measure coronary blood flow in a swine model using digital subtraction X-ray angiography in order to provide a means of objectively assessing epicardial coronary stenosis significance (Molloi et al., 1996; Molloi et al., 1998). The method was based on a first-pass distribution theory where the volume of the vascular bed supplied by a major coronary artery is modelled as a reservoir with a single input. Contrast agent was injected into the coronary artery during image acquisition with a dual-energy digital subtraction angiography system. Tissue-suppressed energy-subtracted images were used to calculate signal intensities within a selected region of interest containing the myocardium subtended by the coronary artery. The signal density was plotted against time to generate time-density curves of pixel density within the region of interest. Blood flow was determined in the vascular bed supplied by the left anterior descending (LAD) coronary artery using the time-density curve as follows.

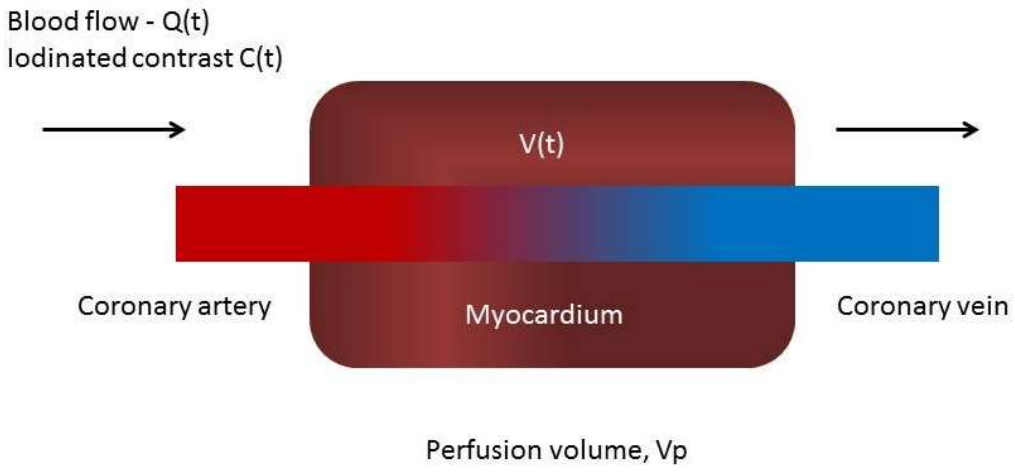


**Figure 1.4: Schematic of flow model demonstrating first pass distribution theory. Adapted from Molloi *et al* (Molloi et al., 1996).** The volume of the myocardial bed (Vp) supplied by a coronary artery is modelled as a reservoir with a single input which supplies a blood flow of Q(t). The injection of iodinated contrast results in concentration C(t) in the blood.

The coronary artery supplies the myocardium with blood at a flow rate of Q(t). When iodinated contrast agent with concentration of iodine C(t) is injected, it accumulates within the myocardium before exiting through the venous system and eventually the coronary vein. During the time before the contrast agent starts to exit the system (Δt), the volume of contrast is calculated as

$$\Delta V = \int_{t}^{t+\Delta t} Q(t)C(t)dt$$

If the contrast input concentration is constant [C(t) =C], then the equation becomes

$$\Delta V = C \int_{t}^{t+\Delta t} Q(t)dt$$

The average volumetric flow for the same time Δt can be calculated as

$$\underline{Q} = \frac{1}{\Delta t}\int_{t}^{t+\Delta t} Q(t)dt$$

So, average volumetric flow can be written as

$$\underline{Q} = \frac{\Delta V}{C\Delta t}$$

If the change in contrast agent volume (ΔV) during a short time frame (Δt) during which all of the contrast material is accumulating in the myocardium, and the iodine concentration of the contrast agent are known, the average volumetric flow can be calculated (Molloi et al., 1996). The injection of contrast agent is performed at a sufficient volume and rate to replace the entire blood volume in the coronary artery with contrast agent, for a short period of time. Therefore, the iodine concentration of the contrast agent is assumed to be same as C.

The pixel value in a digital subtraction image is directly proportional to the volume of contrast agent in that area. Therefore, the volume of contrast agent in the vascular bed is proportional to the integrated change in X-ray signal density ($\Delta D_I$) in that region. It represents the difference in signal intensity change over the region corresponding to the vascular bed over time Δt.

$$\Delta V = \frac{A}{\mu_I}\Delta D_I$$

'A' is the pixel area and $\mu_I$ is the attenuation coefficient of iodine.

A calibration phantom was used to measure the pixel area and attenuation coefficient of iodine. This consisted of an array of cylindrical cells 7mm diameter and 10mm depth with a range of iodine concentrations (figure 1.6).

So, the flow equation can be re-written as

$$\underline{Q} = \frac{1}{C}\frac{1}{\Delta t}\frac{A}{\mu_I}\Delta D_I$$

Δt can be calculated from the frame rate of X-ray image acquisition.

During coronary angiography, invasive blood pressure is continuously monitored. Myocardial resistance can be calculated by dividing the arterial driving pressure by coronary blood flow (CBF) (Aarnoudse et al., 2004b).

$$\text{Myocardial resistance } (\mathrm{R}_{myo}) = \frac{Arterial\ driving\ pressure}{CBF}$$

Arterial driving pressure is calculated from the pressure in the coronary artery distal to any coronary artery stenosis of interest, measured by a pressure sensitive coronary guidewire advanced into the coronary artery ($P_d$). The coronary venous pressure or right atrial pressure ($P_{RA}$) is subtracted from $P_d$ to calculate the arterial driving pressure.

$$R_{myo} = \frac{P_d - P_{RA}}{CBF}$$

$P_{RA}$ is not measured routinely although it can be measured relatively easily by advancing a catheter connected to a pressure transducer into the right atrium. The right atrial pressure is small and often negligible in most patients unless they have another clinical condition causing elevation of right sided pressures. Assuming $P_{RA}$ to be negligible,

$$R_{myo} = \frac{P_d}{CBF}$$

In the absence of significant coronary artery stenosis or if the stenosis has been treated with percutaneous coronary intervention, $P_d$ will be the same as the aortic pressure ($P_a$), which can be measured without the need for pressure sensitive coronary guide wires. So, in the absence of stenosis, the equation becomes

$$R_{myo} = \frac{P_a}{CBF}$$

The stenotic resistance can also be calculated if from the aortic pressure and the driving pressure.

$$Stenotic\ resistance = \frac{(P_a - P_d)}{CBF}$$

Zhang *et al* reported using the same principle to quantify the myocardial resistance by using the pressure data available during cardiac catheterisation and found that myocardial resistance provided the most accurate method of assessing microcirculation (Zhang et al., 2011). Their method made use of a calibration phantom with an array of cylindrical cells with varying concentrations of iodine and a look up table for varying values of X-ray beam energies (kVp) and object thickness. The two assumptions that this method makes are that the flow measurements are made before the contrast starts exiting the perfusion volume and that the input iodine concentration is constant. This method has not been attempted in human subjects.

This thesis aims to study a similar method of absolute coronary blood flow quantification in humans for the first time.

**Table 1.5: Summary of techniques used for assessing coronary physiology.**

| Technique | Invasive /Non-invasive & Method | Advantages | Disadvantages |
|---|---|---|---|
| *Surrogate indices of coronary/myocardial blood flow in the catheterisation laboratory* | | | |
| Coronary flow reserve (CFR) | Thermodilution/Doppler coronary wire | Can assess coronary stenosis and microcirculation | Cannot distinguish between microvascular disease and coronary stenosis.<br>Affected by haemodynamic conditions. |
| Fractional Flow reserve (FFR) | Pressure sensitive coronary wire | Can assess significance of coronary stenosis.<br>Robust evidence base for FFR guided revascularisation.<br>Reproducible. | Cannot assess microcirculation.<br>Influenced by conditions causing high microvascular resistance. |
| Instantaneous wave-free ratio (iFR) | Pressure sensitive coronary wire | Surrogate for FFR, Good correlation at extreme values of FFR at assessing coronary stenoses.<br>Avoids the use of adenosine. | Cannot assess microcirculation. Not very accurate at intermediate values of FFR. |
| Index of microcirculatory resistance (IMR) | Thermodilution | Can assess microcirculation. | Cannot assess coronary stenoses. |
| *Non-invasive methods of myocardial flow quantification* | | | |
| Myocardial contrast echocardiography | Non-invasive, no ionising radiation | Does not use tracer kinetics, widely available and cheap | Operator and image quality dependant. |
| Positron emission tomography (PET) | Non-invasive, uses radioactive tracer | Able to quantify regional myocardial blood flow accurately | Limited clinical utility as not available for decision making in the catheterisation laboratory.<br>Not widely available. |

| | | | |
|---|---|---|---|
| Cardiac magnetic resonance (CMR) | Non-invasive | High spatial resolution. No ionising radiation. | Non-volumetric ventricular imaging, relatively complex post processing steps. Limited clinical utility as not available in the catheterisation laboratory. Still a research tool. |
| Dynamic Computed Tomography Imaging (CT) | Non invasive | High spatial resolution. Anatomic and functional study using one modality | Uses ionising radiation. Risk of contrast induced renal injury. |
| *Invasive methods of coronary flow quantification in the catheterisation lab* | | | |
| TIMI myocardial perfusion grade (TMPG) | Invasive but no need for coronary wire | Easily available, semi-quantitative tool for assessing myocardial perfusion. | Can be subjective. It is a crude method. |
| Doppler wire method of coronary flow calculation | Doppler coronary wire | Coronary flow calculation using flow velocity from Doppler wire | Operator dependant. Lacks reproducibility. |
| Thermodilution method of volumetric coronary flow measurement | Continuous thermodilution | Volumetric coronary blood flow measurements | Cannot distinguish between coronary stenosis and micro circulation. Special infusion catheter needed. |
| X-ray based techniques | Assessment of signal intensity change | Non-invasive, should be able to be applied easily in the catheter lab | Technique not validated in humans. |

CFR- Coronary flow reserve, FFR- Fractional flow reserve, iFR- Instantaneous wave-free ratio, PET- Positron emission tomography, CT- Computed Tomography, CMR- Cardiac magnetic resonance, TMPG- Thrombolysis in myocardial infarction myocardial perfusion grade.

## 1.6 Importance of absolute coronary blood flow measurements and clinical applications

The potential applications of being able to assess coronary flow and in turn the resistance to flow are many. The situation where epicardial coronary disease co-exists with microvascular disease is common. It is often difficult to assess the relative contribution of each to limitation of coronary flow. Methods to assess coronary flow, when combined with indices such as FFR or other measures of stenotic resistance can assess the differential contribution of epicardial coronary stenoses and microvascular disease towards causing myocardial ischaemia and angina. Smalling *et al* demonstrated in an animal model that myocardial function is dependent on coronary flow rather than pressure (Smalling et al., 1985). In the stable setting, a flow based decision-making process may allow optimal patient selection, the key benefit is the ability to evaluate flow impairment not only due to obstructive CAD but also due to microvascular dysfunction (van de Hoef et al., 2015a) .

Although FFR is widely used before and after PCI as a surrogate to measure improvements in blood flow, there is now emerging evidence that increases in FFR measurements do not reflect increases in absolute coronary blood flow (Hamaya et al., 2019). As discussed previously, a normal FFR does not mean that the myocardium is perfused adequately.

Atherosclerosis is a gradual progressive process and often micro-circulatory dysfunction precedes the development of angiographic stenosis, perfusion defects or regional wall motion abnormalities (RWMA) on functional imaging

(Quyyumi et al., 1995; Cox et al., 1989). Murthy *et al* studied over 2700 patients referred for rest/stress positron emission tomography for a median of 1.4 years and found that coronary microvascular dysfunction, as measured by coronary flow reserve (CFR), was an independent predictor of cardiac mortality (Murthy, Venkatesh L. et al., 2011). Being able to measure coronary flow without additional instrumentation of coronary arteries offers the opportunity for better risk stratification in the catheterisation laboratory and guide treatment.

Coronary flow measurements are useful not only for comprehensive assessment of coronary artery disease and microvascular disease, but also in noncoronary cardiac diseases (Camici et al., 1996). Coronary blood flow measurements may help in assessing the prognosis and for monitoring the effectiveness of risk reduction strategies (Waller et al., 2014; Camici and Rimoldi, 2009; van de Hoef et al., 2015b).

### 1.6.1 ST elevation myocardial infarction

Acute ST-elevation myocardial infarction (STEMI) is the subtype of acute coronary syndrome characterised by complete occlusion of epicardial coronary artery with thrombus and coronary spasm. Prompt revascularisation with primary PCI has proved to be the corner stone in treating these patients and has reduced mortality (Roe et al., 2010). However, post infarct conditions such as myocardial dysfunction and heart failure are still common (Rosamond et al., 2012). In spite of prompt revascularisation with primary PCI techniques, further myocardial damage can occur due to a combination of factors such as embolisation of athero-thrombotic debris, release of harmful chemicals and associated reperfusion injury (Fröhlich et al., 2013). In a study of patients who

died from acute coronary syndromes, 73% had distal embolisation causing occlusion of intramyocardial arteries associated with microinfarcts (Falk, 1985). Another study that looked at patients who died after coronary balloon angioplasty found even higher proportion (81%) of patients with coronary micro emboli (Saber et al., 1993). The adequacy of revascularisation can be assessed by coronary angiography demonstrating no residual epicardial coronary artery stenosis, however assessing the adequacy of reperfusion also requires evaluation of the microvascular function, which is now established as a strong prognostic factor post MI (Wu, K.C. et al., 1998; Bolognese et al., 2004). Despite advances in treatment, more than 50% of patients treated with PCI for acute myocardial infarction experience further myocardial damage and increase in infarct size from microvascular impairment commonly due to distal embolisation of atherothrombotic debris and other factors (Niccoli et al., 2009). The most extreme form of microvascular impairment is evident on coronary angiogram images and has been termed ‘no-reflow’ phenomenon. (Eeckhout and Kern, 2001). Coronary angiography cannot evaluate microvascular function other than in conditions such as ‘no reflow’. No-reflow is an independent predictor of mortality (Brosh et al., 2007). It is not possible to accurately identify less severe forms of microvascular impairment from angiography alone. Out of the many factors that cause microvascular impairment, microvascular obstruction, as identified by CMR has been associated with increased cardiovascular complications, larger infarct size (IS) and predicts long term adverse prognosis (Wu, K.C. et al., 1998). Assessing coronary flow may help to identify less obvious MVO in the catheterisation laboratory and help immediately target therapies.

Cardiac MRI can assess the pathophysiological consequences of MI such as infarct size, microvascular obstruction, myocardial salvage, myocardial haemorrhage and LV dysfunction and it has been shown to provide independent prognostic information (Eitel et al., 2014; Regenfus et al., 2015; Carrick et al., 2016b). If conditions such as MVO are identified early, more intense vasodilator, antithrombotic therapy and other therapies currently being evaluated for myocardial protection can be employed to improve outcomes (Rawitscher et al., 1997). However, performing a CMR scan is not feasible in a timescale that would allow immediate delivery of therapy after primary PCI. Therefore, it is highly desirable to have a method to assess the effectiveness of reperfusion in the catheterisation laboratory. Measuring coronary or myocardial blood flow offers the best way to assess reperfusion.

Traditional methods of assessing reperfusion include measuring ST segment resolution on surface ECG (Barbagelata et al., 2005), TIMI flow grade and use of myocardial blush grades such as TIMI myocardial perfusion grades. Other methods such as using biomarkers (Licka et al., 2002; Arruda-Olson et al., 2011; Tanaka et al., 1997), echocardiography (Califf et al., 1990; Eek et al., 2010), Tc99 Sestamibi SPECT imaging (Gibbons et al., 1989), CMR (Hillenbrand et al., 2000; Kopecky et al., 2003) and Index of Microcirculatory resistance (IMR) (Carrick et al., 2016a) have all been employed. A summary of the various methods is given in table 1.6. Other than the methods employed in the catheterisation laboratory at the end of the primary PCI, others do not provide the information in a timely manner to be useful clinically.

**Table 1.6: Methods to assess infarct size and effectiveness of reperfusion.**

| Method | Advantages | Disadvantages |
|---|---|---|
| ECG | easily available in emergency setting. | It provides indirect measure of infarct size that can be quantitative by utilisation of various scores. |
| Biomarkers | easily available. | need for repeated sampling for peak levels, affected by reperfusion. |
| Echocardiographic techniques | easily available. | operator dependent, not widely used outside research setting. |
| Tc99 Sestamibi SPECT imaging | can assess full thickness infarcts. | Low spatial resolution, hence, misses sub-endocardial infarcts; need for radioactive tracer with limited shelf life and use of ionising radiation. Not available in the catheterisation laboratory. |
| Cardiovascular magnetic resonance imaging (CMR) | current gold standard; high spatial resolution; can detect sub-endocardial infarcts better. | Not universally available, cannot be used in patients with metal implants or those who have claustrophobia. Not available in emergency setting. Not available in the catheterisation laboratory. |
| Index of microcirculatory resistance (IMR) | Numerical value for myocardial resistance correlates with infarct size on CMR.<br>Useful for prompt decision-making in the catheterisation laboratory. | Invasive technique.<br>Requires adenosine to induce hyperaemia. |

ECG- electrocardiogram, Tc99- Technetium 99, SPECT- single-photon emission computed tomography, CMR- Cardiovascular magnetic resonance imaging, IMR- Index of microcirculatory resistance. Reproduced with permission from Parviz, *et al* CRM 2017(Parviz et al., 2017)

Assessing coronary flow may help to identify less obvious microvascular obstruction and help target specific therapies. Although several therapeutic agents have been studied to reduce infarct size, none of the agents have been able to establish itself due to not much evidence base to support its

widespread use. Vasodilators such as adenosine and its analogues has shown some promise in reducing infarct size although the evidence is conflicting (Pitarys et al., 1991; Babbitt et al., 1990; Ross et al., 2005). Other agents such as papaverine, epinephrine and ivabradine have limited evidence (Ishihara et al., 1996; Skelding et al., 2002; Heusch et al., 2011). There is some evidence that intra-coronary thrombolysis with primary PCI may reduce infarct size (Sezer et al., 2007; Sezer et al., 2009) but does not reduce the incidence of microvascular obstruction (McCartney et al., 2019). A number of mechanical devices, such as distal embolic protection devices, have been trialled in infarct size reduction with no proven benefit (Gick et al., 2005; Kelbaek et al., 2008). Thrombectomy devices have also been disappointing in reducing infarct size (Jolly et al., 2016; Elgendy et al., 2015). Several cellular and molecular approaches have been studied in enhancing myocardial recovery post MI and although they showed promise in animal models, human studies have been largely disappointing (Parviz et al., 2019).

Knowledge of impaired coronary flow after reperfusion may also allow the cardiologists to use adjunctive technologies such as intra-aortic balloon pump, Impella ventricular support device, or coronary sinus occlusion systems, although the evidence for their clinical utility is currently sparse. This information could also be useful in risk stratifying patients for timing of intervention to non-culprit artery lesions and decisions regarding timing of discharge and follow-up.

### 1.6.2 Decision making regarding revascularisation.

FFR and non-hyperaemic indices such as iFR have large evidence base to support their use in decision making regarding revascularisation, especially in

angiographically intermediate stenoses (De Bruyne, B. et al., 2012; De Bruyne, B. et al., 2014; Gotberg et al., 2017; Davies et al., 2017). The potential pitfalls in using FFR as a gold standard when it is in fact a surrogate of myocardial blood flow have been described earlier in this chapter. Decision making based on myocardial blood flow is feasible in some patients using PET techniques and may lead to better selection of cases where myocardial blood flow can be accurately predicted (Bober et al., 2019). If coronary blood flow could be reliably estimated in the catheter laboratory, especially without the need for instrumenting the coronary artery with a guidewire, it may provide information that can be used alongside FFR/iFR or on its own for clinical decision making in coronary revascularisation.

### 1.6.3 Assessing the impact of percutaneous coronary intervention.

The ultimate aim of PCI is to improve blood flow to the myocardium. However this may not always be achieved after PCI due to a variety of reasons, including the presence of microvascular dysfunction type 2 or type 3 or PCI procedure leading to type 4 microvascular dysfunction or no reflow phenomenon (Camici and Crea, 2007). No-reflow phenomenon is an independent predictor of mortality (Brosh et al., 2007). It has been suggested that performing FFR measurements before and after PCI offers a way of indirectly assessing the impact of PCI on myocardial blood flow, however recent data indicate that changes in FFR may not always reflect improvement in myocardial blood flow (Hamaya et al., 2019; Kanaji et al., 2017). The use of FFR in acute coronary syndromes is less well established than in stable coronary disease. A method to directly measure coronary blood flow in the

catheter laboratory would offer a way of comparing blood flow before and after intervention and help clinicians understand the reasons for patients not improving symptomatically after PCI procedure (Li et al., 2015).

### 1.6.4 Myocardial infarction with no obstructive coronary arteries

Myocardial infarction is usually associated with a partial or complete blockage of an epicardial coronary artery or its branches. However in some cases electrocardiographic and biochemical evidence of myocardial infarction was seen in spite of having unobstructed arteries on the angiogram (Beltrame, 2013). This has been termed myocardial infarction with no obstructive coronary arteries (MINOCA). In spite of the unobstructed arteries, the prognosis in these patients is comparable to patients with acute MI associated with one or two vessel CAD (Kang, W.Y. et al., 2011; Grodzinsky et al., 2015). CMR is useful in understanding the underlying pathology and cause in 87% of cases of MINOCA (Pathik et al., 2016). A number of pathologies have been found as causes underlying MINOCA which include coronary plaque disruption (plaque erosion and plaque rupture), coronary thrombosis or embolism, coronary spasm and microvascular dysfunction (Tavella et al., 2018). It would be an advantage to be able to diagnose the underlying cause at the time of the angiogram. Patients with MINOCA may need comprehensive evaluation of coronary physiology and/or intra-coronary imaging using intravascular ultrasound or optical coherence tomography based on clinical suspicion.

Measuring coronary blood flow in the catheterisation laboratory may help understand the underlying pathophysiology and make early clinical diagnosis and management decisions.

### 1.6.5 Angina with no obstructed coronary arteries

Angina with no obstructed coronary arteries and ischaemia with no obstructed coronary arteries are terms coined recently to describe angina or presence of ischaemic heart disease where coronary arteries appear nonobstructed on coronary angiography (Corcoran et al., 2018a; Bairey Merz et al., 2017). Cardiac syndrome X is a term that was used previously to describe this entity and is often stigmatised by its association with obesity, female sex and psychology leading sometimes to patients being offered no treatment (Berry, 2017). Although the arteries appear normal on coronary angiography, assessment of microvasculature has revealed abnormal microvascular resistance (Luo et al., 2014; Sara et al., 2015). Microvascular angina and vasospastic angina have been thought to be responsible for majority of such cases although other mechanisms such as hypertension, valvular heart disease, anaemia, myocardial diseases, coronary anomalies, congenital heart diseases, myocardial bridging etc. also may contribute to this clinical syndrome. Non-invasive imaging modalities such as CMR may be better suited to evaluate these patients due to the better safety profile compared to invasive tests. However, a large proportion of patients are assessed with invasive angiography and measuring coronary blood flow will help to understand the pathophysiological processes at play (Rahman et al., 2019).

### 1.6.6 Myocardial diseases

Myocardial blood flow and flow reserve have been noted to be severely blunted in hypertrophic cardiomyopathy and the degree of impairment predicts ventricular remodelling and prognostic outlook (Cecchi et al., 2003; Olivotto et

al., 2006). Myocardial blood flow is also noted to be impaired in patients with idiopathic dilated cardiomyopathy and is thought to play a pathophysiologic role (Neglia et al., 1995; van den Heuvel et al., 2000). Patients with diseases such as cardiac sarcoid, Anderson-Fabry disease, Freidreich's ataxia, cardiac amyloid also have microvascular dysfunction and impairment of myocardial blood flow (Kul et al., 2017; Elliott et al., 2006; Tomberli et al., 2013; Kruse et al., 2017; Dorbala et al., 2014; Gregory et al., 2007). Rijnierse *et al* found significant differences in myocardial blood flow in patients with ischaemic cardiomyopathy and the ability to induce ventricular arrhythmias (Rijnierse et al., 2014).

Non-invasive modalities such as echocardiography, CT, CMR and PET will remain the main stay in diagnosis and risk stratification in myocardial diseases and cardiomyopathies, but some of these patients are investigated with a coronary angiogram as part of their work up. The ability to estimate coronary blood flow without additional instrumentation of coronary arteries may provide clinical information that can be useful in diagnosis and clinical decision making in these conditions.

### 1.6.7 Assessing impact of pharmacologic and other risk reduction strategies

The ability to reliably quantify absolute coronary blood flow in the catheterisation laboratory may provide a quick and easy method to assess the impact of drugs and other pharmacotherapeutic agents on the coronary microcirculation. In moderately hypertensive patients, angiotensin receptor blocker Valsartan was noted to improve coronary microcirculation assessed by PET even before reductions in blood pressure was achieved (Higuchi et al.,

2007). Similarly improvements in myocardial blood flow was noted in hypertensive patients with a combination of perindopril and indapamide and in patients with familial hyperlipidaemia, with insulin sensitizer thiazolidinedione, pioglitazone added to conventional lipid-lowering therapy (Naoumova et al., 2007). Assessing coronary blood flow invasively in the cardiac catheterisation laboratory provides another method to evaluate these drug effects in real time and provides the opportunity to test different agents at varying doses.

## 1.7 Need for newer techniques.

The reasons why FFR should not be considered the gold standard for assessment of coronary physiology and blood flow have been discussed earlier in this chapter. Measurement of coronary or myocardial blood flow and resistance would provide a better comprehensive understanding of the pathological processes at play. Although non-invasive methods such as PET scanning can be useful in selected patients, it is not practical to be applied to most patients. CFVR assessment by thermodilution or Doppler wire provides velocity measurements which are often used as surrogates for coronary flow. Both methods are cumbersome and involve instrumentation of coronary arteries. The continuous thermodilution method of measuring volumetric coronary flow is similarly cumbersome and time consuming with the need for special catheters, pumps, and connectors. It would be highly desirable to have a method of assessing coronary flow which is reliable and easy to use in the catheterisation laboratory at the time of coronary angiography, to facilitate a comprehensive assessment of coronary physiology.

An X-ray based technique to quantify blood flow, if it can be successfully employed in humans would be highly promising. Coronary blood flow calculation using digital subtraction angiography as described in a swine model by Molloi *et al* uses a calibration phantom and a look up chart, which can pose practical difficulties when applied to human subjects (Molloi et al., 1998; Molloi et al., 2012).

A large proportion of diagnostic coronary angiography is undertaken in centres without the capacity for instrumentation of the coronary artery with a coronary guidewire. Therefore, a technique that can be applied widely without the requirement to instrument the coronary artery would be a welcome addition to the cardiologists' armamentarium.

## 1.8 Development of a method of X-ray coronary blood flow quantification in Leeds

Dr Andrew Davies (research project co-supervisor) developed a software package for analysing X-ray angiographic image signal intensity at the University of Leeds. The software and the method of flow quantification was developed to improve on the method developed by Molloi et al(Molloi et al., 1998). The software was written in MATLAB (MathWorks, Natick, Massachusetts, US). The calculation of blood flow using this custom software and workflow is referred to as 'X-ray Blood Flow' (XBF) in this thesis. The key difference in the method is the avoidance of the calibration phantom. This is described in more detail in the next section. The original idea to study coronary blood flow using this software was conceived by my supervisors Dr Andrew Davies and Professor Sivananthan. Dr Davies in collaboration with Dr David

Barmby performed early bench studies using a chamber and injecting contrast before imaging with X-ray and applying the XBF software. The results of these experiments showed good correlation between the XBF calculated signal intensity change and the rate of injection of contrast. The data from these experiments is not included in this thesis. The results from these experiments led to the development of the research that forms the basis of this thesis.

X-ray coronary angiogram ‘raw data’, extracted from the catheterisation laboratory X-ray system before the manufacturer’s proprietary post processing is applied, are analysed by the XBF software. The XBF software also can analyse images in Digital Imaging and Communications in Medicine (DICOM) format. DICOM is the most used image format after post processing has been applied for clinical use.

Angiogram images of an acquisition cine loop that starts just before the contrast agent flows into a particular coronary artery of interest and continues over several cardiac cycles until the contrast agent is seen appearing in the coronary venous system is typically used for XBF analysis. This image loop is loaded in the XBF software, which has a viewer interface that allows the visualisation of the coronary angiogram images (figure1.5). Images can be viewed whilst playing in a loop or visualised frame by frame. Individual frames can be selected and analysed. At the initial stage of a typical coronary angiogram cine-loop, the X-ray system stabilises and there is no contrast entering the coronary artery. Images from this phase form the ‘mask images’ which are then subtracted from the images in subsequent frames to remove all background objects. This also helps to eliminate the difference between patients of different body habitus. As the contrast enters the coronary artery

under study and the myocardial bed it subtends, the signal intensity in a user-defined region of interest (ROI) selected to include this myocardial bed (seen on the left side of the user interface in figure 1.5) starts to reduce. The XBF software measures the signal intensity in each frame and plots it in a graphical format on the right-hand side of the interface. As the heart contracts and relaxes during the cardiac cycle, there is some variation in signal intensity in a sinusoidal pattern due to increase in X-ray attenuation as the tissue density and overlap changes during contraction of the heart (seen on the right side of the user interface in figure 1.5). The XBF software automatically analyses the change in signal intensity that occurs with the cardiac cycle and selects the frames where image intensity is lowest or highest and identifies them as systolic or diastolic phase images, respectively. This automatic selection can be manually overridden if necessary. The image frames in a particular phase of the cardiac cycle can be used or all the image frames can be used for analysis. The image frames during the period when the contrast steadily accumulates in the ROI are selected manually. The software can calculate the sum, mean or median of signal intensities in each frame.

The reduction in signal intensity as contrast flows through the coronary artery territory in the ROI is proportional to the mass of contrast agent in the ROI. This is plotted by the XBF custom software against time to obtain a time-intensity curve (TIC). The gradient of this TIC curve during the initial phase when the signal intensity change is the steepest is selected (seen on the right side of the user interface in figure 1.5). This method is performed for the calibration sequence and the measurement sequences during rest and

hyperaemia. The ratio of the gradient of each measurement sequence to the gradient of the calibration sequence gives the coronary blood flow.

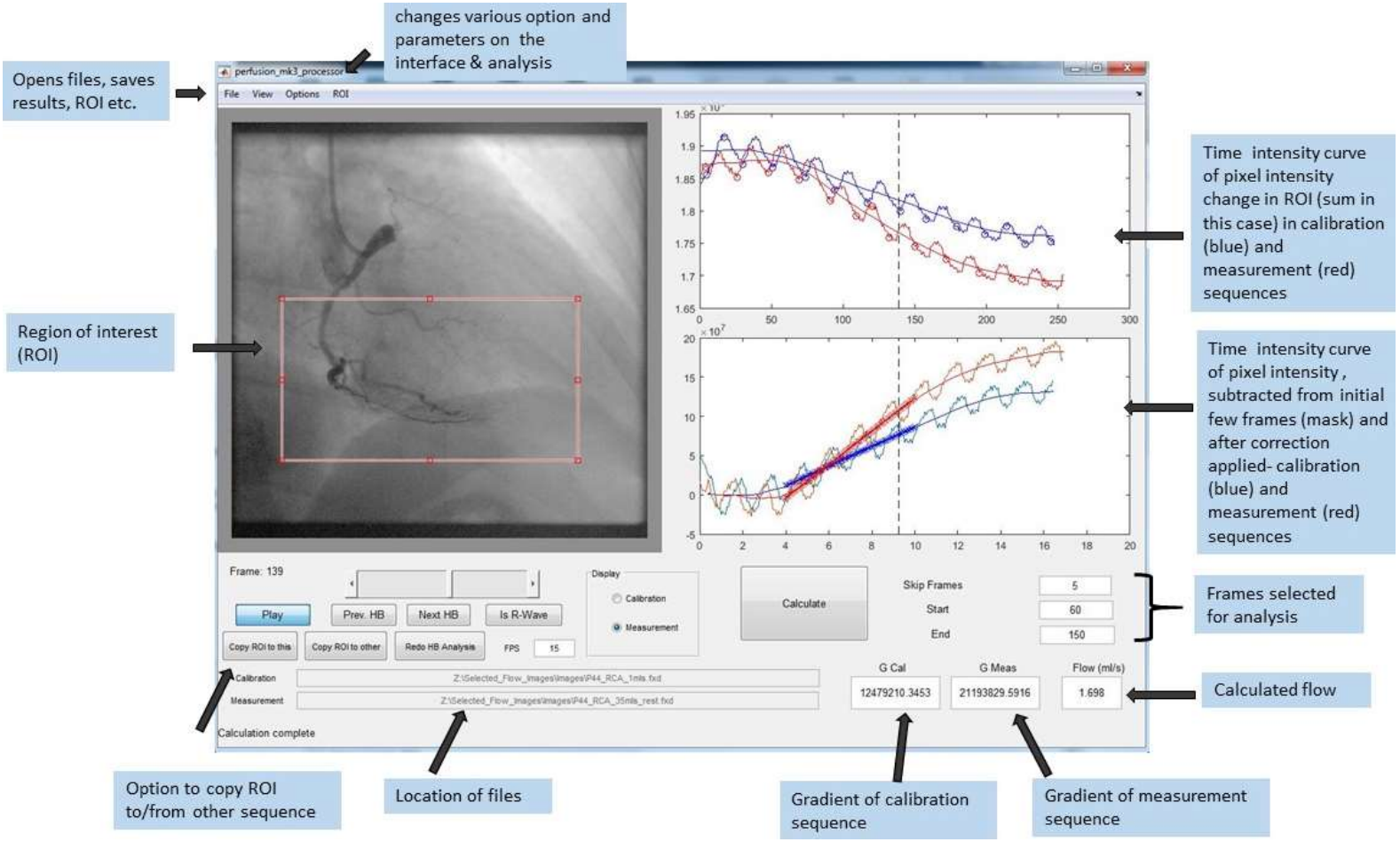


**Figure 1.5: Flow Processor software user interface.** On the right-hand side, the time intensity curves (TIC) generated from signal intensity analysis can be seen. The calibration sequence is analysed first (blue TIC) and then the measurement sequence is analysed (red TIC). The ratio of their gradients gives flow.

### 1.8.1 Differences of the XBF method to the method proposed by Molloi et al.

Molloi *et al* used a calibration phantom with an array of cells with a range of iodine thickness to calibrate the video densitometric iodine signal (Molloi et al., 1998). We did not attempt to calibrate using a phantom. Although for experimental purposes this would have been feasible, when translating to clinical use in patients an iodine-containing X-ray calibration phantom would pose problems. Iodine is liable to degradation and a phantom would need to be refilled with correct amounts of iodine at regular intervals. This would be impractical for clinical use. A phantom could be affixed to patient's chest; however, the phantom will not necessarily be at the same level as the heart, which would lead to error. The phantom must be in the image frame even if the image is acquired at an oblique angle. This would mean repositioning the phantom between imaging sequence. Finally, a phantom in this position may also interfere with the region of interest for coronary flow assessment.

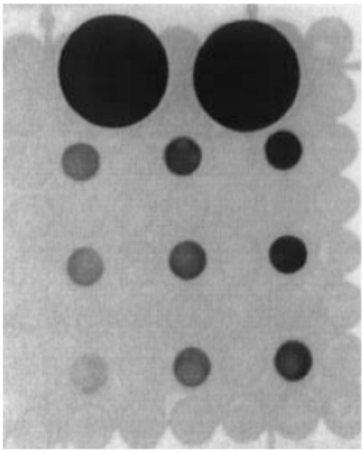

**Figure 1.6: An image of the calibration phantom used by Molloi *et al* (Molloi et al., 1998).** It has an array of cylindrical cells of 7mm diameter and 10mm in depth. A range of iodine thicknesses (0-125mg/cm$^2$) were calibrated. The two large circles were used for pixel calibration.

Instead of an iodine containing phantom, a technique of injecting contrast at a known low rate, such that all the contrast flows into the coronary artery, was used as a calibration sequence against which the measurement sequences were compared. This represents a more user-friendly calibration method that can be employed easily in patients.

## 1.9 Conclusion

The ability to quantify coronary blood flow and microvascular resistance in real time remains highly desirable for comprehensive coronary physiology assessment. The ability to perform coronary blood flow quantification reliably in the catheterisation laboratory could help in diagnosis, risk stratification and clinical decision making in a variety of clinical conditions. It would offer most benefit in understanding the integrity of microvasculature and myocardial perfusion. Thermodilution-based coronary blood flow quantification has been attempted in humans with some success, however, it remains a cumbersome process requiring instrumentation of coronary arteries with coronary guide wires and specially designed microcatheters. X-ray based blood flow quantification method pioneered by Molloi *et al* is promising in its ability to use the data available from standard X-ray angiography to quantify coronary blood flow without any need for instrumenting coronary arteries, thereby avoiding the associated additional risk. Although the results from animal work reported by Molloi *et al* were encouraging, this technology has thus far not been translated to humans where the use of the calibration method required would be very difficult if not impossible. If this method could be used successfully in humans, it would offer great potential to study the coronary microcirculation both in

clinical setting as well as research studies. Bespoke software to enable quantification of X-ray coronary blood flow has been developed at the University of Leeds. The project described in this thesis was designed to validate this XBF method in a bench model and assess the feasibility of its use to quantify coronary flow in patients undergoing cardiac catheterisation.

# Chapter 2 Hypothesis, Aim and Objectives

## 2.1 Background

In the previous chapter, the importance of assessing coronary blood flow physiology and measurement of coronary blood flow were discussed. Molloi *et al* have shown that absolute blood flow quantification can be performed using X-ray signal intensity analysis in swine (Molloi et al., 1998; Molloi et al., 2004), although this method has not been investigated in human subjects.

The development of bespoke XBF software by Dr Andrew Davies to analyse signal intensity change in X-ray angiographic images and the new calibration technique described in more detail in chapter 3, paved the way to a clinical research project on coronary blood flow quantification from X-ray angiography which forms the basis for this thesis.

## 2.2 Hypotheses

- Quantification of coronary blood flow using X-ray signal intensity analysis of X-ray coronary angiogram images is feasible in patients undergoing clinical coronary angiography.
- Assessment of myocardial microvasculature using measurements of coronary blood flow from X-ray angiography can predict outcomes following primary percutaneous coronary intervention for acute myocardial infarction.

## 2.3 Aim

The aim of the project was to validate a bio-imaging technique for quantifying coronary blood flow from X-ray angiography in humans and investigate its utility in the setting of acute myocardial infarction.

## 2.4 Objectives

- To validate the technique of quantifying coronary blood flow from X-ray signal intensity analysis in a bench model allowing experimental modulation of epicardial and microvascular coronary resistance.
- To assess the feasibility of the technique of quantifying coronary blood flow from X-ray signal intensity analysis in humans undergoing routine coronary angiography or percutaneous coronary intervention for coronary heart disease.
- To determine the feasibility of applying X-ray based quantification of coronary flow to assess myocardial resistance immediately after coronary reperfusion in patients undergoing primary percutaneous coronary intervention for acute ST segment elevation myocardial infarction.

## 2.5 Design of study

The research study involved three arms.

a) Bench study.

b) Human validation study.

c) Human STEMI study.

The bench study was based on a phantom, where coronary circulation was simulated. Actual flow rates were compared against the flow measured from the XBF method. This was carried out with support from St Jude Medical and School of Engineering, University of Bradford.

The human validation study was a pilot study, aiming primarily to compare the coronary blood flow calculations by XBF method and the continuous thermodilution method. The study tested the feasibility, adverse events, and effect size to inform the design of a larger study. The validation study aimed to recruit about 30 patients undergoing coronary angiography for clinical reasons and attempted to quantify the coronary blood flow using X-ray signal intensity analysis and compare the results to those obtained from continuous thermodilution method.

The STEMI study was a proof-of-concept study, designed to investigate the feasibility of performing coronary flow assessment by XBF method in an emergency setting. The patients underwent subsequent cardiac MRI to quantify infarct size. The flow and resistance values obtained in the catheterisation laboratory were compared against the CMR parameters. The aim was to recruit 15 STEMI patients and compare coronary artery flow measurements to cardiac magnetic resonance scan infarct parameters. The CMR research group (Professor Sven Plein, Dr Pankaj Garg) at the University of Leeds were our collaborators in this study.

Phillips Healthcare helped support the study by allowing software modification of the catheterisation laboratory X-ray system.

# Chapter 3 General Methods

Coronary angiography involves projection of images of arteries opacified with radio-opaque contrast medium. This provides 2-dimensional imaging of the lumen, which is widely used to diagnose and plan treatment of patients with CAD. Coronary artery blood flow measurement using X-ray angiography has been attempted before as described in chapter 1. The most successful of these attempts were by Molloi *et al* (Molloi et al., 1996).The technique employed in this thesis was based on the principle used by Molloi and colleagues in a swine model (Molloi et al., 1996). This method was adapted for use in humans in our study.

For a short period of time during coronary angiography when contrast is injected into the coronary artery, before the injected contrast reaches the venous system, the rate of accumulation of contrast in the myocardium supplied by the artery is proportional to the rate of contrast flow in the artery. At a set rate of injection, the factors that determine the coronary blood flow such as microvascular resistance and lesion resistance also determine the rate of contrast accumulation. When a parallel beam of X-rays passes through the body, the degree of attenuation depends on scattering and absorption processes. The intensity of X-rays after attenuation can be derived from the Lambert-Beer law.

$$I = I_0 e^{-\mu x}$$

Where $I_0$ is the incident X-ray intensity and $I$ is X-ray intensity transmitted through the body, μ the linear absorption coefficient and x is the sample thickness.

The linear attenuation coefficient μ is a property of the absorbing material and it also depends on the energy of the X-rays. The linear attenuation is proportional to density of the absorbing material. It is therefore convenient to normalise the linear attenuation coefficient to the density of the material, giving the mass attenuation coefficient. The mass attenuation coefficient is calculated by dividing the linear attenuation coefficient by the density of the material (μ/ρ, ρ is the density of the material).

The above equation can be re written as

$$I = I_0 e^{-(\frac{\mu}{\rho})\rho x}$$

If the radiographic factors are kept constant, then the mass attenuation coefficient $\mu/\rho$ is a constant and the attenuation is proportional to $\rho x$ or in the case coronary angiography, mass of contrast in the artery. As mass equals concentration times volume, the attenuation is proportional to volume for a given concentration of the contrast agent. The rate of change of signal intensity on angiographic image due to X-ray attenuation is therefore proportional to the volume of contrast flowing in the coronary artery. If the relationship of signal intensity to iodine mass and the concentration of iodine in the contrast medium are known, the rate of flow can be calculated. Using flow and pressure data, the resistance to the flow (myocardial resistance) can be calculated. Myocardial mass supplied by the individual coronary artery is not known.

To measure coronary blood flow in a method suitable for use in patients, two injections of contrast are used. First, a calibration sequence when contrast is injected into a coronary artery at a known low rate (1 ml/s). At this low rate of injection, all the contrast is assumed to flow into the coronary artery. This calibration sequence is used to calculate the relationship between signal

intensity change produced by the known flow rate of contrast. Then a measurement sequence is performed during which the aortic input of blood into the coronary artery is replaced entirely by contrast agent by injecting at a higher rate. Therefore, contrast is expected to flow into the artery at the native vessel coronary flow rate. By measuring the rate of change in signal intensity in the measurement run and knowing the relationship between signal intensity and the known contrast volume from the calibration sequence, the arterial blood flow in the coronary artery can be calculated. Myocardial resistance can be calculated from the measured flow and distal pressure measurement from the artery (or aortic pressure if there is no epicardial artery stenosis). Pressure data are obtained simultaneously and therefore the resistance to the flow can also be calculated (Resistance = Pressure/Flow).

## 3.1 Changes to X-ray imaging equipment

To perform this study, we made several changes to the way the study images were acquired. Modern catheter laboratory X-ray equipment has several in-built processes both during acquisition and post processing to optimise the output image quality and X-ray dose reduction.

a) Automatic dose control

Automatic dose control (ADC) is a proprietary system of the X-ray equipment manufacturer. It analyses the previous image acquired and changes the dose to optimise the acquired image. The system adjusts the tube voltage, tube current and pulse duration in response to changes in patient thickness to achieve a constant signal level. During research image acquisition, we set the

machine to fix the radiographic output after 5 frames. This would fix the X-ray current and voltage (mA, ms & kV) for the rest of the acquisition.

b) Automatic gain control

Automatic gain control (AGC) is a system that analyses the middle of the acquired image and provides a forward feedback to adjust the pixel intensities so that the image intensity at the centre remains constant at 960 (chosen by manufacturer, Phillips Healthcare). This was disabled for research acquisitions.

c) Filter

We introduced a 0.1mm Copper filter setting within the X-ray tube as standard to reduce X-ray dose. Any additional wedge filtering during image acquisition was avoided.

d) Post processing

The post processing algorithms were disabled, so that the raw X-ray images were exported to the data capture system. DICOM files sent to the imaging archive were stored without compression or further post processing.

e) No increase in zoom mode: No magnification was used during the research protocol.

## 3.2 Safety considerations

There were three potential sources of participants coming to harm because of the research study. These were related to

1. Risk from exposure to X-rays.
2. Risk related to iodinated contrast agent.
3. Risk from the interventional procedure.

### 3.2.1 X-ray dose control

When an X-ray beam passes through the human body, some X-ray photons will be removed from the X-ray beam through interactions with matter (e.g. Photoelectric effect and Compton scatter). This ionises the atoms in the tissue by energising electrons. Such ionisation can cause damage to the cells and DNA.

X-rays have two main detrimental effects to humans.

- Deterministic effects mainly damage the skin. The threshold for this effect to occur is 2 Gy. Severity increases with the dose of X-rays received.
- Stochastic effects usually related to fatal cancer and birth defects due to DNA damage. Although the likelihood of these effects increases with the total dose of X-rays, severity is not affected by dose and there is no threshold level.

We calculated the additional dose of X-rays received by patients during the study and concluded that the additional cancer risk was less than 1in 4800 (<0.04%).

If the patient had more than two previous imaging techniques involving ionising radiation exposure within 6 months of recruitment, or similar planned for the 6 months following participation in this study, they were excluded from the study. Total dose received is related to the patient's body habitus, with patient with larger body mass receiving higher doses. For this reason, patients weighing more than 100 kg were excluded from the study. If any patient received an X-ray dose which exceeded clinical criteria, the Leeds General Infirmary skin care protocol was followed.

### 3.2.2 Minimisation of risk from iodinated contrast

Iodinated contrast agents can cause a variety of adverse effects including allergic reactions, anaphylaxis, and contrast induced kidney injury. The iso-osmolar and non-ionic agent Iodixanol was used for the study which minimised adverse events. Any patient with previous history of contrast allergy was excluded from the study. Any patient with pre-existing renal impairment defined by serum creatinine>200 or eGFR<60ml/min/1.73 m² was excluded from the study. During the procedure intravenous fluids were administered at the operator's discretion if contrast requirements were high for clinical reasons.

### 3.2.3 Minimisation of risk from the interventional procedure

Standard guiding catheters were used for the procedure. The Certus™ pressure wire (St Jude Medical) was used for temperature and pressure measurements. This guidewire has a soft flexible tip with a hydrophilic coating to reduce friction. Standard techniques and precautions were undertaken when instrumenting the arteries.

## 3.3 Addressing breathing movements

Any patient movement, particularly movement of the chest due to inspiration and expiration, pose a significant problem to the XBF method. During inspiration and expiration, not only is there movement of heart along with the movement of the diaphragm, but there is also significant change in interposition of other tissues such as bones and lungs, which move in and out of the region of interest, thereby altering the background X-ray signal intensity.

Breathing movements render the images difficult and in most cases impossible for analysis.

During image acquisition for this study, patients were asked to hold their breath in the same respiratory phase (usually end expiration) for several seconds. Prior to acquiring the images, one or two practice breath holds were performed to make sure the patient understood what was required of them and performed the task adequately. Patients who could not hold their breath for 10-15 seconds were excluded at the time of screening. Common reasons for exclusion included severe obstructive airways disease and heart failure.

## 3.4 Identifying the phase of cardiac cycle

During our initial approach, we wanted to use images from the same phase of the cardiac cycle as the heart should be in the same position, negating the effects of cardiac movement. One way to potentially do this is to use ECG to identify the same phases of the cardiac cycle. However, this proved to be very difficult as the image files acquired did not have ECG data embedded in them. Manual superimposition of ECG proved to be challenging. Therefore, we explored alternative options.

One way to do this was to introduce a way of marking easily identifiable landmarks on the coronary artery. Landmarks used were tip of the catheter, origin of side branches, and the opaque section on the pressure wire. We then drew a line that connects these points and identified those image frames where the selected points and the line had the same relationship to the artery as in the reference image. This worked well in the absence of respiratory movements or ectopic beats.

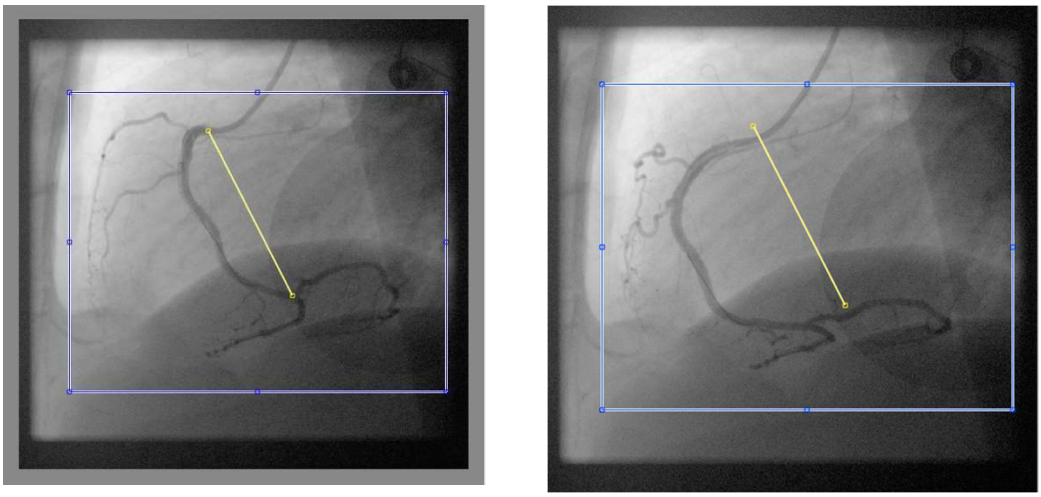

**Figure 3.1: Example of using landmarks to identify same cardiac phase.** In this case, the tip of the catheter and the origin of the postero-lateral ventricular branch were used as the two landmarks and a line was drawn to connect these points. The right panel illustrates how an image frame during a different cardiac phase appears different in relation to the landmarks and the line.

However, after testing the analysis in different phases, we decided to use all the frames for analysis, irrespective of the cardiac cycle. If all frames are used in the software, the TIC is filtered to smooth the cardiac phase related variation. A Gaussian filter (bell shaped) filter is used.

## 3.5 Region of interest

To calculate the signal intensities within the myocardium supplied by the coronary artery of interest, a region of interest (ROI) is drawn around the heart. Selection of the ROI is obviously important and especially so in the case of left coronary artery (LCA) as the separation of the left anterior descending branch (LAD) and left circumflex branch (LCx) territories was thought to be important. A variety of shapes and polygons to select the area

of the interest were attempted. The ability to modify the shape of the ROI was helpful to exclude areas that may impart error. The general rules regarding selection of ROI were:

- Select a region than corresponds to the myocardial territory supplied by the coronary artery.
- An image frame is chosen where the whole coronary artery is filled, and the myocardial blush is most intense.
- A region of interest is drawn around the area and copied to all the selected frames. This ROI can also be copied from the calibration sequence to the measurement sequences and if the gantry angle and the catheterisation laboratory table height or position has not been changed and breath is held in the same respiratory phase, the selected ROI should be similar across the sequences.
- When ROI is selected, care is taken to exclude the aortic root completely to avoid signal change due to the spill of contrast into the aortic root during systole. Similarly, in some patients the descending aorta may be in the frame, which is difficult to identify and as far as possible excluded from the ROI.

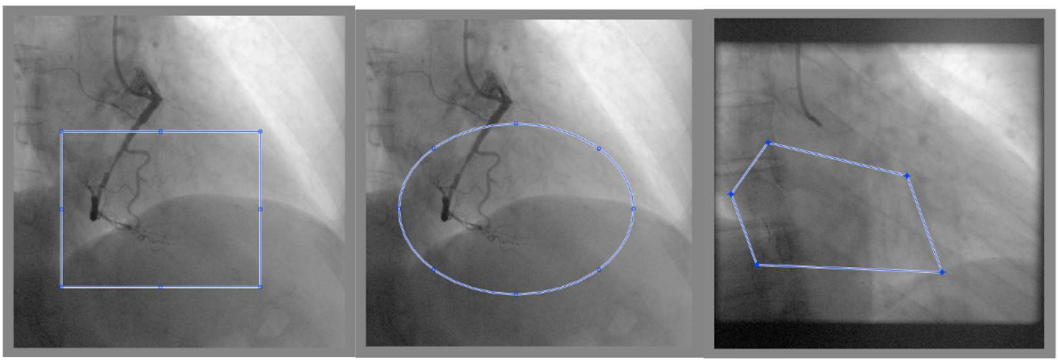

**Figure 3.2: Examples of different types of regions of interest**

## 3.6 Pressure wire and RadiAnalyser Xpress

Pressure wire™ Certus™ (St Jude Medical, Minnesota, US) was used in all studies. This wire has a micro-sensor located at 30mm from the tip, which can simultaneously measure coronary pressure as well as temperature at the location of the sensor, with an accuracy of 1mm Hg and 0.02°C, respectively. The wire has a diameter of 0.014 inch with medium weight support. The operating pressure range is -30 to +300 mmHg with a zero drift of <7mm Hg/h. The length of the wire is 175 cm with a flexible segment at the tip of 31cm. This segment incorporates the sensor element and a radio-opaque tip of 3cm length. The sensor enables simultaneous recording of pressure as well as acting as a thermistor enabling temperature measurement at the location of that sensor, with an accuracy of 0.02°C. The shaft of this wire works as an additional electric resistance and acts as a second thermistor. This provides the input signal when a fluid of different temperature reaches the proximal thermistor. The radio opaque tip is hydrophobic, but the body of the wire is coated with a hydrophilic polymer coating. The distal end of the wire attached to the proximal connector which connected to the RadiAnalyser Xpress console.

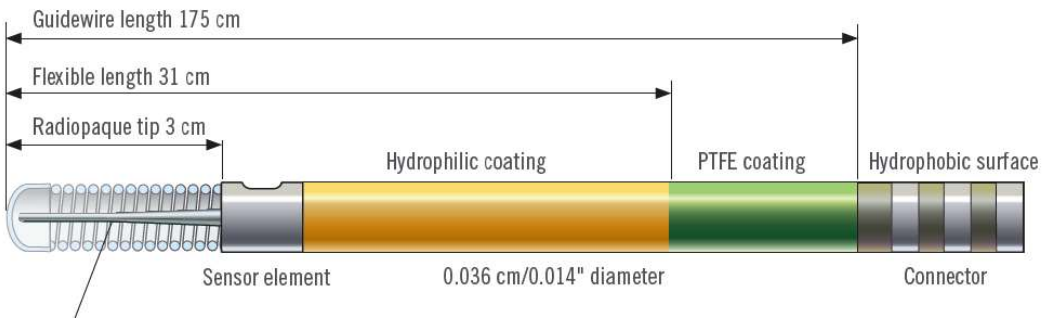


**Figure 3.3: Diagram of a Pressure wire Certus,** (courtesy of St Jude Medical, Minnesota, US)

The RadiAnalyser Xpress console is a lightweight and portable instrument that serves as the user interface for the St Jude FFR assessment system. It is capable of simultaneous assessment of FFR, IMR and CFR. The pressure accuracy quoted by the manufacturer is ±1 mmHg plus ± 1% (<50 mmHg) ± 3% (>50 mmHg) ±3 % (50 to 300 mmHg). The temperature range is 15-42 ˚C with a relative temperature accuracy 0.05 ˚C or 10% ΔT, whichever greatest.

## 3.7 Data extraction, storage, and governance

X-ray data were acquired raw without post-processing and extracted from the system on to a computer system with a dedicated hardware and software for data capture. Post-processed DICOM images transferred to clinical archive at Leeds General Infirmary were also extracted. The correct image sequences were identified and saved in preparation for the XBF software to be applied. The raw data capture did not record any patient identifiers, so additional anonymisation was not necessary. The data was copied to external hard drives and transferred to secure storage at the University of Leeds.

Pressure, temperature, and mean transit time data were extracted from the RadiAnalyser Xpress system to allow calculations.

# Chapter 4 - Validation of X-ray derived flow measurements in bench models

## 4.1 Introduction

Molloi and others proved that coronary blood flow quantification was possible in animal models (Molloi et al., 1998; Molloi et al., 2004). The XBF method developed by Dr Andrew Davies (AD) had some differences compared to that described by Molloi *et al (Molloi et al., 1998)*, the main one being the use of a separate calibration sequence rather than the use of an iodine-containing calibration phantom as explained in section 1.8.1. This chapter reports bench testing on phantoms mimicking the human coronary circulation to evaluate the accuracy of this technique prior to embarking on human studies.

Creating a phantom that simulates the complexity of coronary microcirculation is extremely difficult. This is because of the small size of the microcirculation and the time-varying resistance properties of the myocardium. We therefore decided to first test our method on a static model where the flow remains constant. We started with a simple phantom to test the basic principle and then we went through a phase of iterative development of more robust phantom with more realistic flow to determine if the XBF method can produce reproducible results in clinically relevant context. The XBF software interface and its use are described in section 1.8. Specific methods and protocols used for each of the bench experiments conducted are given below.

## 4.2 Direct injection phantom

The aim of this experiment was to prove that the basic principle of measuring flow was possible without the need for a calibration phantom. In this experiment, we assessed the correlation between contrast flow rate measured in vitro by the XBF method and true flow rate by allowing contrast to accumulate at a known rate in a glass reservoir.

### 4.2.1 Methods

*Model:* The model included a glass jar which acted as a reservoir. The jar had an inlet tubing for contrast agent which was attached to a piece of sponge to create a substrate for slow accumulation of contrast. The system was set up on a cardiac catheter laboratory table at the Leeds General Infirmary. The contrast agent was pumped in using an automated pressure injector (Angiomat Illumena, Mallinckrodt, St Louis, Missouri) through the inlet tubing. The outlet tubing collected the contrast agent for drainage. The automated pressure injector was set up to deliver Iodixanol 652mg/mL (Visipaque 320, GE Healthcare, Chalfont St. Giles, UK), which contains 320mg/ml organically bound iodine, at different flow rates.

The changes to the X-ray equipment are detailed in chapter 3, section 3.1. The collimators were brought in to frame the field of view. Large field of view was selected (25cm) and image acquisition was set at 15 frames/second. The X-ray tube was positioned so that the jar was at the isocentre of the X-ray beam. The pressure injector pump with contrast medium was connected to the inlet. A few frames were acquired before contrast was injected during every sequence to provide mask images. The X-ray acquisition was continued until

the sponge was seen to be saturated with contrast. A schematic diagram of the model is illustrated in figure 4.1. The contrast agent is denser than water, so it would sink to the bottom of the jar making it easy to flush away.

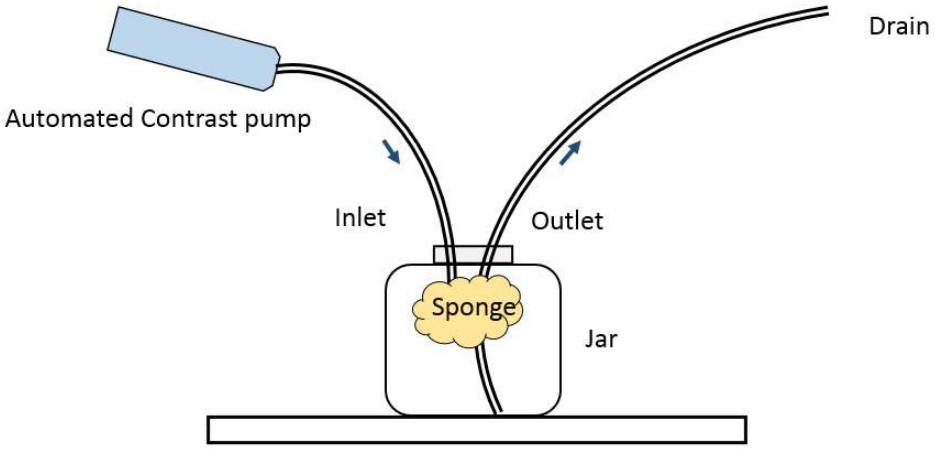


**Figure 4.1: Schematic diagram representing the model used in direct injection phantom experiment.** The model included a glass jar which acted as a reservoir. The jar had an inlet tubing for contrast agent which was attached to a piece of sponge to create a substrate for slow accumulation of contrast**.**

*Protocol:* We performed injections at different flow rates of contrast agent directly injected into the jar using the automated pressure injector. The following flow rates were used 1ml/s, 2ml/s, 3ml/s, 4ml/s, and 5ml/s. Injections were repeated three times for each flow rate. Between each injection the phantom was injected with warm water to wash away the contrast agent.

*XBF analysis:* The raw images were extracted and analysed using XBF method for signal intensity change with time. The ROI was drawn around the glass jar. The first few frames when X-ray parameters were stabilising were excluded and subsequent frames when there was no contrast flow was used as the mask. As the contrast flowed into the jar, the sponge slowly became

saturated with contrast producing a reduction in X-ray signal intensity in the ROI. These imaging frames were then subtracted from the mask image and signal intensity change with each frame was plotted.

The XBF software interface during the image analysis is shown in figure 4.2.

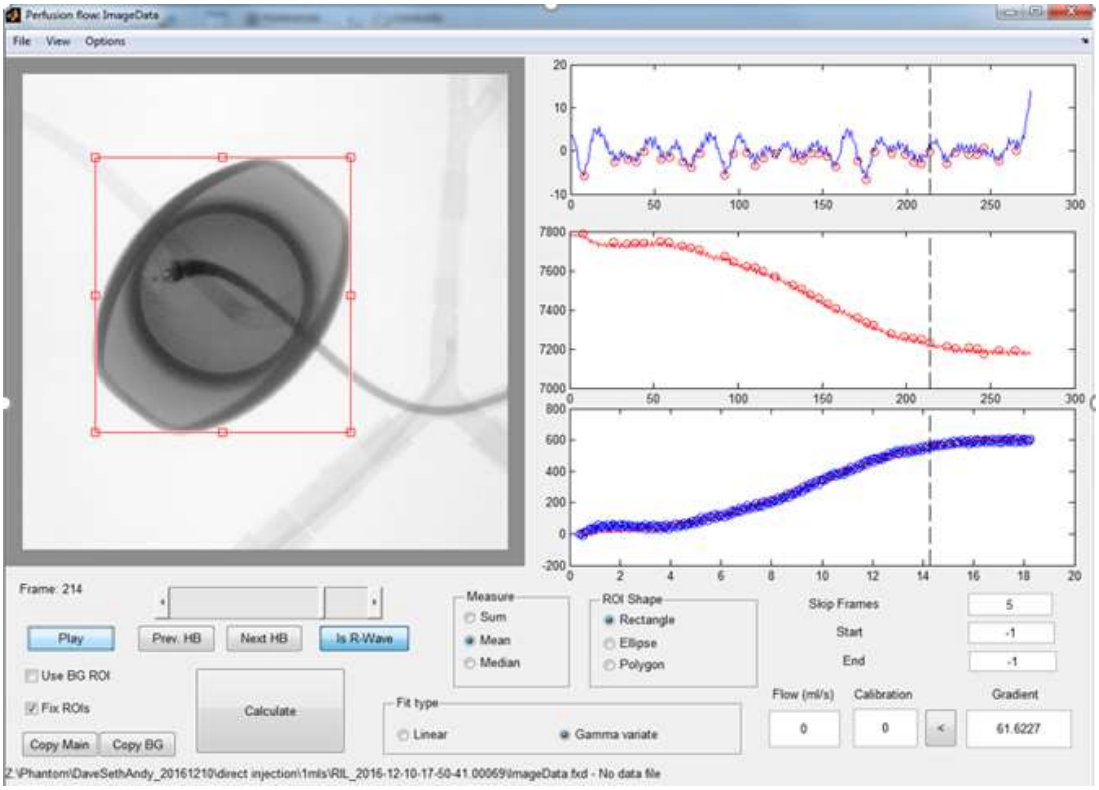


**Figure 4.2: Example of the image acquired during direct injection phantom experiment demonstrating the ROI around the jar with contrast accumulating.** In this frame the contrast injection is just starting to opacify the sponge that simulates the microvasculature. On the right-hand side, the time intensity curve is plotted (red and blue curves)

Contrast flow rates were calculated at each experimental injection rate using the arithmetic sum of signal intensities in each frame, and time intensity curve gradients within the region of interest. The mean of the gradients at 1ml/s contrast injection were used for calibration. Experiments were performed in triplicate.

### 4.2.2 Results

Sum of signal intensities in the XBF values at different flow rates and the time intensity curve (TIC) gradients from which these were derived are shown in table 4.1. Mean data from the three experimental repeats are plotted in figure 4.3, demonstrating an excellent correlation (R=0.99) between actual contrast flow rate and the XBF derived measures.

**Table 4.1: Calculated contrast flow rates using XBF method based in direct injection phantom experiment.**

| **Contrast injection rate ml/s** | **TIC gradient-based signal intensities in ROI** | | | **Calibration = mean of 1ml/s TIC gradients** | **Calculated flow rates using XBF method. ml/s (% error)** | | |
|---|---|---|---|---|---|---|---|
| | **Run 1** | **Run 2** | **Run 3** | | **Run 1** | **Run 2** | **Run 3** |
| **1** | 46.32 | 49.87 | 55.44 | 50.55 | 0.92 (8) | 0.99 (1) | 1.10 (10) |
| **2** | 95.57 | 112.30 | 103.91 | | 1.89 (5.5) | 2.22 (11) | 2.06 (3) |
| **3** | 139.65 | 132.10 | 144.62 | | 2.76 (8) | 2.61 (13) | 2.86 (4.7) |
| **4** | 228.74 | 190.89 | 212.46 | | 4.52 (13) | 3.78 (5.5) | 4.20 (5) |
| **5** | 304.76 | 261.97 | 295.15 | | 6.03 (20.6) | 5.18 (3.6) | 5.84 (16.8) |

TIC- time intensity curve, XBF- X-ray blood flow, ROI- region of interest.

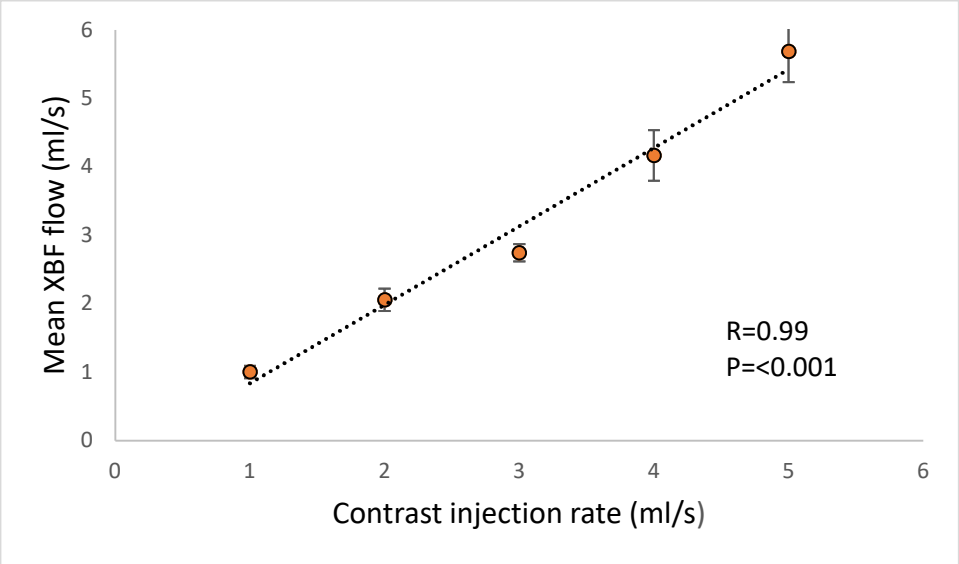


**Figure 4.3: Correlation between the mean of calculated flow rates from XBF methods to the actual rate of contrast injection.** Error bars showing standard deviations.

### 4.2.3 Discussion

This experiment was a simple study where contrast agent was injected directly into a glass reservoir at different rates, firstly a low flow rate which was also used as the calibration sequence and then higher flow rates which were the measurement sequences. In the simple direct injection model, X-ray signal intensity analysis of injected contrast agent using the XBF method was able to calculate the flow rates which correlated very well to the actual injection rates. This experiment proved that if a known small mass of contrast agent can be introduced, then that can be used for calibration. This is a key difference between XBF method and the method described by Molloi *et al* (Molloi et al., 1998). The direct injection phantom experiment proved that the XBF method

using a custom computer software to analyse signal intensity change during injection of contrast was able to accurately measure the injection rate.

This phantom has obvious limitation that the flow is direct from pump and flow being affected by the injection, whereas in reality, coronary flow is derived off the aortic flow.

## 4.3 Coronary circulation phantom

The aim of this experiment was to test the concept of measuring flow using X-ray signal intensity analysis using a robust model of coronary circulation by comparing the actual flow rate to that measured by XBF and thermodilution techniques.

The phantom used in this experiment was developed through iterative process. We conducted experiments during this process of development which are detailed in Appendix 1. During this process, we found issues mainly with the pump and issues due to the difference in viscosities between contrast and the circulating fluid which was causing variation in flow when contrast was introduced. To negate the effects of the viscosity difference between the contrast and the ‘blood’ in the model, we made some refinements. We used a blood mimicking fluid (BMF) instead of warmed tap water which was used in earlier attempts. A solution of 40% Glycerol and 60% water was made and warmed to 37$^{o}$C in a water bath. In order to ensure that glycerol and water remained mixed at constant temperature, the water bath was regularly stirred. We also changed the contrast agent used from Iodixanol 652mg/ml (Visipaque 320, GE Healthcare, Chalfont St. Giles, UK) to Iohexol 302mg/ml (Omnipaque

140, GE Healthcare, Chalfont St. Giles, UK) which had comparable viscosity to the BMF. Iohexol 302mg/ml has 140 mg of organically bound iodine per ml. A comparison of the viscosities of various iodinated contrast agents are given in table 4.2 (Stacul, 2001).

**Table 4.2: Viscosity of current iodinated contrast media.** The contrast agents used in this research are highlighted in bold.

| **Contrast agent** | **Iodine concentration mg/ml** | **Viscosity at 37 °C centipoise(cP)** |
|---|---|---|
| Diatrizoate | 370 | 8.4 |
| Iothalamate | 400 | 9 |
| Ioxithalamate | 380 | 8.5 |
| Metrizoate | 350 | 3.4 |
| Ioxaglate | 320 | 9.5 |
| Iobitridol | 350 | 10 |
| Iohexol | 350 | 11.2 |
| **Iohexol** | **140** | **1.5** |
| Iomeprol | 350 | 8.1 |
| Iopamidol | 370 | 9.8 |
| Iopentol | 350 | 12 |
| Iopromide | 350 | 9.5 |
| Ioversol | 350 | 8.5 |
| Ioxilan | 350 | 7.8 |
| **Iodixanol** | **320** | **11.1** |
| Iotrolan | 320 | 9 |

A more reliable and robust pump (Grant GD120, Grant Instruments Ltd, Shepreth, UK) and water-bath system with connected tubing was created to simulate the human physiologic circulation as closely as possible. The

integrated pump in this machine had a maximum pressure output of 310mbar and maximum flow rate of 17 l/min. This model was created in collaboration with Professor Hadj Benkreira and Matthew Palmer of University of Bradford. The changes made to the phantom are summarised below.

1. The submersible pump was changed to a more powerful Grant GD120 pump and heated water bath.
2. The circulating fluid was changed from tap water to a blood mimicking fluid (BMF), 40% Glycerol with higher viscosity.
3. The BMF was kept warmed at a constant temperature of 37 degrees and stirred to ensure adequate mixing of glycerol with water.
4. The use of Iohexol 302 mg/ml, which has comparable viscosity to BMF.
5. The tubing was connected without any possibility of leak.
6. The reservoir for the coronary microcirculation was changed to a jar filled with beads.
7. A flow meter to monitor any drop in flow real time.
8. Thermodilution protocol was performed using a dedicated infusion microcatheter called Rayflow (Hexacath, Rueil-Malmaison, France).

### 4.3.1 Methods

*Model:* As already explained, the Grant GD120 pump and water bath system proved a much more robust set up, and the flow rate was unaffected when contrast was introduced into the system. Figure 4.4 shows a schematic diagram of the model.

The model was set up on the cardiac catheterisation laboratory table at LGI. There was a large water bath which was filled with BMF (40% Glycerol) and kept warm at 37$^{o}$ C. The pump would take in the BMF and circulate it through

a large bore silicone tube analogous to the aorta. The tube had a resistance screw to increase the pressure in the system and affect the flow rate. This tube could be accessed through a branch tubing connected to a one-way valve. The tube gave off a smaller tube analogous to the coronary artery which had a resistance screw (R1) which could introduce resistance akin to a coronary artery stenosis. The coronary artery tubing was connected to a reservoir to simulate the microcirculation. For this model, we used a glass jar filled with beads as the reservoir to simulate the microvasculature, which worked well. The jar was a closed system free of leaks and the outlet tubing had another resistance screw (R2) to introduce microvascular resistance. There was also a flow meter attached to the outlet tubing to measure the flow through the reservoir system. The BMF when circulating with no contrast agent would return to the water bath. Once contrast agent is in the system, the circulating fluid could drain off with the aid of 3 way tap systems in order not to allow mixing of contrast to BMF in the water bath reservoir.

A 7 Fr coronary guiding catheter was introduced via the branch tubing valve with the tip of the catheter engaging the branch tubing analogous to the coronary artery. A Tuohy Borst valve was attached to the proximal end of the guiding catheter. The side port of the valve Y connector was connected to a pressure transducer and automated contrast injector for introduction of contrast agent. A pressure and temperature sensitive guide wire (Pressure wire Certus, St Jude Medical, Minnesota, US) was introduced via the Tuohy Borst valve with the tip of the guide wire positioned in the coronary artery tubing so that the pressure transducer and thermistor is beyond the resistance

screw R1. The pressure wire was attached to RadiAnalyser Xpress console (St Jude Medical, Minnesota, US).

*Protocol:* The model allowed simultaneous measurement of actual flow while performing the X-ray protocol. Thermodilution protocol could have been run soon after, however we ran into some problems with RadiAnalyser Xpress malfunction. Further performing thermodilution alongside was logistically more difficult. So thermodilution experiments were performed separately. Several flow settings were used by altering the resistances.

**Figure 4.4: Schematic diagram of phantom used in coronary circulation phantom.** Resistance R1 introduces lesion resistance while R2 introduces microvascular resistance. Resistance R3 can increase or decrease the pressure and flow within the tubing analogous to coronary artery.

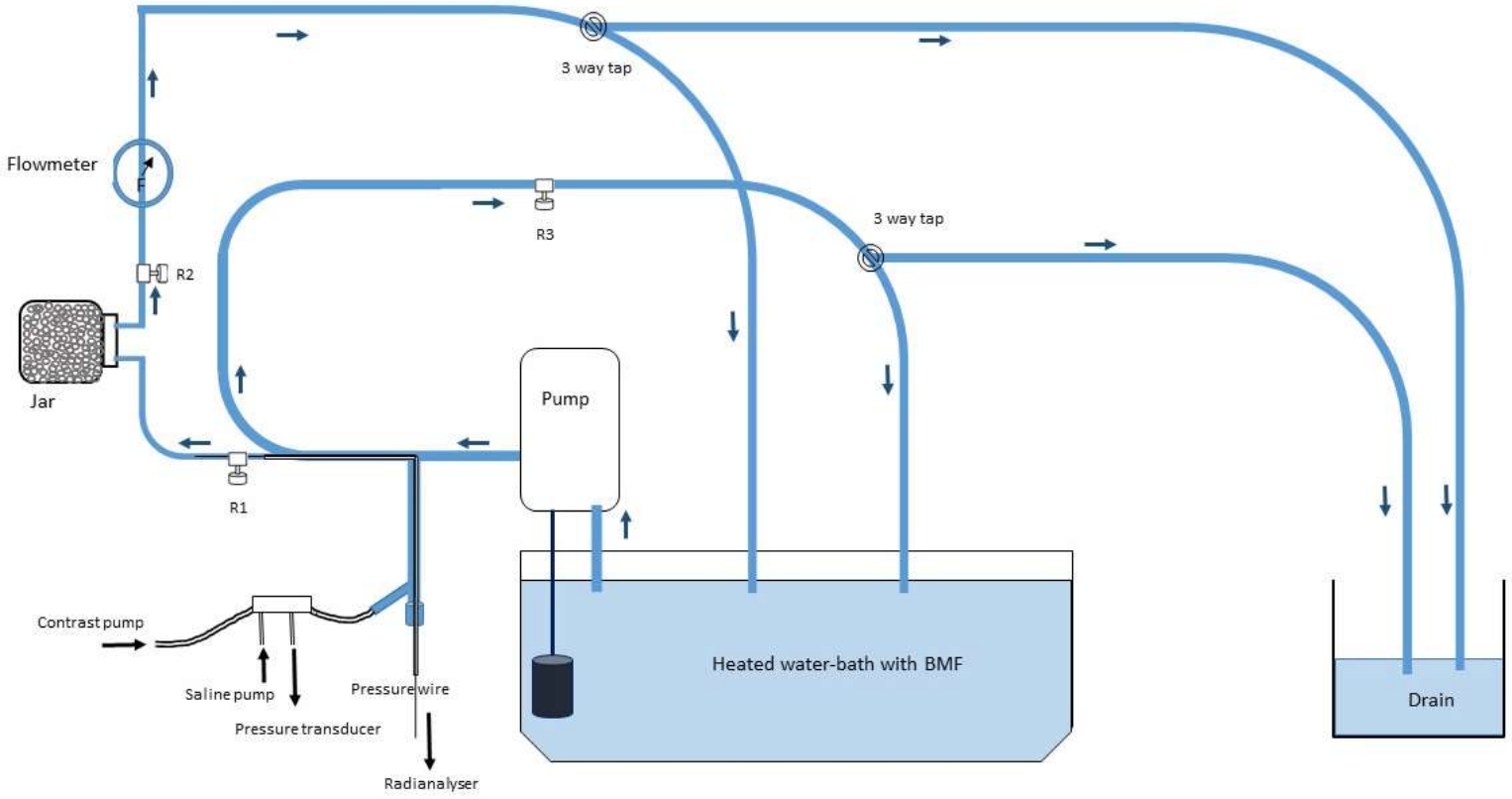

#### 4.3.1.1 X-ray protocol

The changes made to the X-ray equipment are the same as explained in chapter 3, section 3.1. Modern X-ray systems use sophisticated non-linear image enhancement algorithms, and these make the relationship between signal intensity and iodine mass vary within a sequence. The XBF method requires changes to the X-ray system to be implemented, ensuring that the same radiographic factors are used in the calibration and measurement sequences, and that they remain the same during each sequence.

We used both Iohexol 302mg/ml (Omnipaque 140, GE Healthcare, Chalfont St. Giles, UK) contrast agent which had a comparable viscosity to plasma and BMF and Iodixanol 652mg/mL (Visipaque 320, GE Healthcare, Chalfont St. Giles, UK) which was used in previous experiment and human studies. This was done to study the impact of the higher viscosity contrast agent in the phantom. Resistance was introduced to the system primarily by altering the lesion resistance and pump settings and flow rates were varied. The contrast injection rates of 0.5, 1, 2, 3 and 4 ml/s were used in the experiment and each run was performed two or three times. The actual flow was measured by measuring the output in unit time and correlated with the flow meter.

The collimators were brought in to frame the field of view. Large field of view was selected (25cm) and image acquisition was set at 15 frames/second. The X-ray tube was positioned so that the jar was at the isocentre of the X-ray beam. The pressure injector pump with contrast medium was connected to the guiding catheter side port. A few frames were acquired before the start of contrast injection to provide mask images. The X-ray acquisition was started

prior to any contrast injection and continued until the contrast agent was seen to filter through the beads. The first injection of 1ml/s injection was used as calibration sequence.

*XBF analysis:* The raw images were extracted and analysed using XBF method for signal intensity change with time. The region of interest (ROI) was set to include the jar and analysis performed to calculate signal intensities in each frame. The first few frames when X-ray parameters were stabilising were excluded automatically and subsequent frames (starting from 1second into the sequence) when there was no contrast flow was used as the mask. As the contrast flowed into the jar, a reduction in X-ray signal intensity was observed in the ROI. These imaging frames were then subtracted from the mask image and signal intensity change with each frame was plotted. This is proportional to the rate of flow within the tubing. The analysis was performed for the calibration sequence and the measurement sequence.

#### 4.3.1.2 Thermodilution protocol

The actual flow rates were measured using the time to drain 30ml of BMF rather than the flow meter readings. We did not compare the XBF flow and thermodilution directly but compared each of them independently with actual flow. Thermodilution experiments were carried out using a microcatheter called Rayflow™ (Hexacath, Rueil-Malmaison, France)

Rayflow is a dual lumen monorail infusion catheter with 4 side holes a short distance from the distal end. Saline infusion is delivered through the outside lumen and exits the catheter via the side holes. There are also holes connecting both lumens that ensures that the thermistor on the pressure wire

can measure the temperature of saline infusate. It is described in more detail in chapter 5, section 5.2.4.2.

Three settings were used with different flow meter readings (table 4.3), but actual flow was measured in each of the experiments.

**Table 4.3: Different flow settings for thermodilution study in coronary circulation phantom.**

| Setting | Flow meter reading | ml/s |
|---|---|---|
| A | 240cml/min | 4 ml/s |
| B | 200ml/min | 3.33 ml/s |
| C | 155ml/min | 2.58 ml/s |

For each setting we performed three measurements. The saline injection was performed at 0.3ml/s through the Rayflow microcatheter (Qi). The temperature of the BMF when mixed with saline at room temperature (T) was measured. The pressure wire was then pulled back into the microcatheter to measure the temperature of the infusate (Ti). The flow rate of BMF was calculated using the equation.

$$Q_b = Q_i(T_i/T)$$

## 4.3.2 Results

### 4.3.2.1 Flow meter calibration

There was a flow meter attached to the outlet of the reservoir. This was designed and calibrated to measure the flow of water. The flow rate was lower when BMF was used. We calibrated the flow meter for BMF by tabulating the flow meter readings at the different absolute flow rates of BMF which is shown in table 4.4 and in figure 4.5. Although the readings were different when BMF

was used instead of water, the change in flow rate and the readings correlated well.

Although during the experiment we did not use the flow meter to measure the flow, it served as a useful tool to monitor for any significant variation in flow rate during the experiments.

In addition, we also compared the flow with altered lesion resistance to see if the relationship between the flow and the pressure is maintained in the phantom. This is presented in table 4.5 and figure 4.6.

**Table 4.4: Measured flow rates of Blood mimicking fluid (BMF) and Flow meter readings in coronary circulation phantom**

| Flow meter reading (cc/min) | Measured flow (ml/min) |
|---|---|
| 300 | 187.5 |
| 280 | 181.8 |
| 260 | 166.2 |
| 240 | 149.2 |
| 220 | 133.0 |
| 200 | 104.4 |
| 200 | 104.4 |
| 240 | 139.2 |
| 250 | 150.8 |
| 225 | 136.0 |
| 215 | 123.0 |
| 195 | 110.0 |
| 165 | 95.1 |
| 155 | 76.2 |
| 145 | 58.0 |
| 100 | 36.6 |

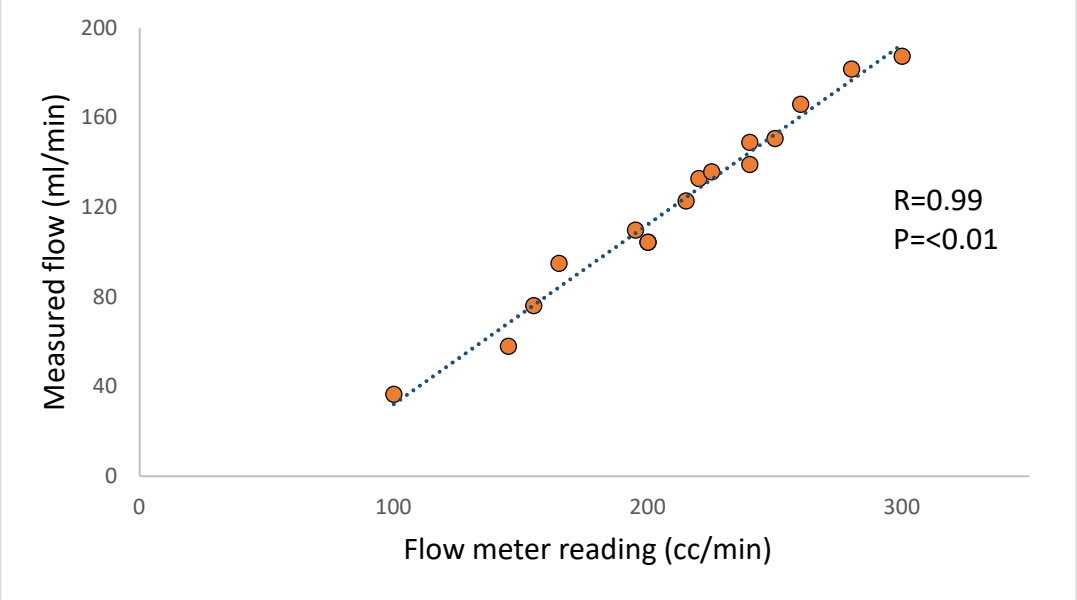


**Figure 4.5: Calibration of flow meter by correlating the flow meter readings and the measured actual flow rate in the coronary circulation phantom.**

**Table 4.5: Pressure readings for various flow rates in coronary circulation phantom.**

| Flow meter Cc/min | Actual flow ml/min | Pa mmHg | Pd mmHg | Pd/Pa |
|---|---|---|---|---|
| 250 | 150.8 | 100 | 100 | 1.00 |
| 225 | 136.0 | 104 | 91 | 0.88 |
| 215 | 123.0 | 105 | 85 | 0.81 |
| 195 | 110.0 | 105 | 75 | 0.71 |
| 165 | 95.1 | 105 | 68 | 0.65 |
| 155 | 76.2 | 106 | 58 | 0.55 |
| 145 | 58.0 | 109 | 51 | 0.47 |
| 100 | 36.6 | 108 | 41 | 0.38 |

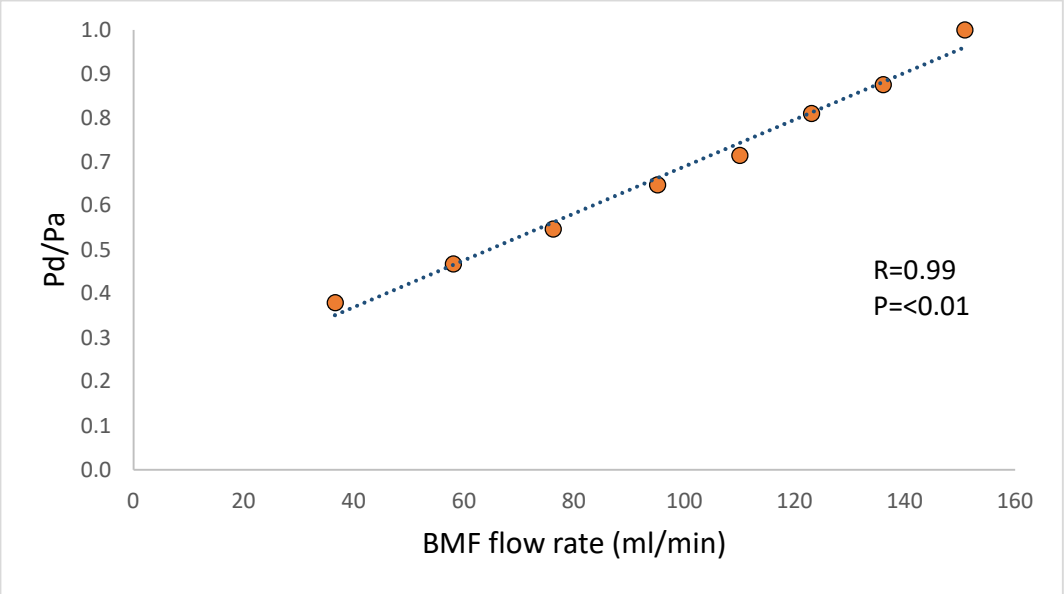


**Figure 4.6: Calibration of flow meter. Scatter plot showing the relationship of different flow rates with corresponding Pd/Pa in the coronary circulation phantom showing that the relationship between flow and pressure is maintained at various flow rates.** Pd/Pa is the ratio of the pressure distal to the lesion resistance to the pressure in the proximal tubing.

The calibration study showed that there was excellent correlation of flow meter readings to the actual flow rates of BMF. It also maintained the linear pressure-flow relationship that is expected in hyperaemic coronary circulation.

#### 4.3.2.2 XBF flow measurement results

The first XBF measurement of the gradient of the time intensity curve (TIC) of actual flow rate of 1ml/s was used as the calibration value. The results have been presented in table 4.6. The relationship between XBF measured flow and actual flow in Iohexol 302mg/ml studies are shown in figure 4.7. There is excellent correlation and agreement between XBF measured flow in the coronary circulation phantom experiment using Iohexol 302mg/ml and the actual flow. The results of correlation between XBF measured flow and actual flow in Iodixanol 652mg/ml studies are shown in figure 4.8. There is excellent correlation and agreement between XBF measured flow and actual flow using Iodixanol 652mg/ml. There was excellent reproducibility of X-ray measurements, when the measurement sequences were repeated, which is evident from the coefficients of variation in table 4.6.

**Table 4.6: Comparison of actual flow rates and XBF measured flow rates in coronary circulation phantom.**

| Contrast agent | Setting | Contrast injection rate ml/s | Run No | Calibration-TIC gradient of first 1ml/s run | TIC gradients of measurement run | XBF Flow ml/s | Coefficients of variation (%) |
|---|---|---|---|---|---|---|---|
| Iohexol 302mg/ml (Omnipaque 140) | 1 | **1** | 1 | 50.91 | calibration | NA | NA |
| | | | 2 | 50.91 | 53.71 | **1.06** | **1.64** |
| | | | 3 | | 54.97 | **1.08** | |
| | 2 | **0.5** | 1 | | 19.10 | **0.38** | **12.75** |
| | | | 2 | | 24.39 | **0.48** | |
| | | | 3 | | 23.58 | **0.46** | |
| | 3 | **2** | 1 | | 103.93 | **2.04** | **1.61** |
| | | | 2 | | 104.28 | **2.05** | |
| | | | 3 | | 101.81 | **2.00** | |
| | | | 4 | | 105.88 | **2.08** | |
| | 4 | **3** | 1 | | 142.80 | **2.80** | **1.73** |
| | | | 2 | | 146.44 | **2.88** | |
| | | | 3 | | 142.84 | **2.81** | |
| | | | 4 | | 147.71 | **2.90** | |
| | 5 | **4** | 1 | | 171.12 | **3.36** | **1.81** |
| | | | 2 | | 174.71 | **3.43** | |
| | | | 3 | | 177.41 | **3.48** | |
| Iodixanol 652mg/mL (Visipaque 320) | 6 | **1** | 1 | 102.86 | calibration | NA | NA |
| | | | 2 | 102.86 | 97.56 | **0.95** | **2.62** |
| | | | 3 | | 101.25 | **0.98** | |

| | | | | | | | |
|---|---|---|---|---|---|---|---|
| | 7 | **0.5** | 1 | | 46.65 | **0.45** | **2.39** |
| | | | 2 | | 48.19 | **0.47** | |
| | | | 3 | | 48.89 | **0.48** | |
| | 8 | **2** | 1 | | 182.22 | **1.77** | **1.41** |
| | | | 2 | | 185.46 | **1.80** | |
| | | | 3 | | 187.37 | **1.82** | |
| | 9 | **3** | 1 | | 256.34 | **2.49** | **0.28** |
| | | | 2 | | 257.34 | **2.50** | |
| | 10 | **4** | 1 | | 280.08 | **2.72** | **3.01** |
| | | | 2 | | 266.49 | **2.59** | |
| | | | 3 | | 265.40 | **2.58** | |
| | | | 4 | | 261.60 | **2.54** | |

Two different contrast agents Iohexol 302mg/ml and Iodixanol 652mg/ml were studied at incremental flow rates from 0.5-4ml/s. The first XBF measurement the TIC gradient of actual flow rate of 1ml/s was used as calibration. TIC- time intensity curve, XBF- X-ray blood flow, NA- not applicable.

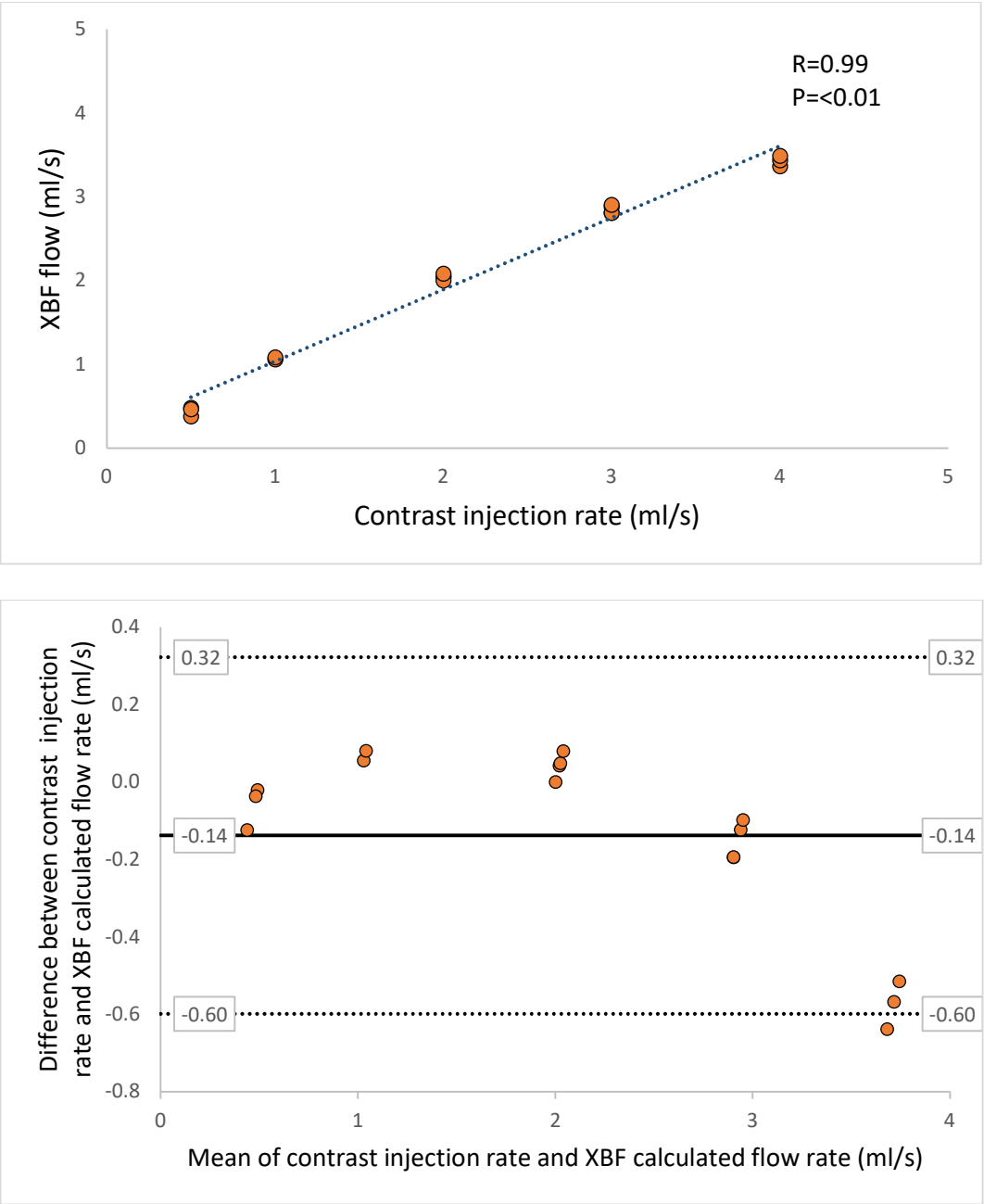


**Figure 4.7: Relationship between actual flow (ml/s) to the XBF flow (ml/s) in coronary circulation phantom using Iohexol 302mg/ml (Omnipaque 140). Upper panel showing scatter plot and lower panel showing Bland-Altman plot.** In the Bland-Altman plot, the solid line represents the mean of the differences between measurements and the dotted lines represent the 95% confidence intervals for the mean of the differences between measures.

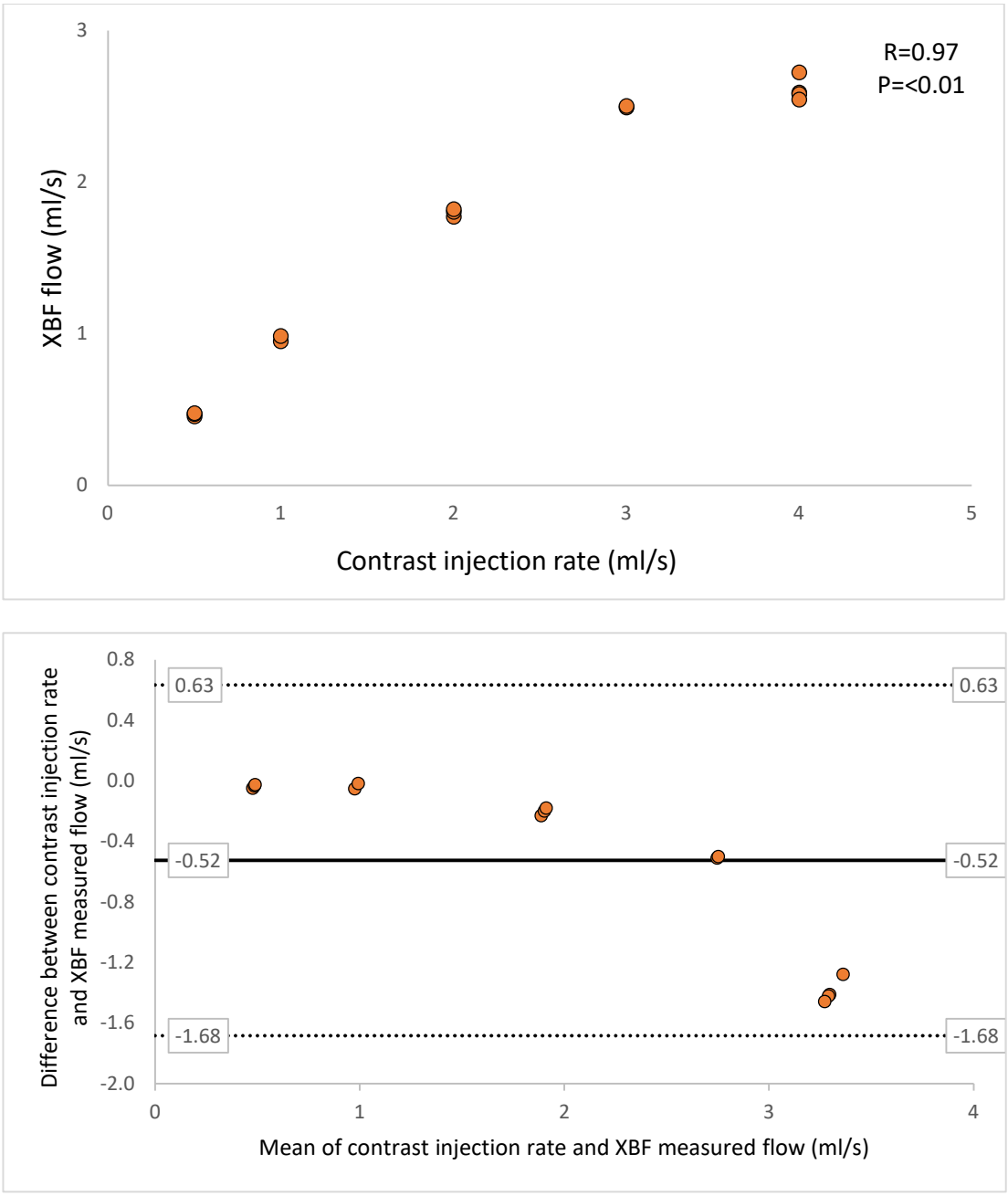


**Figure 4.8: Relationship between actual flow (ml/s) to the XBF flow (ml/s) in coronary circulation phantom using Iodixanol 652mg/ml (Visipaque 320). Upper panel showing scatter plot and lower panel showing Bland-Altman plot.** In the Bland-Altman plot, the solid line represents the mean of the differences between measurements and the dotted lines represent the 95% confidence intervals for the mean of the differences between measures.

#### 4.3.2.3 Thermodilution

The continuous thermodilution method of flow quantification was performed using the coronary circulation phantom. A pressure and temperature sensitive pressure wire (Pressure wire Certus, St Jude Medical, Minnesota, US) was placed in the coronary artery tubing. An infusion microcatheter, Rayflow (Hexacath, Rueil-Malmaison, France) was used to infuse saline at room temperature at a rate of 0.3ml/s. The actual flow was correlated with the thermodilution measured flow and is shown in table 4.7 and in figure 4.9. The thermodilution protocol was repeated for each flow meter setting three times. There is excellent correlation between the actual flow and thermodilution measured flow with a Pearson's coefficient (R) of 0.93. The agreement between the two measurements is also good as illustrated in the corresponding Bland-Altman plot.

**Table 4.7: Comparison of actual flow rates to the flow rates measured by continuous thermodilution method using Rayflow catheter in coronary circulation phantom.**

| Flow meter Setting | Run No | 30 ml time (s) | Actual flow ml/s | Qi ml/s | T °C | Ti °C | Q Thermo-dilution flow ml/s | Coefficient of variation (%) |
|---|---|---|---|---|---|---|---|---|
| A 4 ml/s | 1 | 12.3 | 2.44 | 0.30 | 1.00 | 7.70 | 2.31 | 6.74 |
| | 2 | 12.6 | 2.38 | 0.30 | 0.99 | 8.34 | 2.53 | |
| | 3 | 11.8 | 2.54 | 0.30 | 0.89 | 7.84 | 2.64 | |
| B 3.33 ml/s | 1 | 15.2 | 1.97 | 0.30 | 1.32 | 7.55 | 1.72 | 15.76 |
| | 2 | 15.4 | 1.95 | 0.30 | 1.38 | 9.44 | 2.05 | |
| | 3 | 15.3 | 1.96 | 0.30 | 1.15 | 5.74 | 1.50 | |
| C 2.58 ml/s | 1 | 23.7 | 1.27 | 0.30 | 1.73 | 7.78 | 1.35 | 3.86 |
| | 2 | 24.4 | 1.23 | 0.30 | 1.83 | 7.60 | 1.25 | |
| | 3 | 24.7 | 1.21 | 0.30 | 1.64 | 7.17 | 1.31 | |

Qi=infusion rate of saline (0.3ml/s), T= temperature of BMF mixed with saline, Ti=temperature of infusate (saline), Q= BMF flow from thermodilution method

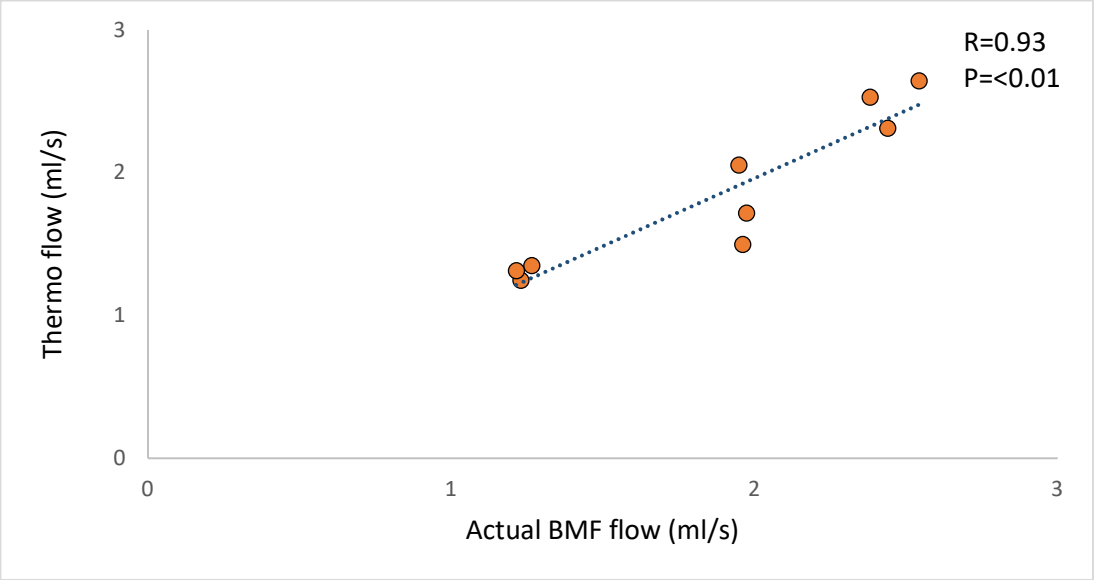


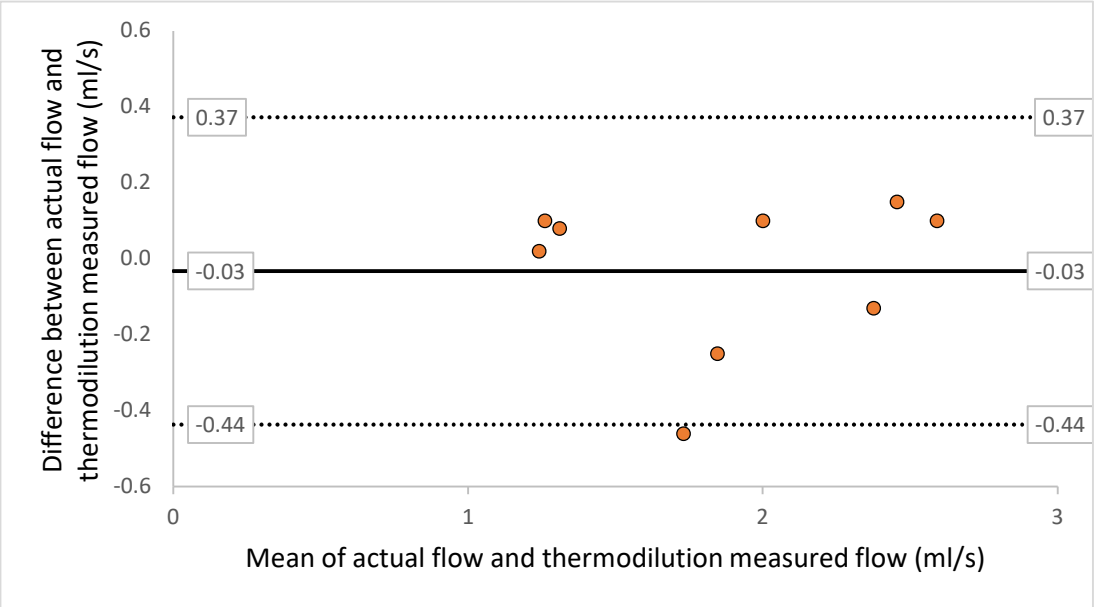


**Figure 4.9: Relationship between actual flow rate of BMF and continuous thermodilution measured flow in coronary circulation phantom. Upper panel shows scatter plot and lower panel shows Bland-Altman plot.** In the Bland-Altman plot, the solid line represents the mean of the differences between measurements and the dotted lines represent the 95% confidence intervals for the mean of the differences between measures.

### 4.3.3 Discussion

In this chapter, we set out to determine whether assessment of flow of contrast using assessment of X-ray signal intensity was feasible, accurate and reproducible. Our objective was to validate the technique of quantifying coronary blood flow from X-ray signal intensity assessment in a bench model allowing experimental modulation of epicardial and microvascular coronary resistance.

The coronary circulation phantom had a well-designed model that performed well with reliable flow at varying rates with maintained linear pressure and flow relationship. The pump needed to maintain a constant flow regardless of the load imposed so that the output of the pump remains the same independent of the viscosity of the perfusate or the resistance of the load applied. Grant GD120 machine with integral pump as explained in section 4.3 performed better than the submersible pump used in previous experiments (Appendix 1). There was excellent correlation and agreement with little systematic error (bias) between the XBF measured flow and the actual flow. Although there was excellent correlation and agreement between XBF flow and actual flow with both Iohexol 302mg/ml (Omnipaque 140) and Iodixanol 652mg/ml (Visipaque 320), at low injection rates, it is obvious that at higher injection rates (especially with the more viscous Iodixanol 625mg/ml) the maximum flow measured by the XBF method plateaued. On reviewing why this was the case, we discovered that as the flow rate increases there was contrast flowing back into the tubing causing this effect. This is demonstrated in figure 4.10. Where

the X-ray images of the junction of the origin of the coronary artery tubing where the guiding catheter tip sits and delivers the contrast agent.

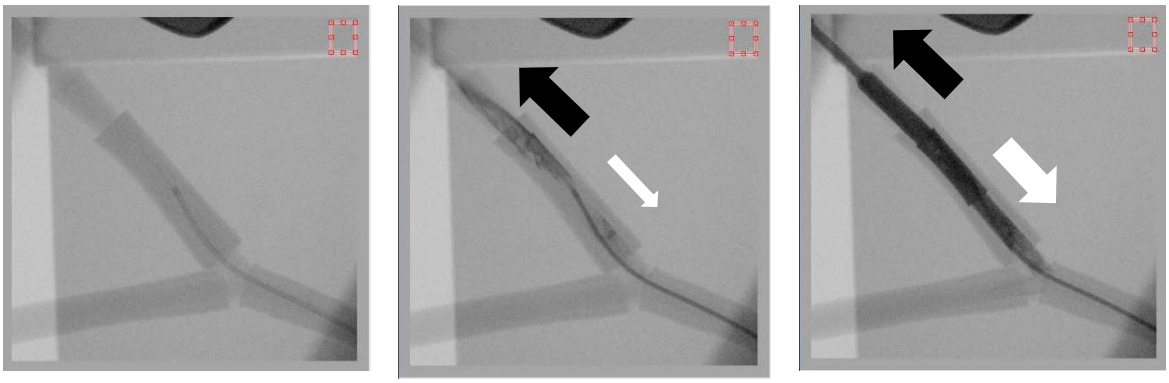

Before contrast injection

At low flow rate, most of the contrast flowing forwards(black arrow) with some contrast flowing backwards (white arrow)

At higher flow rate the backflow is much more (indicated by thicker white arrow)

**Figure 4.10: X-ray images of the junction of the 'coronary artery' in the model demonstrating the higher back flow of contrast at higher flow rates.** At low flow rate, most of the contrast flowing forwards (black arrow) with some contrast flowing backwards (white arrow). At higher flow rate the backflow is much more (indicated by thicker white arrow)

This is consistent with our expectation that the measured flow initially would be linear (and equal to) the low injection rates as was the case in the direct injection phantom experiment. But as the maximum flow rate through the ‘coronary artery’ tubing was reached with higher rates of contrast injection, there was much more spillage back to the ‘aorta’. This means further increasing the injection rates would have no impact on the forward flow. Therefore, in the experiment using Iodixanol 652mg/ml (figure 4.8), the higher flow rate values obtained during 4ml/s injection is close to the maximum flow rate.

We also tested the thermodilution method of blood flow estimation and found that the thermodilution measured flow also correlated with the actual flow.

Although there was good correlation between the thermodilution measured flow and actual flow, Pearson's coefficient of correlation was 0.99 for XBF method with Iohexol 302mg/ml (Omnipaque 140) and 0.93 with the thermodilution method. This suggests that in this experiment XBF method was more accurate than the thermodilution method.

Although the model used in the coronary circulation phantom produced reliable flow rates, this model cannot simulate the complex dynamic forces influencing the coronary blood flow in humans which is an obvious limitation.

## 4.4 Conclusion

This chapter demonstrates that it is possible to measure flow accurately and reproducibly using the XBF method of X-ray signal intensity analysis in a cardiac phantom. Injection of contrast did not alter the native flow rate and therefore we can infer that using a lower flow rate contrast injection provides a convenient and reliable way of calibration for the XBF method.

# Chapter 5 -Validation of X-ray derived calculation of coronary blood flow in human subjects

## 5.1 Introduction

The bench work reported in Chapter 4 established that calculation of flow using X-ray signal intensity analysis was feasible. The next step was to translate this to humans to see if this was feasible in the clinical setting in patients undergoing coronary angiography. Here a study was conducted in human subjects recruited from patients attending the cardiac catheterisation laboratory at the Leeds General Infirmary. The plan was to compare coronary blood flow calculated from the XBF method to flow measured using a continuous thermodilution method.

## 5.2 Methods

### 5.2.1 Cardiac catheterisation laboratory equipment

Cardiac catheter laboratory number 6 at the Leeds General Infirmary was initially equipped for the conduct of this project. This catheterisation laboratory was equipped with a Phillips Allura Xper FD10 cardiovascular X-ray system (Philips Healthcare, Best, the Netherlands). Software changes were made to the catheter laboratory to enable the radiographer to choose the required X-ray settings for the study.

Later in the project, Cardiac catheter laboratory number 2 was also equipped with the necessary changes. This laboratory was equipped with a Phillips

Allura Clarity (Philips Healthcare, Best, the Netherlands) cardiovascular X-ray system.

An automated pressure injector (Angiomat Illumena, Mallinckrodt, St Louis, Missouri) was filled with the contrast agent ready for injection.

Images were acquired at 15 frames per second with a 25cm field of view. Appropriate collimation was employed to centre the image on the heart.

### 5.2.2 Data capture

The catheterisation laboratories were equipped with a dedicated computer system, with the software for capture of X-ray data before the application of the manufacturer's post-processing software. The captured images were stored initially on the computer's hard disc drive and then copied to the University of Leeds system for analysis.

### 5.2.3 Thermodilution

A pressure wire was connected to a dedicated console (RadiAnalyzer™ Xpress, St Jude Medical, Minnesota, US), which processed the pressure and temperature information and displayed the information on its interface screen. RadiAnalyser Xpress displays the FFR and the mean transit time for thermodilution measurements. A second automated pressure injector (Angiomat Illumena, Mallinckrodt, St Louis, Missouri) was filled with sterile 0.9% NaCl infusion solution at room temperature.

Both pumps could be connected to the injection manifold with connector tubing. Care was taken not to introduce air into the system at the time of connecting the tubing.

### 5.2.4 Mixing of saline and blood

In studies performed in early phase of recruitment, saline was injected directly through the guiding catheter. In later studies a specially designed infusion catheter, Amicath (IHT Cordynamic, Barcelona, Spain) was employed to infuse saline into the coronary artery to ensure adequate mixing of saline with the blood. Towards the end of our study, the infusion catheter designed by the proponents of thermodilution method of coronary blood flow measurement (Aarnoudse et al., 2007) became commercially available. This catheter called Rayflow (Hexacath, Rueil-Malmaison, France) was used in a small number of cases.

#### 5.2.4.1 Amicath™

Amicath™ is a 6 French compatible microcatheter marketed by IHT Cordynamic, Barcelona, Spain, for intracoronary use with a dual-lumen, rapid-exchange monorail design. It has an increasing distal to proximal profile from 0.017 inch to 0.059 inch. One lumen is used to accommodate the pressure wire (0.014 inch) (figure 5.1). The other lumen allows the injection of saline, which exits through four small distal side holes ensuring good mixing of saline with the blood. The total length of the catheter is 140 cm, with a distal shaft of 25cm length. The tip tapers to a 0.017-inch diameter at a length of 2mm. The catheter has an overall crossing profile of 0.023 inch. There are four radio-opaque markers on the catheter at 0, 10, 20 and 30 mm from the tip. There are 4 side holes at the proximal marker. This catheter has been previously used safely in research studies (Miranda-Guardiola et al., 2009).

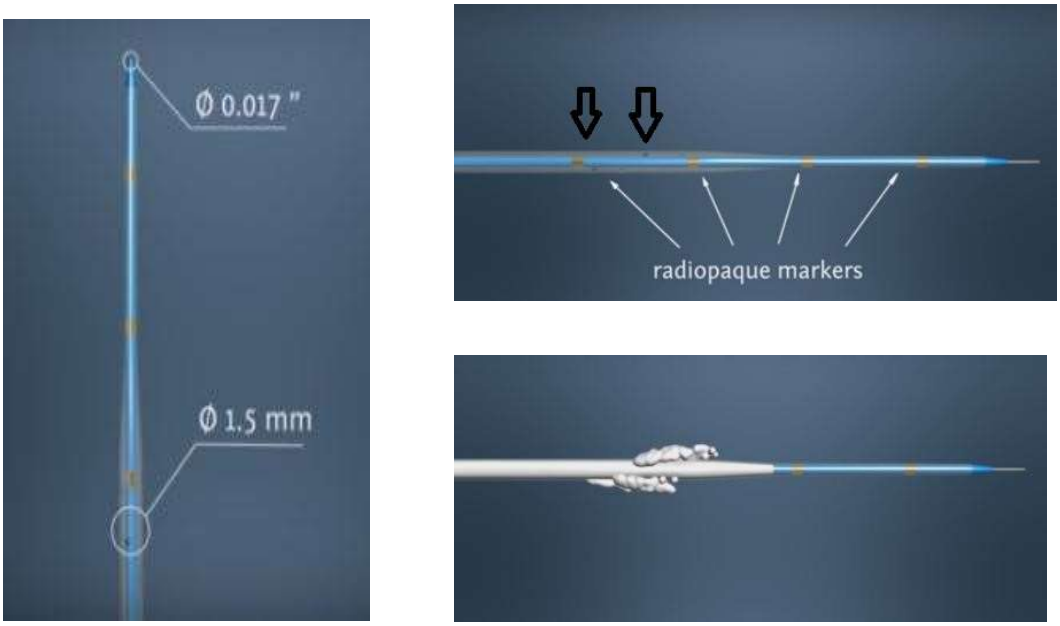


**Figure 5.1: Images showing Amicath design**. The left panel shows the tapered design and the diameters at various points. The right upper panel shows the radio-opaque markers at 10mm intervals and location of perfusion holes (black arrows). The right lower panel shows a cartoon of perfusion through the holes. Image courtesy IHT Cordynamic.

#### 5.2.4.2 Rayflow™

Rayflow™ is a dual lumen monorail infusion catheter marketed by Hexacath, Rueil-Malmaison, France. It is a 6 Fr compatible device (0.84mm diameter) with 4 side holes a short distance from the distal end (figure 5.2). The distal end hole fits snugly over the pressure wire. The saline infusion is delivered through the outside lumen and exits the catheter via the side holes. There are also holes connecting both lumens that ensures that the thermistor on the pressure wire can measure the temperature of saline infusate. This has been validated in coronary blood flow measurements using thermodilution (van 't Veer et al., 2016).

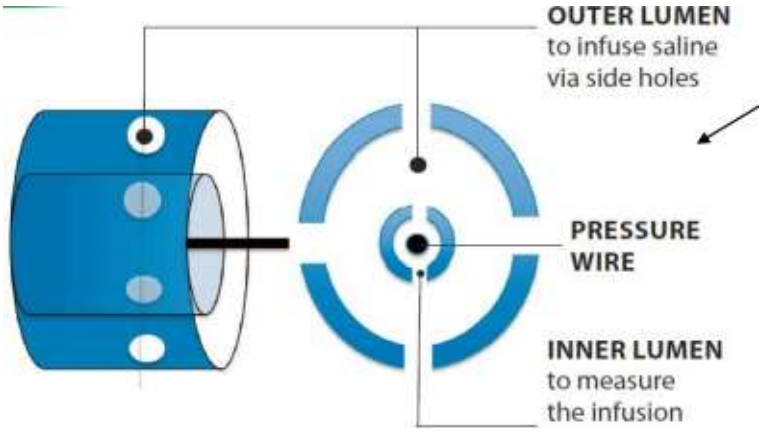


**Figure 5.2: Rayflow design.** The cross section at the level of the infusion holes, demonstrating the unique dual lumen design of 4 outer holes for perfusion and 2 inner holes connecting the two lumens for measuring the temperature of the infusate (Image courtesy of Hexacath).

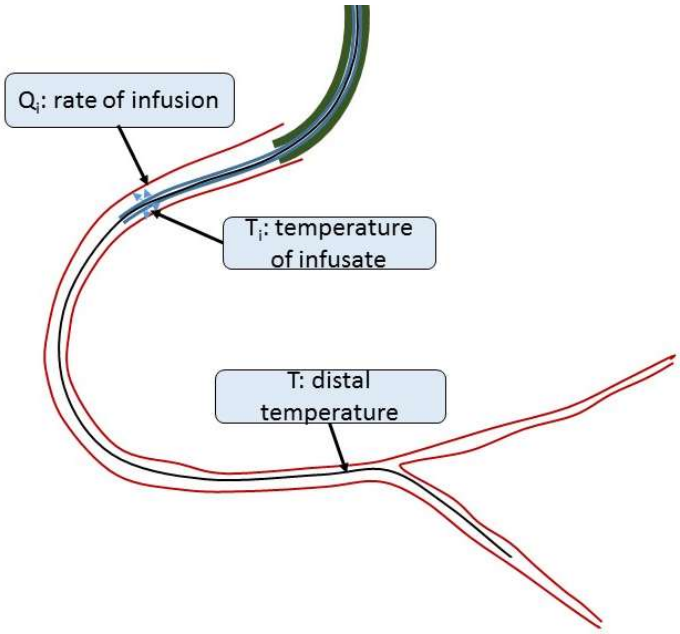


**Figure 5.3: Use of Rayflow in coronary artery to assess coronary blood flow.** The pressure wire with a thermistor is advanced to the distal artery and Rayflow catheter advanced over the wire to the proximal vessel. Saline at room temperature is infused through the Rayflow catheter. $T_i$ is the temperature of the infusate (saline) measured inside the catheter, by the thermistor when the pressure wire is pulled back into the Rayflow catheter. T is the distal temperature from the blood and saline mixture measured by the thermistor on the pressure wire. Qi is the rate of infusion of saline, set on the pressure injector.

Coronary blood flow (ml/min) $Q = \frac{T_i}{T} \times 1.08 \times Q_i$

The correction factor 1.08 is applied to compensate for the difference in specific heat between saline and blood.

Resistance to flow (mm Hg/min/ml) $R = \frac{P}{Q}$

P is the distal pressure.

#### 5.2.4.3 Difference between Amicath and Rayflow microcatheters

There are some important differences in the design of Amicath and Rayflow. Both are 6 French guide catheter compatible rapid exchange monorail design dual lumen catheters with 4 infusion holes at the distal end of the outer lumen. Amicath has a tapered tip which reduces from 1.5mm to 0.43 mm (0.017 inch). The infusion holes are between the 20mm and 30 mm radio-opaque markers which means there is a redundant catheter tip of 20-30 mm distal to infusion holes, which will occupy some volume in the artery and arguably impacts on the flow. The Rayflow catheter has a non-tapered tip which measures 0.84mm in diameter. The infusion holes are positioned much closer to the tip of the catheter which means less redundant catheter in the artery. Rayflow catheter also has two holes that connect the inner lumen to the outer lumen near the tip, which enables the measurement of the infusate by simply withdrawing the thermistor element of the pressure wire to the location of these holes. In the case of Amicath, to achieve the same measurement, Amicath has to be withdrawn into the guide catheter and the pressure wire has to be pulled back with the thermistor element sitting within the guide catheter but just distal to the tip of the Amicath. This is more cumbersome.

### 5.2.5 Hyperaemic agents

Induction of hyperaemia is of paramount importance when assessing coronary physiology. As described in chapter 1, coronary blood flow is very closely regulated, primarily by the distal compartment of coronary circulation. A variety of agents have been employed for induction of hyperaemia including intravenous (IV) or intracoronary (IC) adenosine, adenosine triphosphate, nitroprusside, papaverine, nicorandil, and dobutamine (De Bruyne, Bernard et al., 2003). Intravenous or intracoronary adenosine is the most widely used agent.

#### 5.2.5.1 Adenosine

There are four recognised subtypes of Adenosine receptors $A_1$, $A_{2A}$, $A_{2B}$, and $A_3$. The physiological effects of adenosine on cardiovascular system are vasodilation (A2A), Bradycardia (A2B), slowing of A-V nodal conduction (A1), reduction of atrial contractility (A1), Inhibition of cardiac pacemakers (A1), Inhibition of platelet aggregation (A2A), antagonises stimulatory effects of catecholamines (A1) (Shryock and Belardinelli, 1997). Adenosine acts on endothelium and smooth muscle cells to produce vasodilation. The increase in myocardial blood flow is primarily due to the action at A2A receptors. It is generally safe and effective with reproducible hyperaemic effects. The dose of adenosine generally used is 140μg/kg/min as intravenous infusion. Hyperaemia is achieved at around a minute after the commencement of the infusion and lasts until about a minute after the discontinuation of the infusion. Although the original studies described using central venous access for IV adenosine infusion, in clinical practice a large bore peripheral venous cannula

is often used with good effect. In clinical practice, intracoronary adenosine is used at a dose of 40 µg in the right coronary artery (RCA) and 60 µg in the left coronary artery (LCA). However a recent study suggests 100 µg and 200 µg doses for RCA & LCA respectively (Adjedj et al., 2015). AV nodal block is seen commonly with IC administration (especially RCA). Intravenous administration can cause bronchoconstriction, contraindicating its use in patients with history of severe asthma. Adenosine infusion can induce a very unpleasant sensation of dyspnoea and pressure sensation in the chest.

#### 5.2.5.2 Regadenoson

Regadenoson is a selective A2A receptor agonist has been used for inducing hyperaemia (Al Jaroudi and Iskandrian, 2009). This agent has been widely used in nuclear cardiology for myocardial perfusion studies. The main advantages of using this agent as opposed to adenosine is the ease of use (400 µg IV bolus via a peripheral IV cannula) and the excellent side effect profile (Prasad et al., 2014; Iskandrian et al., 2007). Regadenoson has been used safely in patients with mild to moderate asthma (Leaker et al., 2008).

### 5.2.6 Ethical approval

A formal ethical approval application was made to the NHS Health Research Authority, Research Ethics Committee, Yorkshire, and the Humber- Leeds Bradford. Ethical approval was granted on 14 October 2013 (Appendix 2).

### 5.2.7 Patient selection

Patients attending the cardiac catheterisation laboratory at the Leeds General Infirmary for PCI procedures and coronary angiogram with a view to proceeding to PCI were recruited to the study. The detailed inclusion and

exclusion criteria are given in table 5.1. Patients were approached, usually on the day prior to the procedure and given detailed explanation about the research project. A patient information leaflet was given to the patients deemed to be suitable for recruitment (Appendix 3). After having adequate time to read the leaflet and ask for any clarifications, willing volunteers were requested to sign the consent form (Appendix 4). Patients who were having the procedures for either stable angina or acute coronary syndromes (ACS) were considered for the study. However, among patients with ACS, those presenting as an emergency or with ST elevation myocardial infarction (STEMI) were not included.

**Table 5.1: Inclusion and Exclusion criteria**

| | |
|---|---|
| **Inclusion criteria** | All patients attending cardiac catheter laboratory at LGI for coronary angiography or PCI. |
| **Exclusion criteria** | Patients presenting as emergency, commonly following STEMI.<br>Patients with multi-vessel disease.<br>Patients with normal coronary arteries.<br>Patients < 18 years old.<br>Pregnancy / breast feeding.<br>Inability to provide informed consent.<br>Previous coronary artery bypass grafts.<br>Asthma or significant respiratory impairment.<br>Patient weight > 100 kg.<br>Resting heart rate > 80 /min.<br>Atrial Fibrillation.<br>Renal impairment (serum creatinine>200 μmol/l or eGFR<60ml/min/1.73 m²).<br>Previous sensitivity to iodine-based contrast media<br>Permanent pacemaker / implantable cardioverter-defibrillator device.<br>More than two previous imaging techniques involving ionising radiation exposure within 6 months of recruitment, or similar planned for the 6 months following participation in this study.<br>Any other condition considered by the investigators likely to compromise patient safety or successful data collection.<br>Haemodynamic instability. |

LGI- Leeds General Infirmary, PCI- Percutaneous coronary intervention, STEMI- ST elevation myocardial infarction, eGFR- estimated glomerular filtration rate.

### 5.2.8 Patient preparation

Patient's identity was verified and indication for the procedure double checked. Informed consent was sought for the procedure using the standard consent form at the Leeds General Infirmary. In addition, consent for the research study was reaffirmed. An 18-20-gauge venous cannula was placed in patient's forearm as per usual clinical practice. Patient was then transferred to the catheterisation laboratory table. Arterial access routes were chosen as per clinical indication. In majority of patients, the right radial artery was used as per usual practice. The access site was prepared and cleaned with antiseptic solution and the patient was draped. Intravenous sedation with Diazepam was offered if patient was anxious. Local anaesthesia was given with 2% Lidocaine solution infiltrated around the access site. A 6 French size sheath was used, and standard diagnostic and guiding catheters were used for the procedure.

Adenosine infusion was pre-prepared in a syringe driver pump to deliver at an infusion rate of 140microgram/kg/min. If regadenoson was used as the hyperaemic agent, a bolus of 400mg was prepared in advance, along with a 20 ml syringe of saline flush.

Coronary angiography was performed as per standard practice. A standard 6 Fr guiding catheter suitable for the patient's anatomy was chosen for pressure wire studies and the PCI. Anticoagulation was established with weight adjusted unfractionated heparin. Adequacy of anticoagulation was checked at 30-minute intervals by activated clotting time (ACT) assays.

### 5.2.9 Study protocol

The protocol involved two parts a) the Thermodilution protocol and b) the X-ray protocol.

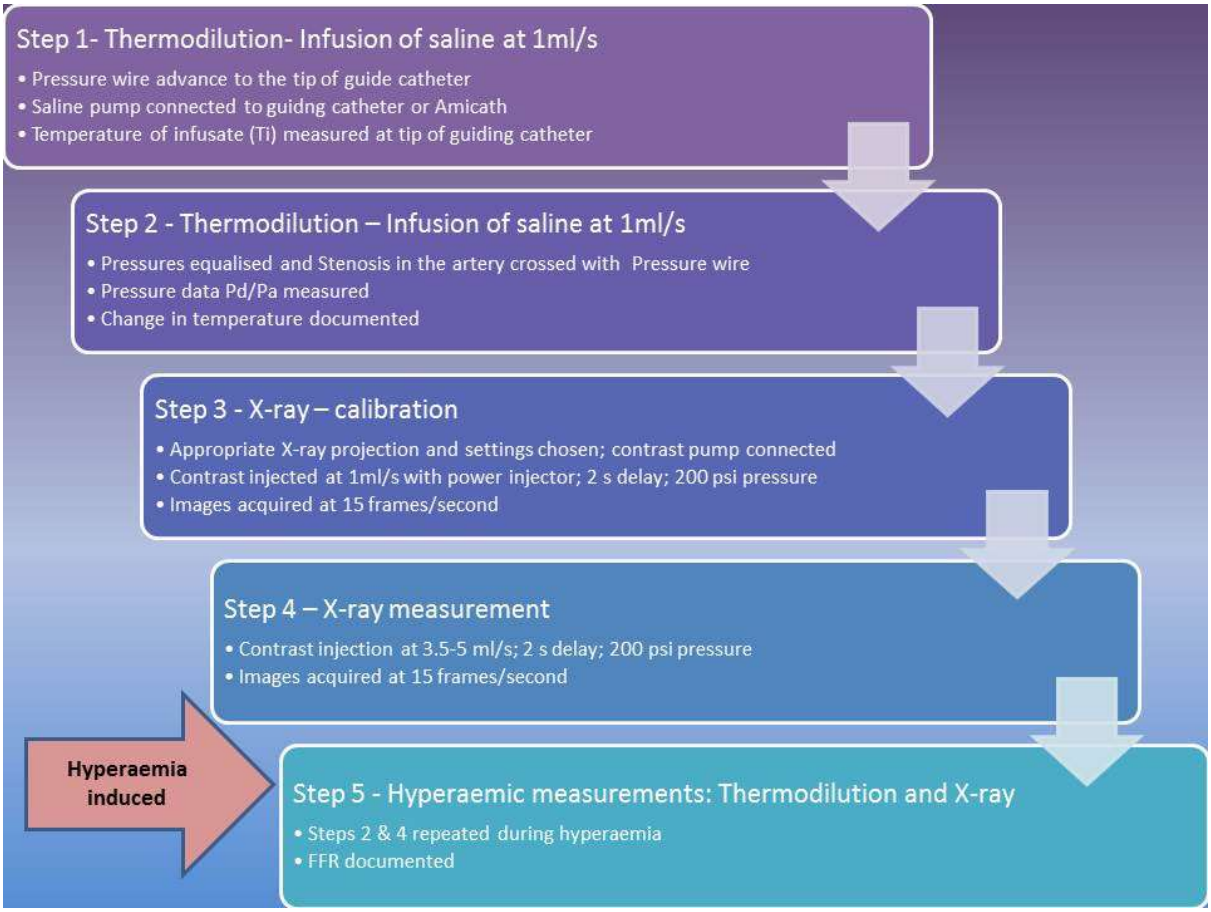


**Figure 5.4: Schematic diagram showing study protocol in the catheterisation laboratory.**

#### 5.2.9.1 Thermodilution protocol (part 1)

A pressure wire (Certus, St Jude Medical) was selected and connected to the RadiAnalyser Xpress console. The wire was flushed, and calibration was completed as usual practice. 'Thermo' section on the RadiAnalyser Xpress menu was selected. The temperature was set to zero. The pressure wire was then advanced to the tip of the guiding catheter, with the sensor element still

within the guiding catheter. The saline Pressure injector was connected to the manifold and saline infusion was infused at 1ml/second.

*Pressure injector settings for saline:* The pressure injector was set to inject 30ml of saline at 1ml/s, with no injection delay and no rate rise. The pressure was set to 200psi, and the injection was hand triggered. The settings remain the same for all the steps in the thermodilution protocol.

In later studies, we used infusion microcatheters Amicath and Rayflow to infuse the saline into the coronary artery to ensure adequate mixing of saline with the blood. In such cases the injector pump was connected to the hub of the microcatheter. When using the Rayflow catheter, the rate of infusion of saline was reduced to 0.3ml/s as instructed by the manufacturer. The drop in temperature was recorded. This is the temperature of infusate (Ti) at the tip of the guiding catheter (figure 5.5).

The pressure wire was then advanced into the coronary artery and the two pressure traces (aortic and distal pressures) were equalised with the sensor element placed at the tip of the guiding catheter. The pressure wire was then advanced further and manipulated past the coronary lesion and the sensor element placed beyond the lesion. In cases where advancing the wire past the stenotic lesion was difficult with the pressure wire, a suitable standard coronary guide wire was used first and pressure wire advanced alongside it.

Saline infusion was then restarted at 1ml/s and the temperature change was recorded. The change in temperature (T) was documented (figure 5.6).


**Figure 5.5: Thermodilution protocol- part 1.** Pressure wire placed within guiding catheter to record the temperature of the infusate (Ti). There was no simultaneous distal pressure recording as the manifold setup did not allow that when infusing saline. Therefore, the Pa value and FFR value are erroneous.


**Figure 5.6: Thermodilution protocol- part 2.** Pressure wire placed within the coronary artery to record the temperature of the blood missed with saline (T). There was no simultaneous distal pressure recording as the manifold setup did not allow that when infusing saline. Therefore, the Pa value and FFR value are erroneous.

#### 5.2.9.2 X-ray protocol

The saline pump was disconnected, and the contrast pressure injector was connected to the manifold. A radiographic projection appropriate for the coronary artery was chosen to minimise the overlap from different coronary artery territories. The collimators were brought in to frame the field of view. Large field of view was selected (25cm). Image acquisition was set at 15 frames/second. The X-ray tube was positioned so that the patient's heart was centred in the frame. The patient was then instructed to hold the breath. Image acquisition was performed in breath hold for several seconds or until the contrast was seen entering the coronary venous system.

#### 5.2.9.3 Calibration sequence

The first image acquired was acquired with contrast injected through the automated pressure injector at a rate of 1ml/s. This injection was intended to deliver all the contrast material into the coronary artery without any spillage.

*Pressure injector settings for contrast:*

- Volume - 4ml
- Rate of injection - 1ml/s
- Inject delay- 2 seconds or approximately 1.5 heart beats after the start of X-ray acquisition, coupled to the catheter laboratory X-ray system or manually triggered.
- Injection rate rise- None
- Injection pressure- 200 psi.

#### 5.2.9.4 X-ray measurement sequence 1

Injector settings were then changed for the measurement sequence. This injection intended to momentarily replace the entire blood volume at the origin of the coronary artery with contrast agent. An injection rate of 3-5 ml/s was chosen based on the size of the coronary artery and the area of myocardium supplied. Images were acquired with patient in breath hold.

*Pressure injector settings for contrast:*

- Volume - 12-20 ml (lower for RCA)
- Rate - 3-5 ml/s. Depending on the size and myocardium supplied by the artery.
- Delay of 2 seconds or approximately 1.5 heart beats.
- Inject delay- Coupled to the catheter lab laboratory system or manually triggered.
- Injection rate rise- None.
- Injection pressure- 200 psi.

#### 5.2.9.5 X-ray measurement sequence 2

This was performed after induction of hyperaemia as previously indicated. Pump settings were identical to those of measurement sequence 1.

#### 5.2.9.6 Thermodilution protocol (part 2)

During hyperaemia, the thermodilution sequence was repeated to calculate flow. The contrast pressure injector was changed for the saline pressure injector. The pressure injector settings were the same as for the rest sequence.

### 5.2.10 Data capture and post processing

X-ray data were captured by the dedicated data capture computer system in the catheterisation laboratory. Data were then transferred to the university computer system for analysis using the XBF software.

Thermodilution and pressure data were copied from the RadiAnalyser Xpress console to the university system. No patient identifiable data were transferred out of the Leeds General Infirmary system. DICOM images transferred to the clinical image archive were also anonymised and copied. The correct image sequences were identified in preparation for the XBF software to be applied.

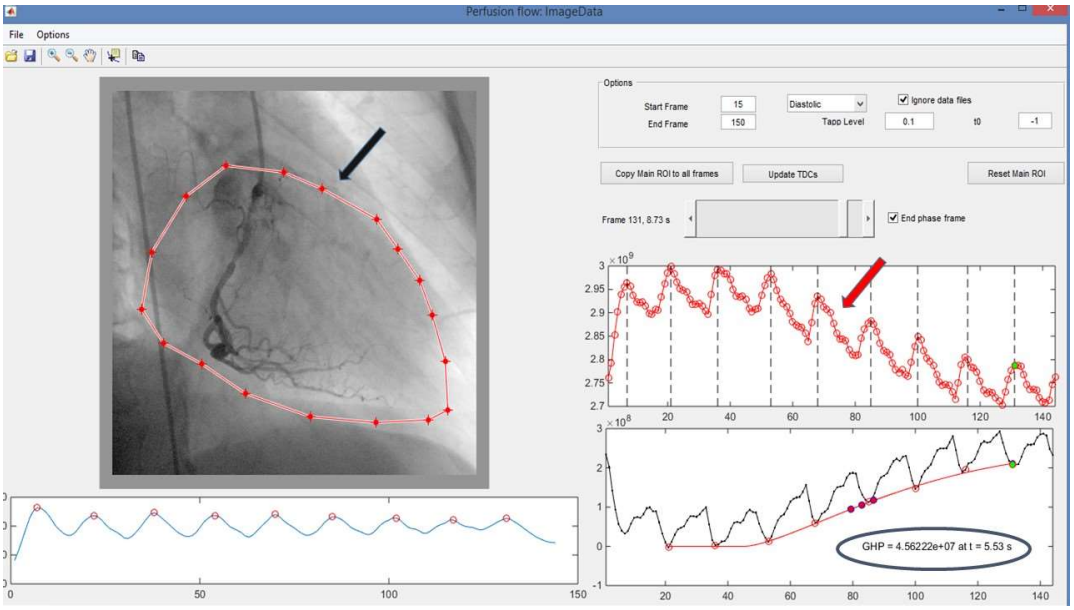


**Figure 5.7: An example of X-ray image analysis using an earlier version of the XBF software.** A region of interest has been chosen around the coronary artery (RCA in this case) and the myocardial territory- black arrow. Signal intensity change plotted on a graph (red arrow). Diastolic phase images selected, and the rate of signal intensity change plotted, and the gradient calculated (black oval)

### 5.2.11 Primary and secondary endpoints

The primary endpoint was the correlation between the XBF calculated coronary blood flow and the thermodilution coronary blood flow.

The secondary endpoints

1. Correlation between the XBF calculated coronary blood flow and the thermodilution coronary blood flow in right coronary artery cases.
2. Correlation between coronary flow reserves from XBF method and thermodilution.
3. Inter-observer and intra-observer variability of XBF method coronary blood flow estimation
4. Safety of performing the X-ray signal intensity analysis in human beings as defined by the rate of clinically relevant adverse patient events.

Independent analyses for right coronary artery (RCA) and left coronary artery (LCA) were planned based on their different branching and territorial supply.

### 5.2.12 Sample size and power calculation

This was a pilot study designed to test the methods, safety, and feasibility of performing coronary blood flow calculation using X-ray signal intensity analysis in human subjects. As this is the first study of this technology in humans, precision and variance of XBF-derived measurements were not known when the study was designed. Further, there are no accepted normal values of coronary blood flow available. Therefore, it was not possible to perform conventional sample size or power calculations. However, the total recruitment size was informed by previous studies in similar study populations

to inform mechanisms (Aarnoudse et al., 2007; Siebes et al., 2004; Li et al., 2015).

## 5.3 Results

Forty-five patients were recruited to the study. The first three patients were used to optimise the protocol and breath hold technique.

During the initial phase, a suitable microcatheter was not available commercially. During later phases we used Amicath and Rayflow microcatheters for left coronary artery cases. The patients were grouped according to this which is detailed in table 5.2.

Patients were recruited over a period of 26 months (January 2015 – March 2017) from those attending cardiac catheter laboratory for angiography for stable coronary artery disease or acute coronary syndromes excluding STEMI.

**Table 5.2: Groups of LCA cases depending on use of microcatheter.**

| | | | |
|---|---|---|---|
| Group A | No microcatheter used | Patients 1-18 | January 2015-October 2015 |
| Group B | Amicath microcatheter for LCA cases. No microcatheter for RCA cases | Patients 19-36 | October 2015-July 2016 |
| Group C | Rayflow microcatheter for LCA cases, No microcatheter for RCA | Patients 37-45 | March 2017 |

RCA- right coronary artery, LCA- left coronary artery.

### 5.3.1 Patient characteristics

Baseline characteristics are summarised in table 5.3. None of the patients suffered adverse events linked to the research protocol.

**Table 5.3: Patient characteristics of patients recruited to the human validation study.**

| | |
|---|---|
| Number of patients recruited | 45 |
| Mean age (SD) years | 61.4 (10.4) |
| Male gender (%) | 34 (75.5%) |
| Clinical syndrome | Stable 18 (40%) |
| | Acute coronary syndrome 27 (60%) |
| Artery studied | LAD 18 (40%) |
| | LCX 3 (7%) |
| | RCA 24 (53%) |
| Hypertension (%) | 19 (42%) |
| Hypercholesterolemia (%) | 16 (36%) |
| Diabetes (%) | 4 (9%) |
| Smoking (%) | Ex-smoker 6 (13%) |
| | Current smoker 8 (18%) |

SD – Standard Deviation. LAD- left anterior descending artery, LCx- Left Circumflex artery, RCA- Right Coronary artery.

### 5.3.2 Quality of images analysis

X-ray image data captured and transferred from the catheter laboratory were analysed offline for the quality and suitability for further analysis.

The quality of the images was graded on a scale of 1-3 as indicated in table 5.4. The results from the image quality analysis are detailed in table 5.5.

**Table 5.4: Grading scheme used for classifying the images based on quality and suitability for analysis.**

| Grade | Description |
|---|---|
| 1 | Significant problems, not suitable for analysis, e.g., breathing artefact |
| 2 | Some problems, may be suitable for analysis with correction, may lead to errors, e.g., breathing towards the end/minor movements |
| 3 | Good quality images, suitable for analysis |

**Table 5.5: Assessment of quality of X-ray images with regards to the suitability for further assessment.**

| Study No | Vessel | Image quality score pre-PCI | | | Image quality score post-PCI | | Comments |
|---|---|---|---|---|---|---|---|
| | | Calibration | Rest | Hyperaemic | Rest | Hyperaemic | |
| P1 | RCA | NP | NP | NP | NP | NP | |
| P2 | LCA | 1 | 1 | NP | NP | NP | |
| P3 | RCA | 2 | 2 | 2 | NP | NP | Descending Aorta overlying region on interest |
| P4 | RCA | 1 | 1 | NP | NP | NP | |
| P5 | RCA | 2 | 2 | 2 | NP | NP | Descending Aorta overlying ROI; Some filling of LCA from overspill |
| P6 | RCA | 1 | 1 | NP | NP | NP | Descending Aorta overlying region on interest |
| P7 | LAD | 1 | 1 | 1 | NP | NP | Framing issue |
| P8 | RCA | 1 | 1 | 1 | NP | NP | |
| P8 | LCX | 1 | 1 | 1 | NP | NP | |
| P9 | LAD | 2 | 3 | NP | 3 | NP | |
| P10 | LAD | 1 | 3 | 1 | NP | NP | |
| P11 | LAD | 1 | 3 | 3 | NP | NP | |
| P12 | LAD | 3 | 3 | 1 | NP | NP | |
| P13 | RCA | 3 | 2 | 3 | NP | NP | Some contrast filling of LCA |
| P14 | RCA | 1 | 1 | 2 | NP | 3 | Contrast filling of LCA |
| P15 | RCA | 3 | 2 | 1 | NP | NP | Some contrast filling of LCA, corrected with frame selection; Descending Aorta, corrected with ROI |
| P16 | RCA | 1 | 1 | 1 | 1 | NP | |
| P17 | RCA | 1 | 3 | 1 | NP | NP | catheter not well engaged |
| P18 | RCA | 3 | 3 | 1 | NP | NP | Framing issue |
| P19 | LAD | 3 | 3 | 3 | NP | 1 | |
| P20 | LAD | 3 | 3 | NP | 1 | 3 | |
| P21 | RCA | 3 | 3 | 2 | NP | NP | |
| P22 | LAD | 3 | 3 | 3 | 3 | NP | |
| P23 | RCA | 3 | 2 | 2 | NP | NP | AR seen, corrected for descending Aorta |

| | | | | | | | |
|---|---|---|---|---|---|---|---|
| P24 | LAD | 1 | 1 | 1 | NP | NP | Framing issue and descending Aorta |
| P25 | LAD | 2 | 3 | 1 | NP | NP | |
| P26 | LAD | 3 | 3 | 1 | 3 | 2 | |
| P27 | RCA | 3 | 2 | 1 | 2 | 1 | Some contrast in LCA; descending Aorta corrected; early breathing in post rest, corrected |
| P28 | RCA | 2 | 2 | 2 | NP | NP | |
| P29 | RCA | 2 | 3 | NP | 3 | 1 | Descending Aorta corrected |
| P30 | LAD | 3 | 3 | 3 | NP | NP | |
| P31 | LCX | 3 | 3 | 3 | NP | NP | |
| P32 | LAD | 3 | 1 | 1 | NP | NP | |
| P33 | RCA | 2 | 2 | 2 | NP | NP | |
| P34 | RCA | 3 | 3 | 3 | NP | NP | Descending Aorta corrected |
| P35 | RCA | 1 | 1 | 1 | 1 | NP | X-ray settings incorrect |
| P36 | RCA | 3 | 2 | 2 | 2 | NP | Some frames skipped by image capture system |
| P37 | LAD | 3 | 3 | 2 | NP | NP | Framing issue; some filling of LCA |
| P38 | RCA | 2 | 2 | 1 | NP | NP | AR noted |
| P39 | LAD | 2 | 2 | 2 | NP | NP | Descending Aorta corrected |
| P40 | LAD | 2 | 2 | 2 | NP | NP | Minor framing issue |
| P41 | RCA | 3 | 2 | 2 | NP | NP | Some filling of LCA |
| P42 | LCx | 3 | 3 | 1 | NP | NP | |
| P43 | LAD | 3 | 3 | 2 | NP | NP | |
| P44 | RCA | 2 | 2 | 2 | NP | NP | |
| P45 | LAD | 3 | NP | 3 | 3 | NP | |

NP- not performed, AR- Aortic regurgitation, LCA- Left coronary artery, RCA- Right coronary artery, LAD- Left anterior descending artery, LCx- Left circumflex artery, ROI- region of interest. Where it is not specified, the problem is with breathing during image acquisition. Major breathing was easy to identify, however subtle breathing was more difficult and often not identified until after the images are analysed. Images which were graded 1 were excluded from analysis. Any error in the calibration sequence will impact the whole study and if the calibration sequence was unsuitable then the whole case had to be excluded from analysis. Subsequent analyses reported in this chapter were only performed on images graded 2 or above.

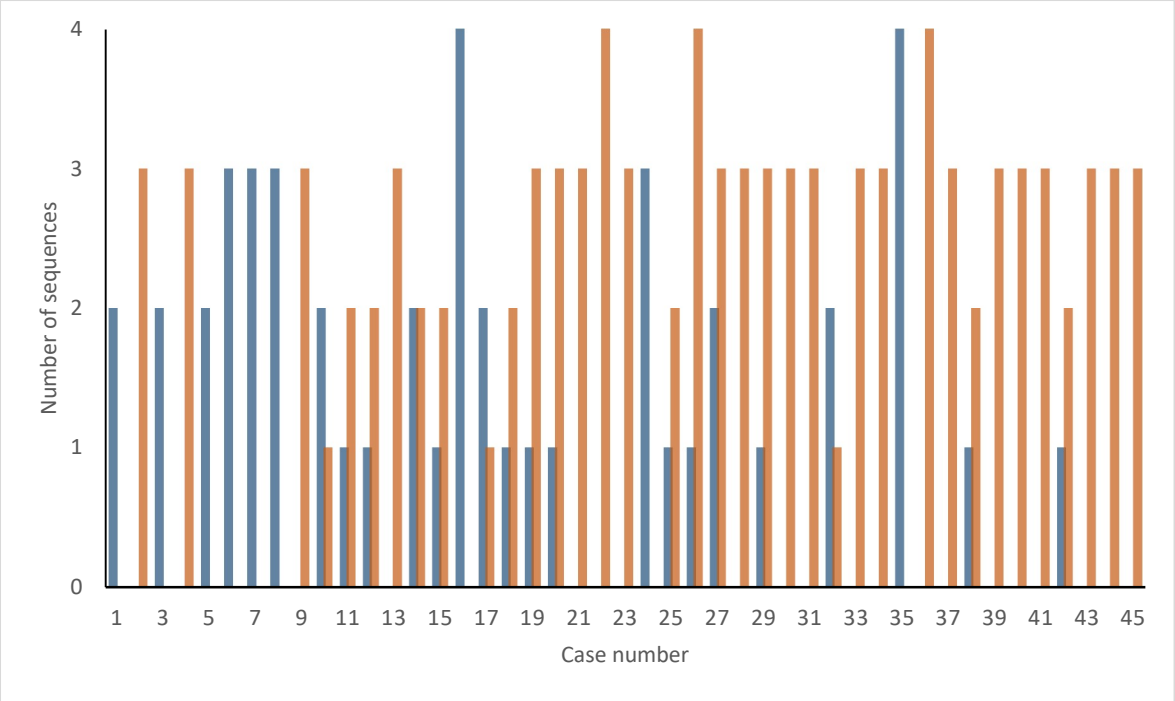


**Figure 5.8:** A histogram chart showing the change in data quality and rejection rates over time demonstrating improvement with increasing experience. Blue bars represent grade 1 images which were rejected, and orange bars represent grade 2 and 3 images which were included in the analysis.

As illustrated in figure 5.8, the proportion of images suitable for analysis generally increased with time and experience. Case number 35 is an anomaly because the X-ray settings were wrongly selected. The main driver for the change was eliminating breathing movements. This was done through breath hold practice prior to image acquisition. As we gained more experience, we were able to spot subtle breathing movements and where appropriate repeat the acquisition. We also learnt to identify issues such as catheter dislodgement or improper engagement, especially with breath hold in end inspiration and overlying descending aorta in the region of interest. As the operators and the team got more experience, we were able to get more hyperaemic sequences which were a challenge during earlier cases because of difficulties with breath hold during hyperaemia.

### 5.3.3 Blood flow analysis

Study sequences with image quality sufficient to be analysed were identified and analysed using the XBF method. Images were loaded on to the software and the image frames where the contrast flows into the coronary artery and there is a steady change in X-ray signal intensity were chosen. A region of interest to include the whole of the heart was chosen in the case of RCA (figure 5.9) and a region of interest to include an arbitrary region supplied by the LAD or LCx arteries were chosen in the case of LCA cases. The gradients of time intensity curves were calculated from the signal intensity changes and coronary blood flow calculated.

The blood flow calculated was then compared to the blood flow calculated using the thermodilution method. The results from the analysis are detailed in table 5.6.

Mean XBF measurements were 1.77 ml/s during rest and 2.5 ml/s during hyperaemia. The mean thermodilution blood flow results were 2.07ml/s and 2.51ml/s during rest and hyperaemia, respectively. Blood flow results categorised according to the artery studied are given in table 5.7.

**Table 5.6: X-ray derived calculation of CBF in human subjects**

| Patient No | Vessel | Pre/Post PCI | Condition | XBF flow ml/s | Thermo Flow ml/s |
|---|---|---|---|---|---|
| 5 | RCA | Pre | rest | 1.58 | 2.60 |
| 5 | RCA | Pre | hyperaemia | 2.58 | 4.10 |
| 9 | LAD | Pre | rest | 2.61 | 2.72 |
| 9 | LAD | post | rest | 2.48 | 2.33 |
| 12 | LAD | Pre | rest | 1.68 | 11.08* |
| 13 | RCA | pre | rest | 1.23 | 1.80 |
| 13 | RCA | pre | hyperaemia | 2.83 | 2.50 |
| 14 | RCA | post | hyperaemia | 2.25 | 3.30 |
| 15 | RCA | pre | rest | 1.92 | 2.30 |
| 18 | RCA | pre | rest | 1.13 | 1.60 |
| 19 | LAD | Pre | rest | 1.85 | 3.46 |
| 19 | LAD | Pre | Hyperaemia | 3.16 | 3.43 |
| 20 | LAD | Pre | rest | 1.25 | 1.51 |
| 20 | LAD | post | hyperaemia | 1.34 | 1.48 |
| 22 | LAD | pre | rest | 1.57 | 2.81 |
| 22 | LAD | pre | hyperaemia | 2.62 | 3.49 |
| 22 | LAD | post | rest | 1.69 | 2.39 |
| 23 | RCA | pre | rest | 1.99 | 2.90 |
| 23 | RCA | pre | hyperaemia | 2.63 | 2.80 |
| 25 | LAD | pre | rest | 1.27 | 2.99 |
| 26 | LAD | pre | rest | 1.58 | 2.61 |
| 26 | LAD | post | rest | 1.63 | 3.17 |
| 26 | LAD | post | hyperaemia | 1.85 | 4.65 |
| 27 | RCA | pre | rest | 1.27 | 1.30 |
| 27 | RCA | post | rest | 1.48 | 1.60 |
| 29 | RCA | pre | rest | 1.31 | 2.20 |
| 29 | RCA | post | rest | 3.18 | 2.60 |
| 30 | LAD | pre | rest | 1.71 | 2.82 |
| 30 | LAD | pre | hyperaemia | 3.03 | 2.99 |
| 31 | LCx | pre | rest | 2.06 | 1.33 |
| 31 | LCx | pre | hyperaemia | 3.13 | 1.93 |
| 34 | RCA | pre | rest | 1.27 | 1.60 |
| 34 | RCA | pre | hyperaemia | 1.00 | 1.29 |
| 36 | RCA | pre | rest | 1.16 | 1.50 |
| 36 | RCA | pre | hyperaemia | 2.22 | 1.70 |
| 36 | RCA | post | rest | 1.80 | 1.70 |
| 37 | LAD | pre | rest | 2.56 | 1.69 |
| 37 | LAD | pre | hyperaemia | 3.50 | 2.43 |
| 39 | LAD | pre | rest | 3.50 | 1.22 |
| 39 | LAD | pre | hyperaemia | 4.32 | 1.26 |
| 40 | LAD | pre | rest | 1.91 | 2.09 |
| 40 | LAD | pre | hyperaemia | 1.79 | 1.87 |
| 41 | RCA | pre | rest | 1.20 | 2.00 |
| 41 | RCA | pre | hyperaemia | 2.35 | 2.10 |
| 42 | LCx | pre | rest | 1.93 | 0.61 |
| 43 | LAD | pre | rest | 1.19 | 0.68 |
| 43 | LAD | pre | hyperaemia | 1.82 | 0.70 |
| 45 | LAD | pre | rest | 1.71 | 1.71 |
| 45 | LAD | post | rest | 1.93 | 2.40 |
| 45 | LAD | post | hyperaemia | 2.52 | 3.07 |

*Thermodilution measurement fault. LCA- Left coronary artery, RCA- Right coronary artery, LAD- Left anterior descending artery, LCx- Left circumflex artery, Thermo – thermodilution.

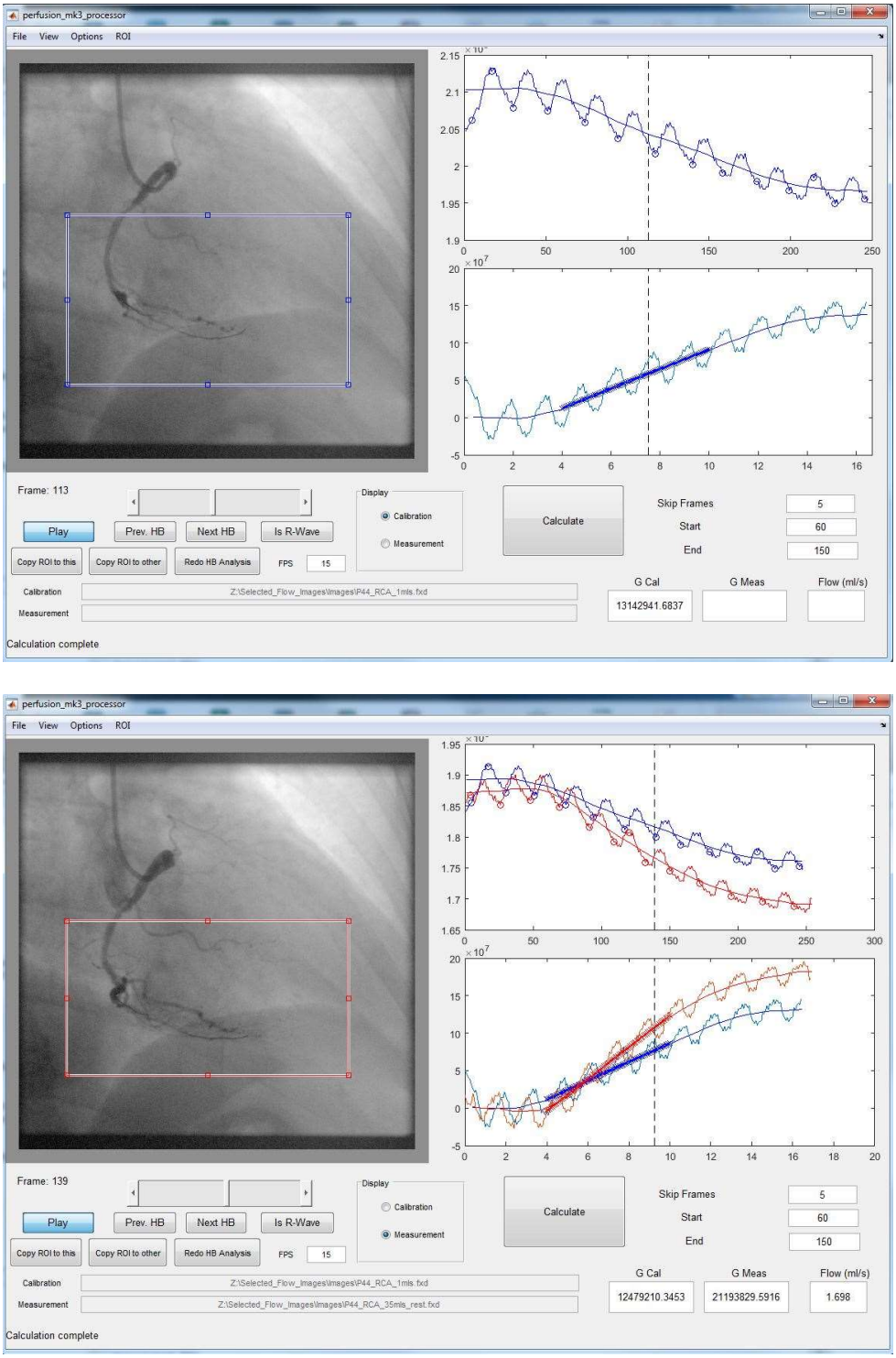


**Figure 5.9: An example of coronary blood flow analysis.** Here in an RCA case, the top panel is the calibration sequence and the bottom panel measurement sequence. Frames 60-150 have been selected in both sequences. A region of interest to include the RCA myocardial territory has been selected around the heart.

**Table 5.7: Summary of blood flow results per artery**

| Vessel | Condition | Sample size | Mean XBF blood flow (SD) ml/s | Mean thermodilution blood flow (SD) ml/s |
|---|---|---|---|---|
| All arteries | Rest | 32 | 1.77(0.58) | 2.07(0.71) |
| | Hyperaemia | 18 | 2.50(0.79) | 2.51(1.06) |
| LAD | Rest | 17 | 1.89(0.59) | 2.29(0.76) |
| | Hyperaemia | 10 | 2.60(0.92) | 2.54(1.21) |
| RCA | Rest | 13 | 1.58(0.56) | 1.98(0.50) |
| | Hyperaemia | 7 | 2.27(0.60) | 2.54(0.96) |
| LCx | Rest | 2 | 2.00(0.09) | 0.97(0.51) |
| | Hyperaemia | 1 | 3.13* | 1.93* |

* only one sample
LAD- Left anterior descending artery, LCx- Left circumflex artery, RCA- Right coronary artery, XBF- X-ray blood flow, SD- Standard deviation.

#### 5.3.3.1 Comparison XBF flow and thermodilution, all patients' data

Coronary blood flow measurements derived from thermodilution and XBF are plotted in figure 5.10. These data include all experimental data points (right and left coronary arteries, at rest and hyperaemia, pre and post PCI). Although the values were within a plausible range, there was no significant correlation between XBF and thermodilution derived flow, which was the reference standard.

To investigate if there was any influence of hyperaemia and differential induction of hyperaemia with the use of saline during thermodilution and contrast during XBF, rest and hyperaemic measurements were examined separately. In theory, hyperaemia using adenosine, or its analogues should negate the effects of saline or contrast on the microcirculation. The results are illustrated in figure 5.10. When blood flow calculated using XBF and thermodilution at rest and hyperaemic conditions were selected and

compared, there was no significant correlation between XBF flow and thermodilution flow.

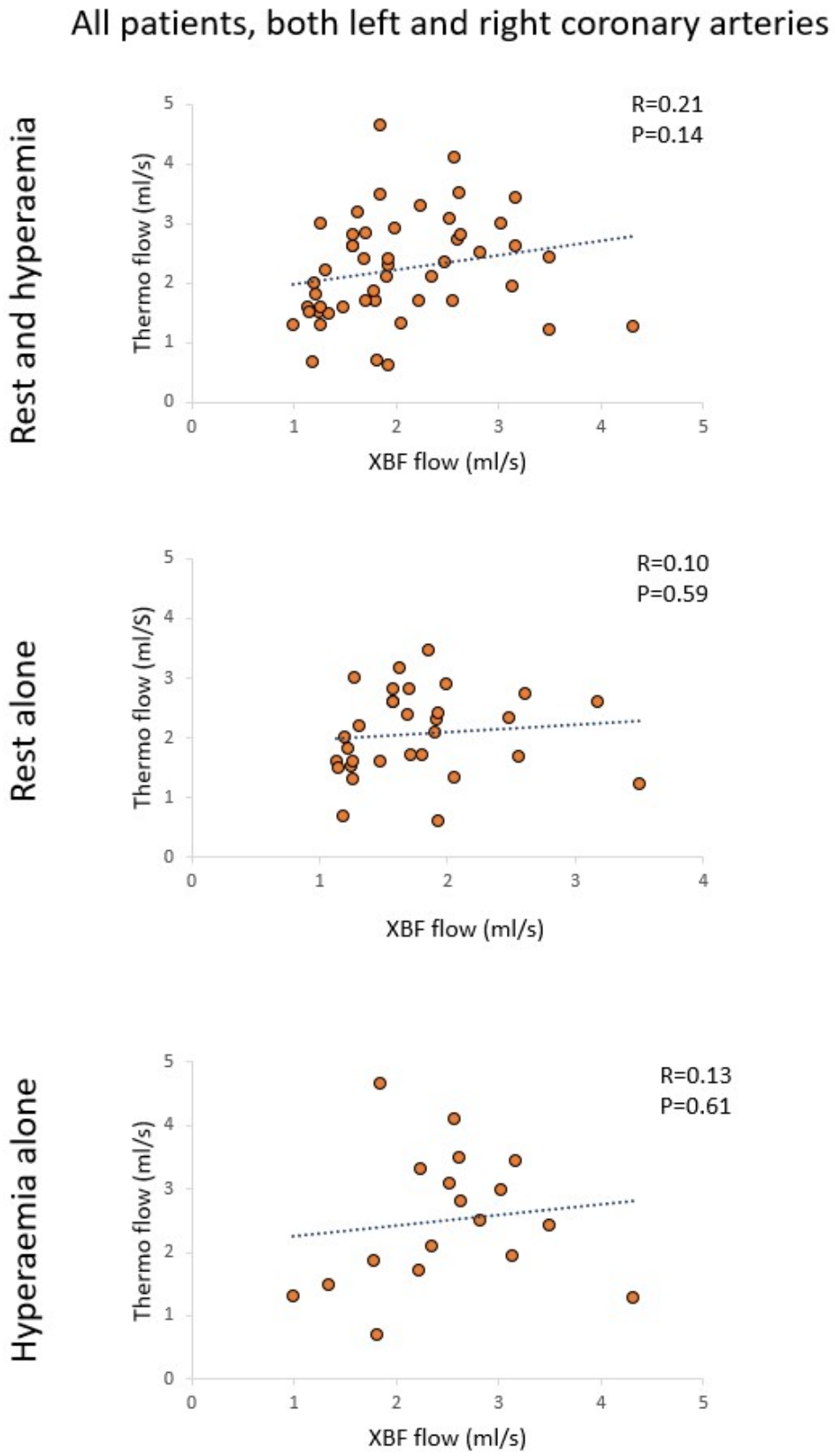


**Figure 5.10: Scatter plots showing the relationship between XBF blood flow plotted and thermodilution blood flow in all patients.**

.

#### 5.3.3.2 Comparison of blood flow in right coronary artery cases

The blood flow in RCA and LCA were analysed separately. The results of the XBF calculated blood flow in all patients who had RCA studied in both rest and hyperaemic conditions are presented in figure 5.11. There was good correlation seen when the flow measured in RCA alone was selected and compared between XBF and thermodilution techniques with a Pearson's coefficient value (R) of 0.67. There was also good agreement between the two methods as illustrated in the corresponding Bland-Altman plot.

There was good correlation between XBF measured blood flow in RCA when rest conditions were compared alone and when hyperaemic conditions were compared alone with Pearson's coefficient of correlation of 0.64 and 0.61 respectively (figures 5.12 & 5.13). There was also good agreement between the two methods as illustrated in the Bland-Altman plots. However, when selecting the images during different conditions and analysing separately, the sample sizes were small and there was relatively wide scatter and the assumptions about the distribution of the data may not hold true.

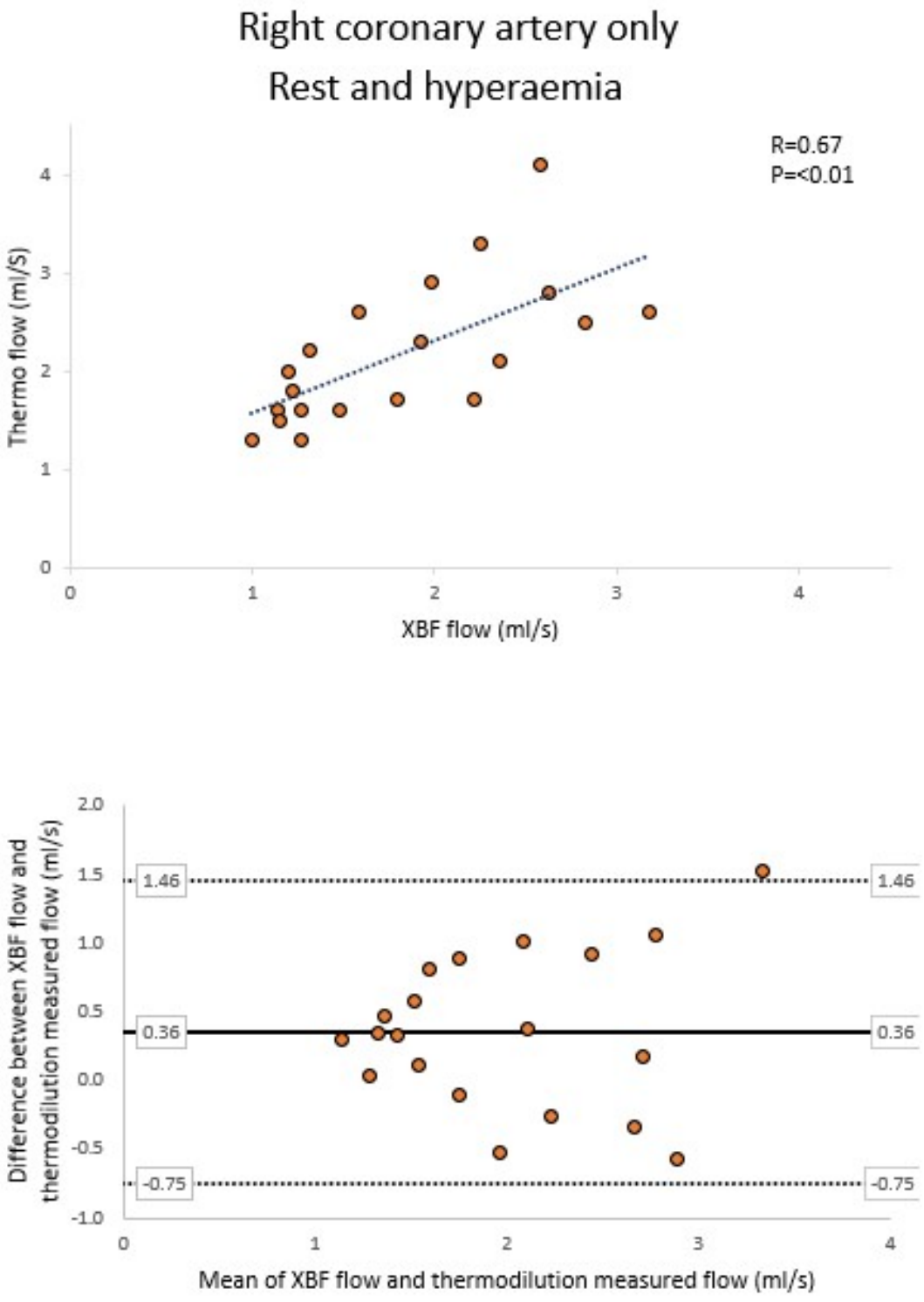


**Figure 5.11: Comparison between XBF measured flow in right coronary artery cases during rest and hyperaemia.** Upper Panel showing scatter plot and lower panel showing Bland Altman plot. In the Bland-Altman plot, the solid line represents the mean of the differences between measurements and the dotted lines represent the 95% confidence intervals for the mean of the differences between measures.

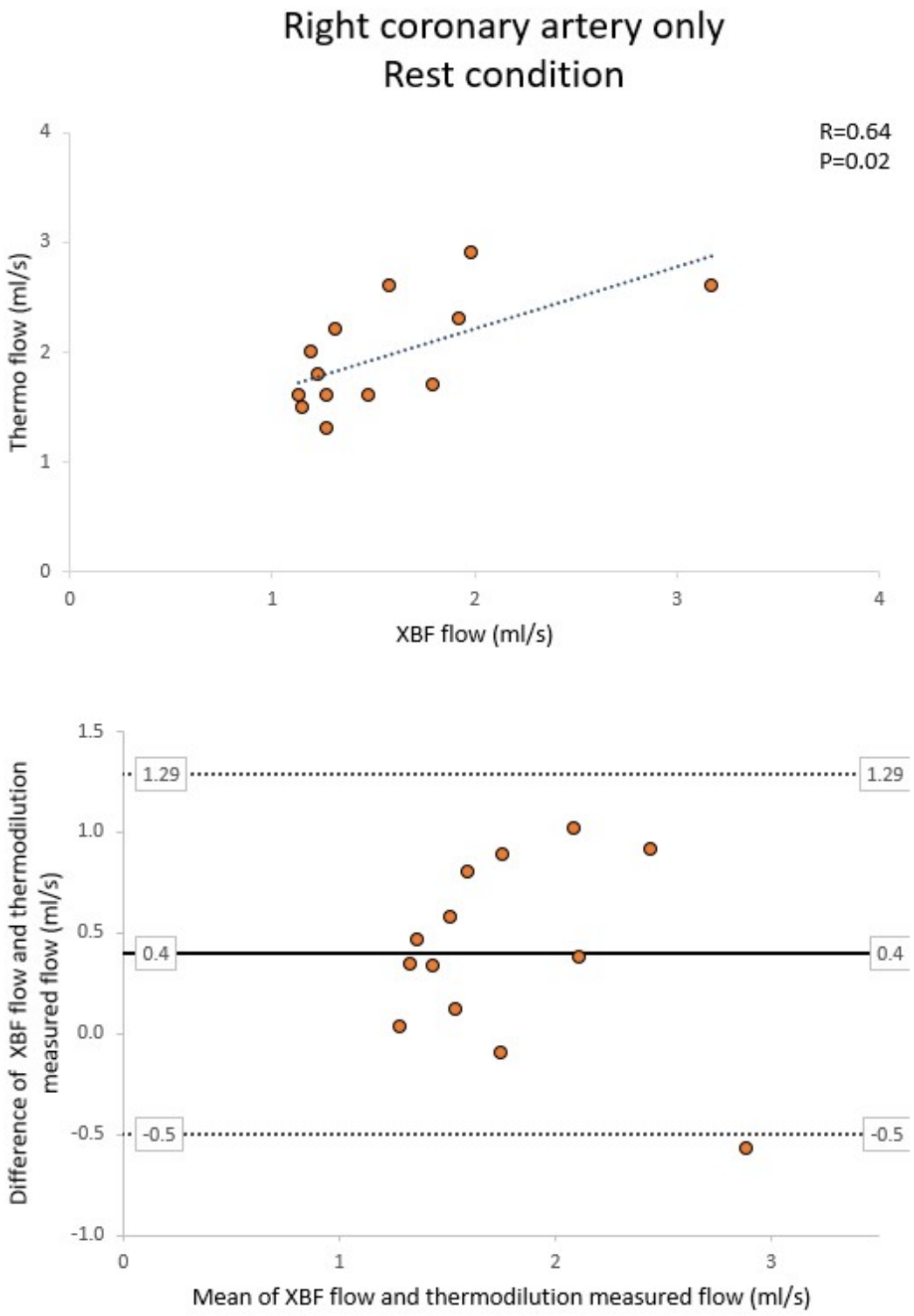


**Figure 5.12: Comparison between XBF measured flow in right coronary artery cases during rest condition only.** Upper Panel showing scatter plot and lower panel showing Bland-Altman plot. In the Bland-Altman plot, the solid line represents the mean of the differences between measurements and the dotted lines represent the 95% confidence intervals for the mean of the differences between measures.

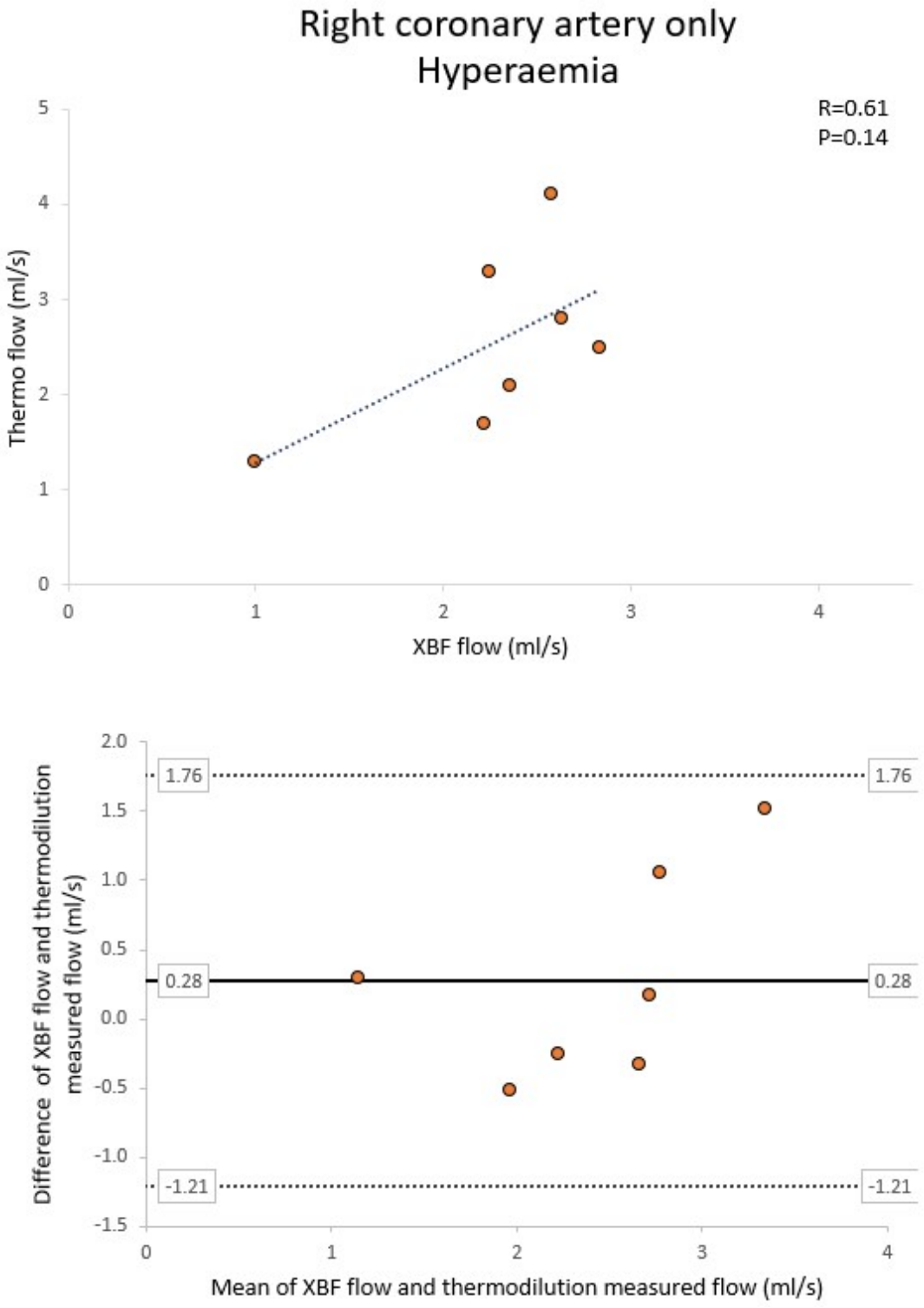


**Figure 5.13: Comparison between XBF measured flow in right coronary artery cases during hyperaemic condition only.** Upper Panel showing scatter plot and lower panel showing Bland-Altman plot. In the Bland-Altman plot, the solid line represents the mean of the differences between measurements and the dotted lines represent the 95% confidence intervals for the mean of the differences between measures.

#### 5.3.3.3 Comparison of blood flow in left coronary artery cases.

Patients in whom coronary flow was measured in the left coronary artery were analysed separately for any correlation between XBF and thermodilution flow. The results of the comparison between all LCA cases in both rest and hyperaemia are illustrated in figure 5.14. There was no correlation between XBF blood flow and thermodilution blood flow when cases in rest and hyperaemia were assessed together. The rest and hyperaemic conditions were compared. There was no correlation seen when LCA blood flow measured by XBF and thermodilution when rest and hyperaemic conditions were compared separately.

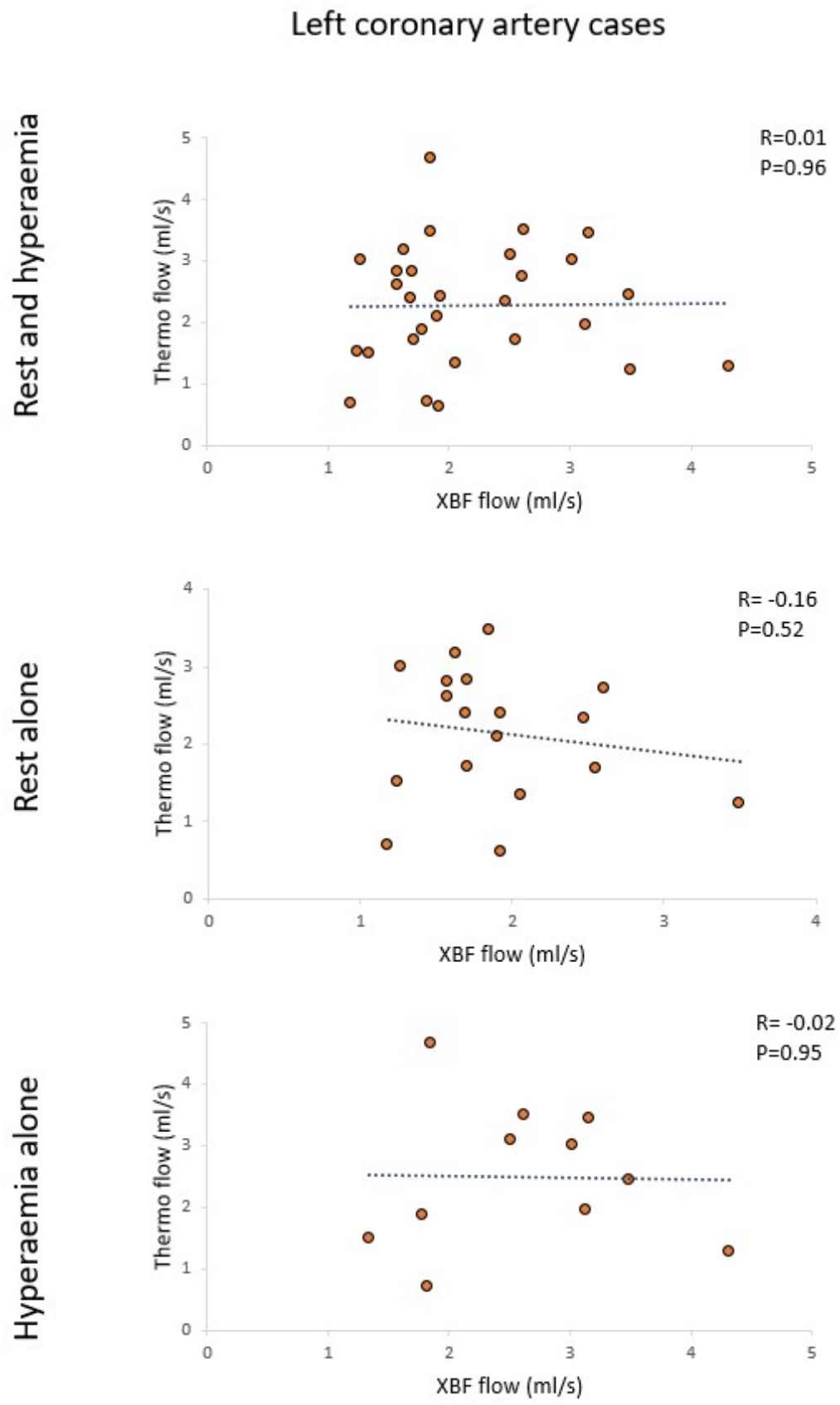


**Figure 5.14: Scatter plots showing the relationship between XBF blood flow and thermodilution blood flow in left coronary arteries.**

#### 5.3.3.4 Comparison of coronary flow reserve

Coronary flow reserve (CFR) was calculated by both XBF and thermodilution methods in those patients with rest and hyperaemic flow data available in the same condition (i.e., pre-PCI or post PCI) and compared to see if there was any correlation. Thermodilution CFR ($CFR_{thermo}$) was calculated not by the standard method of bolus thermodilution and mean transit time, but coronary blood flow calculated using continuous thermodilution and then CFR calculated using the ratio of hyperaemic blood flow to the rest blood flow. However, it must be borne in mind that measuring absolute coronary blood flow has only been validated during the maximal hyperaemic state. Therefore, it is not valid to describe the thermodilution derived ratio of flow during hyperaemia induced by adenosine and at rest as actual CFR. Furthermore, the saline infusion itself may have an impact on the degree of hyperaemia, therefore the rest phase may not be true rest phase.

The results are summarised in table 5.8 and illustrated in figure 5.15. There was only weak correlation between CFR measured by XBF method and that measured by thermodilution method with a Pearson's coefficient of 0.31.

In cases where there were paired values for blood flow with XBF and thermodilution in both rest and hyperaemia, CFR was calculated using XBF ($CFR_{XBF}$) and thermodilution ($CFR_{thermo}$) were compared in right and left coronary arteries separately. $CFR_{XBF}$ and $CFR_{thermo}$ showed good correlation with Pearson's coefficient of 0.61 in RCA but there was no correlation between $CFR_{XBF}$ and $CFR_{thermo}$ in LCA cases. However, when considering the individual coronary arteries separately, the sample sizes were small and there

was relatively wide scatter and the assumptions about the distribution of the data may not hold true.

| Patient No | Vessel | XBF | thermo | CFR XBF | CFR Thermo |
|---|---|---|---|---|---|
| 5 | RCA | 1.58 | 2.60 | 1.63 | 1.58 |
| 5 | RCA | 2.58 | 4.10 | | |
| 13 | RCA | 1.23 | 1.80 | 2.31 | 1.39 |
| 13 | RCA | 2.83 | 2.50 | | |
| 19 | LAD | 1.85 | 3.46 | 1.71 | 0.99 |
| 19 | LAD | 3.16 | 3.43 | | |
| 22 | LAD | 1.57 | 2.81 | 1.67 | 1.24 |
| 22 | LAD | 2.62 | 3.49 | | |
| 23 | RCA | 1.99 | 2.90 | 1.32 | 0.97 |
| 23 | RCA | 2.63 | 2.80 | | |
| 26 | LAD | 1.63 | 3.17 | 1.14 | 1.47 |
| 26 | LAD | 1.85 | 4.65 | | |
| 30 | LAD | 1.71 | 2.82 | 1.77 | 1.06 |
| 30 | LAD | 3.03 | 2.99 | | |
| 31 | LCx | 2.06 | 1.33 | 1.52 | 1.46 |
| 31 | LCx | 3.13 | 1.93 | | |
| 34 | RCA | 1.27 | 1.60 | 0.79 | 0.81 |
| 34 | RCA | 1.00 | 1.29 | | |
| 36 | RCA | 1.16 | 1.50 | 1.92 | 1.13 |
| 36 | RCA | 2.22 | 1.70 | | |
| 37 | LAD | 2.56 | 1.69 | 1.37 | 1.44 |
| 37 | LAD | 3.50 | 2.43 | | |
| 39 | LAD | 3.50 | 1.22 | 1.23 | 1.03 |
| 39 | LAD | 4.32 | 1.26 | | |
| 40 | LAD | 1.91 | 2.09 | 0.94 | 0.89 |
| 40 | LAD | 1.79 | 1.87 | | |
| 41 | RCA | 1.20 | 2.00 | 1.97 | 1.05 |
| 41 | RCA | 2.35 | 2.10 | | |
| 43 | LAD | 1.19 | 0.68 | 1.54 | 1.03 |
| 43 | LAD | 1.82 | 0.70 | | |
| 45 | LAD | 1.93 | 2.40 | 1.30 | 1.28 |
| 45 | LAD | 2.52 | 3.07 | | |

LCA- Left coronary artery, RCA- Right coronary artery, LAD- Left anterior descending artery, LCx- Left circumflex artery, Thermo – thermodilution.

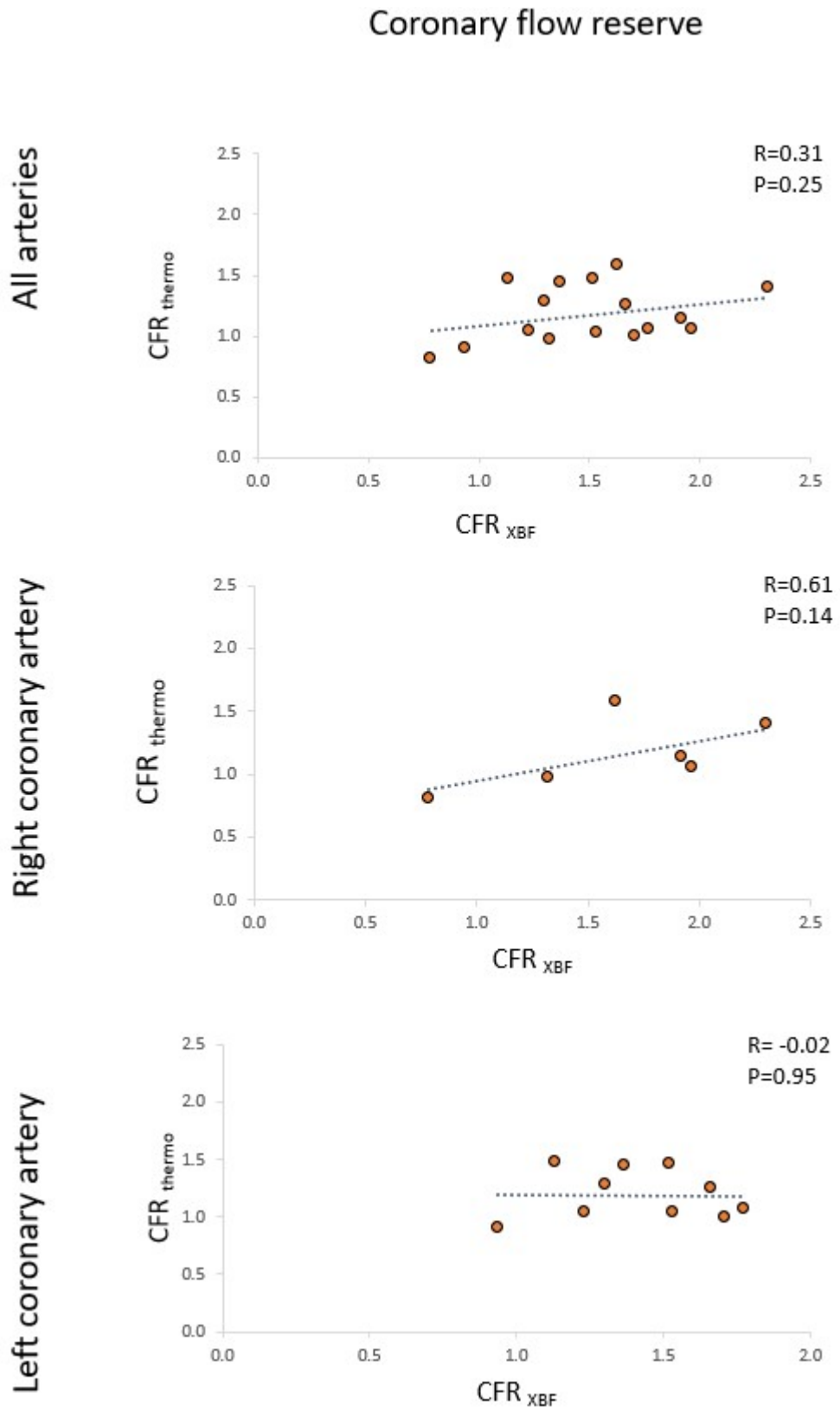


**Figure 5.15: Scatter plots showing the relationship between coronary flow reserve calculated from XBF method and thermodilution methods.**

#### 5.3.3.5 Impact of microcatheter use in left coronary artery cases.

LCA cases were categorised according to the type of microcatheter used for saline infusion. Results were compared within each of the categories to ascertain if their X-ray and thermodilution measured coronary blood flow were correlated when a specific microcatheter was used for the thermodilution technique. Only one LCA patient (Patient 9) in group A (no microcatheter used) had suitable images for analysis. In groups B and C there were 5 and 6 patients with images suitable for analysis. These data are presented in figure 5.16. There was no significant correlation found between XBF measured coronary flow and thermodilution measured flow in LCAs in group B and group C.

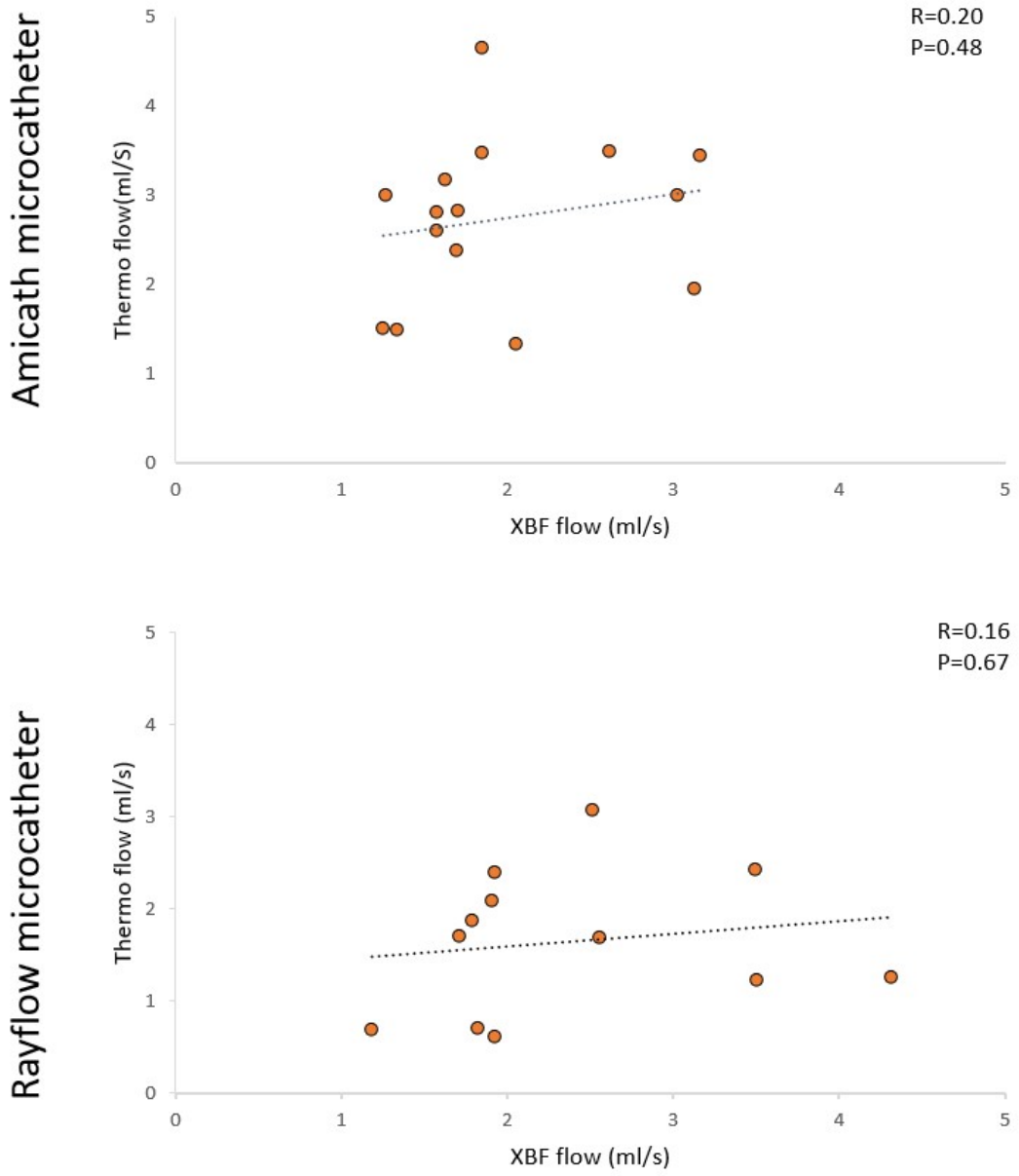


**Figure 5.16: Relationship between XBF blood flow and thermodilution blood flow in LCA cases in group B & group C (Amicath and Rayflow microcatheters respectively).**

### 5.3.3.6 Impact of saline infusion on hyperaemia.

De Bruyne et al reported that infusing saline through the Rayflow microcatheter at a rate of 15ml/min or more induced steady state hyperaemia (De Bruyne, B. et al., 2017). This data was published after the completion of

our research studies and therefore we were not aware of this at the time. The thermodilution data was analysed retrospectively to verify if we observed similar findings. In patients whom thermodilution measured blood flow was available in both rest and adenosine induced hyperaemic state are available are presented in table 5.9

**Table 5.8: Results of thermodilution data in patients with paired results during rest and hyperaemia (induced by adenosine)**

| Patient No | Vessel | Condition | Microcatheter | Thermo Flow ml/s | Ratio of hyperaemic flow/rest flow |
|---|---|---|---|---|---|
| 5 | RCA | rest | None | 2.6 | 1.58 |
| 5 | RCA | hyperaemia | | 4.1 | |
| 13 | RCA | rest | None | 1.8 | 1.39 |
| 13 | RCA | hyperaemia | | 2.5 | |
| 19 | LAD | rest | Amicath | 3.46 | 0.99 |
| 19 | LAD | hyperaemia | | 3.43 | |
| 22 | LAD | rest | Amicath | 2.81 | 1.24 |
| 22 | LAD | hyperaemia | | 3.49 | |
| 23 | RCA | rest | None | 2.9 | 0.97 |
| 23 | RCA | hyperaemia | | 2.8 | |
| 26 | LAD | rest | Amicath | 3.17 | 1.47 |
| 26 | LAD | hyperaemia | | 4.65 | |
| 30 | LAD | rest | Amicath | 2.82 | 1.06 |
| 30 | LAD | hyperaemia | | 2.99 | |
| 31 | LCx | rest | Amicath | 1.33 | 1.46 |
| 31 | LCx | hyperaemia | | 1.93 | |
| 34 | RCA | rest | None | 1.6 | 0.81 |
| 34 | RCA | hyperaemia | | 1.29 | |
| 36 | RCA | rest | None | 1.5 | 1.13 |
| 36 | RCA | hyperaemia | | 1.7 | |
| 37 | LAD | rest | Rayflow | 1.69 | 1.44 |
| 37 | LAD | hyperaemia | | 2.43 | |
| 39 | LAD | rest | Rayflow | 1.22 | 1.03 |
| 39 | LAD | hyperaemia | | 1.26 | |
| 40 | LAD | rest | Rayflow | 2.09 | 0.89 |
| 40 | LAD | hyperaemia | | 1.87 | |
| 41 | RCA | rest | None | 2 | 1.05 |
| 41 | RCA | hyperaemia | | 2.1 | |
| 43 | LAD | rest | Rayflow | 0.68 | 1.03 |
| 43 | LAD | hyperaemia | | 0.7 | |
| 45 | LAD | rest | Rayflow | 2.4 | 1.28 |
| 45 | LAD | hyperaemia | | 3.07 | |

In most of the cases the thermodilution measured flow increased after induction of hyperaemia with adenosine. The ratio of the hyperaemic flow and rest flow should represent $CFR_{thermo}$, however as thremodilution flow was not validated in non-hyperaemic state, it is not strictly correct to call it CFR. The mean of $CFR_{thermo}$ measured in all patients is 1.18 with a standard deviation of 0.23. These values were similar when the patients with different microcatheter groups were compared mean $CFR_{thermo}$ of 1.2 and 1.13 for the Amicath group and Rayflow, respectively. Due to the small sample size, it is difficult to draw any definite conclusions regarding the ability of saline infusion to induce maximum hyperaemia.

#### 5.3.3.7 Impact of quality of images

As explained in section 5.3.2, the quality of X-ray images was variable. I performed analysis of RCA cases with only the best quality images to assess the impact of image quality on the results. The results are presented in figure 5.17 and there is better correlation when good quality images are used for analysis. I undertook a similar analysis of selected LCA cases with good quality images but did not see a meaningful relationship between XBF and thermodilution measured flow.

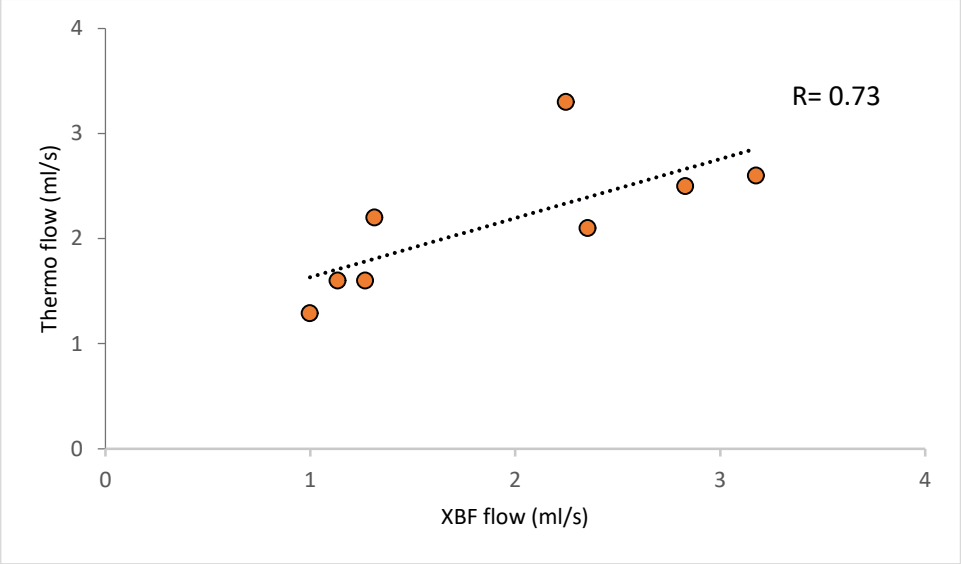


**Figure 5.17: Relationship between XBF blood flow and thermodilution blood flow in RCA cases with good image quality only; both rest and hyperaemic.**

### 5.3.4 Observer variability

The results obtained by two independent observers in a select number of cases were compared for inter-observer variability and results obtained by the same observer on 2 different occasions for intra-observer variability.

#### 5.3.4.1 Inter-observer variability

A select number of images were analysed by two observers, the author, and Dr Andrew Davies (AD) independently and blinded to each other's results. A rectangular ROI was chosen, and care was taken to avoid the aortic root contrast spill. Other than that, observers were free to choose the size and position of the ROI and the frames to be analysed. XBF blood flow results were obtained and compared. The results indicate good reproducibility of results and agreement between observers as shown in figure 5.18.

#### 5.3.4.2 Intra-observer variability

A select number of images were analysed by the author twice on two separate days selecting a new ROI and frames for analysis independently. There was excellent correlation and agreement between the results obtained in both analyses demonstrating excellent intra-observer repeatability as illustrated in figure 5.19.

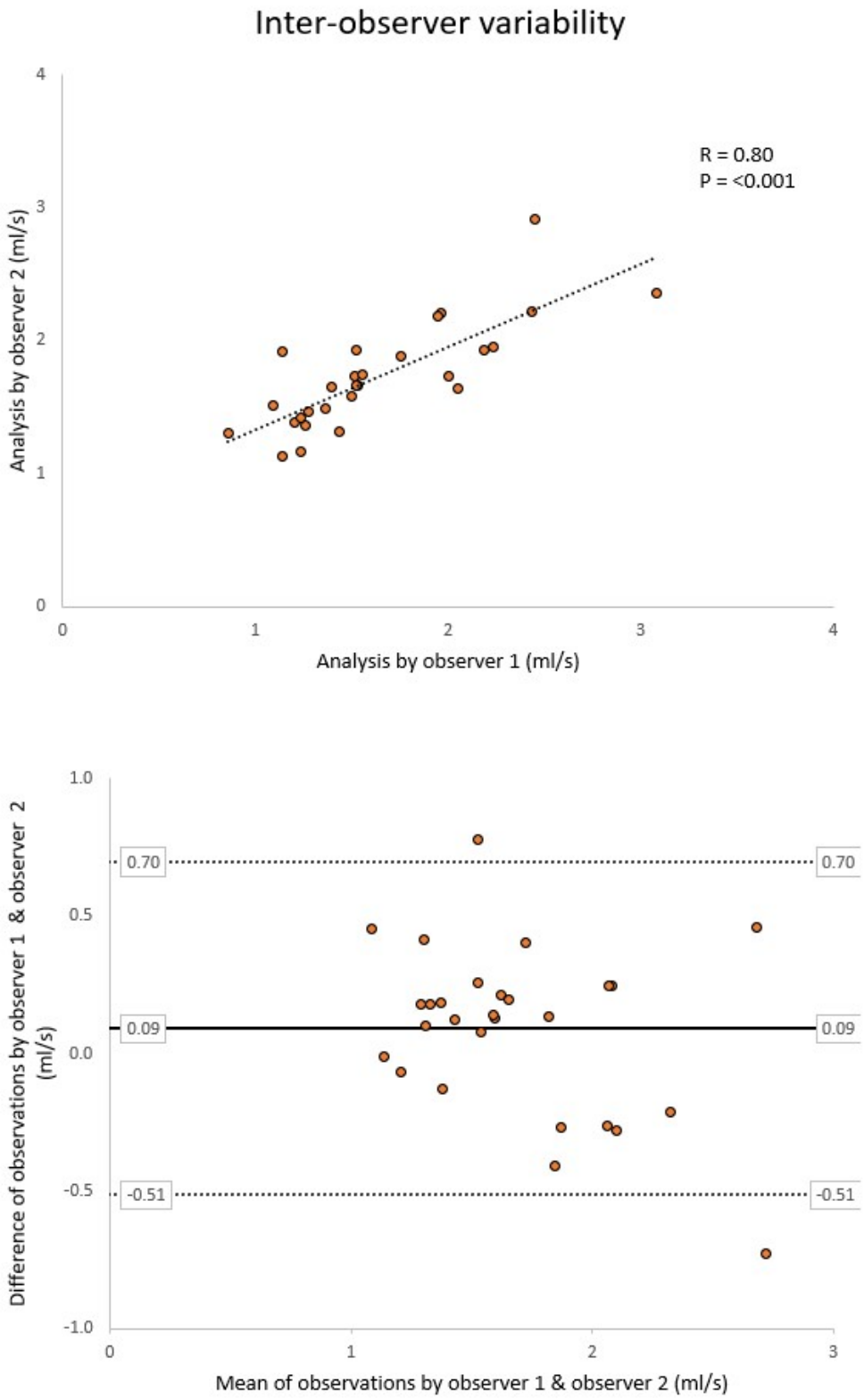


**Figure 5.18: Comparison of analyses by 2 independent observers to assess inter-observer variability of XBF blood flow.** Upper Panel showing scatter plot and lower panel showing Bland-Altman plot. In the Bland-Altman plot, the solid line represents the mean of the differences between measurements and the dotted lines represent the 95% confidence intervals for the mean of the differences between measures.

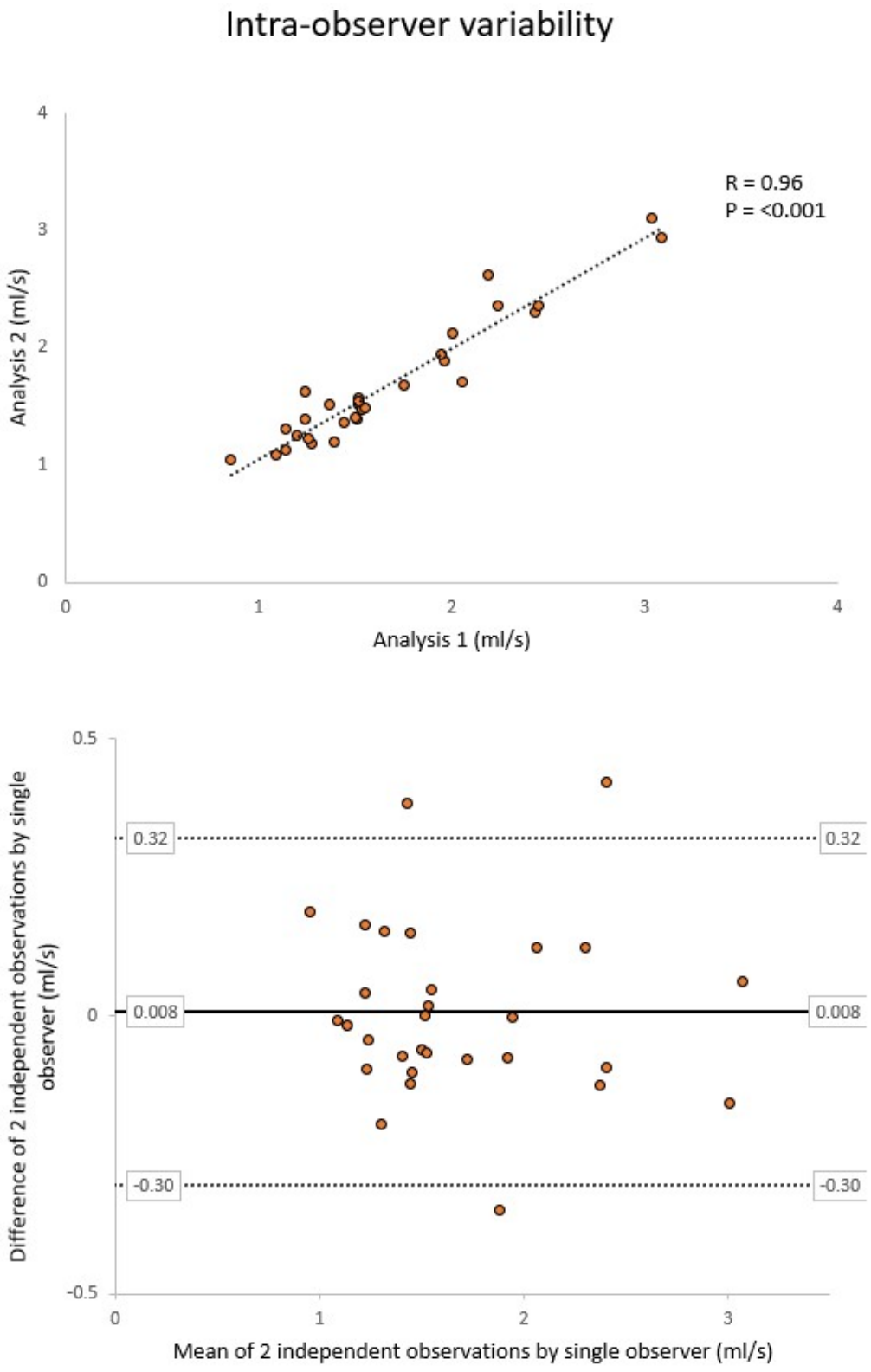


**Figure 5.19: Comparison of 2 independent XBF blood flow analyses of same images by the same observer.** Upper Panel showing scatter plot and lower panel showing Bland-Altman plot. In the Bland-Altman plot, the solid line represents the mean of the differences between measurements and the dotted lines represent the 95% confidence intervals for the mean of the differences between measures.

## 5.4 Discussion

In this chapter, the objective was to assess the feasibility of the XBF technique in quantifying coronary blood flow from X-ray signal intensity analysis in humans undergoing routine coronary angiography or coronary intervention for coronary heart disease. We recruited 45 patients attending cardiac catheter procedures at the Leeds General Infirmary and analysed the coronary blood flow using XBF method and compared them to the continuous thermodilution method of coronary blood flow quantification. This study established the feasibility and safety of performing the study protocol in humans. None of the participants suffered any study related complications or increase in length of stay in hospital.

When the XBF flow from all data points were compared to the corresponding blood flow measurement using thermodilution, no significant correlation was seen. There was also no significant correlation between the CFR measurements using the two techniques when all data points were included. It must be borne in mind that continuous thermodilution method of flow quantification was only validated during hyperaemic state and the blood flow measured without pharmacological induction of hyperaemia cannot be regarded as true rest flow and therefore $CFR_{thermo}$ cannot be regarded as true coronary flow reserve.

In contrast, we found that there was good correlation and agreement with little systematic error (bias) between the XBF measured coronary blood flow and thermodilution measured blood flow in right coronary artery, but we did not find any significant correlation between the two in the case of left coronary artery. The blood flow measurements in RCA correlated well when rest and

hyperaemic measurements were analysed separately and when CFR was analysed. On the other hand, there was no correlation seen in the case of LCA cases when rest and hyperaemic measurements were analysed separately or when CFR was analysed.

The inter-observer and intra-observer variabilities were noted to be low and excellent correlation and agreement was noted between analyses by the same observer at different times and between different observers.

Potential factors which may have contributed to discrepant reliability of XBF measurements from the right and left coronary arteries are discussed below.

### 5.4.1 Potential reasons for discrepant results in left coronary artery.

In the validation study, in contrast to the good correlation noted in RCA cases, the LCA cases did not show any correlation between XBF and thermodilution. There are some important anatomic differences between RCA and LCA. The RCA is devoid of any major branches that supply the left ventricle until it bifurcates in the distal vessel. The LCA on the other hand divides early into LAD and LCx and each of these major branches further giving off sizable side branches early (Loukas et al., 2013). This can cause problems with thermodilution method, especially if a dedicated microcatheter is not used for the delivery of saline. In the human validation study of the thermodilution method of volumetric blood flow quantification, there were almost three times as many RCAs studied as there were LCAs (Aarnoudse et al., 2007). So, it is not clear whether the thermodilution method is accurate in LCA. We did not use this criterion for patient selection in our study and that may have impacted on the flow calculation using thermodilution by introducing error due to

diversion of the saline to side branches. The XBF method can also be affected by this during calibration sequence if the contrast can be differentially directed to the LAD or LCx branches.

There are also differences in flow patterns in right and left coronary arteries. The majority (85%) of the blood flow in LCA occurs during diastole but in RCA the blood flow is not as dominant in diastole and in fact has a systolic predominance. This is thought to be due to the higher myocardial compression forces acting on LCA during systole and the resultant retrograde flow which is more pronounced. This may cause some of the contrast injected during the calibration sequence to spill out of the left coronary artery during systole which could introduce error. The posterior descending branch of RCA is subject to the similar forces generated by the left ventricular myocardium and exhibits the same flow pattern as the LCA (Chatzizisis et al., 2007). It is possible that the difference in flow pattern could have influenced the discrepant results in LCA.

In thermodilution method, adequate mixing of blood with the infused saline is necessary to obtain reliable results. The proponents of this method used a specially designed microcatheter (Rayflow), which only became commercially available during the very late stages of the project (Aarnoudse et al., 2007). Although prior to that we tried a different microcatheter (Amicath) for this purpose in the LCA cases, this was cumbersome. There are differences in design of these microcatheters which have been explained in detail earlier in section 5.2.4.3. It can be argued that not using the dedicated Rayflow microcatheter in most cases led to the inadequate mixing of saline with contrast agent. It would be interesting to study the impact of different

microcatheters on thermodilution method. We were however hampered by time constraints in pursuing this study. In the analysis of results from different groups of patients according the microcatheter used, we did not find any significant differences between the two microcatheter groups.

In LCA cases, we had to choose a region of interest for quantification of pixel intensity that corresponded to the area of myocardium supplied by the artery of interest (LAD or LCx). Our choice of ROI and the division of LAD and LCx territories were arbitrarily based on the extent of the artery branches. It is possible that this could have been the source of significant error. Further the impact of overlapping myocardial territories of LAD and LCx is a problem only affecting LCA as studies involving RCA, all the contrast in the myocardium would be in the RCA territory.

### 5.4.2 Difficulties in measuring coronary flow from X-ray.

The image intensity of a contrast filled vessel is dependent on several factors such as patient's size and body habitus, X-ray beam energy, projection angle, X-ray image detector position and the performance of the anti-scatter grid.

In biological systems there is overlap of various tissues which impart different intensity change depending on the ability of the X-rays to penetrate the tissue. There is overlap of different coronary territories when imaging the heart. Scatter is another problem. Some of the X-rays are invariably scattered by the tissues which is difficult to quantify. So, there will be some degree of inherent error in any X-ray based technique.

Any movement, especially breathing movements and the heart movement with each contraction poses the biggest challenge when utilising subtracted X-ray images for analysis. Cardiac catheterisation is undertaken without general

anaesthesia and most patients can be asked to remain still, to limit voluntary movements. The ability to hold the breath varies from patient to patient and depends on their clinical condition, haemodynamic situation, comorbidities, and effect of medications. A patient who can hold the breath for 10-15 seconds can help avoid breathing movements becoming a problem. It is difficult to correct for heart motion especially in presence of ectopic beats or arrhythmias. But using images in the same phase of the cardiac cycle offers a way to overcome the effects of cardiac motion.

### 5.4.3 Sources of error in XBF method

One of the sources of error in XBF method are the assumptions that are made for this method. During the calibration sequence, the injection made at low flow rate of 1ml/s is assumed to flow into the coronary artery completely so that all the iodine in the injected contrast agent goes to the region of interest. This depends on the catheter being well engaged coaxially at the coronary ostium. Some spillage of contrast into the aortic root was seen, especially in systole. In LCA, this was more prominent unsurprisingly because most of the coronary flow occurs during diastole. The assumption that all the contrast enters the artery during calibration is crucial to the XBF method.

We also assume that at the higher volume and rate, the measurement sequence injection momentarily replaces all the blood at the coronary ostium with contrast agent, so that the contrast agent flows down the coronary artery at the normal flow rate. It is difficult to verify that this is the case during the measurement injection.

Collateral blood supply to the myocardium in the region of interest is not accounted for when using the XBF method. However, XBF method aims to quantify the coronary blood flow and not the myocardial blood flow.

Any amount of breathing during image acquisition causes problems with data analysis (figure 5.20). However, if the breathing is towards the end of the sequence, after the contrast has started to accumulate in the myocardium, the data may still be analysable by disregarding the later frames in a sequence.

End expiration or mid inspiration was found to be a better respiratory phase for breath hold, to ensure that the guiding catheter was not dislodged from the coronary ostium. Practising holding breath beforehand increased the chances of obtaining good quality images. We learnt about the most suitable angiographic projection for different coronary arteries and choosing the right field of view. Early experience was invaluable in developing the catheterisation laboratory team’s familiarity with the protocol.

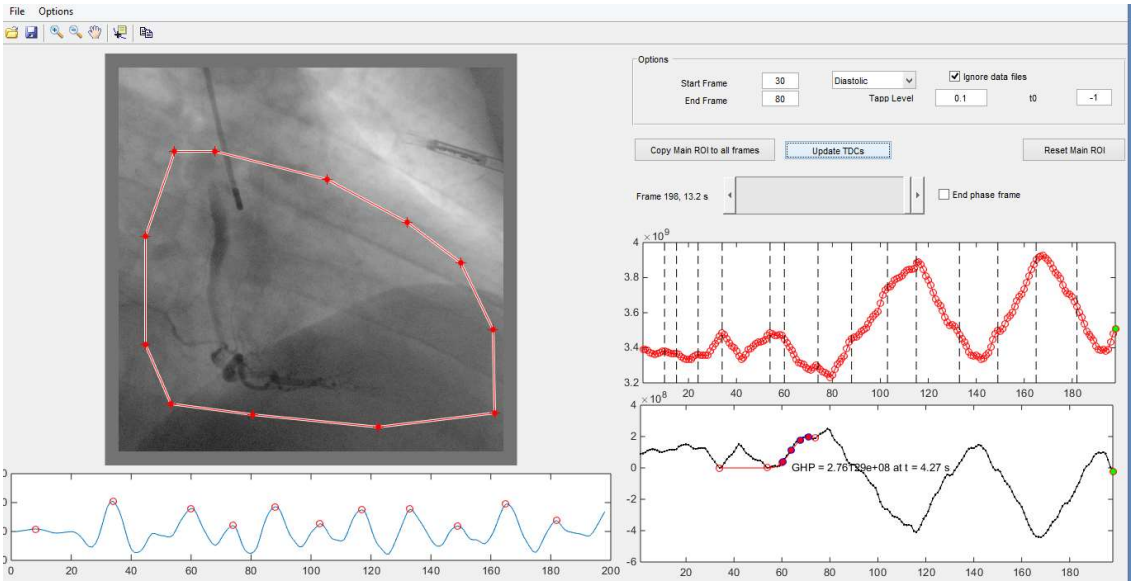


**Figure 5.20 Example of breathing movements producing significant problems with data analysis.** This is an earlier version of the XBF software. The time intensity curve of the right-hand side is dominated by changes in intensity due to changing tissue overlap during breathing. In this case, the image was not suitable for analysis.

Even subtle forms of breathing can cause error in measurement. In the example shown in figure 5.21 and 5.22, breathing movement is evident on careful analysis of the image frames.

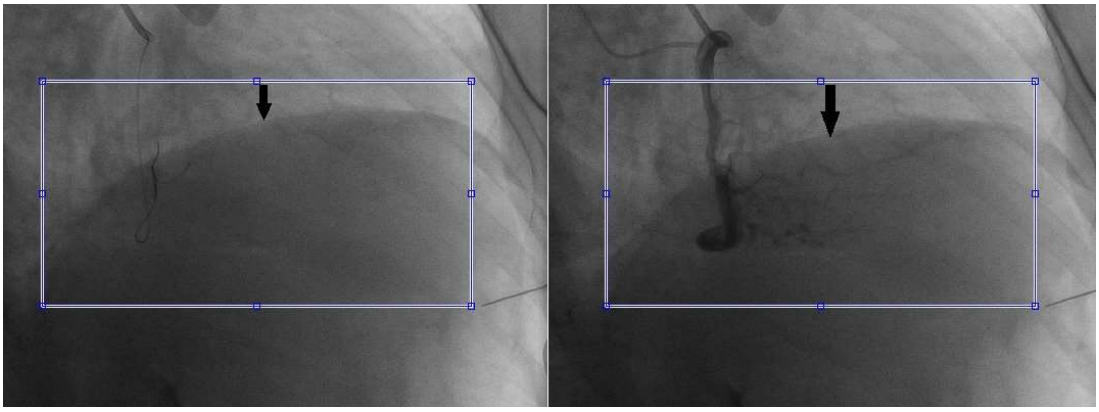

**Figure 5.21: Example of subtle breathing movement obvious by analysing the position of diaphragm as the image sequence progresses.** Here the ROI has remained in the same position and the diaphragm has moved down as evidenced by the increased length of the black arrow that points to the edge of diaphragm on the right panel.

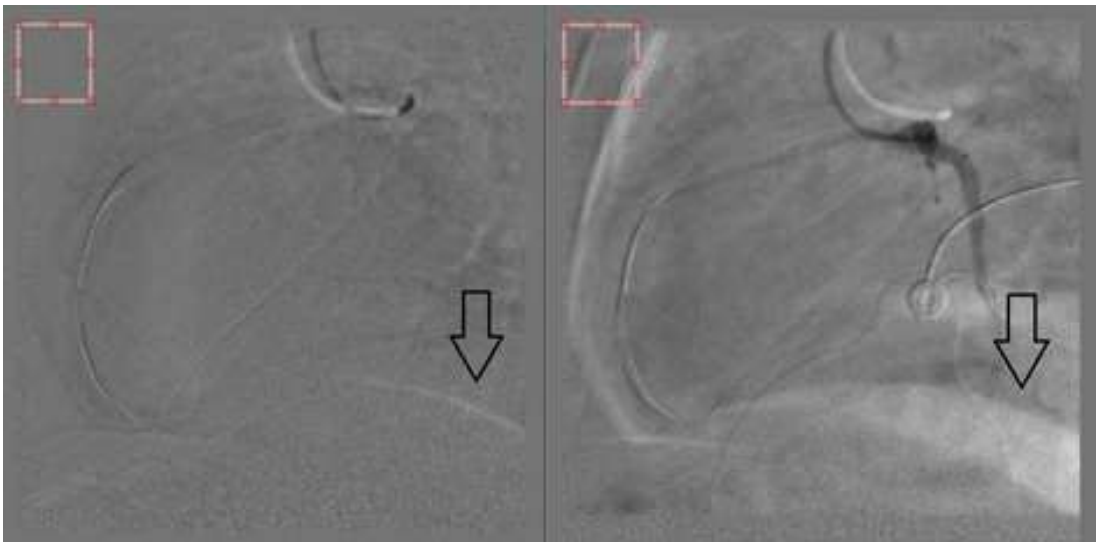

**Figure 5.22: Another example of subtle breathing; when a subtracted image is analysed the diaphragmatic movement is more obvious.** Here in the right panel, the diaphragm has moved down widening the less dense area compared to the image on the left panel.

There is spillage of contrast into aortic root during contrast injection through the guide catheter, especially during the measurement sequence. This is entirely expected as the measurement sequence contrast injection is aimed to replace all the blood at the coronary ostium with contrast. However, some of

this contrast may fill the other coronary artery and introduce error. This effect is understandably much less noticeable during the calibration run which is at a much slower rate. There is some spillage of contrast during the calibration run especially during systole and some amount of error must be being introduced as a result.

In an extreme case, where the RCA was originating from the left coronary sinus (an anatomical variant), this effect can be seen in a much more pronounced way with all of the coronary tree being filled well during the measurement sequence (figure 5.23). There were less obvious forms of the other coronary artery filling as illustrated in figure 5.24.

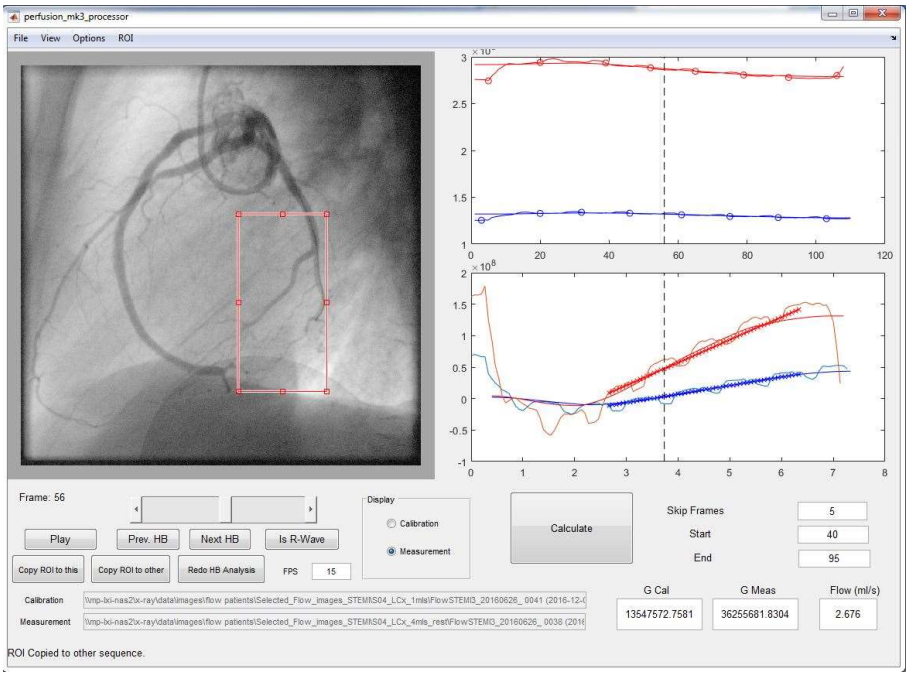


**Figure 5.23: In one of the cases the RCA was originating anomalously from the left coronary sinus and there was good filling of the RCA during injection into LCA no doubt introducing error in flow calculation.** This was not very well noticeable during the calibration run. During the measurement run, there is a lot of spillage of contrast into the aortic root, which in this case filled the RCA which was originating quite close to the LCA.

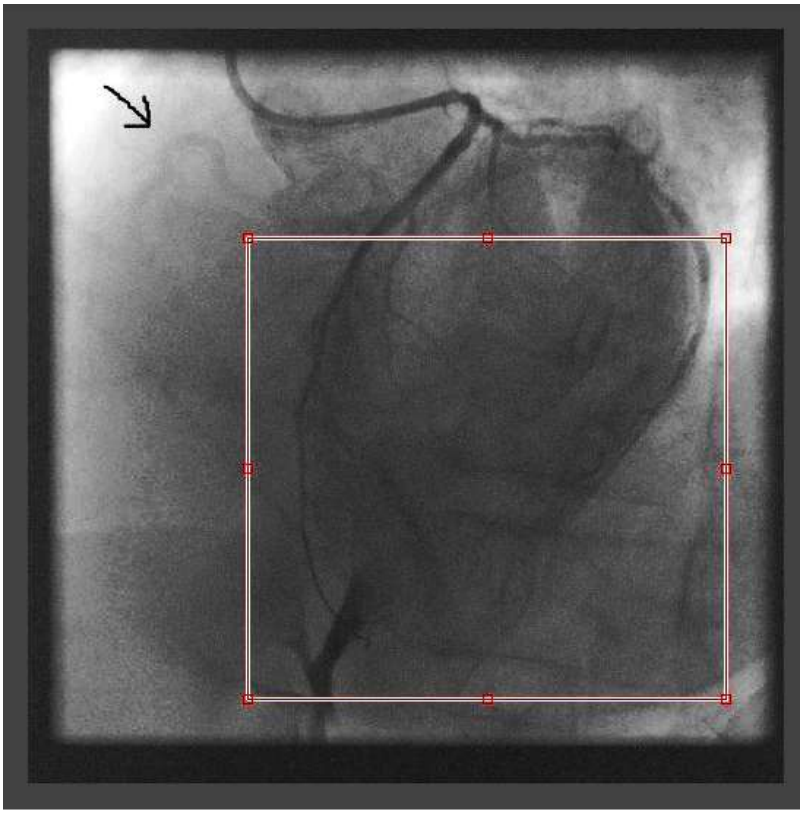

**Figure 5.24: In this example the tortuous RCA is seen filling faintly (black arrow) from spillage of contrast into aorta.**

In some patients the descending aorta can be seen within the region of interest and will no doubt impart error as some of the spilled contrast in the aortic root will be seen to travel down the descending aorta and contribute to the density change. An example is shown in figure 5.25. Sometimes correction can be performed by using a ROI that excludes the aorta, especially if it is only impacting on the ROI marginally. But this is difficult to perform during calibration sequence.

Corrections of ROI must be done just to correct for the spillage of contrast into the aortic root as in the example shown in figure 5.26. In this example the high diagonal could not be included and will impart error.

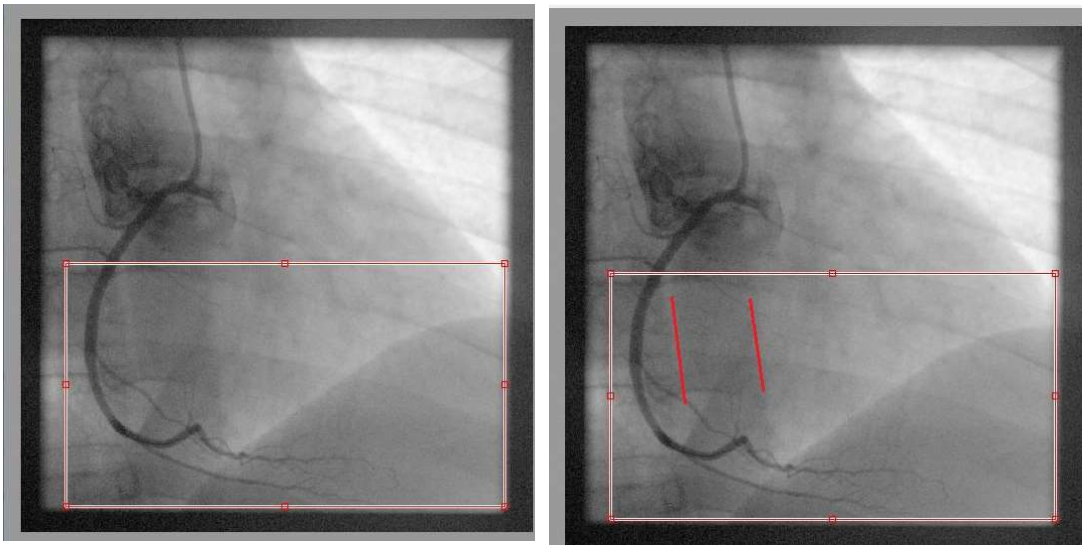

**Figure 5.25: Example where descending aorta is seen to traverse the region of interest introducing error. (Highlighted in red on right panel).** These changes can be subtle and often not recognised until a subtracted image is analysed.

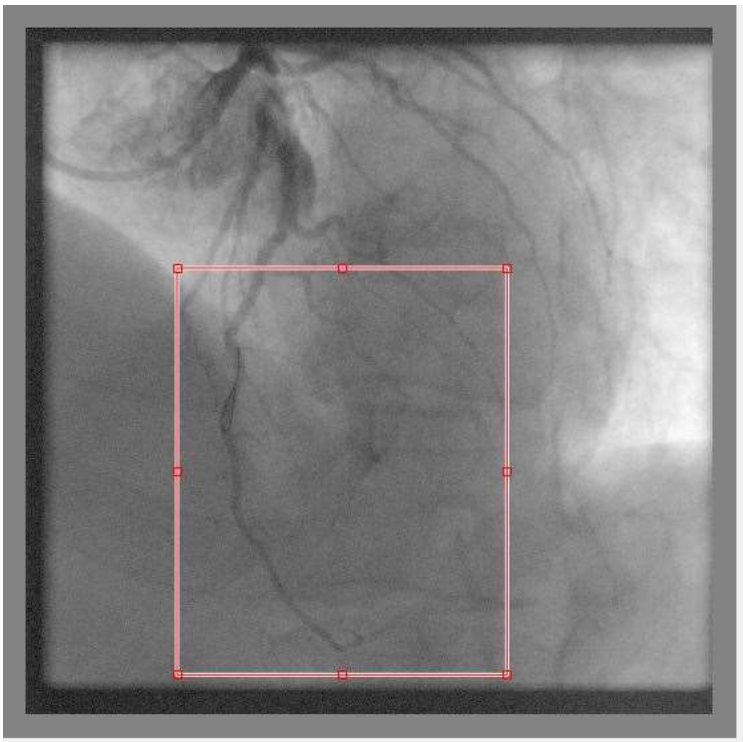

**Figure 5.26: Example of correction for aortic root contrast spillage.** The area close to the catheter has increased density if included in the ROI. This means that in this example of LAD analysis, some of the diagonal territory had to be excluded.

The spillage of contrast can also impart error if there is aortic regurgitation (AR). This is much more difficult to correct as the AR usually imparts density change within the LV cavity which coincides with the ROI. The XBF method in its current form may be unsuitable to use if there is significant AR. This problem is illustrated in figure 5.27.

Frame selection is also very important as the venous phase of the contrast flow through the coronary artery becomes more obvious towards the end of the sequence (figure 5.28). This can be corrected by selecting frames during the earlier coronary artery filling phase of the sequence. However, different areas of myocardium may clear at varying rates. For e.g., in the case of a septal branch from the LAD which is close to the catheter contrast that may go through arterioles and capillaries and reach the venous system quickly and possibly even before an apical branch of the same artery sees any contrast. On angiography, we notice contrast in the venous system only when most of the contrast is in the vein. So completely correcting for this may be very difficult.

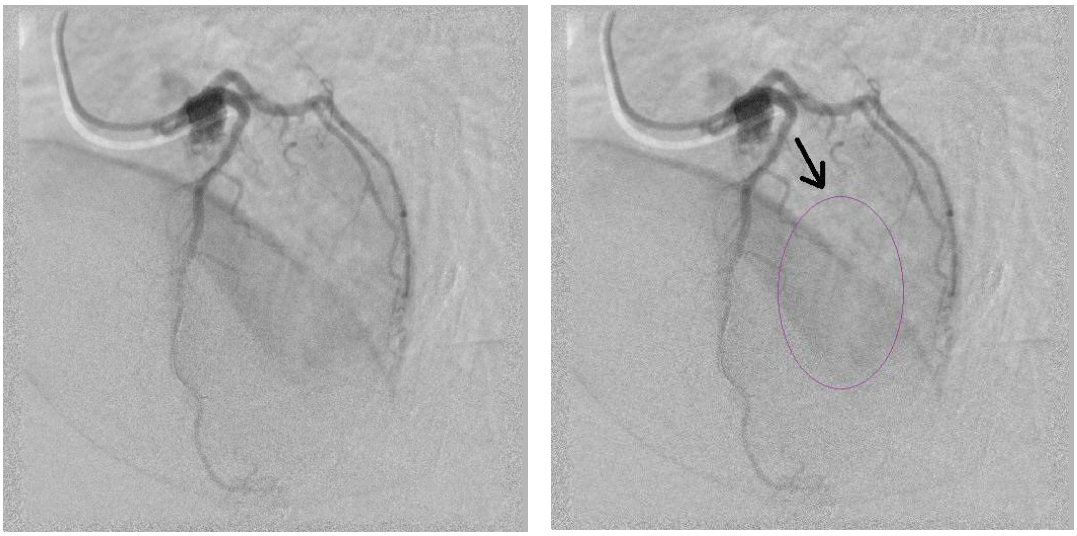

**Figure 5.27: Example of AR imparting density change which is more obvious when a subtracted image is analysed. (Purple oval and black arrow)**

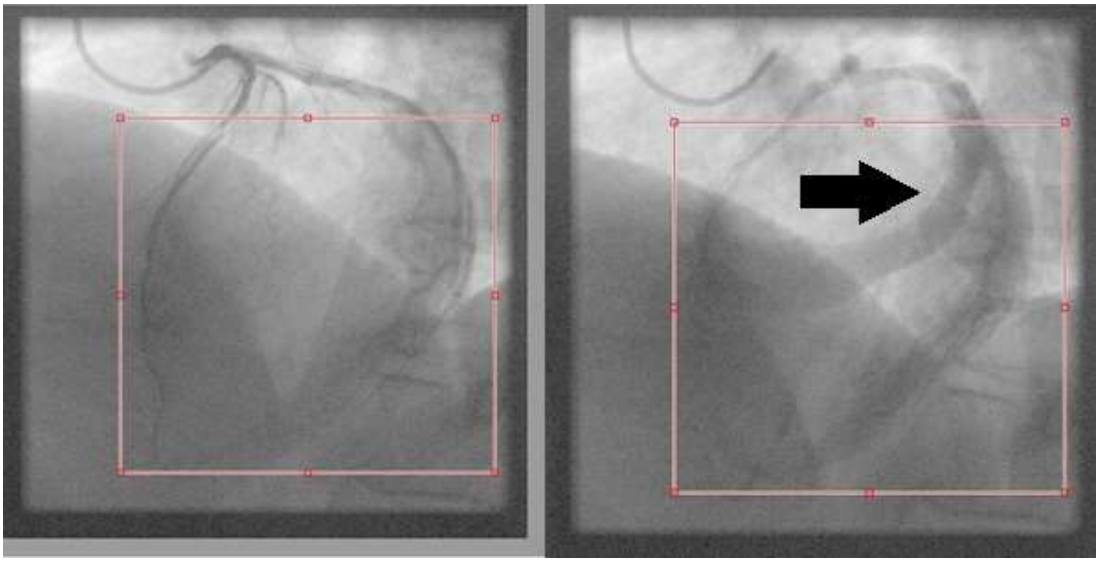

**Figure 5.28: Example where the venous phase is clearly visible during the later frames of the sequence. In this example the coronary sinus (black arrow) is clearly visible during the later phase of the angiogram.**

## 5.5 Limitations in the project and methodology

The ability to hold the breath and remain still is crucial for deployment of the XBF technique. Patients who have conditions that prevent them from doing so are not suitable to undergo blood flow quantification by XBF method.

### 5.5.1 Data capture software and hardware

The data capture software installed on a computer system in one of the catheterisation laboratories sometimes malfunctioned would skip several image frames during data capture. These events were random and unpredictable. The problem was easier to spot when a large number of consecutive frames were not captured as the impact of the skipped frames was obvious to naked eye while playing back the image sequence. But when

the number of skipped frames was small, the effect was not so obvious. These were detected only when the number of image frames in the captured data were compared to the number of frames in the DICOM files. These understandably posed problems to image analysis. Unfortunately, these problems were usually discovered only after the research protocol was completed, which meant that repeat image acquisition could not be undertaken. Furthermore, it was not immediately obvious how to resolve this issue. Although the usual corrective measures such as clearing up disk space on the PC and re-installing the software were undertaken, we could not resolve the problem completely.

### 5.5.2 Effect of contrast agent and saline on coronary circulation

The intracoronary injection of contrast agents has long been recognised to produce hemodynamic effects, which are mainly attributable to the physical and chemical properties of the contrast material (De Bruyne, Bernard et al., 2003; Tatineni et al., 1992). Injection of contrast agent induces some degree of hyperaemia. It has been known for decades that contrast agent injection into coronary arteries produces an increase in coronary blood flow and has recently been used to perform contrast FFR (Guzman and West, 1959; Johnson et al., 2016). Contrast injection itself can therefore produce alterations in CBF (Bassan et al., 1975; Baile et al., 1999; KLOSTER et al., 1972). However, hyperaemic blood flow induced by adenosine should be relatively unaffected. The contrast medium that we use is significantly more viscous than human blood, which is further affected by temperature. The high viscosity and osmolality relative to blood, sodium content, and pH are some of the properties that are thought to cause these hemodynamic effects.

The rate of clearance of the contrast depends on number of factors - microvascular resistance, myocardial scar, coronary venous pressure, and LV end diastolic pressure all of which may affect the trans-myocardial gradient, and the effect of high viscosity in the capillaries. The clearance of contrast could be at a completely different rate to that of blood.

Different available contrast agents and their viscosities are summarised in section 4.3. Excellent results were obtained in the bench experiments using Iohexol 302mg/ml (Omnipaque 140, GE Healthcare, Chalfont St. Giles, UK) which has a comparable viscosity to the blood mimicking fluid used at 1.5 centipoise (cP). The viscosity of whole blood at physiological haematocrit of 45 is about 3.2 cP. It is possible that using a more viscous contrast agent Iodixanol 652mg/mL (Visipaque 320, GE Healthcare, Chalfont St. Giles, UK) which has a viscosity of 11.1 cP at 37degrees, could have had an impact on the analysis. However non-ionic contrast agents have lower osmolality and its effect on blood rheology may be lower (Smedby, 1992). Pijls *et al* noted that isotonic, non-ionic contrast agents with low iodine content such as Iohexol 302mg/ml had only a moderate influence on coronary blood flow compared to hypertonic and ionic contrast agents (Pijls, N.H. et al., 1988). Further studies are required before an ideal contrast agent can be selected.

Similarly, injection of saline into coronary arteries also seems to alter the microvascular resistance and blood flow. De Bruyne *et al* in their study found that intracoronary infusion of saline at a rate 15ml/min or more produced maximal hyperaemia, which could not be augmented by additional intravenous infusion of adenosine (De Bruyne, B. et al., 2017). It is possible that saline and contrast induce varying degrees of hyperaemia which may have impacted on

the results. In theory, measuring the flow using the two techniques at maximal hyperaemia induced by adenosine should compensate for such difference. However, acquiring good quality images with breath hold was challenging during adenosine induced hyperaemia. We achieved that in a smaller number of patients.

### 5.5.3 Normal values and gold standard method of quantifying blood flow to the myocardium

There are few data available about the normal range of CBF rates in humans. This is partly because the flow rates vary according to the amount of myocardium supplied and this is variable in different individuals. In addition, physiological states determine the CBF rates as described previously and therefore variable within the same subject. Furthermore, gender, age and body mass index have been shown to influence the myocardial blood flow rate and may have to be corrected or taken into account when analysing normal ranges of coronary blood flow (Danad et al., 2012). Chareonthaitawee *et al* in their study of myocardial blood flow using PET proved the heterogeneity that exists in normal individuals and highlighted the difficulty in establishing the lower limit of normal myocardial blood flow (Chareonthaitawee et al., 2001).

There is currently no gold standard for measuring coronary blood flow. Although PET is regarded widely as the best method of myocardial blood flow quantification (Kuhle et al., 1992), this method measures the uptake of radioactive tracer by the myocardium and gives blood flow in ml/minute/gram of tissue. It is not possible to easily calculate the myocardial mass supplied by the individual coronary artery and therefore this is not the same as coronary blood flow calculated by XBF method. Furthermore, collateral blood flow is not

accounted for. It was not feasible to perform cardiac PET scanning at LGI as there was no PET scanner on site. In addition, PET scanning would have added additional radiation. Adding a PET scanning protocol, which would invariably have to be scheduled at a separate time and most likely another day, means that the factors influencing the coronary blood flow may be completely different on that day and hence the flow rates could be different too. Arguably, pharmacological agents such as adenosine can correct for this difference by inducing hyperaemia.

Thermodilution method of absolute coronary blood flow estimation is still only used as a research tool more than a decade after it was originally proposed. There are no normal values of coronary flow established yet.

## 5.6 Conclusion

In this chapter, it was demonstrated that the XBF method can be safely undertaken in humans. The results had good agreement when analysed repeatedly and between observers. When compared to the thermodilution method of coronary blood flow quantification, results from XBF method correlated well with good agreement in right coronary artery cases. There was no correlation noted in cases where left coronary artery was studied.

# Chapter 6 -Relationship between X-ray derived coronary blood flow and resistance to Index of microcirculatory resistance and infarct characteristics in acute myocardial infarction.

## 6.1 Introduction

The ability to measure coronary blood flow in real time would potentially be of great value in the setting of acute myocardial infarction. Knowledge of absolute coronary blood flow and myocardial resistance should in theory enable clinicians to assess tissue level perfusion after opening the occluded epicardial coronary artery by primary PCI (PPCI). If reperfusion is deemed to be suboptimal either due to microvascular obstruction or other reasons, patients can be appropriately risk stratified and management strategy modified.

In the previous chapter, the XBF coronary blood flow was seen to correlate with thermodilution measured coronary blood flow in right coronary artery. Although the XBF blood flow in the left coronary artery did not show similar correlation, this could have been mainly due to technical issues with the thermodilution technique.

In this chapter, the XBF technique was applied in STEMI patients to determine whether XBF derived coronary blood flow and myocardial resistance could predict outcomes measured by subsequent cardiovascular magnetic resonance imaging (CMR). In patients assessed by a pressure wire in the catheter laboratory, Carrick *et al* reported that high IMR values measured after reperfusion were associated with subsequent left ventricular dysfunction and

adverse clinical outcomes following PPCI (Carrick et al., 2016a). Payne *et al* demonstrated that microvascular resistance measured by IMR during PPCI predicts myocardial salvage and left ventricular ejection fraction (LVEF) (Payne et al., 2012).

The intention of the study described here was to investigate if myocardial resistance and coronary blood flow measures calculated from the XBF method would correlate with CMR-derived infarct size, myocardial salvage, left ventricular remodelling and change in left ventricular ejection fraction. If this were demonstrated to be the case, the XBF method could have a significant clinical role in risk stratification after primary PCI in STEMI patients.

## 6.2 Methods

Patients who present with STEMI are often very ill and revascularisation should be performed promptly. To avoid any delay in completion of primary PCI, the research protocol commenced only after PCI and stenting of the infarct-related artery (IRA) had been completed.

### 6.2.1 Ethical amendment

There were modifications that needed to be made to the research protocol and consent process to study patients presenting with acute STEMI. A substantial amendment was made to the research protocol to include patients presenting with ST elevation MI. The application for ethical approval of this amendment was made to the NHS Health Research Authority, Research Ethics Committee, Yorkshire, and the Humber- Leeds Bradford and approved on 15 April 2016 (Appendix 6).

### 6.2.2 Patient selection

Patients attending the cardiac catheterisation laboratory at the Leeds General Infirmary for treatment of acute STEMI were screened for inclusion into the study. STEMI was defined as the occurrence of ongoing chest pain for at least 30 min associated with ST segment elevation >2 mm in at least 2 contiguous leads. Detailed inclusion and exclusion criteria are given in table 6.1. Patients were approached after informed consent for the PPCI procedure was obtained and a screen for exclusion criteria was undertaken. The research protocol was briefly explained and if agreeable to take part, the research consent form was signed. PPCI was undertaken as per standard practice in accordance with guidelines (Windecker et al., 2014). All the patients were loaded with dual anti-platelet therapy Aspirin 300mg and Ticagrelor 180mg (or Clopidogrel 600mg). Unfractionated Heparin was used in all patients to achieve anticoagulation during PPCI. Decisions about aspiration thrombectomy and use of glycoprotein 2b/3a inhibitors were left to the operator's discretion.

**Table 6.1: Inclusion and Exclusion criteria**

| | |
|---|---|
| **Inclusion criteria** | All patients attending cardiac catheter laboratory at LGI for primary PCI. |
| **Exclusion criteria** | Patients with previously known multi-vessel disease.<br>Patients < 18 years old.<br>Pregnancy / breast feeding.<br>Inability to provide informed consent.<br>Previous coronary artery bypass grafts.<br>Asthma or significant respiratory impairment.<br>Patient weight > 100 kg.<br>Resting heart rate > 80 /min.<br>Atrial Fibrillation.<br>Previously known renal impairment (serum creatinine>200 μmol/l or eGFR<60ml/min/1.73 $m^2$).<br>Previous sensitivity to iodine-based contrast media.<br>Permanent pacemaker / implantable cardioverter-defibrillator device.<br>Contraindications for CMR study- claustrophobia, metallic foreign bodies, or implants.<br>More than two previous imaging techniques involving ionising radiation exposure within 6 months of recruitment, or similar planned for the 6 months following participation in this study.<br>Any other condition considered by the investigators likely to compromise patient safety or successful data collection.<br>Haemodynamic instability. |

LGI- Leeds General Infirmary, PCI- Percutaneous coronary intervention, STEMI- ST elevation myocardial infarction, eGFR- estimated glomerular filtration rate, CMR- cardiac magnetic resonance.

### 6.2.3 Changes to consent process

Patients with STEMI present as emergency and PPCI should be performed without delay. We designed a shortened version of the patient information leaflet (Appendix 7). Care was taken to exclude patients who were too unwell or had haemodynamic instability. Those who had impaired ability to consent for the study such as after use of opiates for analgesia were also excluded.

### 6.2.4 Study protocol

#### 6.2.4.1 Equipment set up.

The RadiAnalyser Express console (St Jude Medical, Minnesota, US) was used and a pressure wire (Certus, St Jude Medical, Minnesota, US) was connected and calibrated. The pressure wire was then inserted into the IRA alongside the coronary guidewire used for the PPCI. The aortic pressure and the pressure recorded by the pressure wire were equalised at the ostium of the coronary artery as per standard practice. The pressure wire was then advanced further along the IRA to at least 6cm beyond the ostium and beyond the stented segment.

The X-ray protocol was essentially the same as described in the previous chapter. An appropriate X-ray projection angle was chosen to separate out the coronary territories (right anterior oblique, RAO or lateral for RCA, left anterior oblique-cranial, LAO cranial or lateral for LCA). Large field of view was chosen without any magnification or filters. An automated pressure injector (Angiomat Illumena, Mallinckrodt, St Louis, Missouri) was filled with contrast agent Iodixanol 652mg/mL (Visipaque 320, GE Healthcare, Chalfont St. Giles, UK), pre-warmed and kept warm in the pump. After ensuring that the system is free

of air, it was connected to the manifold attached to the guide catheter. Contrast injection was performed with the patients holding their breath in expiration. Care was taken to ensure that the guide catheter was engaged well at the coronary ostium.

#### 6.2.4.2 X-ray calibration sequence

Calibration sequence was performed by acquiring the X-ray images at 15 frames a second and then after about 2 seconds the contrast injection was started at 1ml/s. The pressure injector delivered this for 4 seconds at 200psi and the rate of injection was set constant. The acquisition was continued until the contrast agent was seen to exit the coronary venous system.

#### 6.2.4.3 X-ray measurement sequence - rest

The pressure injector was then set to deliver contrast agent at 3-5ml/s, depending on the size of the coronary artery. The injection was delivered for 4 seconds in total at 200psi at the constant rate. The acquisition was performed during breath-hold and until contrast agent was seen in the venous system.

#### 6.2.4.4 Measurement of index of microcirculatory resistance

As opposed to the continuous thermodilution employed in Chapter 5, pressure wire derived IMR measurements were used in the STEMI cohort in this study. This was because in this study, the intention was to assess whether XBF-derived blood flow and resistance predicts adverse infarct parameters on CMR, rather than compare XBF-derived blood flow measurements to another method of coronary blood flow quantification. IMR has been shown to predict clinical outcomes following STEMI (Carrick et al., 2016a). As microcatheters

are not required for IMR measurement, an IMR-based protocol is more appropriate and less time intensive to deploy in the setting of STEMI.

As explained already, the pressure and temperature sensitive guidewire was inserted into the infarct related artery, after calibration and equalisation, placed in the distal part of the IRA. The appropriate mode (CFR/thermo) was selected on the RadiAnalyser Express console that can record both temperature and pressure. Boluses of saline (3ml) were hand injected into the guiding catheter briskly to generate thermodilution curves. Hyperaemia was induced using adenosine or regadenoson. The mean transit time (Tmn) was calculated from the curves and the distal coronary pressure (Pd) was obtained from the Pressure wire. IMR was then calculated as

$$IMR = Pd \times Tmn$$


**Figure 6.1: Example of IMR measurement in a STEMI patient.** The thermodilution curves (blue- rest traces, yellow-hyperaemic traces) are seen in the bottom half of the screen while the top half shows the pressure tracing. In this case IMR is high at 59

#### 6.2.4.5 X-ray measurement sequence – hyperaemic

The pressure injector was set up to deliver the same volume of contrast as the rest measurement sequence (3-5ml/s constant rate injection at 200psi) and images were acquired as before under breath hold.

#### 6.2.4.6 Myocardial resistance calculation.

Myocardial resistance ($R_{myo}$) was calculated using the pressure measurement from the artery ($P_d$) using the Pressure wire. In the absence of significant epicardial stenosis, Aortic pressure ($P_a$) should be the same as $P_d$. If we assume that right atrial pressure ($P_{RA}$) is negligible then $P_d$ equals the driving pressure.

$$\text{Myocardial resistance } (R_{myo}) = \frac{Arterial\ driving\ pressure}{CBF}$$

$$R_{myo} = \frac{P_d - P_{RA}}{CBF}$$

Assuming $P_{RA}$ to be negligible

$$R_{myo} = \frac{P_d}{CBF}$$

#### 6.2.4.7 Cardiovascular magnetic resonance (CMR) imaging protocol

Patients participating in the XBF STEMI study were invited to take part in another research project (3TSTEMI – REC: 12/YH/0169) conducted by the CMR research group at the University of Leeds (Investigators: Dr Pankaj Garg & Professor Sven Plein, Leeds Institute of Cardiovascular and Metabolic Medicine, University of Leeds). Participation in this study was entirely voluntary. Upon consenting to taking part in the CMR study, patients received two CMR scans. The first scan was performed within 7 days of their presentation with STEMI (acute scan). A follow-up scan was performed at 3 months (convalescent scan). All CMR scanning was performed on a1.5 Tesla MRI scanner (Ingenia, Philips, Best, the Netherlands). A dedicated cardiac phased array receiver coil was used (1.5 T: 24 channels; 3 T: 32 channel).

At the start of the scan, a free breathing, low resolution survey scan was used to mark the anatomical landmarks. Images of each pulsed sequence were scrutinised for any artefacts and sequence repeated until good quality images were obtained for reporting.

After the survey, the following balanced cines were acquired: horizontal long axis (HLA), vertical long axis (VLA) and short axis left ventricular cine stack.

The cines were acquired during breath hold, with a balanced steady state free precession (bSSFP). The breath hold was usually between 8-10 seconds. The number of phases throughout the cardiac cycle acquired was 30. The SAX LV cine stack had ten-millimetre slice gap.

After the cine acquisition, T2W-imaging was performed in the pre-planned left ventricular short-axis with a slice gap of 10mm.

After this, the patients were given a bolus of Gadolinium DTPA, (gadopentetate dimeglumine; Magnevist, Bayer, Berlin, Germany) at a dose of 0.1 mmol/kg.

Early gadolinium enhancement images were acquired in long and short axes looking for gadolinium enhancement in the infarcted area, immediately post gadolinium administration. Late gadolinium enhancement imaging was performed after 10-15 minutes of administration of gadolinium.

The images were analysed by a Level 3 certified CMR cardiologist (PG) who was blinded to all X-ray, pressure wire and thermodilution data. Images were analysed offline using commercially available software (cvi42 v4.1.5, Circle Cardiovascular Imaging Inc., Calgary, Canada). LV mass, volume and function were calculated by drawing endocardial and epicardial contours manually on the short axis cine images in end systole and end diastole. Trabeculation and papillary muscles were excluded. The late gadolinium images were analysed for infarct size and presence of MVO. Any areas of reduced enhancement present early within the area of gadolinium enhancement and persisting on repeated imaging represented MVO. The acute phase scan was analysed for the scar size, microvascular obstruction (MVO), LV dimensions, LV stroke volume (SV), LV ejection fraction (EF) and

end diastolic mass (EDM). The convalescent phase scan was analysed from LV dimensions, EF, and SV to assess the remodelling. Area at Risk (AAR) was quantified using the full-width at half maximum (FWHM) thresholding method (Garg et al., 2017).

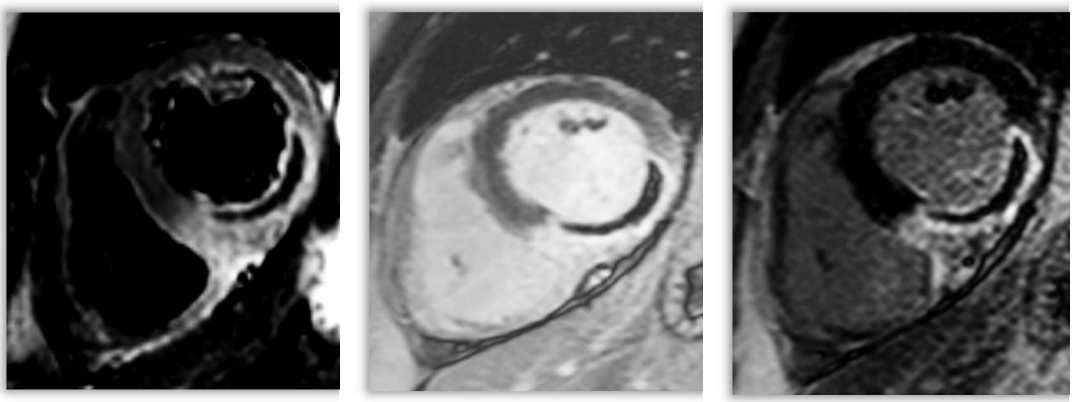

| T2 W SPIR imaging | Early Gadolinium enhancement imaging | Late Gadolinium enhancement imaging |
|---|---|---|

**Figure 6.2 T2-weighted imaging demonstrating myocardial oedema (hyperintense) in the infero-lateral wall which also has a dark core (hypointense) area.** This hypointense area is also there on EGE-imaging and LGE-imaging and is sandwiched between the transmural scar in the infero-septal region.

### 6.2.5 Definitions

*Time to revascularisation:* The time to revascularisation is defined as the time from symptom onset to first device/balloon time during PPCI to re-establish blood flow in the IRA.

*Scar size (Infarct size):* CMR scans were analysed for presence of late gadolinium enhancement. The myocardial mass of the late gadolinium enhancement was determined using validated semi-automated thresholding method - full-width at half maximum (FWHM) (Flett et al., 2011; Amado et al., 2004). The scar size was expressed as percentage of myocardial mass (scar size %).

*Area at risk (AAR):* The area at risk was calculated by measuring the hyperintense area on T2 weighted images.

*Myocardial salvage:* Myocardial salvage is defined as the difference between AAR and scar size (Botker et al., 2012).

*Myocardial salvage index (MSI):* myocardial salvage index can be calculated as the proportion of salvaged AAR.

$$MSI = \frac{AAR - scar\ size}{AAR}$$

*LV dimensions and functional indices:* The standard LV dimensions of end diastolic volume (LVEDV), end systolic volume (LVESV), left ventricular stroke volume (LVSV), left ventricular ejection fraction (LVEF), and end diastolic mass (EDM) was calculated by drawing endocardial and epicardial contours on short axis cine slices. The LV remodelling was assessed by subtracting the EDV on acute scan from EDV on convalescent scan (∆LVEDV). Similarly change in LVEF (∆LVEF) was calculated by subtracting the LVEF measured on the acute scan from the LVEF on convalescent scan.

### 6.2.6 Clinical data collection, anonymisation and storage and data analysis

Clinical data were collected from the patient's notes after the procedure. Patient outcome data were obtained from data collected as part of National Institute for Cardiovascular Outcomes Research (NICOR) national audit.

Raw X-ray images were captured by a dedicated computer system and software in the control room. The raw data did not have any patient identifiable information.

DICOM images from the research protocol were identified and anonymised and transferred to the hospital archive without compression and saved as a separate study folder. Both these sets of data were copied and analysed later using the XBF software (figure 6.3). Haemodynamic data and thermodilution data were acquired on the RadiAnalyser system with the study participant ID number as the identifier. The patients underwent CMR scans within the first 7 days and then repeated after 3 months. The CMR data were stored in the hospital's radiology images archive.

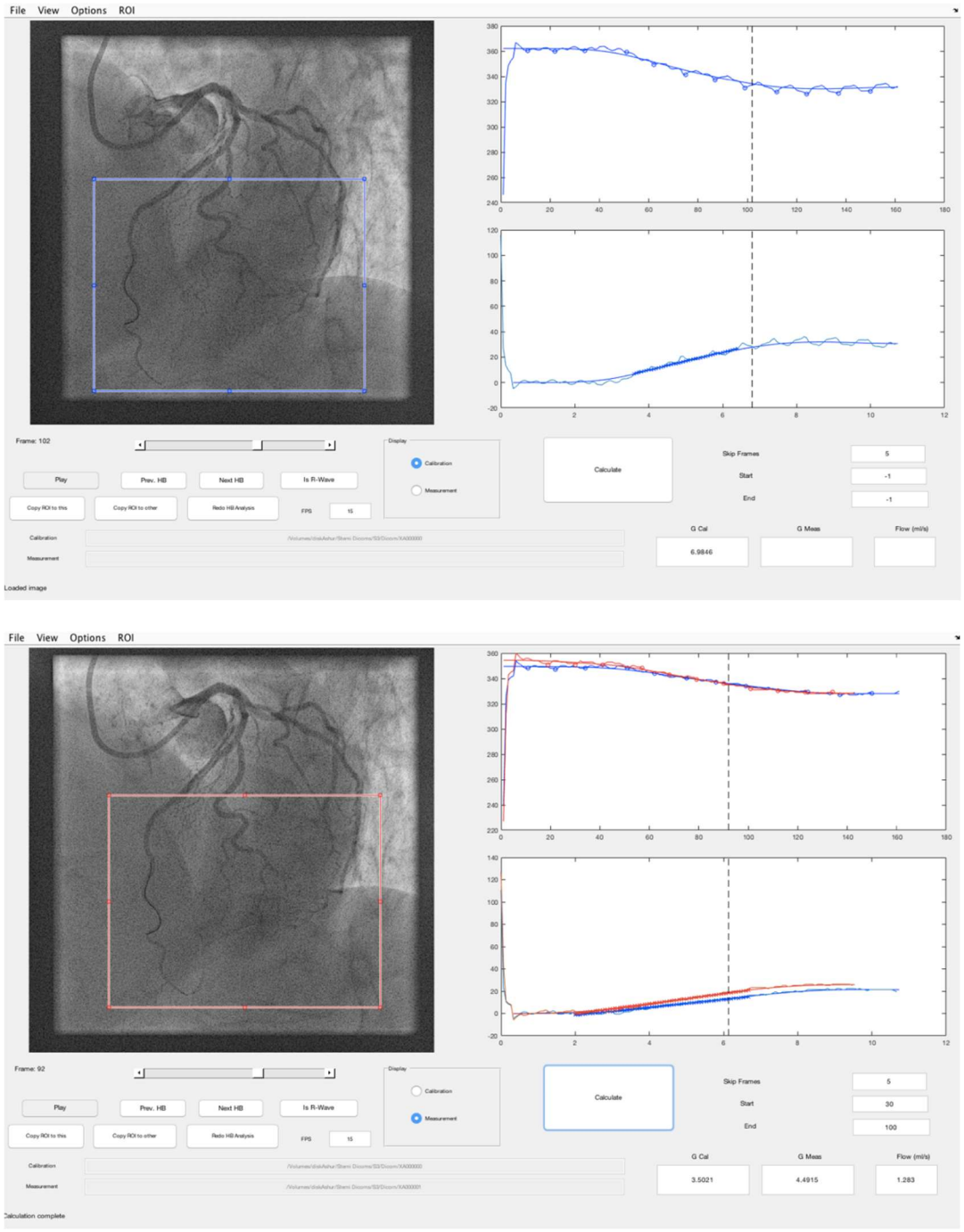


**Figure 6.3: Example of image analysis using XBF software in a STEMI patient.** In this case DICOM images were used.

### 6.2.7 Primary and secondary endpoints

The primary endpoint was the relationship between the myocardial resistance calculated from XBF method in the infarct related artery (IRA) after reperfusion and stent deployment and CMR-measured myocardial scar, myocardial salvage index (MSI) and remodelling assessed by change in end diastolic volume and ejection fraction.

The secondary endpoints were

1. Correlation between XBF coronary blood flow and the CMR scar size, myocardial salvage index (MSI) and LV remodelling assessed by change in LV end diastolic volume and change in LV ejection fraction.
2. Correlation between myocardial resistance from XBF method and IMR
3. Safety of performing XBF coronary blood flow and resistance studies in patients presenting with acute STEMI.

### 6.2.8 Sample size and power calculation

As in the validation study, the STEMI study was also a pilot study designed to test the methods, safety, and feasibility of performing coronary blood flow calculation using X-ray signal intensity analysis in patients presenting as emergency with acute myocardial infarction. Precision and variance of XBF measurements were not known when the study was designed. Further, there were no accepted normal values of coronary blood flow available. Design and recruitment to this study overlapped with completion of the validation study, so the results from the validation study were not available for power calculation. Therefore, it was not possible to perform conventional sample size or power calculations for this study. The recruitment size was

informed by previous studies in similar study populations to inform mechanisms (Wijnbergen et al., 2016; Ahn et al., 2016).

## 6.3 Results

Twenty-four patients were recruited to the study between May 2016 and March 2017.

### 6.3.1 Patient characteristics

Patient characteristics are summarised in table 6.2. Twenty-one patients out of 24 completed the acute CMR scan, out of which 20 completed both acute and convalescent CMR scans.

**Table 6.2: Patient characteristics of participants of the STEMI study**

| | |
|---|---|
| Number of patients recruited | 24 |
| Mean age (SD) years | 63.9 (10.8) |
| Male gender (%) | 17 (70.8%) |
| Artery studied | LAD 10 (42%) |
| | LCx 2 (8%) |
| | RCA 12 (50%) |
| Hypertension (%) | 3 (12.5%) |
| Hypercholesterolemia (%) | 1 (4%) |
| Diabetes (%) | 2 (8%) |
| Smoking (%) | Ex-smoker 3 (12.5%) |
| | Current smoker 6 (25%) |
| Completed CMR acute (%) | 21 (87.5%) |
| Completed CMR convalescent (%) | 20 (83.3%) |

CMR- Cardiac magnetic resonance, SD- standard deviation, LAD- Left anterior descending artery, LCx- Left circumflex artery, RCA- Right coronary artery.

### 6.3.2 Patient outcomes

None of the patients recruited to the study had any procedure related complications. All the patients tolerated the procedure well including the research component. Clinical outcomes are summarised in the table 6.3.

**Table 6.3: Summary of patient outcomes**

| | |
|---|---|
| Total number of patients recruited | 24 |
| TIMI flow grade post PPCI | TIMI 3 - 23 (96%)<br>TIMI 2 – 1 (4%) |
| Mean time to revascularisation | 359.6 minutes |
| Median time to revascularisation | 234 minutes |
| Patients who received dual antiplatelet therapy with Aspirin and Ticagrelor | 24 (100%) |
| Major in-lab complications | 0 |

TIMI- Thrombolysis in myocardial infarction, PPCI- Primary percutaneous coronary intervention.

Two patients were incidentally found to have LV thrombi on their CMR scans, which were reported to the clinical teams and led to change in management plan with anticoagulation.

Patient records were accessed after a mean of 43.4 (SD 2.8) months after the procedure. All patients were alive. The only major adverse cardiac event was that of repeat revascularisation with CABG, 13 months after the PPCI in one of the patients who had progression of left main stem disease.

### 6.3.3 Quality of images analysis

As with the validation study, there were difficulties in acquiring good quality data. For the STEMI study the research team had learnt from the early experience with the validation study and the workflow had undergone updates and fine tuning. STEMI patients presented acutely and were more unwell and

often in pain compared to the previous cohort of patients. This led to difficulties in breath holding in some patients especially during hyperaemia.

Images were analysed for their quality and suitability to be analysed. Image quality and suitability were sometimes not obvious at the time of data acquisition. Major issues like obvious breathing led us to repeat the image acquisition. Where there were issues with raw X-ray data, we used the DICOM data for analysis.

The image sequences were analysed for their quality and suitability for analysis. During some of the cases, the image acquisition software malfunctioned and skipped some image frames. In such cases, the DICOM files were used for analysis.

The grading system described in section 5.3.2 was used to grade the quality of the images with grade 3 being good quality images and grade 1 poor quality, not suitable for analysis. Grade 2 images could be analysed after making adjustments to correct the error such as adjusting the ROI or selecting the frames to avoid frames with breathing etc. Only grades 2 or 3 images were included in the analysis.

**Table 6.4: Data quality of STEMI patients graded from 1-3, where 3 is best quality data and 1 not analysable data.**

| Study number | Vessel | Calibration | Rest | Hyperaemic | Comments |
|---|---|---|---|---|---|
| S1 | LAD | 3 | 3 | 2 | Some skip in hyperaemic file |
| S2 | LAD | 2 | 2 | 2 | Hyperaemia file skips |
| S3 | LAD | 3 | 3 | 3 | |
| S4 | LCx | 2 | 2 | 2 | RCA fills from overspill |
| S5 | LAD | 3 | 3 | 3 | |
| S6 | RCA | 2 | 2 | 2 | |
| S7 | LAD | 2 | 2 | 2 | |
| S8 | LAD | 2 | 2 | 2 | Framing issue |
| S9 | LAD | 2 | 2 | 2 | Framing issue |
| S10 | LCx | 3 | 2 | 2 | |
| S11 | LAD | 1 | 3 | 3 | Calibration file faulty |
| S12 | RCA | 3 | 2 | 2 | |
| S13 | RCA | 3 | 3 | 3 | |
| S14 | RCA | 2 | 3 | 3 | |
| S15 | RCA | 2 | 2 | 2 | Minor breathing |
| S16 | LAD | 2 | 2 | 2 | Framing issue |
| S17 | RCA | 3 | 3 | 3 | Framing issue & settings |
| S18 | RCA | 3 | 3 | 3 | |
| S19 | RCA | 3 | 3 | 3 | |
| S20 | RCA | 3 | 3 | 3 | |
| S21 | RCA | 3 | 3 | 3 | |
| S22 | LAD | 2 | 3 | 3 | |
| S23 | RCA | 3 | 3 | 3 | |
| S24 | RCA | 3 | 3 | 3 | |

LAD- Left anterior descending artery, LCx- Left circumflex artery, RCA- Right coronary artery.

Patient number S11 was excluded from further analysis as the calibration file was faulty and hence XBF analysis could not be performed.

### 6.3.4 Correlation between raw and DICOM images

As described above, when there were issues with raw X-ray data capture, we used DICOM data for analysis. In order to ensure that DICOM images were appropriate for analysis and yielded comparable results to raw data files, we carried out a comparison of raw image data and DICOM-derived data in patients in which both were available (figure 6.4). Raw images and DICOM images were analysed sequentially keeping the region of interest and frames selected for analysis the same, to minimise intra-observer variability. The results from DICOM and raw data are tabulated in table 6.5 There was excellent correlation and agreement between the results from DICOM and raw data as illustrated in figure 6.5.

**Table 6.5: Summary of XBF blood flow using analysis of raw images and DICOM images.**

| **Rest and Hyperaemic flow rates calculated from Raw images. ml/s** | **Rest and Hyperaemic flow rates calculated from DICOM images. ml/s** |
|---|---|
| 1.18 | 1.26 |
| 1.77 | 1.72 |
| 3.94 | 3.75 |
| 1.34 | 1.36 |
| 0.94 | 1.16 |
| 1.76 | 1.57 |
| 2.02 | 2.05 |
| 2.14 | 2.23 |
| 1.72 | 1.77 |
| 1.17 | 1.23 |
| 1.09 | 1.30 |
| 2.11 | 2.05 |
| 4.10 | 3.93 |
| 1.86 | 1.94 |
| 1.19 | 1.54 |
| 1.27 | 1.13 |
| 2.42 | 2.22 |
| 2.75 | 2.82 |
| 2.83 | 2.68 |
| 1.98 | 2.01 |

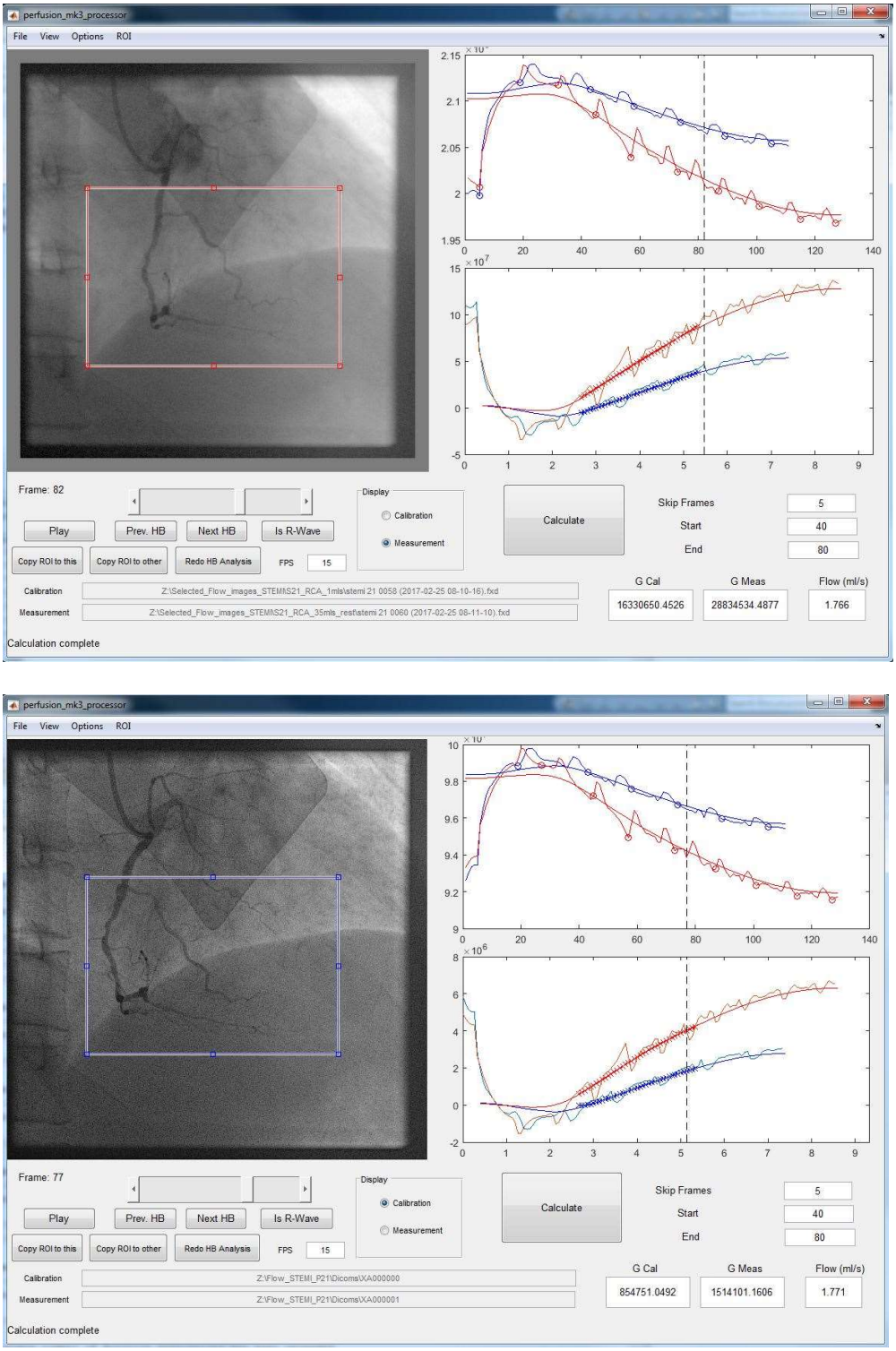


**Figure 6.4: Example of same patient's data in raw format and DICOM format analysed.** The frames selection and ROI have been kept the same. A defibrillator pad is visible in the upper aspect of the X-ray image.

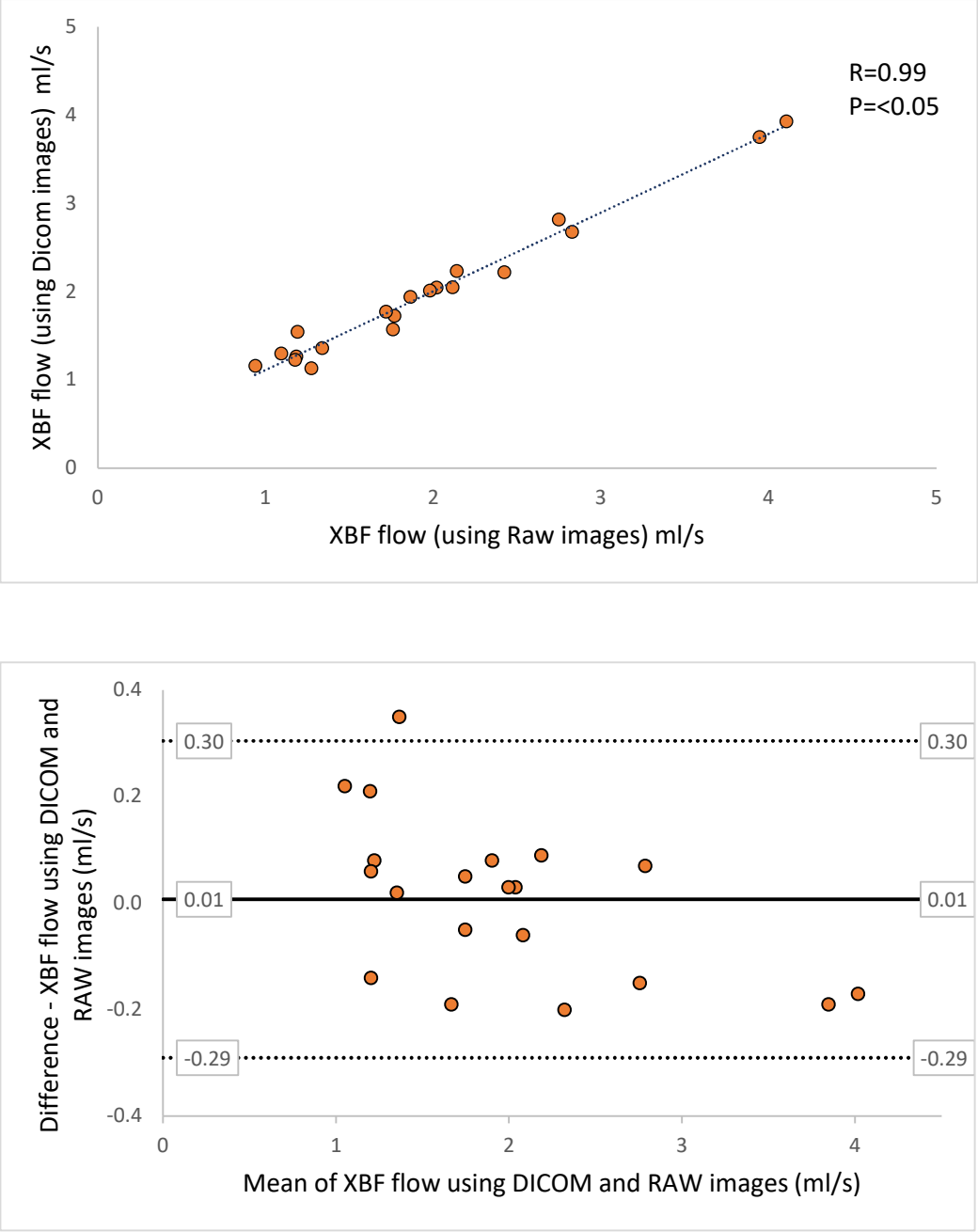


**Figure 6.5: Relationship between XBF blood flow calculated from Raw X-ray images and DICOM images.** The same ROI was used. Upper panel shows scatter plot and lower panel shows the Bland-Altman plot. In the Bland-Altman plot, the solid line represents the mean of the differences between measurements and the dotted lines represent the 95% confidence intervals for the mean of the differences between measures.

There was excellent correlation and agreement between XBF blood flow calculated from raw X-ray images and DICOM images R=0.99 (figure 6.5). Allowing for intra-observer variability, there was no difference between the results from the raw images to that of DICOM. Therefore, in cases where raw data acquisition was problematic either due to issues with the computer hardware or software, analysis of DICOM data was deemed to be adequate.

### 6.3.5 X-ray data results

X-ray data for all the STEMI patients were analysed using the XBF software. In cases where the raw X-ray data capture had been problematic due to equipment malfunction, such as several image frames being omitted from the saved file, DICOM files were used for analysis. The results have been summarised in the tables 6.6 and 6.7.

**Table 6.6: Results of coronary blood flow and myocardial resistance calculated using XBF method in all STEMI patients.**

| Patient No | Raw/Dicom images used | IRA | XBF blood flow | | Pd | Myocardial resistance ($R_{myo}$) |
|---|---|---|---|---|---|---|
| | | | Rest flow ml/s | Hyperaemic Flow ml/s | mm Hg | mmHg.s/ml |
| S1 | Raw | LAD | 3.19 | 5.70 | NP | NP |
| S2 | Raw | LAD | 1.10 | 1.41 | 89* | 63.12 |
| S3 | Raw | LAD | 1.50 | 1.73 | 110 | 63.58 |
| S4 | Raw | LCx | 0.84 | 2.65 | 111* | 41.89 |
| S5 | Raw | LAD | 1.50 | 1.95 | 72 | 36.92 |
| S6 | Dicom | RCA | 1.43 | 1.88 | 71 | 37.77 |
| S7 | Raw | LAD | 2.14 | 2.07 | 65 | 31.40 |
| S8 | Raw | LAD | 2.57 | 3.20 | 99 | 30.94 |
| S9 | Dicom | LAD | 1.45 | 1.61 | 54 | 33.54 |
| S10 | Raw | LCx | 1.14 | 1.91 | 84 | 43.98 |
| S12 | Raw | RCA | 1.46 | 1.73 | 53 | 30.64 |
| S13 | Raw | RCA | 0.94 | 1.19 | 65 | 54.62 |
| S14 | Dicom | RCA | 2.85 | 1.75 | 103 | 58.86 |
| S15 | Raw | RCA | 0.98 | 0.34 | 65 | 191.18 |
| S16 | Raw | LAD | 3.26 | 2.68 | 58 | 21.64 |
| S17 | Dicom | RCA | 1.61 | 1.56 | 84 | 53.85 |
| S18 | Raw | RCA | 2.02 | 2.42 | 74 | 30.58 |
| S19 | Dicom | RCA | 2.08 | 2.23 | 61 | 27.35 |
| S20 | Raw | RCA | 2.13 | 2.75 | 82 | 29.82 |
| S21 | Raw | RCA | 1.72 | 2.83 | 66 | 23.32 |
| S22 | Dicom | LAD | 1.53 | 2.11 | 50 | 23.70 |
| S23 | Raw | RCA | 2.59 | 2.61 | 76 | 29.12 |
| S24 | Dicom | RCA | 2.30 | 2.91 | 70 | 24.05 |

* In patients S2 and S4 the mean Pd at rest was taken. IRA- infarct related artery, Pd- distal pressure from coronary artery, RCA- Right coronary artery, LAD- Left anterior descending artery, LCx- Left circumflex artery, NP –not performed.

**Table 6.7: Summary of XBF blood flow and resistance in STEMI patients**

| IRA (number of cases) | Parameter | | | Unit |
|---|---|---|---|---|
| All arteries (23) | CBF at rest | Mean | 2.03 | ml/s |
| | | Median | 1.61 | ml/s |
| | | SD | 0.70 | ml/s |
| | CBF hyperaemic | Mean | 2.23 | ml/s |
| | | Median | 2.07 | ml/s |
| | | SD | 1.00 | ml/s |
| | Myocardial resistance (Rmyo) | Mean | 44.63 | mmHg.s/ml |
| | | Median | 32.47 | mmHg.s/ml |
| | | SD | 35.30 | mmHg.s/ml |
| LAD (9) | CBF at rest | Mean | 2.03 | ml/s |
| | | Median | 1.53 | ml/s |
| | | SD | 0.80 | ml/s |
| | CBF hyperaemic | Mean | 2.50 | ml/s |
| | | Median | 2.07 | ml/s |
| | | SD | 1.32 | ml/s |
| | Myocardial resistance (Rmyo) | Mean | 38.11 | mmHg.s/ml |
| | | Median | 32.47 | mmHg.s/ml |
| | | SD | 16.35 | mmHg.s/ml |
| LCx (2) | CBF at rest | Mean | 0.99 | ml/s |
| | | SD | 0.21 | ml/s |
| | CBF hyperaemic | Mean | 2.28 | ml/s |
| | | SD | 0.52 | ml/s |
| | Myocardial resistance (Rmyo) | Mean | 42.94 | mmHg.s/ml |
| | | SD | 1.48 | mmHg.s/ml |
| RCA (12) | CBF at rest | Mean | 1.84 | ml/s |
| | | Median | 1.87 | ml/s |
| | | SD | 0.60 | ml/s |
| | CBF hyperaemic | Mean | 2.02 | ml/s |
| | | Median | 2.06 | ml/s |
| | | SD | 0.76 | ml/s |
| | Myocardial resistance (Rmyo) | Mean | 49.26 | mmHg.s/ml |
| | | Median | 30.61 | mmHg.s/ml |
| | | SD | 46.40 | mmHg.s/ml |

IRA – Infarct related artery, LAD- Left anterior descending artery, LCx- Left circumflex artery, RCA- Right coronary artery, CBF- Coronary blood flow, Rmyo- myocardial resistance calculated by XBF method, SD- standard deviation

### 6.3.6 Cardiovascular magnetic resonance imaging results

Patients 1, 14 and 24 did not undergo CMR scan, due to claustrophobia and other logistic reasons. Patient 8 only underwent acute phase scan.

The results are detailed in table 6.8. The results of the CMR scan categorised according to IRA are detailed in table 6.9. As expected, the LAD which supplies more myocardium than other arteries had largest scar%.

**Table 6.8: Summary of CMR results of all patients.**

| Patient No | IRA | Acute Scan | | | | | | | | | | Convalescent scan | | | |
|---|---|---|---|---|---|---|---|---|---|---|---|---|---|---|---|
| | | Scar grams | Scar % | MVO grams | LVEDV ml | LVESV ml | LVSV ml | LVEF % | LVEDM grams | AAR % | MSI | LVEDV ml | LVESV ml | LVSV ml | LVEF % |
| S2 | LAD | 42 | 49 | 6 | 124 | 72 | 52 | 42 | 86 | 61 | 0.32 | 137 | 84 | 53 | 39 |
| S3 | LAD | 9 | 9 | 0 | 125 | 50 | 75 | 60 | 108 | 25 | 0.62 | 147 | 66 | 81 | 55 |
| S4 | LCx | 12 | 13 | 0 | 109 | 41 | 67 | 62 | 89 | 15 | 0.23 | 92 | 33 | 59 | 64 |
| S5 | LAD | 16 | 13 | 0 | 164 | 68 | 96 | 58 | 123 | 29 | 0.46 | 156 | 64 | 92 | 59 |
| S6 | RCA | 12 | 8 | 0 | 202 | 95 | 107 | 53 | 160 | 22 | 0.45 | 186.5 | 64 | 122.5 | 67 |
| S7 | LAD | 34 | 18 | 7 | 258 | 183 | 74 | 29 | 187 | 42 | 0.20 | 362 | 254 | 108 | 30 |
| S8 | LAD | 10 | 7 | 1 | 203 | 94 | 109 | 54 | 138 | 36 | 0.15 | NA | NA | NA | NA |
| S9 | LAD | 30 | 24 | 7 | 119 | 51 | 68 | 57 | 126 | 15 | 0.33 | 128 | 62 | 66 | 51 |
| S10 | LCx | 5 | 6 | 0 | 131 | 75 | 57 | 43 | 90 | 60 | 0.24 | 139 | 70 | 70 | 50 |
| S11 | LAD | 46 | 29 | 17 | 187 | 139 | 48 | 26 | 160 | 36 | 0.76 | 249 | 170 | 79 | 32 |
| S12 | RCA | 9 | 8 | 0 | 152 | 66 | 86 | 57 | 114 | 15 | 0.66 | 150 | 55 | 96 | 64 |
| S13 | RCA | 7 | 6 | 0 | 133 | 61 | 72 | 54 | 120 | 22 | 0.66 | 122 | 39 | 83 | 68 |
| S15 | RCA | 14 | 10 | 0 | 136 | 61 | 75 | 55 | 137 | 50 | 0.72 | 165 | 56 | 109 | 66 |
| S16 | LAD | 9 | 8 | 0 | 183 | 100 | 83 | 45 | 110 | 24 | 0.48 | 160 | 70 | 91 | 57 |
| S17 | RCA | 10 | 10 | 3 | 100 | 30 | 70 | 70 | 95 | 19 | 0.63 | 111 | 31 | 80 | 72 |
| S18 | RCA | 13 | 8 | 0 | 187 | 98 | 88 | 47 | 159 | 31 | 0.71 | 160 | 70 | 91 | 57 |
| S19 | RCA | 7 | 4 | 2 | 183 | 89 | 94 | 51 | 164 | 33 | 0.96 | 198 | 92 | 106 | 54 |
| S20 | RCA | 1 | 1 | 0 | 187 | 104 | 83 | 44 | 177 | 19 | 0.37 | 210 | 104 | 105 | 50 |
| S21 | RCA | 12 | 9 | 0 | 211 | 112 | 99 | 47 | 134 | 45 | 0.30 | 208 | 101 | 98 | 47 |
| S22 | LAD | 32 | 26 | 0 | 173 | 85 | 88 | 51 | 123 | 44 | 0.35 | 190 | 102 | 87 | 46 |
| S23 | RCA | 28 | 34 | 5 | 144 | 72 | 72 | 50 | 85 | 14 | 0.30 | 132 | 65 | 67 | 51 |

IRA- infarct related artery, MVO- microvascular obstruction, LV- left ventricle, EDV- end diastolic volume, ESV- end systolic volume, EF- ejection fraction, EDM- End diastolic mass, scar- myocardial scar, LV- left ventricle, Scar % - myocardial scar expressed as a % of LV mass, AAR-area at risk, MSI- myocardial salvage index, NA- not available (scan not performed).

**Table 6.9: CMR results summary by infarct related artery (IRA)**

| IRA (Number of cases) | Parameter | Number (%) | Mean | Median | SD |
|---|---|---|---|---|---|
| All arteries (21) | Scar (g) | | 17.05 | 12 | 12.77 |
| | Scar% | | 14.29 | 9 | 11.79 |
| | No of cases with MVO (%) | 8 (38%) | | | |
| | LVEF | | 50.24 | 51 | 10.2 |
| | AAR | | 31.27 | 29 | 14.56 |
| | MSI | | 0.47 | 0.45 | 0.22 |
| LAD (9) | Scar | | 25.33 | 30 | 14.59 |
| | Scar% | | 20.33 | 18 | 13.51 |
| | No of cases with MVO (%) | 5 (56%) | | | |
| | LVEF | | 46.89 | 51 | 12.49 |
| | AAR | | 34.61 | 36 | 13.57 |
| | MSI | | 0.41 | 0.35 | 0.19 |
| LCx (2) | Scar | | 8.5 | NA | 4.95 |
| | Scar% | | 9.5 | NA | 4.95 |
| | No of cases with MVO (%) | 0 | | | |
| | LVEF | | 52.5 | NA | 13.44 |
| | AAR | | 37.57 | NA | 31.73 |
| | MSI | | 0.24 | NA | 0.01 |
| RCA (10) | Scar | | 11.3 | 11 | 6.99 |
| | Scar% | | 9.8 | 8 | 8.95 |
| | No of cases with MVO (%) | 3(30%) | | | |
| | LVEF | | 52.8 | 52 | 7.27 |
| | AAR | | 27 | 22 | 12.45 |
| | MSI | | 0.58 | 0.65 | 0.21 |

IRA- Infarct related artery, LAD- Left anterior descending artery, LCx- Left circumflex artery, RCA- Right coronary artery, Scar % - myocardial scar expressed as a % of LV mass, MVO- microvascular obstruction, LVEF- Left ventricular ejection fraction, AAR- area at risk as % of LV mass, MSI- myocardial salvage index.

### 6.3.7 Relationship between XBF measured resistance and blood flow with CMR infarct parameters and LV remodelling.

The primary endpoint was the correlation between myocardial resistance calculated from XBF method in the infarct related artery (IRA) and CMR measured myocardial scar, remodelling assessed by change in end diastolic volume and ejection fraction.

The comparison between myocardial resistance ($R_{myo}$) calculated by XBF method and myocardial scar expressed as a percentage of total left ventricular mass (scar%) shows weak correlation between $R_{myo}$ and scar% with Pearson's coefficient (R) of 0.31. Correlation between MSI and $R_{myo}$ showed no correlation.

The change in left ventricular end diastolic volume (ΔLVEDV) and the change in left ventricular ejection fractions (ΔLVEF) were calculated from the two CMR scans and compared to the $R_{myo.}$ Change in LVEDV was calculated by subtracting the LVEDV measured from the acute CMR scan from the LVEDV measured from the convalescent CMR scan. Similarly, change in LV EF percentage (ΔLV EF) was calculated by subtracting the LV EF at the acute CMR scan from the LVEF at the convalescent CMR scan. There was no correlation between ΔLVEDV and $R_{myo}$ and very weak negative correlation between ΔLVEF and $R_{myo.}$ These results are illustrated in figure 6.6.

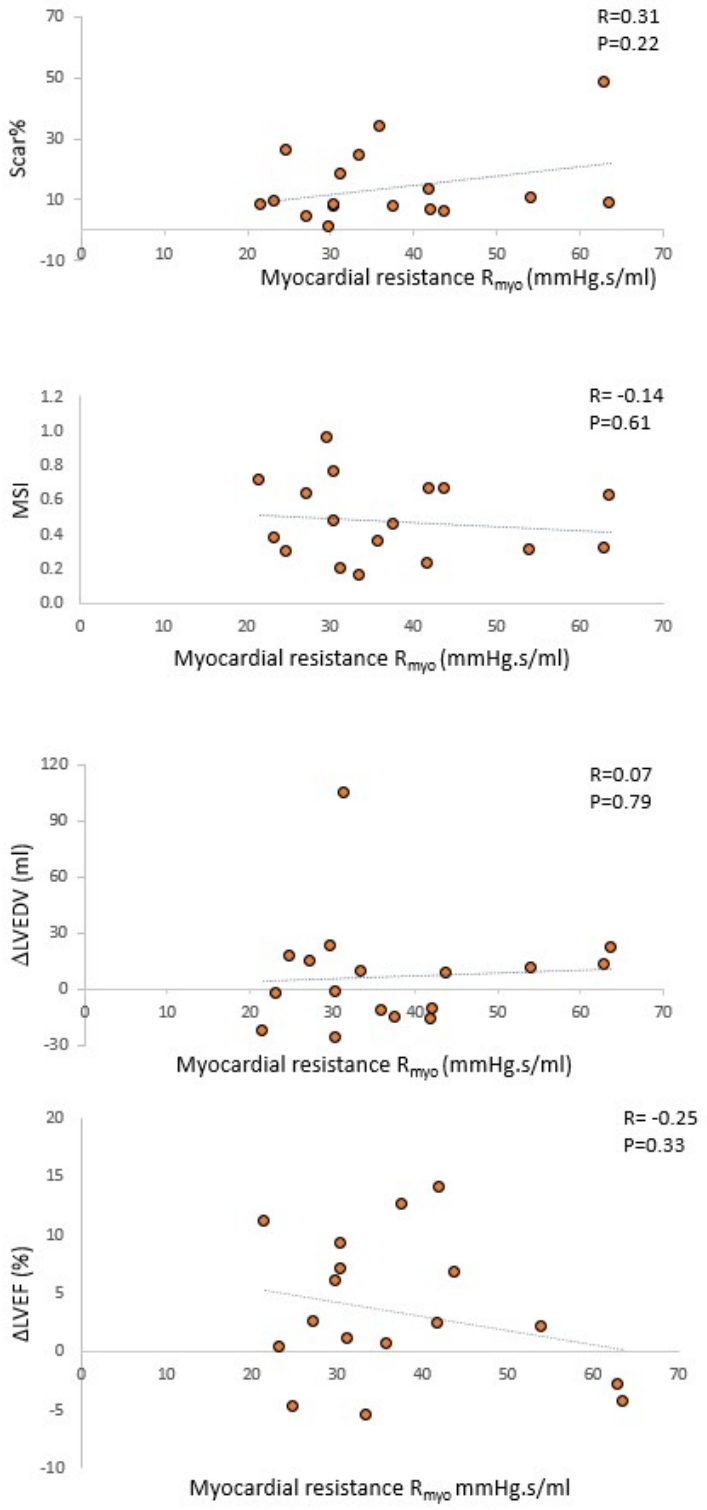


**Figure 6.6: Relationships between myocardial resistance (Rmyo) from XBF method to CMR infarct parameters- a) myocardial scar expressed as percentage of total myocardial mass (Scar%) b) Myocardial salvage index (MSI) c) change in LV end diastolic volume (ΔLVEDV) d) change in LV ejection fraction (ΔLVEF)**

The hyperaemic coronary blood flow calculated using the XBF method was compared with the CMR scar% and myocardial salvage index (MSI). The results are illustrated in figure 6.7 and there was weak negative correlation between scar% and hyperaemic XBF flow and very weak positive correlation between MSI and XBF flow.

The change in left ventricular end diastolic volume (ΔLVEDV) and the change in left ventricular ejection fractions (ΔLVEF) were calculated from the two CMR scans and compared to the hyperaemic XBF blood flow. The results are also illustrated in figure 6.7. There was no significant correlation seen between XBF blood flow during hyperaemic post PPCI and ΔLVEDV or ΔLVEF.

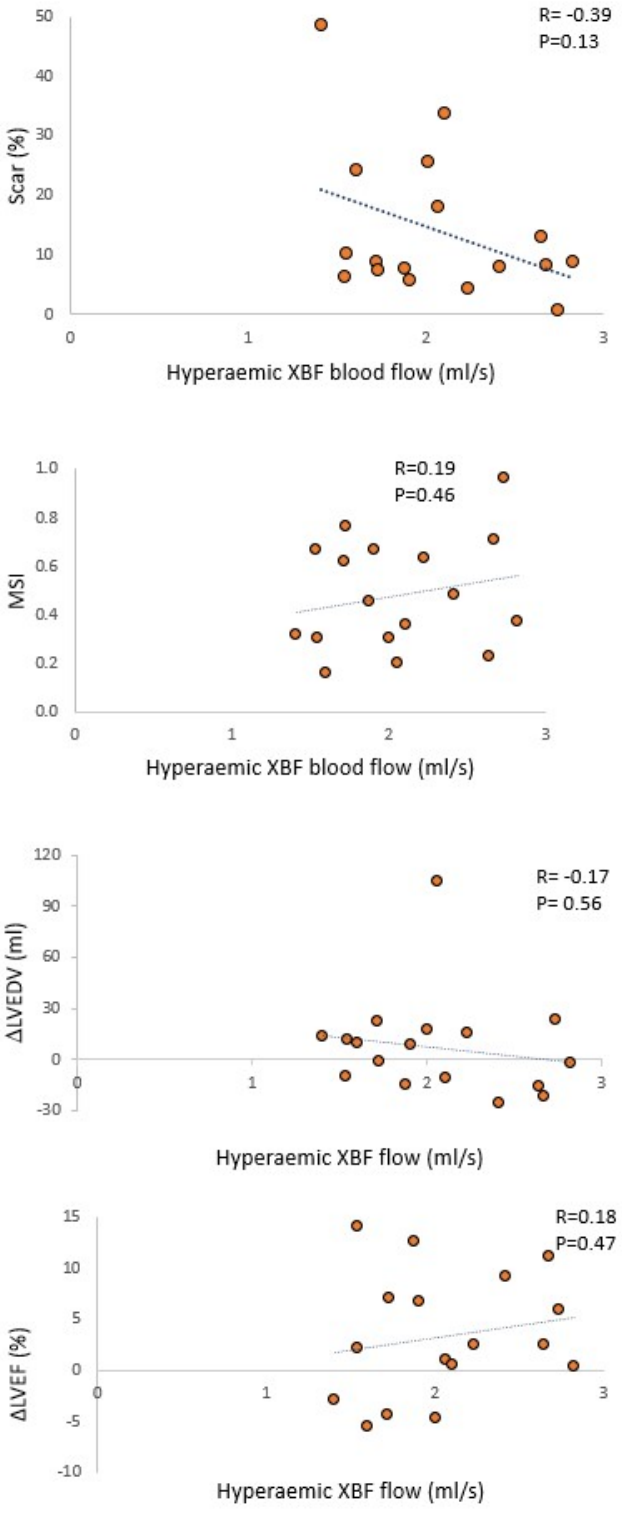


**Figure 6.7: Relationships between hyperaemic coronary blood flow calculated from XBF method (ml/s) to CMR infarct parameters- a) myocardial scar expressed as percentage of total myocardial mass (Scar%) b) Myocardial salvage index (MSI) c) change in LV end diastolic volume (ΔLVEDV) d) change in LV ejection fraction (ΔLVEF).**

### 6.3.8 Pressure wire indices of microvascular function and resistance

The pressure wire evaluation involved assessing the IMR in the case of STEMI patients and this was performed after the primary PCI was completed. The results are detailed in table 6.10.

**Table 6.10: Results of pressure-wire derived indices of coronary physiology.**

| Study no | FFR | Mean TT_baseline | Mean TT_hyperaemic | Mean Pd | IMR | CFR |
|---|---|---|---|---|---|---|
| | | seconds | seconds | mm Hg | | |
| S1 | NP | NP | NP | NP | NP | NP |
| S2 | NA | 0.99 | 1.54 | 89* | 24 | 0.64 |
| S3 | NA | 1.77 | 1.11 | 110 | 122.1 | 1.59 |
| S4 | 0.99 | 0.32 | NP | 111* | NP | NP |
| S5 | 0.97 | 0.62 | 0.31 | 72 | 22.32 | 2.00 |
| S6 | NA | 0.37 | 0.23 | 71 | 16.33 | 1.61 |
| S7 | 0.89 | 0.61 | 0.58 | 65 | 37.7 | 1.05 |
| S8 | 0.97 | 1.16 | 0.6 | 99 | 59.4 | 1.93 |
| S9 | 1.00 | 0.22 | 0.2 | 54 | 10.8 | 1.10 |
| S10 | 0.95 | 0.62 | 0.22 | 84 | 18.48 | 2.82 |
| S11 | 0.93 | 0.58 | 0.67 | 79 | 52.93 | 0.87 |
| S12 | 1.00 | 0.25 | 0.16 | 53 | 8.48 | 1.56 |
| S13 | 1.03 | 0.96 | 0.4 | 65 | 26 | 2.40 |
| S14 | 0.97 | 0.92 | 0.53 | 103 | 54.59 | 1.74 |
| S15 | 0.90 | 0.48 | 0.17 | 65 | 11.05 | 2.82 |
| S16 | 0.94 | 0.37 | 0.23 | 58 | 13.34 | 1.61 |
| S17 | 1.01 | 1.43 | 1.03 | 84 | 86.52 | 1.39 |
| S18 | 0.97 | 0.44 | 0.38 | 74 | 28.12 | 1.16 |
| S19 | 0.92 | 2.34 | 0.75 | 61 | 45.75 | 3.12 |
| S20 | 0.84 | 0.25 | 0.15 | 82 | 12.3 | 1.67 |
| S21 | 0.83 | 0.46 | 0.17 | 66 | 11.22 | 2.71 |
| S22 | 0.82 | 0.48 | 0.45 | 50 | 22.5 | 1.07 |
| S23 | 1.07 | 0.76 | 1.19 | 76 | 90.44 | 0.64 |
| S24 | 0.96 | 0.97 | 0.79 | 70 | 55.3 | 1.23 |

* In patients S2 and S4 the mean Pd at rest was taken.

FFR- Fractional flow reserve, IMR- index of microcirculatory resistance, CFR- Coronary flow reserve, TT- transit time, NP- not performed; NA- not available.

For the first case (S1), we did not undertake the thermodilution protocol. For the second, third and sixth patients (S2, S3 and S6) there was a fault with the cable and arterial pressure trace could not be obtained. Therefore, no FFR value is available. In patient 4 (S4), only baseline thermodilution transit times could be obtained again due to technical issues, so IMR value is not available.

### 6.3.9 Correlation between XBF method myocardial resistance and index of microcirculatory resistance

The XBF measured myocardial resistance ($R_{myo}$) was compared with IMR. The results are illustrated in figure 6.8. There was good correlation between the two measures of resistance with a Pearson' coefficient of 0.74.

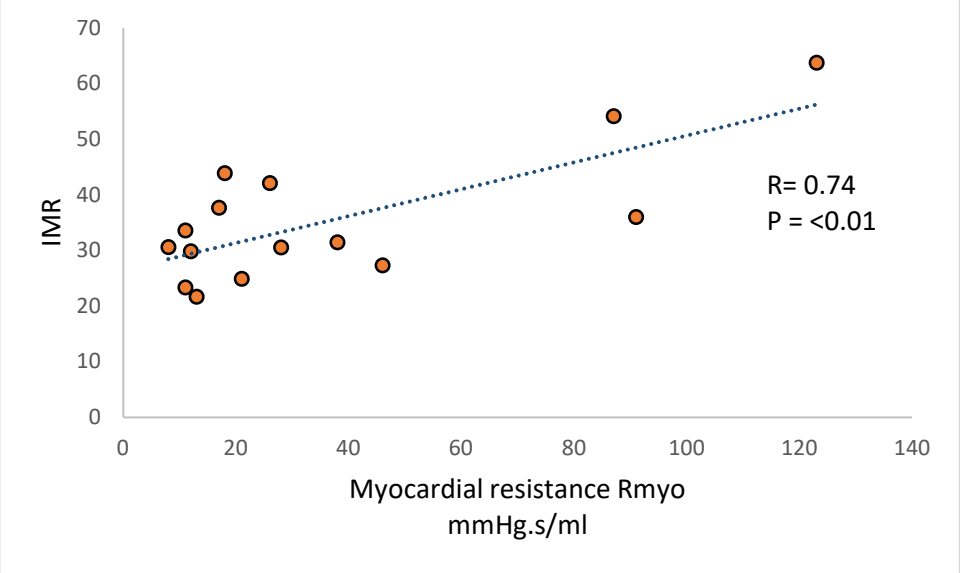


**Figure 6.8: Comparison between IMR and myocardial resistance from XBF method ($R_{myo}$).**

### 6.3.10 Post hoc analysis of right coronary artery cases

In the previous chapter, XBF coronary blood flow measurements correlated well with thermodilution blood flow measurements in right coronary artery cases. Although there were methodological issues with performing continuous thermodilution in left coronary artery mainly related to the microcatheter, there were other differences in XBF analysis in LCA compared to RCA cases such as different gantry angle, difficulties with choosing ROI to avoid overlapping coronary territories of left anterior descending and circumflex branches of LCA. It was therefore considered appropriate to analyse the STEMI cases

where RCA was the IRA separately to ensure that the results were not different.

The relationship of $R_{myo}$ and XBF hyperaemic blood flow measured in the RCA after primary PCI with CMR infarct parameters of scar% and MSI is illustrated in figures 6.9. There is no significant correlation seen. The $R_{myo}$ and XBF hyperaemic blood flow in RCA were then compared to the myocardial salvage index (MSI). There was weak negative correlation between $R_{myo}$ and MSI while the XBF blood flow did not have significant correlation.

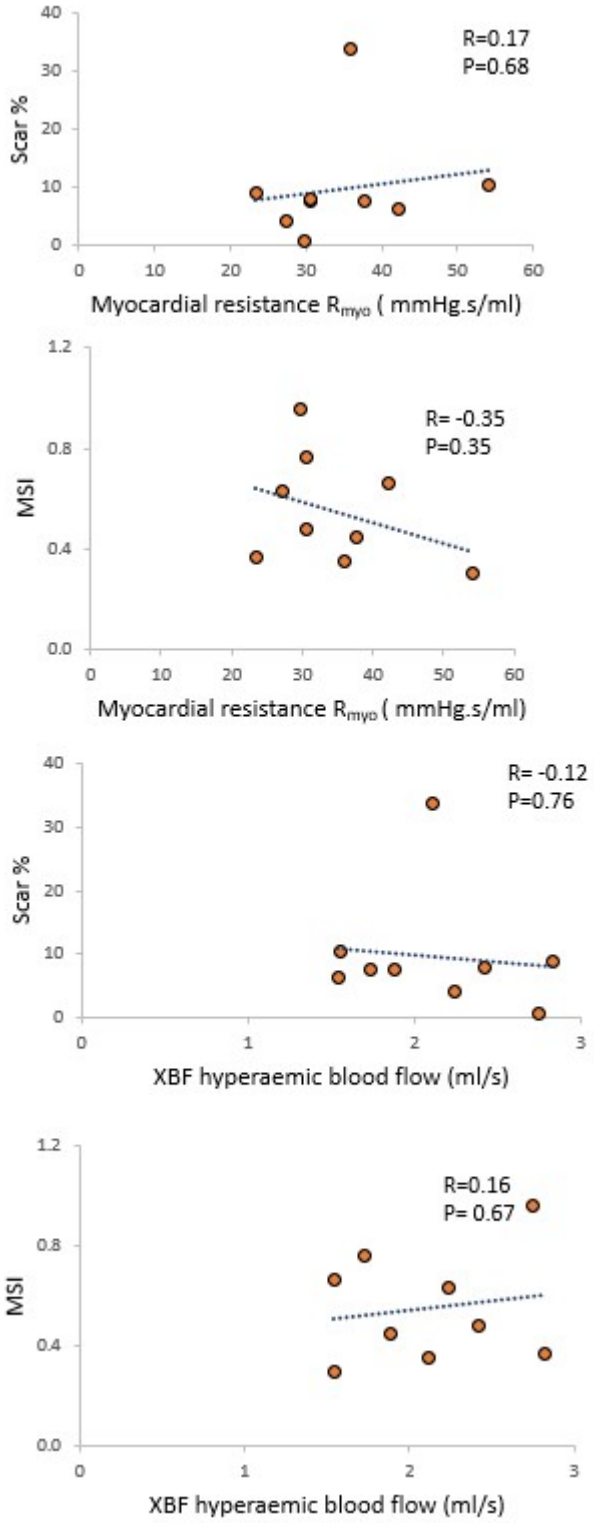


**Figure 6.9: Results in RCA cases alone - a) myocardial resistance ($R_{myo}$) from XBF method and myocardial scar expressed as percentage of total myocardial mass (Scar%) b) myocardial resistance calculated from XBF method ($R_{myo}$) and Myocardial salvage index (MSI) c) hyperaemic XBF blood flow and scar size on CMR, expressed as percentage of total LV mass (Scar%) d) hyperaemic blood flow calculated from XBF method (Rmyo) and Myocardial salvage index (MSI)**

When the XBF measured myocardial resistance (Rmyo) was compared with IMR measured after primary PCI in RCA cases, there appeared to be good correlation with the Pearson's coefficient of 0.59. The results are illustrated in figure 6.10.

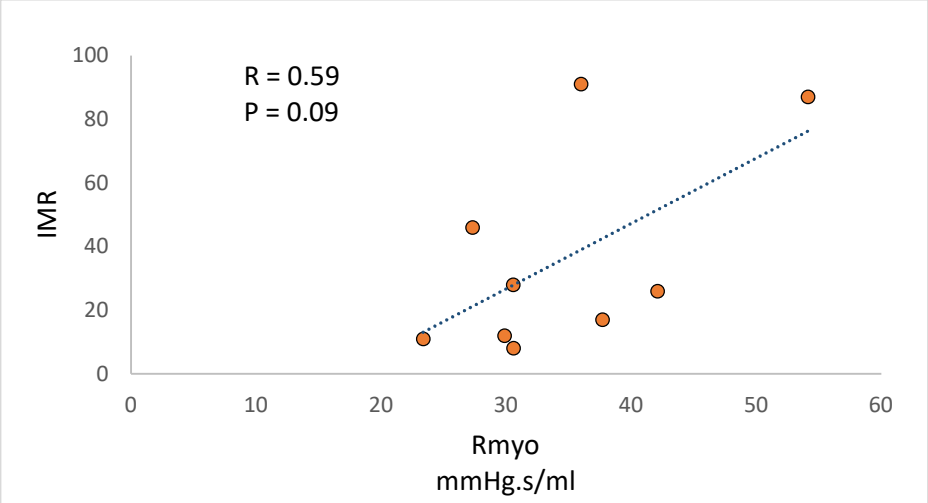


**Figure 6.10: Correlation between XBF measured myocardial resistance ($R_{myo}$) and IMR measured after primary PCI in RCA cases.**

## 6.4 Discussion

Patients presenting with STEMI are a key group of patients where the ability to assess the coronary blood flow and resistance in real time may have significant clinical implications in risk stratification and in choosing different therapeutic options. The aim of this chapter was to investigate if myocardial resistance ($R_{myo}$) and hyperaemic coronary blood flow measured from XBF method were predictive of CMR infarct parameters of scar size (as percentage of LV mass), myocardial salvage index (MSI) and LV remodelling assessed by changes in LV end-diastolic volume and LV ejection fraction.

This study established the safety of performing the research study protocol in patients undergoing PPCI for STEMI. There were no clinically relevant

adverse events and adenosine was well tolerated. Adenosine posed difficulties in breath hold during the hyperaemic sequence.

In planned comparisons of XBF-derived parameters with CMR-derived infarct parameters, XBF-derived $R_{myo}$ was weakly correlated with CMR-derived scar%. The XBF-derived hyperaemic blood flow in the IRA was weakly negatively correlated with CMR-derived scar%. There was no significant correlation between the CMR parameter of MSI, ΔLVEDV or ΔLVEF and the XBF parameters $R_{myo}$ or hyperaemic blood flow. However, when $R_{myo}$ was compared with the established pressure-wire index of microvascular resistance (IMR), a good correlation was observed which was maintained when RCA cases were analysed separately.

Although a weak correlation was noted between $R_{myo}$ and scar%, overall, the results of the STEMI study in terms of primary endpoint must be considered negative.

We have also established that the image analysis can be undertaken using images in standard DICOM format copied without compression and raw X-ray data are not required. Normally, the X-ray images undergo post processing by the X-ray equipment manufacturer's proprietary systems to enhance the images. The raw images are extracted by the dedicated software and computer system before these are applied. We did not know whether the post processing would impact on the pixel intensity assessments. When we compared the results obtained by analysing images from the same patient in raw format and DICOM, we found that there was excellent correlation and agreement with little bias between the two. This implies that in future studies using this technique, raw data extraction and transfer for analysis can be

avoided and standard DICOM images transferred to the archive without compression can be utilised. This reduces the resources required for future studies using this method and serves to streamline the workflow.

There are several potential reasons why the XBF measured parameters did not correlate well with CMR measured infarct parameters.

Immediately after revascularisation, several pathological and compensatory physiological processes are still at play. There is often relative haemodynamic instability which may affect coronary flow measurements. It is possible that early after reperfusion in primary PCI, the patient is still in a volatile haemodynamic state and in a situation where the blood flow and microvascular resistance are continuously changing. There is a varying degree of coronary spasm involved with any acute coronary syndrome (Belle et al., 2016). Microvascular obstruction and spasm usually take time to resolve, aided by pharmacological agents. Reperfusion injury is a phenomenon where further damage is imparted to the ischaemic myocardium despite restoration of blood flow. This is thought to be due to the release of harmful chemicals and is influenced by several factors. This effect is difficult to quantify and is highly variable from patient to patient. Wijnbergen *et al* in their study measuring absolute flow and myocardial resistance noted that the blood flow increased and resistance decreased from acute to sub-acute phase of Acute MI (Wijnbergen et al., 2016). It is possible that coronary blood flow measured in the sub-acute phase using the XBF method may correlate better with CMR measured infarct parameters. However, such measurement may be of limited value as the opportunity to risk stratify and intervene therapeutically may have passed by then.

Although, $R_{myo}$ did not correlate well with CMR assessed scar% or myocardial salvage index or parameters of LV remodelling and function well, it correlated well with IMR. This is encouraging and should be investigated in larger studies looking at clinical outcomes in STEMI patients or surrogate endpoints on CMR. IMR is gaining popularity as a means of assessing the microvascular function in the catheterisation laboratory. There is an increasing evidence base to support the view that presence of MVO is a marker for adverse prognosis (de Waha et al., 2017). Several studies have shown that IMR measured after PPCI in the IRA correlates well with presence of MVO (Bulluck et al., 2016; Fearon, W. F. et al., 2013; Carrick et al., 2016c; McGeoch et al., 2010). Based on these data, we might have expected to see a correlation between $R_{myo}$ and MVO. In our small study, MVO was only present in 8 (38%) patients and in this small number of patients we did not see any signal of a relationship between presence of MVO and $R_{myo}$ or IMR (data not shown). It has been previously noted that there can be discordance between IMR and MVO in about a third of the patients presenting with STEMI (De Maria et al., 2019). Patel *et al* in a cohort of 34 STEMI patients, did not observe a correlation between IMR and MVO (Patel, N. et al., 2015). A larger study may be useful in investigating this relationship.

After the coronary artery stenosis or lesions have been treated the distal pressure in the coronary artery ($P_d$) can be assumed to be the same as aortic pressure ($P_a$). Therefore, $R_{myo}$ can be calculated using XBF method without the need for pressure wires or additional instrumentation of the coronary artery.

## 6.5 Limitations

This is a single centre pilot study which only recruited a small number of patients presenting with STEMI. The methodology suffered from some of the problems with data capture described in previous chapter, section 5.5.1.

Leeds General Infirmary (LGI) is the busiest PPCI centre in the UK performing more than 1100 PPCIs annually. There are 6 cardiac catheterisation laboratories in use at LGI. We had the X-ray data extraction software and computer set up in two catheterisation laboratories. These laboratories were also equipped with the necessary software modification on the X-ray equipment. On days where these catheter laboratories were not available for PPCI, due to other procedures such as structural heart interventions or electrophysiology procedures, recruitment was not possible.

It was challenging to seek consent for the PPCI procedure as well as for the research project in the limited time before PPCI. Patients presenting with STEMI can often be in pain and be seriously unwell. This meant that all but the most motivated and relatively stable patients for taking part in clinical research had to be excluded. A number of these patients had received opiate analgesia for pain, which sometimes caused drowsiness and the consent process for research could not be undertaken.

There were other clinical trials recruiting STEMI patients, which meant that patients had to be shared between other research projects.

Being a busy PPCI centre also means that not infrequently there was a STEMI patient on the way to catheterisation laboratory through the Yorkshire Ambulance service while there was already a patient undergoing PPCI. Therefore, even though the first patient may have consented to taking part in

the study, he/she may have to be excluded in-order to avoid delay in revascularising the second patient.

LGI served a large catchment area with over 2.2 million population. The patients who are from outside Leeds area were transferred back to their local hospitals after 6 hours of observation in the Coronary Care Unit. This meant there would often be difficulties in arranging a CMR scan within seven days of the STEMI. If significant difficulties were anticipated, the patients were excluded from the study.

## 6.6 Conclusion

In this chapter, it was demonstrated that the XBF method can be safely undertaken in patients presenting with STEMI. XBF measured parameters of coronary blood flow and myocardial resistance did not correlate well with CMR measured infarct parameters and measures of LV remodelling. However, XBF measured myocardial resistance in the infarct related artery after primary PCI correlated well with the index of microcirculatory resistance (IMR) measured at the same time. Results from analysis of DICOM images correlated and agreed very well with the results from analysis of raw X-ray data which serves to simplify the workflow.

# Chapter 7 Future directions and conclusions

This research examined the feasibility of using X-ray image signal intensity analysis to calculate coronary blood flow. The aim of the thesis was to refine and validate a bespoke bio-imaging technique (XBF method) for quantifying coronary blood flow from X-ray angiography in humans and investigate its utility in the setting of acute myocardial infarction.

The thesis achieved its first objective of validating the technique of quantifying flow using the XBF method using a bench model of coronary arteries and microcirculation. There was excellent correlation between XBF method measured flow and the actual flow in the model. The results also showed that XBF method was more highly correlated with actual flow than was the thermodilution method.

The thesis also achieved its second objective of testing the feasibility of using the XBF method in humans in the human validation study. The results from validation study indicated good correlation and agreement of XBF blood flow with the continuous thermodilution method of coronary blood flow quantification in the right coronary artery. The results in the left coronary artery did not correlate with the thermodilution flow. There may be several reasons for this which have been discussed in detail. The problem may lie due to errors in XBF method or thermodilution or both.

The third objective of applying XBF method to assess myocardial resistance in patients undergoing primary PCI was also successfully completed in the human STEMI study. The measurements of myocardial resistance from XBF method ($R_{myo}$) correlated well with index of microcirculatory resistance (IMR). However, $R_{myo}$ and coronary blood flow only weakly correlated with myocardial

scar expressed as percentage of the left ventricular mass (scar%) measured by CMR. There was no significant correlation between the $R_{myo}$ or XBF measured coronary blood flow to the myocardial salvage index (MSI) or change in left ventricular dimensions and ejection fraction.

The results from both human studies are mixed and although XBF method has been successfully and safely employed in humans, we have not been successful in demonstrating its clinical utility in STEMI patients. However, $R_{myo}$ correlated well with IMR, which is indeed encouraging, as IMR has been reported to be predictive of CMR infarct parameters. Therefore, it is possible that $R_{myo}$ may also predict the same if a larger study were to be undertaken. Our small pilot study in STEMI patients, was underpowered to detect any clinical outcomes.

The mixed results in the human validation study with good correlation with thermodilution measured blood flow seen only with RCA measurement is likely to be due to the methodological issues with the thermodilution technique related to non-availability of a dedicated microcatheter for most part of the study. The results from the STEMI study in which XBF measured $R_{myo}$ correlated well with IMR in both LCA, and RCA further adds weight to this argument.

During this research we have managed to refine the XBF technique in several ways. The software itself has undergone numerous iterative changes and the current version is robust and delivers consistent reproducible results. We have optimised the data acquisition protocol by streamlining the catheterisation laboratory protocol and proving that DICOM images are just as suitable for blood flow analysis as raw X-ray images.

Although currently the results are obtained after off-line processing and analysis, the workflow can be streamlined to give real time results in the catheterisation laboratory. Such a technique, with its main advantage of not needing additional instrumentation of coronary arteries could prove to be useful in clinical decision making in a variety of clinical settings such as acute MI, microvascular disease, and myocardial diseases.

## 7.1 Future directions

The XBF software needs further optimisation to overcome many of the shortcomings explained in detail in previous chapters. Some of the changes that could be considered in future and potential future direction are given below.

### 7.1.1 Change to calibration sequence

At present we use a calibration sequence performed at a low flow rate (typically 1ml/s) of contrast agent. If any problems are encountered with the calibration sequence any subsequent flow measurements will be erroneous and any errors in the measurement sequence amplified. Some of the common issues we encountered when performing data acquisition were patient breathing, and catheter disengagement from the coronary artery leading to contrast flowing into the aortic root and the ascending and descending aorta.

One option would be to use a guide catheter extension to deliver contrast into the artery of interest without spillage. This would have the advantage of being able to sub select the LAD and LCx in the case of left coronary artery.

Another option to overcome this would be to use an alternative method of calibration. Although it would be possible to try an iodine-filled calibration

phantom as used by Molloi *et al* (Molloi et al., 1998), this is cumbersome and impractical in humans. The calibration phantom would need to be repositioned for each angiographic projection. Furthermore, it is prone to error as the calibration phantom will be at a different distance to the X-ray detector compared to the heart.

Another potential option for calibration is to use the image of the contrast-filled catheter itself. The catheter diameter is known (typically 6 French size).

**Table 7.1: Inner diameter in inches of various guide catheters available commercially**

| Guide (Manufacturer) | Outer Lumen (French) size | | | |
|---|---|---|---|---|
| | 5 | 6 | 7 | 8 |
| Launcher (Medtronic) | 0.058 | 0.071 | 0.081 | 0.090 |
| Vista Brite Tip (Cordis) | 0.056 | 0.070 | 0.078 | 0.088 |
| Mach 1 (Boston Scientific) | NA | 0.070 | 0.081 | 0.091 |
| Viking/Guidant (Abbott) | NA | 0.068 | 0.078 | 0.091 |
| Wiseguide (Boston Scientific) | NA | 0.066 | 0.076 | 0.086 |

The catheter we used were Mach 1 (Boston Scientific) which has an inner diameter of 0.070 of an inch (1.8mm). For e.g. If we select a small square of the catheter filled with contrast (i.e., 1.8 x1.8 mm) in an area with minimal foreshortening, we get the signal intensity change produced by a cylinder of contrast with a diameter of 1.8mm and height of 1.8mm.

The volume can be calculated as

$$V = 3.14 \times 0.9^2 \times 1.8\, mm^3 = 4.578\, mm^3$$

From the signal intensity change produced by 4.578 $mm^3$ of contrast agent with a known concentration of iodine by using the software, we can understand the relationship of iodine to signal intensity in that patient. The signal intensity

produced by the catheter itself and the background tissues should be subtracted from this. This method also has the advantage of being closer to the level of the heart than a phantom stuck on the surface of the chest.

We can then use this and perform calculations of coronary flow based on signal intensity change in the coronary arteries during coronary angiography. The current XBF software would require further optimisation to perform analysis in this way.

### 7.1.2 ECG gating.

During our initial analysis we attempted to choose the diastolic phase images for analysis. This proved challenging as ECG was not embedded in the X-ray images especially the those in raw format. There is the option to embed ECG on the DICOM images. ECG gating in this way can identify the cardiac phases more accurately. However, the later analysis involved analysing all the frames and averaging the result. As the XBF method is based on analysing the signal intensity change induced by the total mass of iodine in the ROI, choosing images of a specific cardiac phase should not make a huge impact. However, it may help to reduce the issues posed by cardiac motion.

### 7.1.3 Changes in choosing region of interest.

Our attempt is to quantify coronary blood flow which is proportional to but not the same as myocardial blood flow. Collateral blood flow from other coronary arteries must be considered for calculating myocardial blood flow. We considered changing the ROI to just fit around the artery and its visible branches. This is possible, but as the coronary artery moves with the cardiac

cycle, the artery will move in and out of a ROI that fits snuggly around the artery and its branches in one frame. Adjusting the ROI in every frame to correct for the artery movement is cumbersome and time-consuming.

During previous animal studies by Molloi *et al* (Molloi et al., 2004), problems were encountered in using a ROI of myocardial perfusion bed and the authors resorted to using a ROI around the arterial outline. This is appropriate as the XBF method attempts to quantify coronary blood flow and not myocardial blood flow or perfusion. This change could be attempted by further developing the XBF flow processor software.

### 7.1.4 Larger patient study

During our pilot studies of human validation and STEMI, we have identified several problems and troubleshooting them as we encountered them and thereby refining and optimising the protocol.

Most clinical end-users do not have the opportunity to extract raw X-ray data from their cardiac imaging systems. Phillips Healthcare supported us in extracting these images for research. Digital Imaging and Communications in Medicine (DICOM) images used in cardiac catheter laboratories for analysis of images for clinical purposes are produced after applying the manufacturers post processing algorithms. In the STEMI study, the results obtained using raw X-ray images and DICOM were compared, and it showed excellent correlation and agreement. Therefore, XBF flow quantification can be undertaken without any additional hardware modifications to catheter laboratory equipment. This paves the way for larger scale clinical studies.

Larger scale clinical studies comparing coronary flow measurements with clinical outcomes or CMR/PET imaging parameters may prove the utility of this technique of assessing coronary flow in the real world.

#### 7.1.4.1 Studies comparing perfused myocardial mass.

The current gold standard to measure myocardial blood flow is with Positron emission tomography (PET). It would be interesting to compare and correlate the coronary blood flow calculated from X-ray signal intensity analysis to the gold standard test of PET. There are considerations of radiation exposure if recruiting patients to such a study. A pragmatic approach would be to screen patients undergoing PET myocardial perfusion imaging, who then go on to coronary angiography. It must also be borne in mind that coronary blood flow is not the same as the myocardial blood flow. Calculating myocardial mass is not possible using X-ray angiography, so flow cannot be correlated to unit of myocardial tissue. Although the LV can be divided into segments roughly corresponding to individual coronary territory, there can be wide variation and overlap in the segments supplied by each coronary between individuals and it is not possible to identify myocardial territory supplied by each individual coronary artery. Another option is to use mathematical algorithms such as Voronoi's algorithm that divides area between predetermined points based on the shortest distance to calculate the myocardial mass supplied by the coronary artery (Kurata et al., 2015). Despite these limitations, in a carefully selected cohort of patients perhaps with single vessel disease, if the coronary blood flow can be correlated to myocardial blood flow, it would be a better validation study.

#### 7.1.4.2 Long term outcome study

Another potential study could be recruiting a large number of patients who undergo coronary angiography and assess the coronary blood flow in the artery of interest. Rather than look for surrogate outcomes, long term follow-up for clinical outcomes such as mortality, myocardial infarction, repeat admissions due to angina, heart failure and changes in LV function. This may help to correlate between coronary blood flow and myocardial resistance to clinical outcomes and may prove its utility in clinical cardiology.

### 7.1.5 Application in CT coronary angiography.

Cardiac CT is replacing invasive coronary angiography in several groups of patients especially those undergoing investigation for stable CAD. As explained in chapter 1, $FFR_{CT}$ is also in wide clinical use to noninvasively predict the functional significance of coronary lesions (Koo et al., 2011; Wu, W. et al., 2016). However, $FFR_{CT}$ attempts to non-invasively predict the FFR which itself is a surrogate measure of coronary blood flow and therefore will be a suboptimal index for a comprehensive assessment of coronary physiology due to the reasons explained in detail in Chapter 1. Newer multidetector row CT scanning machines not only allow detailed imaging of coronary arteries but also allow myocardial CT perfusion (CTP) in the same study. This was first reported by Kurata et al (Kurata et al., 2005). CTP analyses the first pass distribution of contrast material during in the myocardium as a surrogate marker of myocardial blood flow (MBF) using a similar principle used in the XBF method of coronary blood flow quantification. The imaging can be repeated after induction of hyperaemia to assess for ischaemia provoked by stress (Cademartiri et al., 2017). Combining $FFR_{CT}$

with CTP has the potential to provide a non-invasive comprehensive coronary physiology assessment.

## 7.2 Conclusions

The work so far has explored the feasibility of performing coronary blood flow quantification using X-ray signal intensity analysis. The technique was tested in a bench model and human patients. The bench studies prove the concept that blood flow calculations can be accurately made by using the XBF method. We have established that these studies can be safely performed in human patients including those presenting with acute myocardial infarction. In the validation study, we noticed a good correlation in the RCA between thermodilution-derived coronary flow and XBF flow. The technique needs further optimisation to address the issues in LCA. The XBF measured myocardial resistance correlated well with index of microcirculatory resistance but did not correlate well with CMR infarct parameters. With further optimisation and research, the XBF method has the potential to be useful clinically in risk stratifying patients with a wide variety of conditions without additional instrumentation of coronary arteries.

# References

Aarnoudse, W., Fearon, W.F., Manoharan, G., Geven, M., van de Vosse, F., Rutten, M., De Bruyne, B. and Pijls, N.H. 2004a. Epicardial stenosis severity does not affect minimal microcirculatory resistance. *Circulation.* **110**(15), pp.2137-2142.

Aarnoudse, W., Van't Veer, M., Pijls, N.H., Ter Woorst, J., Vercauteren, S., Tonino, P., Geven, M., Rutten, M., van Hagen, E., de Bruyne, B. and van de Vosse, F. 2007. Direct volumetric blood flow measurement in coronary arteries by thermodilution. *J Am Coll Cardiol.* **50**(24), pp.2294-2304.

Aarnoudse, W., van den Berg, P., van de Vosse, F., Geven, M., Rutten, M., Van Turnhout, M., Fearon, W., de Bruyne, B. and Pijls, N. 2004b. Myocardial resistance assessed by guidewire-based pressure-temperature measurement: in vitro validation. *Catheter Cardiovasc Interv.* **62**(1), pp.56-63.

Adjedj, J., Toth, G.G., Johnson, N.P., Pellicano, M., Ferrara, A., Floré, V., Di Gioia, G., Barbato, E., Muller, O. and De Bruyne, B. 2015. Intracoronary Adenosine: Dose–Response Relationship With Hyperemia. *JACC: Cardiovascular Interventions.* **8**(11), pp.1422-1430.

Ahn, S.G., Hung, O.Y., Lee, J.W., Lee, J.H., Youn, Y.J., Ahn, M.S., Kim, J.Y., Yoo, B.S., Lee, S.H., Yoon, J., Kwon, W. and Samady, H. 2016. Combination of the Thermodilution-Derived Index of Microcirculatory Resistance and Coronary Flow Reserve Is Highly Predictive of Microvascular Obstruction on Cardiac Magnetic Resonance Imaging After ST-Segment Elevation Myocardial Infarction. *JACC Cardiovasc Interv.* **9**(8), pp.793-801.

Al Jaroudi, W. and Iskandrian, A.E. 2009. Regadenoson: a new myocardial stress agent. *J Am Coll Cardiol.* **54**(13), pp.1123-1130.

Albertal, M., Voskuil, M., Piek, J.J., de Bruyne, B., Van Langenhove, G., Kay, P.I., Costa, M.A., Boersma, E., Beijsterveldt, T., Sousa, J.E., Belardi, J.A. and Serruys, P.W. 2002. Coronary flow velocity reserve after percutaneous interventions is predictive of periprocedural outcome. *Circulation.* **105**(13), pp.1573-1578.

Amado, L.C., Gerber, B.L., Gupta, S.N., Rettmann, D.W., Szarf, G., Schock, R., Nasir, K., Kraitchman, D.L. and Lima, J.A. 2004. Accurate and objective infarct sizing by contrast-enhanced magnetic resonance imaging in a canine myocardial infarction model. *J Am Coll Cardiol.* **44**(12), pp.2383-2389.

Amigues, I., Russo, C., Giles, J.T., Tugcu, A., Weinberg, R., Bokhari, S. and Bathon, J.M. 2019. Myocardial Microvascular Dysfunction in Rheumatoid ArthritisQuantitation by (13)N-Ammonia Positron Emission Tomography/Computed Tomography. *Circ Cardiovasc Imaging.* **12**(1), pe007495.

Antony, I., Nitenberg, A., Foult, J.M. and Aptecar, E. 1993. Coronary vasodilator reserve in untreated and treated hypertensive patients with and without left ventricular hypertrophy. *J Am Coll Cardiol.* **22**(2), pp.514-520.

Arashi, H., Satomi, N., Ishida, I., Soontorndhada, K., Ebihara, S., Tanaka, K., Otsuki, H., Nakao, M., Jujo, K., Yamaguchi, J. and Hagiwara, N. 2019. Hemodynamic and

Lesion Characteristics Associated with Discordance between the Instantaneous Wave-Free Ratio and Fractional Flow Reserve. *J Interv Cardiol.* **2019**, p3765282.

Arruda-Olson, A.M., Roger, V.L., Jaffe, A.S., Hodge, D.O., Gibbons, R.J. and Miller, T.D. 2011. Troponin T levels and infarct size by SPECT myocardial perfusion imaging. *JACC Cardiovasc Imaging.* **4**(5), pp.523-533.

Babbitt, D.G., Virmani, R., Vildibill, H.D., Jr., Norton, E.D. and Forman, M.B. 1990. Intracoronary adenosine administration during reperfusion following 3 hours of ischemia: effects on infarct size, ventricular function, and regional myocardial blood flow. *Am Heart J.* **120**(4), pp.808-818.

Baile, E.M., Pare, P.D., D'Yachkova, Y. and Carere, R.G. 1999. Effect of contrast media on coronary vascular resistance: contrast-induced coronary vasodilation. *Chest.* **116**(4), pp.1039-1045.

Bairey Merz, C.N., Pepine, C.J., Walsh, M.N. and Fleg, J.L. 2017. Ischemia and No Obstructive Coronary Artery Disease (INOCA): Developing Evidence-Based Therapies and Research Agenda for the Next Decade. *Circulation.* **135**(11), pp.1075-1092.

Barbagelata, A., Di Carli, M.F., Califf, R.M., Garg, J., Birnbaum, Y., Grinfeld, L., Gibbons, R.J., Granger, C.B., Goodman, S.G., Wagner, G.S. and Mahaffey, K.W. 2005. Electrocardiographic infarct size assessment after thrombolysis: insights from the Acute Myocardial Infarction STudy ADenosine (AMISTAD) trial. *Am Heart J.* **150**(4), pp.659-665.

Barbato, E., Aarnoudse, W., Aengevaeren, W.R., Werner, G., Klauss, V., Bojara, W., Herzfeld, I., Oldroyd, K.G., Pijls, N.H. and De Bruyne, B. 2004. Validation of coronary flow reserve measurements by thermodilution in clinical practice. *Eur Heart J.* **25**(3), pp.219-223.

Bassan, M., Ganz, W., Marcus, H.S. and Swan, H.J. 1975. The effect of intracoronary injection of contrast medium upon coronary blood flow. *Circulation.* **51**(3), pp.442-445.

Baumgart, D., Haude, M., Goerge, G., Ge, J., Vetter, S., Dagres, N., Heusch, G. and Erbel, R. 1998. Improved assessment of coronary stenosis severity using the relative flow velocity reserve. *Circulation.* **98**(1), pp.40-46.

Bech, G.J.W., De Bruyne, B., Pijls Nico, H.J., de Muinck Ebo, D., Hoorntje Jan, C.A., Escaned, J., Stella Pieter, R., Boersma, E., Bartunek, J., Koolen Jacques, J. and Wijns, W. 2001. Fractional Flow Reserve to Determine the Appropriateness of Angioplasty in Moderate Coronary Stenosis. *Circulation.* **103**(24), pp.2928-2934.

Beigel, R., Oieru, D., Goitein, O., Chouraqui, P., Konen, E., Shamiss, A., Hod, H., Or, J. and Matetzky, S. 2009. Usefulness of routine use of multidetector coronary computed tomography in the "fast track" evaluation of patients with acute chest pain. *Am J Cardiol.* **103**(11), pp.1481-1486.

Beleslin, B., Ostojic, M., Djordjevic-Dikic, A., Vukcevic, V., Stojkovic, S., Nedeljkovic, M., Stankovic, G., Orlic, D., Milic, N., Stepanovic, J., Giga, V. and Saponjski, J. 2008. The value of fractional and coronary flow reserve in predicting myocardial recovery in patients with previous myocardial infarction. *Eur Heart J.* **29**(21), pp.2617-2624.

Belle, L., Motreff, P., Mangin, L., Range, G., Marcaggi, X., Marie, A., Ferrier, N., Dubreuil, O., Zemour, G., Souteyrand, G., Caussin, C., Amabile, N., Isaaz, K., Dauphin, R., Koning, R., Robin, C., Faurie, B., Bonello, L., Champin, S., Delhaye, C., Cuilleret, F., Mewton, N., Genty, C., Viallon, M., Bosson, J.L. and Croisille, P. 2016. Comparison of Immediate With Delayed Stenting Using the Minimalist Immediate Mechanical Intervention Approach in Acute ST-Segment-Elevation Myocardial Infarction: The MIMI Study. *Circ Cardiovasc Interv.* **9**(3), pe003388.

Beltrame, J.F. 2013. Assessing patients with myocardial infarction and nonobstructed coronary arteries (MINOCA). *J Intern Med.* **273**(2), pp.182-185.

Berry, C. 2017. Stable Coronary Syndromes: The Case for Consolidating the Nomenclature of Stable Ischemic Heart Disease. *Circulation.* **136**(5), pp.437-439.

Berry, C., van 't Veer, M., Witt, N., Kala, P., Bocek, O., Pyxaras, S.A., McClure, J.D., Fearon, W.F., Barbato, E., Tonino, P.A., De Bruyne, B., Pijls, N.H. and Oldroyd, K.G. 2013. VERIFY (VERification of Instantaneous Wave-Free Ratio and Fractional Flow Reserve for the Assessment of Coronary Artery Stenosis Severity in EverydaY Practice): a multicenter study in consecutive patients. *J Am Coll Cardiol.* **61**(13), pp.1421-1427.

Bhatt, D.L. 2015. *Cardiovascular Intervention: A Companion to Braunwald's Heart Disease E-Book.* Elsevier Health Sciences.

Blankstein, R., Shturman, L.D., Rogers, I.S., Rocha-Filho, J.A., Okada, D.R., Sarwar, A., Soni, A.V., Bezerra, H., Ghoshhajra, B.B., Petranovic, M., Loureiro, R., Feuchtner, G., Gewirtz, H., Hoffmann, U., Mamuya, W.S., Brady, T.J. and Cury, R.C. 2009. Adenosine-induced stress myocardial perfusion imaging using dual-source cardiac computed tomography. *J Am Coll Cardiol.* **54**(12), pp.1072-1084.

Bober, R.M., Milani, R.V., Oktay, A.A., Javed, F., Polin, N.M. and Morin, D.P. 2019. The impact of revascularization on myocardial blood flow as assessed by positron emission tomography. *Eur J Nucl Med Mol Imaging.* **46**(6), pp.1226-1239.

Botker, H.E., Kaltoft, A.K., Pedersen, S.F. and Kim, W.Y. 2012. Measuring myocardial salvage. *Cardiovasc Res.* **94**(2), pp.266-275.

Brosh, D., Assali, A.R., Mager, A., Porter, A., Hasdai, D., Teplitsky, I., Rechavia, E., Fuchs, S., Battler, A. and Kornowski, R. 2007. Effect of no-reflow during primary percutaneous coronary intervention for acute myocardial infarction on six-month mortality. *Am J Cardiol.* **99**(4), pp.442-445.

Brush, J.E., Jr., Cannon, R.O., 3rd, Schenke, W.H., Bonow, R.O., Leon, M.B., Maron, B.J. and Epstein, S.E. 1988. Angina due to coronary microvascular disease in hypertensive patients without left ventricular hypertrophy. *N Engl J Med.* **319**(20), pp.1302-1307.

Bulluck, H., Foin, N., Cabrera-Fuentes, H.A., Yeo, K.K., Wong, A.S., Fam, J.M., Wong, P.E., Tan, J.W., Low, A.F. and Hausenloy, D.J. 2016. Index of Microvascular Resistance and Microvascular Obstruction in Patients With Acute Myocardial Infarction. *JACC Cardiovasc Interv.* **9**(20), pp.2172-2174.

Cademartiri, F., Seitun, S., Clemente, A., La Grutta, L., Toia, P., Runza, G., Midiri, M. and Maffei, E. 2017. Myocardial blood flow quantification for evaluation of coronary artery disease by computed tomography. *Cardiovasc Diagn Ther.* **7**(2), pp.129-150.

Califf, R.M., Harrelson-Woodlief, L. and Topol, E.J. 1990. Left ventricular ejection fraction may not be useful as an end point of thrombolytic therapy comparative trials. *Circulation.* **82**(5), pp.1847-1853.

Camici, P.G. and Crea, F. 2007. Coronary microvascular dysfunction. *N Engl J Med.* **356**(8), pp.830-840.

Camici, P.G., d'Amati, G. and Rimoldi, O. 2015. Coronary microvascular dysfunction: mechanisms and functional assessment. *Nat Rev Cardiol.* **12**(1), pp.48-62.

Camici, P.G., Gropler, R.J., Jones, T., L'Abbate, A., Maseri, A., Melin, J.A., Merlet, P., Parodi, O., Schelbert, H.R., Schwaiger, M. and Wijns, W. 1996. The impact of myocardial blood flow quantitation with PET on the understanding of cardiac diseases. *Eur Heart J.* **17**(1), pp.25-34.

Camici, P.G., Olivotto, I. and Rimoldi, O.E. 2012. The coronary circulation and blood flow in left ventricular hypertrophy. *J Mol Cell Cardiol.* **52**(4), pp.857-864.

Camici, P.G. and Rimoldi, O.E. 2009. The clinical value of myocardial blood flow measurement. *J Nucl Med.* **50**(7), pp.1076-1087.

Carrick, D., Haig, C., Ahmed, N., Carberry, J., Yue May, V.T., McEntegart, M., Petrie, M.C., Eteiba, H., Lindsay, M., Hood, S., Watkins, S., Davie, A., Mahrous, A., Mordi, I., Ford, I., Radjenovic, A., Oldroyd, K.G. and Berry, C. 2016a. Comparative Prognostic Utility of Indexes of Microvascular Function Alone or in Combination in Patients With an Acute ST-Segment-Elevation Myocardial Infarction. *Circulation.* **134**(23), pp.1833-1847.

Carrick, D., Haig, C., Ahmed, N., McEntegart, M., Petrie, M.C., Eteiba, H., Hood, S., Watkins, S., Lindsay, M.M., Davie, A., Mahrous, A., Mordi, I., Rauhalammi, S., Sattar, N., Welsh, P., Radjenovic, A., Ford, I., Oldroyd, K.G. and Berry, C. 2016b. Myocardial Hemorrhage After Acute Reperfused ST-Segment-Elevation Myocardial Infarction: Relation to Microvascular Obstruction and Prognostic Significance. *Circ Cardiovasc Imaging.* **9**(1), pe004148.

Carrick, D., Haig, C., Carberry, J., May, V.T.Y., McCartney, P., Welsh, P., Ahmed, N., McEntegart, M., Petrie, M.C., Eteiba, H., Lindsay, M., Hood, S., Watkins, S., Mahrous, A., Rauhalammi, S.M., Mordi, I., Ford, I., Radjenovic, A., Sattar, N., Oldroyd, K.G. and Berry, C. 2016c. Microvascular resistance of the culprit coronary artery in acute ST-elevation myocardial infarction. *JCI Insight.* **1**(6), pe85768.

Cecchi, F., Olivotto, I., Gistri, R., Lorenzoni, R., Chiriatti, G. and Camici, P.G. 2003. Coronary microvascular dysfunction and prognosis in hypertrophic cardiomyopathy. *N Engl J Med.* **349**(11), pp.1027-1035.

Chareonthaitawee, P., Kaufmann, P.A., Rimoldi, O. and Camici, P.G. 2001. Heterogeneity of resting and hyperemic myocardial blood flow in healthy humans. *Cardiovasc Res.* **50**(1), pp.151-161.

Chatzizisis, Y.S., Giannoglou, G.D., Parcharidis, G.E. and Louridas, G.E. 2007. Is left coronary system more susceptible to atherosclerosis than right? A pathophysiological insight. *Int J Cardiol.* **116**(1), pp.7-13.

Chilian, W.M., Layne, S.M., Klausner, E.C., Eastham, C.L. and Marcus, M.L. 1989. Redistribution of coronary microvascular resistance produced by dipyridamole. *Am J Physiol.* **256**(2 Pt 2), pp.H383-390.

Christian, T.F., Rettmann, D.W., Aletras, A.H., Liao, S.L., Taylor, J.L., Balaban, R.S. and Arai, A.E. 2004. Absolute myocardial perfusion in canines measured by using dual-bolus first-pass MR imaging. *Radiology.* **232**(3), pp.677-684.

Corcoran, D., Ford, T.J., Hsu, L.Y., Chiribiri, A., Orchard, V., Mangion, K., McEntegart, M., Rocchiccioli, P., Watkins, S., Good, R., Brooksbank, K., Padmanabhan, S., Sattar, N., McConnachie, A., Oldroyd, K.G., Touyz, R.M., Arai, A. and Berry, C. 2018a. Rationale and design of the Coronary Microvascular Angina Cardiac Magnetic Resonance Imaging (CorCMR) diagnostic study: the CorMicA CMR sub-study. *Open Heart.* **5**(2), pe000924.

Corcoran, D., Young, R., Adlam, D., McConnachie, A., Mangion, K., Ripley, D., Cairns, D., Brown, J., Bucciarelli-Ducci, C., Baumbach, A., Kharbanda, R., Oldroyd, K.G., McCann, G.P., Greenwood, J.P. and Berry, C. 2018b. Coronary microvascular dysfunction in patients with stable coronary artery disease: The CE-MARC 2 coronary physiology sub-study. *Int J Cardiol.* **266**, pp.7-14.

Cox, D.A., Vita, J.A., Treasure, C.B., Fish, R.D., Alexander, R.W., Ganz, P. and Selwyn, A.P. 1989. Atherosclerosis impairs flow-mediated dilation of coronary arteries in humans. *Circulation.* **80**(3), pp.458-465.

Czernin, J., Muller, P., Chan, S., Brunken, R.C., Porenta, G., Krivokapich, J., Chen, K., Chan, A., Phelps, M.E. and Schelbert, H.R. 1993. Influence of age and hemodynamics on myocardial blood flow and flow reserve. *Circulation.* **88**(1), pp.62-69.

Danad, I., Raijmakers, P.G., Appelman, Y.E., Harms, H.J., de Haan, S., van den Oever, M.L., van Kuijk, C., Allaart, C.P., Hoekstra, O.S., Lammertsma, A.A., Lubberink, M., van Rossum, A.C. and Knaapen, P. 2012. Coronary risk factors and myocardial blood flow in patients evaluated for coronary artery disease: a quantitative [15O]H2O PET/CT study. *Eur J Nucl Med Mol Imaging.* **39**(1), pp.102-112.

Davies, J.E., Sen, S., Dehbi, H.M., Al-Lamee, R., Petraco, R., Nijjer, S.S., Bhindi, R., Lehman, S.J., Walters, D., Sapontis, J., Janssens, L., Vrints, C.J., Khashaba, A., Laine, M., Van Belle, E., Krackhardt, F., Bojara, W., Going, O., Harle, T., Indolfi, C., Niccoli, G., Ribichini, F., Tanaka, N., Yokoi, H., Takashima, H., Kikuta, Y., Erglis, A., Vinhas, H., Canas Silva, P., Baptista, S.B., Alghamdi, A., Hellig, F., Koo, B.K., Nam, C.W., Shin, E.S., Doh, J.H., Brugaletta, S., Alegria-Barrero, E., Meuwissen, M., Piek, J.J., van Royen, N., Sezer, M., Di Mario, C., Gerber, R.T., Malik, I.S., Sharp, A.S.P., Talwar, S., Tang, K., Samady, H., Altman, J., Seto, A.H., Singh, J., Jeremias, A., Matsuo, H., Kharbanda, R.K., Patel, M.R., Serruys, P. and Escaned, J. 2017. Use of the Instantaneous Wave-free Ratio or Fractional Flow Reserve in PCI. *N Engl J Med.* **376**(19), pp.1824-1834.

Dayanikli, F., Grambow, D., Muzik, O., Mosca, L., Rubenfire, M. and Schwaiger, M. 1994. Early detection of abnormal coronary flow reserve in asymptomatic men at high risk for coronary artery disease using positron emission tomography. *Circulation.* **90**(2), pp.808-817.

De Bruyne, B., Adjedj, J., Xaplanteris, P., Ferrara, A., Mo, Y., Penicka, M., Flore, V., Pellicano, M., Toth, G., Barbato, E., Duncker, D.J. and Pijls, N.H. 2017. Saline-

Induced Coronary Hyperemia: Mechanisms and Effects on Left Ventricular Function. *Circ Cardiovasc Interv.* **10**(4).

De Bruyne, B., Bartunek, J., Sys, S.U. and Heyndrickx, G.R. 1995. Relation between myocardial fractional flow reserve calculated from coronary pressure measurements and exercise-induced myocardial ischemia. *Circulation.* **92**(1), pp.39-46.

de Bruyne, B., Bartunek, J., Sys, S.U., Pijls, N.H., Heyndrickx, G.R. and Wijns, W. 1996. Simultaneous coronary pressure and flow velocity measurements in humans. Feasibility, reproducibility, and hemodynamic dependence of coronary flow velocity reserve, hyperemic flow versus pressure slope index, and fractional flow reserve. *Circulation.* **94**(8), pp.1842-1849.

De Bruyne, B., Fearon, W.F., Pijls, N.H., Barbato, E., Tonino, P., Piroth, Z., Jagic, N., Mobius-Winckler, S., Rioufol, G., Witt, N., Kala, P., MacCarthy, P., Engstrom, T., Oldroyd, K., Mavromatis, K., Manoharan, G., Verlee, P., Frobert, O., Curzen, N., Johnson, J.B., Limacher, A., Nuesch, E. and Juni, P. 2014. Fractional flow reserve-guided PCI for stable coronary artery disease. *N Engl J Med.* **371**(13), pp.1208-1217.

De Bruyne, B., Hersbach, F., Pijls, N.H., Bartunek, J., Bech, J.W., Heyndrickx, G.R., Gould, K.L. and Wijns, W. 2001. Abnormal epicardial coronary resistance in patients with diffuse atherosclerosis but "Normal" coronary angiography. *Circulation.* **104**(20), pp.2401-2406.

De Bruyne, B., Pijls, N.H., Kalesan, B., Barbato, E., Tonino, P.A., Piroth, Z., Jagic, N., Mobius-Winkler, S., Rioufol, G., Witt, N., Kala, P., MacCarthy, P., Engstrom, T., Oldroyd, K.G., Mavromatis, K., Manoharan, G., Verlee, P., Frobert, O., Curzen, N., Johnson, J.B., Juni, P. and Fearon, W.F. 2012. Fractional flow reserve-guided PCI versus medical therapy in stable coronary disease. *N Engl J Med.* **367**(11), pp.991-1001.

De Bruyne, B., Pijls, N.H.J., Barbato, E., Bartunek, J., Bech, J.-W., Wijns, W. and Heyndrickx, G.R. 2003. Intracoronary and Intravenous Adenosine 5′-Triphosphate, Adenosine, Papaverine, and Contrast Medium to Assess Fractional Flow Reserve in Humans. *Circulation.* **107**(14), pp.1877-1883.

De Maria, G.L., Alkhalil, M., Wolfrum, M., Fahrni, G., Borlotti, A., Gaughran, L., Dawkins, S., Langrish, J.P., Lucking, A.J., Choudhury, R.P., Porto, I., Crea, F., Dall'Armellina, E., Channon, K.M., Kharbanda, R.K. and Banning, A.P. 2019. Index of Microcirculatory Resistance as a Tool to Characterize Microvascular Obstruction and to Predict Infarct Size Regression in Patients With STEMI Undergoing Primary PCI. *JACC Cardiovasc Imaging.* **12**(5), pp.837-848.

de Waha, S., Patel, M.R., Granger, C.B., Ohman, E.M., Maehara, A., Eitel, I., Ben-Yehuda, O., Jenkins, P., Thiele, H. and Stone, G.W. 2017. Relationship between microvascular obstruction and adverse events following primary percutaneous coronary intervention for ST-segment elevation myocardial infarction: an individual patient data pooled analysis from seven randomized trials. *Eur Heart J.* **38**(47), pp.3502-3510.

Dorbala, S., Vangala, D., Bruyere, J., Jr., Quarta, C., Kruger, J., Padera, R., Foster, C., Hanley, M., Di Carli, M.F. and Falk, R. 2014. Coronary microvascular dysfunction is related to abnormalities in myocardial structure and function in cardiac amyloidosis. *JACC Heart Fail.* **2**(4), pp.358-367.

Doucette, J.W., Corl, P.D., Payne, H.M., Flynn, A.E., Goto, M., Nassi, M. and Segal, J. 1992. Validation of a Doppler guide wire for intravascular measurement of coronary artery flow velocity. *Circulation.* **85**(5), pp.1899-1911.

Duncker, D.J., Koller, A., Merkus, D. and Canty, J.M., Jr. 2015. Regulation of coronary blood flow in health and ischemic heart disease. *Prog Cardiovasc Dis.* **57**(5), pp.409-422.

Echavarria-Pinto, M., Escaned, J., Macias, E., Medina, M., Gonzalo, N., Petraco, R., Sen, S., Jimenez-Quevedo, P., Hernandez, R., Mila, R., Ibanez, B., Nunez-Gil, I.J., Fernandez, C., Alfonso, F., Banuelos, C., Garcia, E., Davies, J., Fernandez-Ortiz, A. and Macaya, C. 2013. Disturbed coronary hemodynamics in vessels with intermediate stenoses evaluated with fractional flow reserve: a combined analysis of epicardial and microcirculatory involvement in ischemic heart disease. *Circulation.* **128**(24), pp.2557-2566.

Eeckhout, E. and Kern, M.J. 2001. The coronary no-reflow phenomenon: a review of mechanisms and therapies. *Eur Heart J.* **22**(9), pp.729-739.

Eek, C., Grenne, B., Brunvand, H., Aakhus, S., Endresen, K., Hol, P.K., Smith, H.J., Smiseth, O.A., Edvardsen, T. and Skulstad, H. 2010. Strain echocardiography and wall motion score index predicts final infarct size in patients with non-ST-segment-elevation myocardial infarction. *Circ Cardiovasc Imaging.* **3**(2), pp.187-194.

Eitel, I., de Waha, S., Wöhrle, J., Fuernau, G., Lurz, P., Pauschinger, M., Desch, S., Schuler, G. and Thiele, H. 2014. Comprehensive Prognosis Assessment by CMR Imaging After ST-Segment Elevation Myocardial Infarction. *Journal of the American College of Cardiology.* **64**(12), pp.1217-1226.

Elgendy, I.Y., Huo, T., Bhatt, D.L. and Bavry, A.A. 2015. Is Aspiration Thrombectomy Beneficial in Patients Undergoing Primary Percutaneous Coronary Intervention? Meta-Analysis of Randomized Trials. *Circ Cardiovasc Interv.* **8**(7), pe002258.

Elliott, P.M., Kindler, H., Shah, J.S., Sachdev, B., Rimoldi, O.E., Thaman, R., Tome, M.T., McKenna, W.J., Lee, P. and Camici, P.G. 2006. Coronary microvascular dysfunction in male patients with Anderson-Fabry disease and the effect of treatment with alpha galactosidase A. *Heart.* **92**(3), pp.357-360.

Fearon, W.F., Balsam, L.B., Farouque, H.M.O., Robbins, R.C., Fitzgerald, P.J., Yock, P.G. and Yeung, A.C. 2003. Novel Index for Invasively Assessing the Coronary Microcirculation. *Circulation.* **107**(25), pp.3129-3132.

Fearon, W.F., Low, A.F., Yong, A.S., McGeoch, R., Berry, C., Shah, M.G., Ho, M.Y., Kim, H.-S., Loh, J.P. and Oldroyd, K.G. 2013. Prognostic Value of the Index of Microcirculatory Resistance Measured After Primary Percutaneous Coronary Intervention. *Circulation.* **127**(24), pp.2436-2441.

Fearon, W.F., Low, A.F., Yong, A.S., McGeoch, R., Berry, C., Shah, M.G., Ho, M.Y., Kim, H.S., Loh, J.P. and Oldroyd, K.G. 2013. Prognostic value of the Index of Microcirculatory Resistance measured after primary percutaneous coronary intervention. *Circulation.* **127**(24), pp.2436-2441.

Feher, A. and Sinusas, A.J. 2017. Quantitative Assessment of Coronary Microvascular Function: Dynamic Single-Photon Emission Computed Tomography,

Positron Emission Tomography, Ultrasound, Computed Tomography, and Magnetic Resonance Imaging. *Circ Cardiovasc Imaging.* **10**(8).

Flett, A.S., Hasleton, J., Cook, C., Hausenloy, D., Quarta, G., Ariti, C., Muthurangu, V. and Moon, J.C. 2011. Evaluation of techniques for the quantification of myocardial scar of differing etiology using cardiac magnetic resonance. *JACC Cardiovasc Imaging.* **4**(2), pp.150-156.

Fröhlich, G.M., Meier, P., White, S.K., Yellon, D.M. and Hausenloy, D.J. 2013. Myocardial reperfusion injury: looking beyond primary PCI. *European Heart Journal.* **34**(23), pp.1714-1722.

Ganz, W., Tamura, K., Marcus, H.S., Donoso, R., Yoshida, S. and Swan, H.J. 1971. Measurement of coronary sinus blood flow by continuous thermodilution in man. *Circulation.* **44**(2), pp.181-195.

Garg, P., Broadbent David, A., Swoboda Peter, P., Foley James, R.J., Fent Graham, J., Musa Tarique, A., Ripley David, P., Erhayiem, B., Dobson Laura, E., McDiarmid Adam, K., Haaf, P., Kidambi, A., van der Geest Rob, J., Greenwood John, P. and Plein, S. 2017. Acute Infarct Extracellular Volume Mapping to Quantify Myocardial Area at Risk and Chronic Infarct Size on Cardiovascular Magnetic Resonance Imaging. *Circulation: Cardiovascular Imaging.* **10**(7), pe006182.

Gianrossi, R., Detrano, R., Mulvihill, D., Lehmann, K., Dubach, P., Colombo, A., McArthur, D. and Froelicher, V. 1989. Exercise-induced ST depression in the diagnosis of coronary artery disease. A meta-analysis. *Circulation.* **80**(1), pp.87-98.

Gibbons, R.J., Verani, M.S., Behrenbeck, T., Pellikka, P.A., O'Connor, M.K., Mahmarian, J.J., Chesebro, J.H. and Wackers, F.J. 1989. Feasibility of tomographic 99mTc-hexakis-2-methoxy-2-methylpropyl-isonitrile imaging for the assessment of myocardial area at risk and the effect of treatment in acute myocardial infarction. *Circulation.* **80**(5), pp.1277-1286.

Gibson, C.M., Cannon, C.P., Murphy, S.A., Marble, S.J., Barron, H.V. and Braunwald, E. 2002. Relationship of the TIMI myocardial perfusion grades, flow grades, frame count, and percutaneous coronary intervention to long-term outcomes after thrombolytic administration in acute myocardial infarction. *Circulation.* **105**(16), pp.1909-1913.

Gibson, C.M., Cannon, C.P., Murphy, S.A., Ryan, K.A., Mesley, R., Marble, S.J., McCabe, C.H., Van De Werf, F. and Braunwald, E. 2000. Relationship of TIMI myocardial perfusion grade to mortality after administration of thrombolytic drugs. *Circulation.* **101**(2), pp.125-130.

Gick, M., Jander, N., Bestehorn, H.P., Kienzle, R.P., Ferenc, M., Werner, K., Comberg, T., Peitz, K., Zohlnhofer, D., Bassignana, V., Buettner, H.J. and Neumann, F.J. 2005. Randomized evaluation of the effects of filter-based distal protection on myocardial perfusion and infarct size after primary percutaneous catheter intervention in myocardial infarction with and without ST-segment elevation. *Circulation.* **112**(10), pp.1462-1469.

Gislason-Lee, A.J., Hoornaert, B., Cowen, A.R. and Davies, A.G. 2013. Understanding automated dose control in dynamic X-ray imaging systems. In: *European Congress of Radiology*, *2013-03, Vienna, Austria*.

Go, A.S., Mozaffarian, D., Roger, V.L., Benjamin, E.J., Berry, J.D., Blaha, M.J., Dai, S., Ford, E.S., Fox, C.S., Franco, S., Fullerton, H.J., Gillespie, C., Hailpern, S.M., Heit, J.A., Howard, V.J., Huffman, M.D., Judd, S.E., Kissela, B.M., Kittner, S.J., Lackland, D.T., Lichtman, J.H., Lisabeth, L.D., Mackey, R.H., Magid, D.J., Marcus, G.M., Marelli, A., Matchar, D.B., McGuire, D.K., Mohler, E.R., 3rd, Moy, C.S., Mussolino, M.E., Neumar, R.W., Nichol, G., Pandey, D.K., Paynter, N.P., Reeves, M.J., Sorlie, P.D., Stein, J., Towfighi, A., Turan, T.N., Virani, S.S., Wong, N.D., Woo, D. and Turner, M.B. 2014. Executive summary: heart disease and stroke statistics--2014 update: a report from the American Heart Association. *Circulation.* **129**(3), pp.399-410.

Gotberg, M., Christiansen, E.H., Gudmundsdottir, I.J., Sandhall, L., Danielewicz, M., Jakobsen, L., Olsson, S.E., Ohagen, P., Olsson, H., Omerovic, E., Calais, F., Lindroos, P., Maeng, M., Todt, T., Venetsanos, D., James, S.K., Karegren, A., Nilsson, M., Carlsson, J., Hauer, D., Jensen, J., Karlsson, A.C., Panayi, G., Erlinge, D. and Frobert, O. 2017. Instantaneous Wave-free Ratio versus Fractional Flow Reserve to Guide PCI. *N Engl J Med.* **376**(19), pp.1813-1823.

Gould, K.L. and Lipscomb, K. 1974. Effects of coronary stenoses on coronary flow reserve and resistance. *Am J Cardiol.* **34**(1), pp.48-55.

Gregory, S.A., MacRae, C.A., Aziz, K., Sims, K.B., Schmahmann, J.D., Kardan, A., Morss, A.M., Ellinor, P.T., Tawakol, A., Fischman, A.J. and Gewirtz, H. 2007. Myocardial blood flow and oxygen consumption in patients with Friedreich's ataxia prior to the onset of cardiomyopathy. *Coron Artery Dis.* **18**(1), pp.15-22.

Grodzinsky, A., Arnold, S.V., Gosch, K., Spertus, J.A., Foody, J.M., Beltrame, J., Maddox, T.M., Parashar, S. and Kosiborod, M. 2015. Angina Frequency After Acute Myocardial Infarction In Patients Without Obstructive Coronary Artery Disease. *Eur Heart J Qual Care Clin Outcomes.* **1**(2), pp.92-99.

Gulati, M., Cooper-DeHoff, R.M., McClure, C., Johnson, B.D., Shaw, L.J., Handberg, E.M., Zineh, I., Kelsey, S.F., Arnsdorf, M.F., Black, H.R., Pepine, C.J. and Merz, C.N. 2009. Adverse cardiovascular outcomes in women with nonobstructive coronary artery disease: a report from the Women's Ischemia Syndrome Evaluation Study and the St James Women Take Heart Project. *Arch Intern Med.* **169**(9), pp.843-850.

Guzman, S.V. and West, J.W. 1959. Cardiac effects of intracoronary arterial injections of various roentgenographic contrast media. *Am Heart J.* **58**, pp.597-607.

Hamaya, R., Kanaji, Y., Usui, E., Hoshino, M., Murai, T., Yonetsu, T. and Kakuta, T. 2019. Improvement of Fractional Flow Reserve after Percutaneous Coronary Intervention Does Not Necessarily Indicate Increased Coronary Flow. *Eur Cardiol.* **14**(1), pp.10-12.

Hennigan, B., Oldroyd, K.G., Berry, C., Johnson, N., McClure, J., McCartney, P., McEntegart, M.B., Eteiba, H., Petrie, M.C., Rocchiccioli, P., Good, R., Lindsay, M.M., Hood, S. and Watkins, S. 2016. Discordance Between Resting and Hyperemic Indices of Coronary Stenosis Severity: The VERIFY 2 Study (A Comparative Study of Resting Coronary Pressure Gradient, Instantaneous Wave-Free Ratio and Fractional Flow Reserve in an Unselected Population Referred for Invasive Angiography). *Circ Cardiovasc Interv.* **9**(11).

Heusch, G. 2010. Adenosine and maximum coronary vasodilation in humans: myth and misconceptions in the assessment of coronary reserve. *Basic Res Cardiol.* **105**(1), pp.1-5.

Heusch, G., Skyschally, A. and Schulz, R. 2011. Cardioprotection by ivabradine through heart rate reduction and beyond. *J Cardiovasc Pharmacol Ther.* **16**(3-4), pp.281-284.

Higuchi, T., Abletshauser, C., Nekolla, S.G., Schwaiger, M. and Bengel, F.M. 2007. Effect of the angiotensin receptor blocker Valsartan on coronary microvascular flow reserve in moderately hypertensive patients with stable coronary artery disease. *Microcirculation.* **14**(8), pp.805-812.

Hillenbrand, H.B., Kim, R.J., Parker, M.A., Fieno, D.S. and Judd, R.M. 2000. Early assessment of myocardial salvage by contrast-enhanced magnetic resonance imaging. *Circulation.* **102**(14), pp.1678-1683.

Ho, K.T., Chua, K.C., Klotz, E. and Panknin, C. 2010. Stress and rest dynamic myocardial perfusion imaging by evaluation of complete time-attenuation curves with dual-source CT. *JACC Cardiovasc Imaging.* **3**(8), pp.811-820.

Hoffman, J.I. 2000. Problems of coronary flow reserve. *Ann Biomed Eng.* **28**(8), pp.884-896.

Hoffman, J.I. and Spaan, J.A. 1990. Pressure-flow relations in coronary circulation. *Physiol Rev.* **70**(2), pp.331-390.

Hwang, D., Lee, J.M. and Koo, B.-K. 2016. Physiologic Assessment of Coronary Artery Disease: Focus on Fractional Flow Reserve. *Korean journal of radiology.* **17**(3), pp.307-320.

Ishihara, M., Sato, H., Tateishi, H., Kawagoe, T., Shimatani, Y., Kurisu, S. and Sakai, K. 1996. Attenuation of the no-reflow phenomenon after coronary angioplasty for acute myocardial infarction with intracoronary papaverine. *Am Heart J.* **132**(5), pp.959-963.

Iskandrian, A.E., Bateman, T.M., Belardinelli, L., Blackburn, B., Cerqueira, M.D., Hendel, R.C., Lieu, H., Mahmarian, J.J., Olmsted, A., Underwood, S.R., Vitola, J. and Wang, W. 2007. Adenosine versus regadenoson comparative evaluation in myocardial perfusion imaging: results of the ADVANCE phase 3 multicenter international trial. *J Nucl Cardiol.* **14**(5), pp.645-658.

Jenni, R., Buchi, M., Jakob, M. and Ritter, M. 1998a. Position control of intravascular Doppler guidewire: concept of a tracking indicator and its clinical implications. *Cathet Cardiovasc Diagn.* **44**(1), pp.28-33.

Jenni, R., Buchi, M., Zweifel, H.J. and Ritter, M. 1998b. Impact of Doppler guidewire size and flow rates on intravascular velocity profiles. *Cathet Cardiovasc Diagn.* **45**(1), pp.96-100.

Jeremias, A., Kirtane, A.J. and Stone, G.W. 2017. A Test in Context: Fractional Flow Reserve: Accuracy, Prognostic Implications, and Limitations. *J Am Coll Cardiol.* **69**(22), pp.2748-2758.

Jespersen, L., Hvelplund, A., Abildstrom, S.Z., Pedersen, F., Galatius, S., Madsen, J.K., Jorgensen, E., Kelbaek, H. and Prescott, E. 2012. Stable angina pectoris with no obstructive coronary artery disease is associated with increased risks of major adverse cardiovascular events. *Eur Heart J.* **33**(6), pp.734-744.

Johnson, N.P., Jeremias, A., Zimmermann, F.M., Adjedj, J., Witt, N., Hennigan, B., Koo, B.-K., Maehara, A., Matsumura, M., Barbato, E., Esposito, G., Trimarco, B., Rioufol, G., Park, S.-J., Yang, H.-M., Baptista, S.B., Chrysant, G.S., Leone, A.M., Berry, C., De Bruyne, B., Gould, K.L., Kirkeeide, R.L., Oldroyd, K.G., Pijls, N.H.J. and Fearon, W.F. 2016. Continuum of Vasodilator Stress From Rest to Contrast Medium to Adenosine Hyperemia for Fractional Flow Reserve Assessment. *JACC: Cardiovascular Interventions.* **9**(8), pp.757-767.

Johnson, N.P., Kirkeeide, R.L., Asrress, K.N., Fearon, W.F., Lockie, T., Marques, K.M.J., Pyxaras, S.A., Rolandi, M.C., van 't Veer, M., De Bruyne, B., Piek, J.J., Pijls, N.H.J., Redwood, S., Siebes, M., Spaan, J.A.E. and Gould, K.L. 2013. Does the Instantaneous Wave-Free Ratio Approximate the Fractional Flow Reserve? *Journal of the American College of Cardiology.* **61**(13), pp.1428-1435.

Johnson, N.P., Kirkeeide, R.L. and Gould, K.L. 2012. Is discordance of coronary flow reserve and fractional flow reserve due to methodology or clinically relevant coronary pathophysiology? *JACC Cardiovasc Imaging.* **5**(2), pp.193-202.

Johnson, N.P., Toth, G.G., Lai, D., Zhu, H., Acar, G., Agostoni, P., Appelman, Y., Arslan, F., Barbato, E., Chen, S.L., Di Serafino, L., Dominguez-Franco, A.J., Dupouy, P., Esen, A.M., Esen, O.B., Hamilos, M., Iwasaki, K., Jensen, L.O., Jimenez-Navarro, M.F., Katritsis, D.G., Kocaman, S.A., Koo, B.K., Lopez-Palop, R., Lorin, J.D., Miller, L.H., Muller, O., Nam, C.W., Oud, N., Puymirat, E., Rieber, J., Rioufol, G., Rodes-Cabau, J., Sedlis, S.P., Takeishi, Y., Tonino, P.A., Van Belle, E., Verna, E., Werner, G.S., Fearon, W.F., Pijls, N.H., De Bruyne, B. and Gould, K.L. 2014. Prognostic value of fractional flow reserve: linking physiologic severity to clinical outcomes. *J Am Coll Cardiol.* **64**(16), pp.1641-1654.

Jolly, S.S., James, S.K., Dzavik, V., Cairns, J.A., Mahmoud, K.D., Zijlstra, F., Yusuf, S., Olivecrona, G.K., Renlund, H., Gao, P., Lagerqvist, B., Alazzoni, A., Kedev, S., Stankovic, G., Meeks, B. and Frobert, O. 2016. Thrombus Aspiration in ST Elevation Myocardial Infarction: An Individual Patient Meta-analysis. *Circulation.* **9**(116), p025371.

Kanaji, Y., Murai, T., Yonetsu, T., Usui, E., Araki, M., Matsuda, J., Hoshino, M., Yamaguchi, M., Niida, T., Hada, M., Ichijyo, S., Hamaya, R., Kanno, Y., Isobe, M. and Kakuta, T. 2017. Effect of Elective Percutaneous Coronary Intervention on Hyperemic Absolute Coronary Blood Flow Volume and Microvascular Resistance. *Circ Cardiovasc Interv.* **10**(10).

Kang, S.J., Ahn, J.M., Han, S., Lee, J.Y., Kim, W.J., Park, D.W., Lee, S.W., Kim, Y.H., Lee, C.W., Park, S.W., Mintz, G.S. and Park, S.J. 2013. Sex differences in the visual-functional mismatch between coronary angiography or intravascular ultrasound versus fractional flow reserve. *JACC Cardiovasc Interv.* **6**(6), pp.562-568.

Kang, W.Y., Jeong, M.H., Ahn, Y.K., Kim, J.H., Chae, S.C., Kim, Y.J., Hur, S.H., Seong, I.W., Hong, T.J., Choi, D.H., Cho, M.C., Kim, C.J., Seung, K.B., Chung, W.S., Jang, Y.S., Rha, S.W., Bae, J.H., Cho, J.G. and Park, S.J. 2011. Are patients with angiographically near-normal coronary arteries who present as acute myocardial infarction actually safe? *Int J Cardiol.* **146**(2), pp.207-212.

Kaufmann, P.A., Gnecchi-Ruscone, T., di Terlizzi, M., Schafers, K.P., Luscher, T.F. and Camici, P.G. 2000. Coronary heart disease in smokers: vitamin C restores coronary microcirculatory function. *Circulation.* **102**(11), pp.1233-1238.

Kelbaek, H., Terkelsen, C.J., Helqvist, S., Lassen, J.F., Clemmensen, P., Klovgaard, L., Kaltoft, A., Engstrom, T., Botker, H.E., Saunamaki, K., Krusell, L.R., Jorgensen, E., Hansen, H.H., Christiansen, E.H., Ravkilde, J., Kober, L., Kofoed, K.F. and Thuesen, L. 2008. Randomized comparison of distal protection versus conventional treatment in primary percutaneous coronary intervention: the drug elution and distal protection in ST-elevation myocardial infarction (DEDICATION) trial. *J Am Coll Cardiol.* **51**(9), pp.899-905.

Kellman, P. and Arai, A.E. 2007. Imaging sequences for first pass perfusion --a review. *J Cardiovasc Magn Reson.* **9**(3), pp.525-537.

Kennedy, M.W., Kaplan, E., Hermanides, R.S., Fabris, E., Hemradj, V., Koopmans, P.C., Dambrink, J.-H.E., Marcel Gosselink, A.T., van't Hof, A.W.J., Ottervanger, J.P., Roolvink, V., Remkes, W.S., van der Sluis, A., Suryapranata, H. and Kedhi, E. 2016. Clinical outcomes of deferred revascularisation using fractional flow reserve in patients with and without diabetes mellitus. *Cardiovascular Diabetology.* **15**, p100.

Kern, M.J., Lerman, A., Bech, J.W., De Bruyne, B., Eeckhout, E., Fearon, W.F., Higano, S.T., Lim, M.J., Meuwissen, M., Piek, J.J., Pijls, N.H., Siebes, M. and Spaan, J.A. 2006. Physiological assessment of coronary artery disease in the cardiac catheterization laboratory: a scientific statement from the American Heart Association Committee on Diagnostic and Interventional Cardiac Catheterization, Council on Clinical Cardiology. *Circulation.* **114**(12), pp.1321-1341.

Klein, R., Beanlands, R.S. and deKemp, R.A. 2010. Quantification of myocardial blood flow and flow reserve: Technical aspects. *J Nucl Cardiol.* **17**(4), pp.555-570.

KLOSTER, F.E., FRIESEN, W.G., GREEN, G.S. and JUDKINS, M.P. 1972. Effects of Coronary Arteriography on Myocardial Blood Flow. *Circulation.* **46**(3), pp.438-444.

Kobayashi, Y., Johnson, N.P., Berry, C., De Bruyne, B., Gould, K.L., Jeremias, A., Oldroyd, K.G., Pijls, N.H.J. and Fearon, W.F. 2016. The Influence of Lesion Location on the Diagnostic Accuracy of Adenosine-Free Coronary Pressure Wire Measurements. *JACC Cardiovasc Interv.* **9**(23), pp.2390-2399.

Koo, B.K., Erglis, A., Doh, J.H., Daniels, D.V., Jegere, S., Kim, H.S., Dunning, A., DeFrance, T., Lansky, A., Leipsic, J. and Min, J.K. 2011. Diagnosis of ischemia-causing coronary stenoses by noninvasive fractional flow reserve computed from coronary computed tomographic angiograms. Results from the prospective multicenter DISCOVER-FLOW (Diagnosis of Ischemia-Causing Stenoses Obtained Via Noninvasive Fractional Flow Reserve) study. *J Am Coll Cardiol.* **58**(19), pp.1989-1997.

Kopecky, S.L., Aviles, R.J., Bell, M.R., Lobl, J.K., Tipping, D., Frommell, G., Ramsey, K., Holland, A.E., Midei, M., Jain, A., Kellett, M. and Gibbons, R.J. 2003. A randomized, double-blinded, placebo-controlled, dose-ranging study measuring the effect of an adenosine agonist on infarct size reduction in patients undergoing primary percutaneous transluminal coronary angioplasty: the ADMIRE (AmP579 Delivery for Myocardial Infarction REduction) study. *Am Heart J.* **146**(1), pp.146-152.

Kruse, M.J., Kovell, L., Kasper, E.K., Pomper, M.G., Moller, D.R., Solnes, L., Chen, E.S. and Schindler, T.H. 2017. Myocardial Blood Flow and Inflammatory Cardiac Sarcoidosis. *JACC Cardiovasc Imaging.* **10**(2), pp.157-167.

Kuhle, W.G., Porenta, G., Huang, S.C., Buxton, D., Gambhir, S.S., Hansen, H., Phelps, M.E. and Schelbert, H.R. 1992. Quantification of regional myocardial blood flow using 13N-ammonia and reoriented dynamic positron emission tomographic imaging. *Circulation.* **86**(3), pp.1004-1017.

Kul, S., Kutlu, G.A., Guvenc, T.S., Kavas, M., Demircioglu, K., Yilmaz, Y., Yakar, H.I., Kanbay, A., Boga, S. and Caliskan, M. 2017. Coronary flow reserve is reduced in sarcoidosis. *Atherosclerosis.* **264**, pp.115-121.

Kurata, A., Kono, A., Sakamoto, T., Kido, T., Mochizuki, T., Higashino, H., Abe, M., Coenen, A., Saru-Chelu, R.G., de Feyter, P.J., Krestin, G.P. and Nieman, K. 2015. Quantification of the myocardial area at risk using coronary CT angiography and Voronoi algorithm-based myocardial segmentation. *Eur Radiol.* **25**(1), pp.49-57.

Kurata, A., Mochizuki, T., Koyama, Y., Haraikawa, T., Suzuki, J., Shigematsu, Y. and Higaki, J. 2005. Myocardial perfusion imaging using adenosine triphosphate stress multi-slice spiral computed tomography: alternative to stress myocardial perfusion scintigraphy. *Circ J.* **69**(5), pp.550-557.

Leaker, B.R., O'Connor, B., Hansel, T.T., Barnes, P.J., Meng, L., Mathur, V.S. and Lieu, H.D. 2008. Safety of regadenoson, an adenosine A2A receptor agonist for myocardial perfusion imaging, in mild asthma and moderate asthma patients: a randomized, double-blind, placebo-controlled trial. *J Nucl Cardiol.* **15**(3), pp.329-336.

Lee, J.M., Lee, S.H., Hwang, D., Rhee, T.M., Choi, K.H., Kim, J., Park, J., Kim, H.Y., Jung, H.W., Cho, Y.K., Yoon, H.J., Song, Y.B., Hahn, J.Y., Nam, C.W., Shin, E.S., Doh, J.H., Hur, S.H. and Koo, B.K. 2020. Long-Term Clinical Outcomes of Nonhyperemic Pressure Ratios: Resting Full-Cycle Ratio, Diastolic Pressure Ratio, and Instantaneous Wave-Free Ratio. *J Am Heart Assoc.* **9**(18), pe016818.

Lerman, A., Holmes, D.R., Herrmann, J. and Gersh, B.J. 2007. Microcirculatory dysfunction in ST-elevation myocardial infarction: cause, consequence, or both?The opinions expressed in this article are not necessarily those of the Editors of the European Heart Journal or of the European Society of Cardiology. *European Heart Journal.* **28**(7), pp.788-797.

Li, Y., Yang, D., Lu, L., Wu, D., Yao, J., Hu, X., Long, M., Luo, C. and Du, Z. 2015. Thermodilutional Confirmation of Coronary Microvascular Dysfunction in Patients With Recurrent Angina After Successful Percutaneous Coronary Intervention. *Can J Cardiol.* **31**(8), pp.989-997.

Licka, M., Zimmermann, R., Zehelein, J., Dengler, T.J., Katus, H.A. and Kübler, W. 2002. Troponin T concentrations 72 hours after myocardial infarction as a serological estimate of infarct size. *Heart.* **87**(6), pp.520-524.

Lim, H.S., Tonino, P.A., De Bruyne, B., Yong, A.S., Lee, B.K., Pijls, N.H. and Fearon, W.F. 2014. The impact of age on fractional flow reserve-guided percutaneous coronary intervention: a FAME (Fractional Flow Reserve versus Angiography for Multivessel Evaluation) trial substudy. *Int J Cardiol.* **177**(1), pp.66-70.

Liu, A., Wijesurendra, R.S., Liu, J.M., Greiser, A., Jerosch-Herold, M., Forfar, J.C., Channon, K.M., Piechnik, S.K., Neubauer, S., Kharbanda, R.K. and Ferreira, V.M. 2018. Gadolinium-Free Cardiac MR Stress T1-Mapping to Distinguish Epicardial From Microvascular Coronary Disease. *J Am Coll Cardiol.* **71**(9), pp.957-968.

Loukas, M., Sharma, A., Blaak, C., Sorenson, E. and Mian, A. 2013. The clinical anatomy of the coronary arteries. *J Cardiovasc Transl Res.* **6**(2), pp.197-207.

Luo, C., Long, M., Hu, X., Huang, Z., Hu, C., Gao, X. and Du, Z. 2014. Thermodilution-derived coronary microvascular resistance and flow reserve in patients with cardiac syndrome X. *Circ Cardiovasc Interv.* **7**(1), pp.43-48.

Marcus, M.L., Doty, D.B., Hiratzka, L.F., Wright, C.B. and Eastham, C.L. 1982. Decreased coronary reserve: a mechanism for angina pectoris in patients with aortic stenosis and normal coronary arteries. *N Engl J Med.* **307**(22), pp.1362-1366.

Marks, D.S., Gudapati, S., Prisant, L.M., Weir, B., diDonato-Gonzalez, C., Waller, J.L. and Houghton, J.L. 2004. Mortality in patients with microvascular disease. *J Clin Hypertens (Greenwich).* **6**(6), pp.304-309.

McAlindon, E., Pufulete, M., Harris, J., Lawton, C., Johnson, T., Strange, J., Baumbach, A. and Bucciarelli-Ducci, C. 2018. Microvascular dysfunction determines infarct characteristics in patients with reperfused ST-segment elevation myocardial infarction: The MICROcirculation in Acute Myocardial Infarction (MICRO-AMI) study. *PloS one.* **13**(11), pp.e0203750-e0203750.

McCartney, P.J., Eteiba, H., Maznyczka, A.M., McEntegart, M., Greenwood, J.P., Muir, D.F., Chowdhary, S., Gershlick, A.H., Appleby, C., Cotton, J.M., Wragg, A., Curzen, N., Oldroyd, K.G., Lindsay, M., Rocchiccioli, J.P., Shaukat, A., Good, R., Watkins, S., Robertson, K., Malkin, C., Martin, L., Gillespie, L., Ford, T.J., Petrie, M.C., Macfarlane, P.W., Tait, R.C., Welsh, P., Sattar, N., Weir, R.A., Fox, K.A., Ford, I., McConnachie, A. and Berry, C. 2019. Effect of Low-Dose Intracoronary Alteplase During Primary Percutaneous Coronary Intervention on Microvascular Obstruction in Patients With Acute Myocardial Infarction: A Randomized Clinical Trial. *Jama.* **321**(1), pp.56-68.

McGeoch, R., Watkins, S., Berry, C., Steedman, T., Davie, A., Byrne, J., Hillis, S., Lindsay, M., Robb, S., Dargie, H. and Oldroyd, K. 2010. The index of microcirculatory resistance measured acutely predicts the extent and severity of myocardial infarction in patients with ST-segment elevation myocardial infarction. *JACC Cardiovasc Interv.* **3**(7), pp.715-722.

McKetty, M.H. 1998. The AAPM/RSNA physics tutorial for residents. X-ray attenuation. *Radiographics.* **18**(1), pp.151-163; quiz 149.

Meuwissen, M., Chamuleau, S.A.J., Siebes, M., Schotborgh, C.E., Koch, K.T., de Winter, R.J., Bax, M., de Jong, A., Spaan, J.A.E. and Piek, J.J. 2001. Role of Variability in Microvascular Resistance on Fractional Flow Reserve and Coronary Blood Flow Velocity Reserve in Intermediate Coronary Lesions. *Circulation.* **103**(2), pp.184-187.

Meuwissen, M., Siebes, M., Chamuleau, S.A., van Eck-Smit, B.L., Koch, K.T., de Winter, R.J., Tijssen, J.G., Spaan, J.A. and Piek, J.J. 2002. Hyperemic stenosis resistance index for evaluation of functional coronary lesion severity. *Circulation.* **106**(4), pp.441-446.

Michail, M., Thakur, U., Mehta, O., Ramzy, J.M., Comella, A., Ihdayhid, A.R., Cameron, J.D., Nicholls, S.J., Hoole, S.P. and Brown, A.J. 2020. Non-hyperaemic pressure ratios to guide percutaneous coronary intervention. *Open Heart.* **7**(2).

Miranda-Guardiola, F., Rossi, A., Serra, A., Garcia, B., Rumoroso, J.R., Iniguez, A., Vaquerizo, B., Triano, J.L., Sierra, G. and Bruguera, J. 2009. Angiographic quantification of thrombus in ST-elevation acute myocardial infarction presenting with an occluded infarct-related artery and its relationship with results of percutaneous intervention. *J Interv Cardiol.* **22**(3), pp.207-215.

Molloi, S., Bednarz, G., Tang, J., Zhou, Y. and Mathur, T. 1998. Absolute volumetric coronary blood flow measurement with digital subtraction angiography. *Int J Card Imaging.* **14**(3), pp.137-145.

Molloi, S., Chalyan, D., Le, H. and Wong, J.T. 2012. Estimation of coronary artery hyperemic blood flow based on arterial lumen volume using angiographic images. *Int J Cardiovasc Imaging.* **28**(1), pp.1-11.

Molloi, S., Ersahin, A., Tang, J., Hicks, J. and Leung, C.Y. 1996. Quantification of Volumetric Coronary Blood Flow With Dual-Energy Digital Subtraction Angiography. *Circulation.* **93**(10), pp.1919-1927.

Molloi, S., Zhou, Y. and Kassab, G.S. 2004. Regional volumetric coronary blood flow measurement by digital angiography: In vivo validation1. *Academic Radiology.* **11**(7), pp.757-766.

Moran, A.E., Forouzanfar, M.H., Roth, G.A., Mensah, G.A., Ezzati, M., Flaxman, A., Murray, C.J. and Naghavi, M. 2014. The global burden of ischemic heart disease in 1990 and 2010: the Global Burden of Disease 2010 study. *Circulation.* **129**(14), pp.1493-1501.

Morton, G., Chiribiri, A., Ishida, M., Hussain, S.T., Schuster, A., Indermuehle, A., Perera, D., Knuuti, J., Baker, S., Hedstrom, E., Schleyer, P., O'Doherty, M., Barrington, S. and Nagel, E. 2012. Quantification of absolute myocardial perfusion in patients with coronary artery disease: comparison between cardiovascular magnetic resonance and positron emission tomography. *J Am Coll Cardiol.* **60**(16), pp.1546-1555.

Murthy, V.L., Naya, M., Foster, C.R., Hainer, J., Gaber, M., Di Carli, G., Blankstein, R., Dorbala, S., Sitek, A., Pencina, M.J. and Di Carli, M.F. 2011. Improved cardiac risk assessment with noninvasive measures of coronary flow reserve. *Circulation.* **124**(20), pp.2215-2224.

Murthy, V.L., Naya, M., Foster, C.R., Hainer, J., Gaber, M., Di Carli, G., Blankstein, R., Dorbala, S., Sitek, A., Pencina, M.J. and Di Carli, M.F. 2011. Improved Cardiac Risk Assessment With Noninvasive Measures of Coronary Flow ReserveClinical Perspective. *Circulation.* **124**(20), pp.2215-2224.

Naoumova, R.P., Kindler, H., Leccisotti, L., Mongillo, M., Khan, M.T., Neuwirth, C., Seed, M., Holvoet, P., Betteridge, J. and Camici, P.G. 2007. Pioglitazone improves myocardial blood flow and glucose utilization in nondiabetic patients with combined hyperlipidemia: a randomized, double-blind, placebo-controlled study. *J Am Coll Cardiol.* **50**(21), pp.2051-2058.

Neglia, D., Parodi, O., Gallopin, M., Sambuceti, G., Giorgetti, A., Pratali, L., Salvadori, P., Michelassi, C., Lunardi, M., Pelosi, G. and et al. 1995. Myocardial blood flow response to pacing tachycardia and to dipyridamole infusion in patients with dilated cardiomyopathy without overt heart failure. A quantitative assessment by positron emission tomography. *Circulation.* **92**(4), pp.796-804.

Ng, M.K.C., Yeung, A.C. and Fearon, W.F. 2006. Invasive Assessment of the Coronary Microcirculation: Superior Reproducibility and Less Hemodynamic Dependence of Index of Microcirculatory Resistance Compared With Coronary Flow Reserve. *Circulation.* **113**(17), pp.2054-2061.

Ng, V.G., Lansky, A.J., Toro, S., Parise, H., Cristea, E., Mehran, R. and Stone, G.W. 2016. Prognostic utility of myocardial blush grade after PCI in patients with NSTE-ACS: Analysis from the ACUITY trial. *Catheter Cardiovasc Interv.* **88**(2), pp.215-224.

Niccoli, G., Burzotta, F., Galiuto, L. and Crea, F. 2009. Myocardial no-reflow in humans. *J Am Coll Cardiol.* **54**(4), pp.281-292.

Nitenberg, A., Valensi, P., Sachs, R., Dali, M., Aptecar, E. and Attali, J.-R. 1993. Impairment of Coronary Vascular Reserve and ACh-Induced Coronary Vasodilation in Diabetic Patients With Angiographically Normal Coronary Arteries and Normal Left Ventricular Systolic Function. *Diabetes.* **42**(7), pp.1017-1025.

Nolte, F., van de Hoef, T.P., Meuwissen, M., Voskuil, M., Chamuleau, S.A.J., Henriques, J.P.S., Verberne, H.J., van Eck-Smit, B.L.F., Koch, K.T., de Winter, R.J., Spaan, J.A.E., Tijssen, J.G.P., Siebes, M. and Piek, J.J. 2014. Increased hyperaemic coronary microvascular resistance adds to the presence of myocardial ischaemia. *EuroIntervention.* **9**(12), pp.1423-1431.

Nørgaard, B.L., Leipsic, J., Gaur, S., Seneviratne, S., Ko, B.S., Ito, H., Jensen, J.M., Mauri, L., De Bruyne, B., Bezerra, H., Osawa, K., Marwan, M., Naber, C., Erglis, A., Park, S.J., Christiansen, E.H., Kaltoft, A., Lassen, J.F., Bøtker, H.E. and Achenbach, S. 2014. Diagnostic performance of noninvasive fractional flow reserve derived from coronary computed tomography angiography in suspected coronary artery disease: the NXT trial (Analysis of Coronary Blood Flow Using CT Angiography: Next Steps). *J Am Coll Cardiol.* **63**(12), pp.1145-1155.

Olivotto, I., Cecchi, F., Gistri, R., Lorenzoni, R., Chiriatti, G., Girolami, F., Torricelli, F. and Camici, P.G. 2006. Relevance of coronary microvascular flow impairment to long-term remodeling and systolic dysfunction in hypertrophic cardiomyopathy. *J Am Coll Cardiol.* **47**(5), pp.1043-1048.

Parviz, Y., Vijayan, S. and Lavi, S. 2017. A review of strategies for infarct size reduction during acute myocardial infarction. *Cardiovasc Revasc Med.* **18**(5), pp.374-383.

Parviz, Y., Waleed, M., Vijayan, S., Adlam, D., Lavi, S., Al Nooryani, A., Iqbal, J. and Stone, G.W. 2019. Cellular and molecular approaches to enhance myocardial recovery after myocardial infarction. *Cardiovasc Revasc Med.* **20**(4), pp.351-364.

Patel, M.R., Peterson, E.D., Dai, D., Brennan, J.M., Redberg, R.F., Anderson, H.V., Brindis, R.G. and Douglas, P.S. 2010. Low diagnostic yield of elective coronary angiography. *N Engl J Med.* **362**(10), pp.886-895.

Patel, N., Petraco, R., Dall'Armellina, E., Kassimis, G., De Maria, G.L., Dawkins, S., Lee, R., Prendergast, B.D., Choudhury, R.P., Forfar, J.C., Channon, K.M., Davies, J., Banning, A.P. and Kharbanda, R.K. 2015. Zero-Flow Pressure Measured Immediately After Primary Percutaneous Coronary Intervention for ST-Segment Elevation Myocardial Infarction Provides the Best Invasive Index for Predicting the Extent of Myocardial Infarction at 6 Months: An OxAMI Study (Oxford Acute Myocardial Infarction). *JACC Cardiovasc Interv.* **8**(11), pp.1410-1421.

Pathik, B., Raman, B., Mohd Amin, N.H., Mahadavan, D., Rajendran, S., McGavigan, A.D., Grover, S., Smith, E., Mazhar, J., Bridgman, C., Ganesan, A.N. and Selvanayagam, J.B. 2016. Troponin-positive chest pain with unobstructed coronary arteries: incremental diagnostic value of cardiovascular magnetic resonance imaging. *Eur Heart J Cardiovasc Imaging.* **17**(10), pp.1146-1152.

Payne, A.R., Berry, C., Doolin, O., McEntegart, M., Petrie, M.C., Lindsay, M.M., Hood, S., Carrick, D., Tzemos, N., Weale, P., McComb, C., Foster, J., Ford, I. and Oldroyd, K.G. 2012. Microvascular Resistance Predicts Myocardial Salvage and Infarct Characteristics in ST-Elevation Myocardial Infarction. *J Am Heart Assoc.* **1**(4), p24.

Pepine, C.J., Anderson, R.D., Sharaf, B.L., Reis, S.E., Smith, K.M., Handberg, E.M., Johnson, B.D., Sopko, G. and Bairey Merz, C.N. 2010. Coronary microvascular reactivity to adenosine predicts adverse outcome in women evaluated for suspected ischemia results from the National Heart, Lung and Blood Institute WISE (Women's Ischemia Syndrome Evaluation) study. *J Am Coll Cardiol.* **55**(25), pp.2825-2832.

Perera, D., Biggart, S., Postema, P., Patel, S., Lambiase, P., Marber, M. and Redwood, S. 2004. Right atrial pressure: Can it be ignored when calculating fractional flow reserve and collateral flow index? *Journal of the American College of Cardiology.* **44**(10), pp.2089-2091.

Pijls, N.H., Aengevaeren, W.R., Uijen, G.J., Hoevelaken, A., Pijnenburg, T., van Leeuwen, K. and van der Werf, T. 1991. Concept of maximal flow ratio for immediate evaluation of percutaneous transluminal coronary angioplasty result by videodensitometry. *Circulation.* **83**(3), pp.854-865.

Pijls, N.H., Bos, H.S., Uijen, G.J. and Van der Werf, T. 1988. Is nonionic isotonic iohexol the contrast agent of choice for quantitative myocardial videodensitometry? *Int J Card Imaging.* **3**(2-3), pp.117-126.

Pijls, N.H., De Bruyne, B., Peels, K., Van Der Voort, P.H., Bonnier, H.J., Bartunek, J.K.J.J. and Koolen, J.J. 1996. Measurement of fractional flow reserve to assess the functional severity of coronary-artery stenoses. *N Engl J Med.* **334**(26), pp.1703-1708.

Pijls, N.H., Uijen, G.J., Hoevelaken, A., Pijnenburg, T., van Leeuwen, K.L., Fast, J.H., Bos, H.S., Aengevaeren, W.R. and van der Werf, T. 1990. Mean transit time for videodensitometric assessment of myocardial perfusion and the concept of maximal flow ratio: a validation study in the intact dog and a pilot study in man. *Int J Card Imaging.* **5**(2-3), pp.191-202.

Pijls, N.H., van Son, J.A., Kirkeeide, R.L., De Bruyne, B. and Gould, K.L. 1993. Experimental basis of determining maximum coronary, myocardial, and collateral blood flow by pressure measurements for assessing functional stenosis severity before and after percutaneous transluminal coronary angioplasty. *Circulation.* **87**(4), pp.1354-1367.

Pijls, N.H.J., van Schaardenburgh, P., Manoharan, G., Boersma, E., Bech, J.-W., van't Veer, M., Bär, F., Hoorntje, J., Koolen, J., Wijns, W. and de Bruyne, B. 2007. Percutaneous Coronary Intervention of Functionally Nonsignificant Stenosis: 5-Year Follow-Up of the DEFER Study. *Journal of the American College of Cardiology.* **49**(21), pp.2105-2111.

Pitarys, C.J., 2nd, Virmani, R., Vildibill, H.D., Jr., Jackson, E.K. and Forman, M.B. 1991. Reduction of myocardial reperfusion injury by intravenous adenosine administered during the early reperfusion period. *Circulation.* **83**(1), pp.237-247.

Pitkänen, O.-P., Nuutila, P., Raitakari, O.T., Rönnemaa, T., Koskinen, P.J., Iida, H., Lehtimäki, T.J., Laine, H.K., Takala, T., Viikari, J.S.A. and Knuuti, J. 1998. Coronary Flow Reserve Is Reduced in Young Men With IDDM. *Diabetes.* **47**(2), pp.248-254.

Prasad, A., Zareh, M., Doherty, R., Gopal, A., Vora, H., Somma, K., Mehra, A., Clavijo, L.C., Matthews, R.V. and Shavelle, D.M. 2014. Use of regadenoson for measurement of fractional flow reserve. *Catheter Cardiovasc Interv.* **83**(3), pp.369-374.

Pries, A.R. and Reglin, B. 2017. Coronary microcirculatory pathophysiology: can we afford it to remain a black box? *Eur Heart J.* **38**(7), pp.478-488.

Quyyumi, A.A., Dakak, N., Andrews, N.P., Husain, S., Arora, S., Gilligan, D.M., Panza, J.A. and Cannon, R.O., 3rd. 1995. Nitric oxide activity in the human coronary circulation. Impact of risk factors for coronary atherosclerosis. *J Clin Invest.* **95**(4), pp.1747-1755.

Radjenovic, A., Biglands, J.D., Larghat, A., Ridgway, J.P., Ball, S.G., Greenwood, J.P., Jerosch-Herold, M. and Plein, S. 2010. Estimates of systolic and diastolic myocardial blood flow by dynamic contrast-enhanced MRI. *Magn Reson Med.* **64**(6), pp.1696-1703.

Rahman, H., Corcoran, D., Aetesam-Ur-Rahman, M., Hoole, S.P., Berry, C. and Perera, D. 2019. Diagnosis of patients with angina and non-obstructive coronary disease in the catheter laboratory. *Heart.* **105**(20), pp.1536-1542.

Rawitscher, D., Levin, T.N., Cohen, I. and Feldman, T. 1997. Rapid reversal of no-reflow using Abciximab after coronary device intervention. *Cathet Cardiovasc Diagn.* **42**(2), pp.187-190.

Recio-Mayoral, A., Mason, J.C., Kaski, J.C., Rubens, M.B., Harari, O.A. and Camici, P.G. 2009. Chronic inflammation and coronary microvascular dysfunction in patients without risk factors for coronary artery disease. *Eur Heart J.* **30**(15), pp.1837-1843.

Regenfus, M., Schlundt, C., Krahner, R., Schonegger, C., Adler, W., Ludwig, J., Daniel, W.G. and Schmid, M. 2015. Six-Year Prognostic Value of Microvascular Obstruction After Reperfused ST-Elevation Myocardial Infarction as Assessed by Contrast-Enhanced Cardiovascular Magnetic Resonance. *Am J Cardiol.* **116**(7), pp.1022-1027.

Rigo, F., Sicari, R., Gherardi, S., Djordjevic-Dikic, A., Cortigiani, L. and Picano, E. 2008. The additive prognostic value of wall motion abnormalities and coronary flow reserve during dipyridamole stress echo. *Eur Heart J.* **29**(1), pp.79-88.

Rijnierse, M.T., de Haan, S., Harms, H.J., Robbers, L.F., Wu, L., Danad, I., Beek, A.M., Heymans, M.W., van Rossum, A.C., Lammertsma, A.A., Allaart, C.P. and Knaapen, P. 2014. Impaired hyperemic myocardial blood flow is associated with inducibility of ventricular arrhythmia in ischemic cardiomyopathy. *Circ Cardiovasc Imaging.* **7**(1), pp.20-30.

Roe, M.T., Messenger, J.C., Weintraub, W.S., Cannon, C.P., Fonarow, G.C., Dai, D., Chen, A.Y., Klein, L.W., Masoudi, F.A., McKay, C., Hewitt, K., Brindis, R.G., Peterson, E.D. and Rumsfeld, J.S. 2010. Treatments, trends, and outcomes of acute myocardial infarction and percutaneous coronary intervention. *J Am Coll Cardiol.* **56**(4), pp.254-263.

Rosamond, W.D., Chambless, L.E., Heiss, G., Mosley, T.H., Coresh, J., Whitsel, E., Wagenknecht, L., Ni, H. and Folsom, A.R. 2012. Twenty-two-year trends in incidence of myocardial infarction, coronary heart disease mortality, and case fatality in 4 US communities, 1987-2008. *Circulation.* **125**(15), pp.1848-1857.

Ross, A.M., Gibbons, R.J., Stone, G.W., Kloner, R.A. and Alexander, R.W. 2005. A randomized, double-blinded, placebo-controlled multicenter trial of adenosine as an adjunct to reperfusion in the treatment of acute myocardial infarction (AMISTAD-II). *J Am Coll Cardiol.* **45**(11), pp.1775-1780.

Rossen, J.D. and Winniford, M.D. 1993. Effect of increases in heart rate and arterial pressure on coronary flow reserve in humans. *J Am Coll Cardiol.* **21**(2), pp.343-348.

Rutishauser, W., Bussmann, W.D., Noseda, G., Meier, W. and Wellauer, J. 1970. Blood flow measurement through single coronary arteries by roentgen densitometry. I. A comparison of flow measured by a radiologic technique applicable in the intact organism and by electromagnetic flowmeter. *Am J Roentgenol Radium Ther Nucl Med.* **109**(1), pp.12-20.

Sara, J.D., Widmer, R.J., Matsuzawa, Y., Lennon, R.J., Lerman, L.O. and Lerman, A. 2015. Prevalence of Coronary Microvascular Dysfunction Among Patients With Chest Pain and Nonobstructive Coronary Artery Disease. *JACC Cardiovasc Interv.* **8**(11), pp.1445-1453.

Schindler, T.H., Schelbert, H.R., Quercioli, A. and Dilsizian, V. 2010. Cardiac PET imaging for the detection and monitoring of coronary artery disease and microvascular health. *JACC Cardiovasc Imaging.* **3**(6), pp.623-640.

Seibert, J.A. 2004. X-ray imaging physics for nuclear medicine technologists. Part 1: Basic principles of x-ray production. *J Nucl Med Technol.* **32**(3), pp.139-147.

Sen, S., Asrress, K.N., Nijjer, S., Petraco, R., Malik, I.S., Foale, R.A., Mikhail, G.W., Foin, N., Broyd, C., Hadjiloizou, N., Sethi, A., Al-Bustami, M., Hackett, D., Khan, M.A., Khawaja, M.Z., Baker, C.S., Bellamy, M., Parker, K.H., Hughes, A.D., Francis, D.P., Mayet, J., Di Mario, C., Escaned, J., Redwood, S. and Davies, J.E. 2013. Diagnostic classification of the instantaneous wave-free ratio is equivalent to fractional flow reserve and is not improved with adenosine administration. Results of CLARIFY (Classification Accuracy of Pressure-Only Ratios Against Indices Using Flow Study). *J Am Coll Cardiol.* **61**(13), pp.1409-1420.

Sen, S., Escaned, J., Malik, I.S., Mikhail, G.W., Foale, R.A., Mila, R., Tarkin, J., Petraco, R., Broyd, C., Jabbour, R., Sethi, A., Baker, C.S., Bellamy, M., Al-Bustami, M., Hackett, D., Khan, M., Lefroy, D., Parker, K.H., Hughes, A.D., Francis, D.P., Di

Mario, C., Mayet, J. and Davies, J.E. 2012. Development and validation of a new adenosine-independent index of stenosis severity from coronary wave-intensity analysis: results of the ADVISE (ADenosine Vasodilator Independent Stenosis Evaluation) study. *J Am Coll Cardiol.* **59**(15), pp.1392-1402.

Sen, S., Petraco, R., Mayet, J. and Davies, J. 2014. Wave intensity analysis in the human coronary circulation in health and disease. *Curr Cardiol Rev.* **10**(1), pp.17-23.

Sezer, M., Cimen, A., Aslanger, E., Elitok, A., Umman, B., Bugra, Z., Yormaz, E., Turkmen, C., Adalet, I.S., Nisanci, Y. and Umman, S. 2009. Effect of intracoronary streptokinase administered immediately after primary percutaneous coronary intervention on long-term left ventricular infarct size, volumes, and function. *J Am Coll Cardiol.* **54**(12), pp.1065-1071.

Sezer, M., Oflaz, H., Goren, T., Okcular, I., Umman, B., Nisanci, Y., Bilge, A.K., Sanli, Y., Meric, M. and Umman, S. 2007. Intracoronary streptokinase after primary percutaneous coronary intervention. *N Engl J Med.* **356**(18), pp.1823-1834.

Shryock, J.C. and Belardinelli, L. 1997. Adenosine and adenosine receptors in the cardiovascular system: biochemistry, physiology, and pharmacology. *Am J Cardiol.* **79**(12A), pp.2-10.

Siebes, M., Chamuleau, S.A., Meuwissen, M., Piek, J.J. and Spaan, J.A. 2002. Influence of hemodynamic conditions on fractional flow reserve: parametric analysis of underlying model. *Am J Physiol Heart Circ Physiol.* **283**(4), pp.H1462-1470.

Siebes, M., Verhoeff, B.J., Meuwissen, M., de Winter, R.J., Spaan, J.A. and Piek, J.J. 2004. Single-wire pressure and flow velocity measurement to quantify coronary stenosis hemodynamics and effects of percutaneous interventions. *Circulation.* **109**(6), pp.756-762.

Skelding, K.A., Goldstein, J.A., Mehta, L., Pica, M.C. and O'Neill, W.W. 2002. Resolution of refractory no-reflow with intracoronary epinephrine. *Catheter Cardiovasc Interv.* **57**(3), pp.305-309.

Smalling, R.W., Kelley, K., Kirkeeide, R.L. and Fisher, D.J. 1985. Regional myocardial function is not affected by severe coronary depressurization provided coronary blood flow is maintained. *J Am Coll Cardiol.* **5**(4), pp.948-955.

Smedby, O. 1992. Viscosity of some contemporary contrast media before and after mixing with whole blood. *Acta Radiol.* **33**(6), pp.600-605.

Smith, H.C., Sturm, R.E. and Wood, E.H. 1973. Videodensitometric system for measurement of vessel blood flow, particularly in the coronary arteries, in man. *Am J Cardiol.* **32**(2), pp.144-150.

Stacul, F. 2001. Current iodinated contrast media. *European Radiology.* **11**(4), pp.690-697.

Svanerud, J., Ahn, J.M., Jeremias, A., van 't Veer, M., Gore, A., Maehara, A., Crowley, A., Pijls, N.H.J., De Bruyne, B., Johnson, N.P., Hennigan, B., Watkins, S., Berry, C., Oldroyd, K.G., Park, S.J. and Ali, Z.A. 2018. Validation of a novel non-hyperaemic index of coronary artery stenosis severity: the Resting Full-cycle Ratio (VALIDATE RFR) study. *EuroIntervention.* **14**(7), pp.806-814.

Tanaka, H., Abe, S., Yamashita, T., Arima, S., Saigo, M., Nakao, S., Toda, H., Nomoto, K. and Tahara, M. 1997. Serum levels of cardiac troponin I and troponin T in estimating myocardial infarct size soon after reperfusion. *Coron Artery Dis.* **8**(7), pp.433-439.

Tatineni, S., Kern, M.J., Deligonul, U. and Aguirre, F. 1992. The effects of ionic and nonionic radiographic contrast media on coronary hyperemia in patients during coronary angiography. *Am Heart J.* **123**(3), pp.621-627.

Tavella, R., Pasupathy, S. and Beltrame, J.F. 2018. MINOCA - A personalised medicine approach. *Int J Cardiol.* **267**, pp.54-55.

Tomberli, B., Cecchi, F., Sciagra, R., Berti, V., Lisi, F., Torricelli, F., Morrone, A., Castelli, G., Yacoub, M.H. and Olivotto, I. 2013. Coronary microvascular dysfunction is an early feature of cardiac involvement in patients with Anderson-Fabry disease. *Eur J Heart Fail.* **15**(12), pp.1363-1373.

Tomiyama, Y., Manabe, O., Oyama-Manabe, N., Naya, M., Sugimori, H., Hirata, K., Mori, Y., Tsutsui, H., Kudo, K., Tamaki, N. and Katoh, C. 2015. Quantification of myocardial blood flow with dynamic perfusion 3.0 Tesla MRI: Validation with (15) O-water PET. *J Magn Reson Imaging.* **42**(3), pp.754-762.

Tonino, P.A., De Bruyne, B., Pijls, N.H., Siebert, U., Ikeno, F., van' t Veer, M., Klauss, V., Manoharan, G., Engstrom, T., Oldroyd, K.G., Ver Lee, P.N., MacCarthy, P.A. and Fearon, W.F. 2009. Fractional flow reserve versus angiography for guiding percutaneous coronary intervention. *N Engl J Med.* **360**(3), pp.213-224.

Toth, G.G., De Bruyne, B., Rusinaru, D., Di Gioia, G., Bartunek, J., Pellicano, M., Vanderheyden, M., Adjedj, J., Wijns, W., Pijls, N.H. and Barbato, E. 2016. Impact of Right Atrial Pressure on Fractional Flow Reserve Measurements: Comparison of Fractional Flow Reserve and Myocardial Fractional Flow Reserve in 1,600 Coronary Stenoses. *JACC Cardiovasc Interv.* **9**(5), pp.453-459.

Townsend N, W.K., Bhatnagar P, Smolina K, Nichols and M, L.J., Luengo-Fernandez R, Rayner M 2012. Coronary heart disease statistics 2012 edition. . *British Heart Foundation: London.*

Turgeon, R.D., Pearson, G.J. and Graham, M.M. 2018. Pharmacologic Treatment of Patients With Myocardial Ischemia With No Obstructive Coronary Artery Disease. *Am J Cardiol.* **121**(7), pp.888-895.

van't Veer, M., Pijls, N.H.J., Hennigan, B., Watkins, S., Ali, Z.A., De Bruyne, B., Zimmermann, F.M., van Nunen, L.X., Barbato, E., Berry, C. and Oldroyd, K.G. 2017. Comparison of Different Diastolic Resting Indexes to iFR: Are They All Equal? *Journal of the American College of Cardiology.* **70**(25), pp.3088-3096.

van 't Veer, M., Adjedj, J., Wijnbergen, I., Toth, G.G., Rutten, M.C., Barbato, E., van Nunen, L.X., Pijls, N.H. and De Bruyne, B. 2016. Novel monorail infusion catheter for volumetric coronary blood flow measurement in humans: in vitro validation. *EuroIntervention.* **12**(6), pp.701-707.

van de Hoef, T.P., Bax, M., Damman, P., Delewi, R., Hassell, M.E., Piek, M.A., Chamuleau, S.A., Voskuil, M., van Eck-Smit, B.L., Verberne, H.J., Henriques, J.P., Koch, K.T., de Winter, R.J., Tijssen, J.G., Piek, J.J. and Meuwissen, M. 2013a. Impaired Coronary Autoregulation Is Associated With Long-term Fatal Events in

Patients With Stable Coronary Artery Disease. *Circ Cardiovasc Interv.* **6**(4), pp.329-335.

van de Hoef, T.P., Bax, M., Meuwissen, M., Damman, P., Delewi, R., de Winter, R.J., Koch, K.T., Schotborgh, C., Henriques, J.P., Tijssen, J.G. and Piek, J.J. 2013b. Impact of coronary microvascular function on long-term cardiac mortality in patients with acute ST-segment-elevation myocardial infarction. *Circ Cardiovasc Interv.* **6**(3), pp.207-215.

van de Hoef, T.P., Meuwissen, M., Escaned, J., Davies, J.E., Siebes, M., Spaan, J.A. and Piek, J.J. 2013c. Fractional flow reserve as a surrogate for inducible myocardial ischaemia. *Nat Rev Cardiol.* **10**(8), pp.439-452.

van de Hoef, T.P., Nolte, F., Rolandi, M.C., Piek, J.J., van den Wijngaard, J.P., Spaan, J.A. and Siebes, M. 2012. Coronary pressure-flow relations as basis for the understanding of coronary physiology. *J Mol Cell Cardiol.* **52**(4), pp.786-793.

van de Hoef, T.P., Siebes, M., Spaan, J.A. and Piek, J.J. 2015a. *Fundamentals in clinical coronary physiology: why coronary flow is more important than coronary pressure.* Eur Heart J. 2015 Jun 1. pii: ehv235.

van de Hoef, T.P., Siebes, M., Spaan, J.A. and Piek, J.J. 2015b. Fundamentals in clinical coronary physiology: why coronary flow is more important than coronary pressure. *Eur Heart J.* **36**(47), pp.3312-3319a.

van de Hoef, T.P., van Lavieren, M.A., Damman, P., Delewi, R., Piek, M.A., Chamuleau, S.A., Voskuil, M., Henriques, J.P., Koch, K.T., de Winter, R.J., Spaan, J.A., Siebes, M., Tijssen, J.G., Meuwissen, M. and Piek, J.J. 2014. Physiological basis and long-term clinical outcome of discordance between fractional flow reserve and coronary flow velocity reserve in coronary stenoses of intermediate severity. *Circ Cardiovasc Interv.* **7**(3), pp.301-311.

van den Heuvel, A.F., van Veldhuisen, D.J., van der Wall, E.E., Blanksma, P.K., Siebelink, H.M., Vaalburg, W.M., van Gilst, W.H. and Crijns, H.J. 2000. Regional myocardial blood flow reserve impairment and metabolic changes suggesting myocardial ischemia in patients with idiopathic dilated cardiomyopathy. *J Am Coll Cardiol.* **35**(1), pp.19-28.

Vogel, R., Indermuhle, A., Reinhardt, J., Meier, P., Siegrist, P.T., Namdar, M., Kaufmann, P.A. and Seiler, C. 2005. The quantification of absolute myocardial perfusion in humans by contrast echocardiography: algorithm and validation. *J Am Coll Cardiol.* **45**(5), pp.754-762.

Waller, A.H., Blankstein, R., Kwong, R.Y. and Di Carli, M.F. 2014. Myocardial blood flow quantification for evaluation of coronary artery disease by positron emission tomography, cardiac magnetic resonance imaging, and computed tomography. *Curr Cardiol Rep.* **16**(5), pp.014-0483.

Wei, K., Jayaweera, A.R., Firoozan, S., Linka, A., Skyba, D.M. and Kaul, S. 1998. Quantification of myocardial blood flow with ultrasound-induced destruction of microbubbles administered as a constant venous infusion. *Circulation.* **97**(5), pp.473-483.

White, C.W., Wright, C.B., Doty, D.B., Hiratza, L.F., Eastham, C.L., Harrison, D.G. and Marcus, M.L. 1984. Does visual interpretation of the coronary arteriogram predict

the physiologic importance of a coronary stenosis? *N Engl J Med.* **310**(13), pp.819-824.

Wijnbergen, I., van 't Veer, M., Lammers, J., Ubachs, J. and Pijls, N.H. 2016. Absolute coronary blood flow measurement and microvascular resistance in ST-elevation myocardial infarction in the acute and subacute phase. *Cardiovasc Revasc Med.* **17**(2), pp.81-87.

Windecker, S., Kolh, P., Alfonso, F., Collet, J.P., Cremer, J., Falk, V., Filippatos, G., Hamm, C., Head, S.J., Jüni, P., Kappetein, A.P., Kastrati, A., Knuuti, J., Landmesser, U., Laufer, G., Neumann, F.J., Richter, D.J., Schauerte, P., Sousa Uva, M., Stefanini, G.G., Taggart, D.P., Torracca, L., Valgimigli, M., Wijns, W. and Witkowski, A. 2014. 2014 ESC/EACTS Guidelines on myocardial revascularization: The Task Force on Myocardial Revascularization of the European Society of Cardiology (ESC) and the European Association for Cardio-Thoracic Surgery (EACTS)Developed with the special contribution of the European Association of Percutaneous Cardiovascular Interventions (EAPCI). *Eur Heart J.* **35**(37), pp.2541-2619.

Wu, K.C., Zerhouni, E.A., Judd, R.M., Lugo-Olivieri, C.H., Barouch, L.A., Schulman, S.P., Blumenthal, R.S. and Lima, J.A. 1998. Prognostic significance of microvascular obstruction by magnetic resonance imaging in patients with acute myocardial infarction. *Circulation.* **97**(8), pp.765-772.

Wu, W., Pan, D.R., Foin, N., Pang, S., Ye, P., Holm, N., Ren, X.M., Luo, J., Nanjundappa, A. and Chen, S.L. 2016. Noninvasive fractional flow reserve derived from coronary computed tomography angiography for identification of ischemic lesions: a systematic review and meta-analysis. *Sci Rep.* **6**(29409).

Xaplanteris, P., Fournier, S., Keulards, D.C.J., Adjedj, J., Ciccarelli, G., Milkas, A., Pellicano, M., Van't Veer, M., Barbato, E., Pijls, N.H.J. and De Bruyne, B. 2018. Catheter-Based Measurements of Absolute Coronary Blood Flow and Microvascular Resistance: Feasibility, Safety, and Reproducibility in Humans. *Circ Cardiovasc Interv.* **11**(3), pe006194.

Xaplanteris, P., Fournier, S., Pijls, N.H.J., Fearon, W.F., Barbato, E., Tonino, P.A.L., Engstrøm, T., Kääb, S., Dambrink, J.-H., Rioufol, G., Toth, G.G., Piroth, Z., Witt, N., Fröbert, O., Kala, P., Linke, A., Jagic, N., Mates, M., Mavromatis, K., Samady, H., Irimpen, A., Oldroyd, K., Campo, G., Rothenbühler, M., Jüni, P. and De Bruyne, B. 2018. Five-Year Outcomes with PCI Guided by Fractional Flow Reserve. *New England Journal of Medicine.* **379**(3), pp.250-259.

Yokoyama, I., Momomura, S., Ohtake, T., Yonekura, K., Nishikawa, J., Sasaki, Y. and Omata, M. 1997. Reduced myocardial flow reserve in non-insulin-dependent diabetes mellitus. *J Am Coll Cardiol.* **30**(6), pp.1472-1477.

Yokoyama, I., Ohtake, T., Momomura, S., Nishikawa, J., Sasaki, Y. and Omata, M. 1996. Reduced coronary flow reserve in hypercholesterolemic patients without overt coronary stenosis. *Circulation.* **94**(12), pp.3232-3238.

Yoo, S.H., Yoo, T.K., Lim, H.S., Kim, M.Y. and Koh, J.H. 2012. Index of microcirculatory resistance as predictor for microvascular functional recovery in patients with anterior myocardial infarction. *J Korean Med Sci.* **27**(9), pp.1044-1050.

Zhang, Z., Takarada, S. and Molloi, S. 2011. Assessment of coronary microcirculation in a swine animal model. *Am J Physiol Heart Circ Physiol.* **301**(2), pp.H402-408.

Zhou, W., Bajaj, N., Gupta, A., Sun, Y.P., Divakaran, S., Bibbo, C., Hainer, J., Taqueti, V., Dorbala, S., Blankstein, R., Shah, P., Kaneko, T., Adler, D., O'Gara, P. and Di Carli, M. 2019. Coronary microvascular dysfunction, left ventricular remodeling, and clinical outcomes in aortic stenosis. *J Nucl Cardiol.*

Zimmermann, F.M., Ferrara, A., Johnson, N.P., van Nunen, L.X., Escaned, J., Albertsson, P., Erbel, R., Legrand, V., Gwon, H.C., Remkes, W.S., Stella, P.R., van Schaardenburgh, P., Bech, G.J., De Bruyne, B. and Pijls, N.H. 2015. Deferral vs. performance of percutaneous coronary intervention of functionally non-significant coronary stenosis: 15-year follow-up of the DEFER trial. *Eur Heart J.* **36**(45), pp.3182-3188.

# Appendix 1 - Phantom development experiments

We wanted to create a model that simulated the pulsatile blood flow and to test if the method would work when there is mixing of contrast agent with the circulating fluid. We used a coil of tubing as a reservoir instead of the jar as it was easier to configure and clean between contrast injections. A pump that generates pulsatile blood flow was employed to simulate pulsatile blood flow.

## Experiment 1

### Methods

We adapted a 'wet lab' model borrowed from St Jude Medical (Minnesota, US) which was designed for demonstrating fractional flow reserve (FFR) measurements. The model consists of a closed system of silicon tubing through which fluid can be pumped in a pulsatile fashion simulating blood flow. See figure A1.

*Model:* The system was set up on a cardiac catheter laboratory table at Leeds General Infirmary. A heated water bath was used as a reservoir. A submersible pump (GP1652 High flow submersible pump, Whale pumps, Bangor, Northern Ireland) was used to circulate the water through a large bore silicon tube, which was analogous to the ascending aorta (figure A 1). There was a pressure sensor which connected to the RadiAnalyser Xpress console giving a pressure trace similar to the aortic pressure trace.

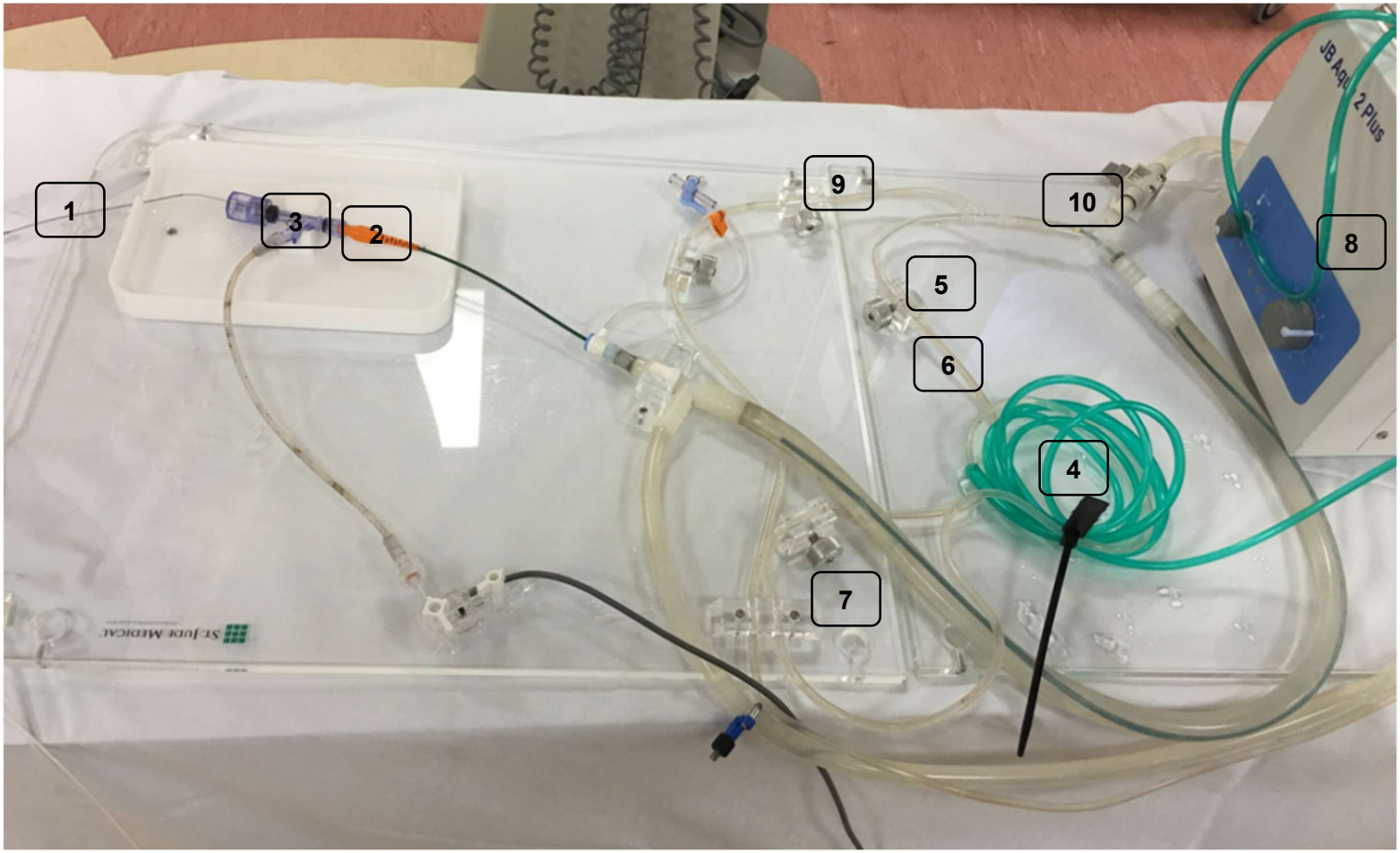


**Figure A 1: Wet lab model adapted for experiment 1.**
1. Pressure wire 2. Guide catheter hub 3. Tuohy Borst valve 4. Coil of tubing (microvasculature) 5. Screw for introducing lesion resistance 6. Coronary artery 7. Screw for introducing distal resistance 8. Reservoir 9. Redundant coronary artery 10. Position of guide catheter tip.

The pressure could be altered by using screws on the tubing to alter the resistance, to simulate a physiological pressure trace. The tube had a 'Y' junction, one of the branching outlets connected as a large bore silicone tube and connected to a sheath similar to the one used in human arteries. This allowed the passage of the catheters and other equipment. The hub of the guiding catheter once introduced through the sheath could be attached to a 'Tuohy Borst valve' system, similar to the one in clinical use in the cardiac catheter laboratory. This system also had a side port that allowed contrast injections and flushes as in the cardiac catheter laboratory set up. There was a water drainage port at this end to clearing the system after use. This was kept closed during the experiments. The other outlet of the Y junction connected to a smaller lumen silicone tubing which divided into two tubes of similar bore analogous to the coronary arteries. These tubes then drained back into a drainage tub but along their course there were external screws which could be tightened to introduce luminal narrowing by compressing the tubing from the outside, by varying the position of the screws, resistances analogous to lesion resistance and micro-vascular resistance could be introduced.

St Jude Medical originally intended this model to demonstrate the practice of measuring FFR. However, for our purpose we needed a model where the contrast could accumulate simulating the accumulation of contrast in the heart during coronary angiography. A model which included branching tubes that progressively reduced in lumen was considered, but this was deemed too complex to set up and more importantly difficult to flush and clear the contrast

medium. A long length of plastic tubing attached to one of the ‘coronary arteries’ which allowed some time for the contrast to fill as it is injected and pumped through the system. The tubing was rolled up to create a roll that would fit in the imaging frame (figure A 2).

The reservoir was filled with warm tap water and kept warm by the heated water bath at a temperature of 40°C. A 7F guiding catheter was advanced through the one-way valve and advanced along the tube up just beyond the ‘Y’ junction and into the origin of the ‘coronary artery’ tubing. One of the branches of this tube was closed off by tightening the resistance screw. The pump was started and allowed to run, and the pressure trace was confirmed on the RadiAnalyser Xpress. A pressure and temperature sensitive guide wire (Pressure wire Certus, St Jude Medical, Minnesota, US) was advanced through the guide catheter. The wire was also connected to the RadiAnalyser Xpress and the pressure traces were equalised with the sensor just outside the tip of the guiding catheter. The wire was advanced along the ‘coronary artery’. The resistance screws were placed such that one screw was proximal to the pressure sensor, which when tightened would simulate increasing lesion resistance by introducing luminal narrowing. The other screw was placed beyond the tip of the wire, which when tightened would introduce distal resistance or hyperaemia. The side port of the one-way valve could be attached to a power injector pump through high connector tubing. The pump was filled with iodinated contrast medium Iodixanol 652mg/mL (Visipaque 320, GE Healthcare, Chalfont St. Giles, UK) and kept warmed.

We attached a graduated reservoir (50 ml syringe) to the outlet of the system before it emptied into the drainage tub, so that we can measure the flow rate.

We used a stopwatch to measure the time it took for the syringe to fill 40 ml and calculated the flow rate from this.

*Protocol*: Iodixanol 652mg/ml was used as the contrast medium, and was pre-warmed to 37 °C. The contrast was drawn up in an automated pressure injector (Angiomat Illumena, Mallinckrodt, St Louis, Missouri) with connector to the manifold. In catheter laboratory 6, the contrast pressure injector was coupled to the X-ray system and set to inject after a delay of two seconds (or more than 1.5 heartbeats). The rate of injection was chosen depending on the stage of the protocol, between 1ml/s to 4ml/s. There was no rate rise set on the injector pump and a maximum pressure of 200psi was set. We designed a set of 5 different set ups for the experiments shown in table A 1. When the pump was switched on the RadiAnalyser would give a reading of the distal pressure/proximal pressure (Pd/Pa), we adjusted the proximal screw to introduce the lesion resistance to correspond to a Pd/Pa of 0.70. The distal screw would be tightened to give a Pd/Pa reading of 0.85. The absolute values were not important as we would measure the true flow rate with each set up.

**Table A 1: Resistance parameters used in experiment 1.**

| Set up | Lesion resistance | Distal resistance |
|---|---|---|
| A | Nil | Nil |
| B | Nil | + |
| C | + | Nil |
| D | + | + |
| E | Nil | ++ |

For each set up we followed two steps shown in table A 2.

**Table A 2: Steps for Experiment 1**

| | |
|---|---|
| Step 1 | Flow measurement |
| Step 2 | X-ray acquisition protocol |

**Step 1: Flow measurement**

Once the resistance settings were set, we measured the time it took for the reservoir to fill from 10ml to 50ml. The measurements were taken on the stopwatch and corresponding reservoir readings. We used the time to fill 40ml to calculate the flow rates during each of the resistance set ups. The times were measured three times and the mean was chosen.

**Step 2: X-ray acquisition protocol**

The changes to the X-ray equipment are detailed in chapter 3, section 3.1. The collimators were brought in to frame the field of view. Large field of view was selected (25cm) and image acquisition was set at 15 frames/second. The X-ray tube was positioned so that the heart model was at the isocentre of the X-ray beam. The power injector pump with contrast medium was connected to the guiding catheter through a connecting tube. A few frames were acquired before contrast was injected, to provide mask images.

*Step 2A: Calibration run.*

Contrast was injected at a rate of 0.5-1 ml /second through the guiding catheter. The injection was continued until contrast was seen to completely fill the tubing. The contrast injection was stopped, and the system kept running to wash out the contrast.

*Step 2B: Measurement run.*

Once the contrast was fully cleared another injection was performed at a set rate of 4 ml/second with the pump set to inject at 400psi. As before, a few mask frames were acquired first and then the contrast injection was performed. The injection was continued until the tubing was completely filled with contrast.

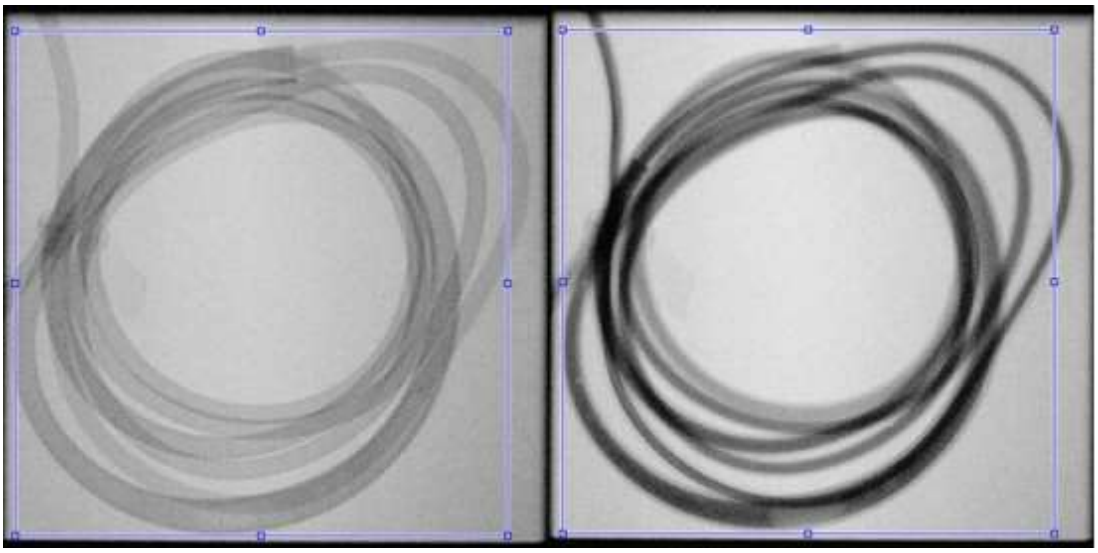

**Figure A 2: The coil of tubing used in experiment 1 to simulate the coronary microvasculature where water was circulated.** The panel on the left with no contrast and panel on the right during contrast injection

*XBF analysis:* The raw images were extracted and analysed using XBF method for signal intensity change with time. The region of interest (ROI) was set to include the entire coil of tubing and analysis performed to calculate signal intensities in each frame. The first few frames when X-ray parameters were stabilising were excluded and subsequent frames when there was no contrast flow was used as the mask. As the contrast flowed into the tubing, a

reduction in X-ray signal intensity was observed in the ROI. These imaging frames were then subtracted from the mask image and signal intensity change with each frame was plotted. This is proportional to the rate of flow within the tubing. The analysis was performed for the calibration sequence and the measurement sequences.

**Results**

The results are summarised in table A 3 and graphically represented in figure A 3.

**Table A 3: Resistance settings and relationship between XBF measured flow, Pd/Pa, and actual flow.**

| Setting | Lesion resistance | microvascular resistance | Pd/Pa | Actual flow ml/s | XBF flow ml/s |
|---|---|---|---|---|---|
| A | 0 | 0 | 0.98 | 2.84 | 8.35 |
| B | 0 | + | 0.98 | 2.74 | 3.36 |
| C | + | 0 | 0.70 | 2.16 | 1.32 |
| D | + | + | 0.85 | 1.59 | 1.77 |
| E | 0 | ++ | 0.93 | 2.18 | 1.32 |

Pd- Pressure distal to lesion resistance, Pa- Pressure in the proximal tubing analogous to aorta (aortic pressure). In setting A, there was no resistance in the system, in setting B, there was microvascular resistance added which reduced the flow but has not altered the Pd/Pa. In setting C, lesion resistance was added, which reduced the actual flow and Pd/Pa. In setting D, both lesion resistance and microvascular resistance were introduced which reduced the flow significantly, but Pd/Pa is higher than in setting C. Setting E is similar to setting B but with more microvascular resistance added.

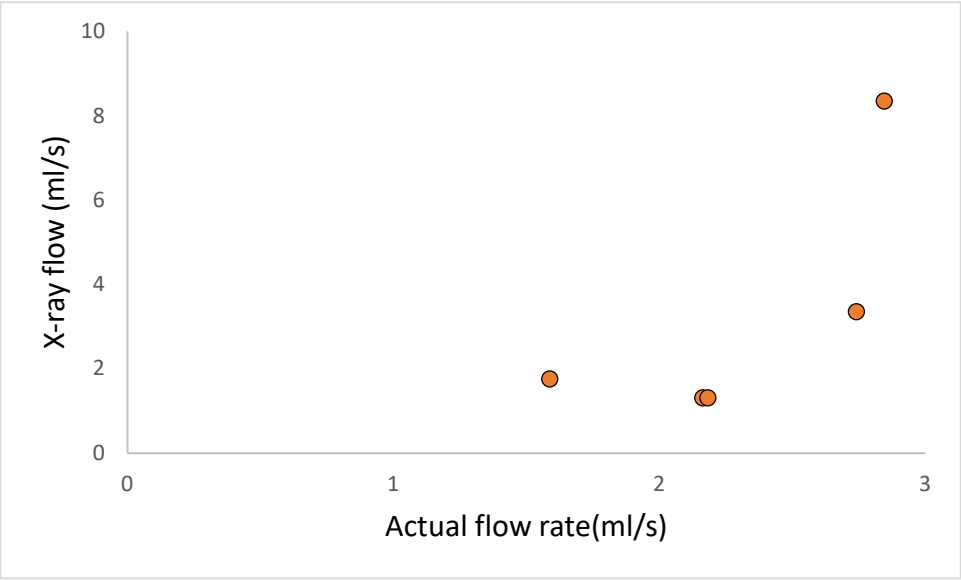


**Figure A 3: Scatter plot showing the relationship between actual flow and flow calculated by the XBF method.** The measured actual flow is plotted on X axis and XBF measured flow is plotted along Y axis.

### Discussion

This experiment was our first attempt at creating a phantom that simulates the coronary artery circulation and pulsatile blood flow.

The actual flow rate and the XBF measured flow correlated poorly. However, there were several issues with the performance of the phantom. The fluid flow rate was dropping when contrast was introduced into the system. The other issues we had were that of air accumulating within the tubing and of leaks which were proving difficult to overcome. We made modifications to the phantom to iron out these issues.

## Experiment 2

### Methods

The model used for experiment 1 had to be modified because of poor performance. The coil of tubing proved difficult to seal and we noticed issues with leaks and air accumulating within the tubing. Therefore, we decided to switch to the plastic jar used in the direct injection phantom experiment was used as the heart model instead of the coil of tubes to which the inlet and outlet tubes were connected. We attempted to reduce leaks and air accumulation within the tubing which was causing unpredictable variation in the flow rate. As explained previously, the jar had a sponge which would absorb the water/contrast medium to simulate the accumulation of blood/contrast in the myocardium. The rest of the tubing, reservoir and pump systems remained the same as for experiment 1.

*Protocol*: Iodixanol 652mg/mL warmed to 37$^{o}$ C was used as the contrast medium, as in experiment 1. The contrast was drawn up in an automated

pressure injector with connector to the manifold. The rate of injection was chosen depending on the stage of the protocol, between 1ml/s to 4ml/s. There was no rate rise set on the injector pump and a maximum pressure of 200psi was set. We designed a set of 4 different set ups for the experiments shown in table A 4. When the pump was switched on the RadiAnalyser would give a reading of the distal pressure/proximal pressure (Pd/Pa), we adjusted the proximal screw to vary the lesion resistance to vary the flow. The absolute values were not important as we would measure the absolute flow rate with each set up.

For the thermodilution protocol we had a second automated pump injector filled with water at room temperature.

**Table A 4: Resistance settings used in experiment 2.**

| Setting | Lesion resistance | Distal resistance |
|---|---|---|
| 1 | Nil | Nil |
| 2 | + | Nil |
| 3 | + | + |
| 4 | Nil | + |

For each setting we followed the following steps

**Table A 5: Steps in protocol experiment 2**

| | |
|---|---|
| Step 1 | Absolute flow measurement |
| Step 2 | Thermodilution protocol |
| Step 3 | X-ray acquisition protocol |

Step 1: **Flow measurement**

Once the resistance settings were set, we measured the time it took for the reservoir to fill from 10ml to 50ml. As in experiment 1, the measurements were taken by using the stopwatch.

Step 2: **Thermodilution protocol**

Another pressure injector was filled with the water at room temperature was connected to the side port of the Tuohy Borst valve. Proximal pressure (Pa) and pressure beyond stenosis (Pa) and the ratio Pd/Pa is documented.

*Step 2 A: Measuring temperature of infusate.*

The pressure wire was pulled back into the guide catheter. The 'thermo' menu was chosen on the RadiAnalyser Xpress and large scale selected. The temperature reading was zeroed. Injection was then commenced at 400 psi and set rate (1 ml/second), for each set up. The infusion continued until a steady reading was obtained and stopped. The drop in temperature was documented and the reading recorded on RadiAnalyser system.

*Step 2B: Measuring temperature after mixing of infusate with water.*

The pressure wire was advanced beyond the proximal screw so that the sensor was about 5cm distal to the screw. The injection was then recommenced with the same pump settings as in the calibration run. The drop in temperature noted and reading saved on the RadiAnalyser Xpress system

Step 3: **X-ray acquisition protocol**

The collimators were brought in to frame the field of view. Large field of view was selected (25cm) and image acquisition was set at 15 frames/second. The X-ray tube was positioned so that the jar was at the isocentre of the X-ray beam. The power injector pump with contrast medium was connected to the guiding catheter through a connecting tube. A few frames were acquired before contrast was injected, to provide mask images.

*Step 3A: Calibration run.*

Contrast was injected at a rate of 0.5-1 ml /second through the guiding catheter. The injection was continued until contrast was seen to completely saturate the sponge in the jar. The contrast injection was stopped, and the system kept running to wash out the contrast.

*Step 4A: Measurement run.*

Once the contrast was fully cleared another injection was performed at a set rate of 3.5- 6ml/second with the pump set to inject at 400psi. As before, a few mask frames were acquired first and then the contrast injection was performed. The injection was continued until the sponge in the jar was completely saturated with contrast (figure A 4). The pressure wire set up were identical to the one used in experiment 1. For the X-ray protocol the entire jar was imaged in the imaging frame and the acquisition protocol and settings were identical.

***XBF analysis:***

The raw images were extracted and analysed using XBF method for signal intensity change with time. The region of interest (ROI) was set to include the jar and analysis performed to calculate signal intensities in each frame. The rest of the analysis was performed in the same way as described previously for previous experiment.

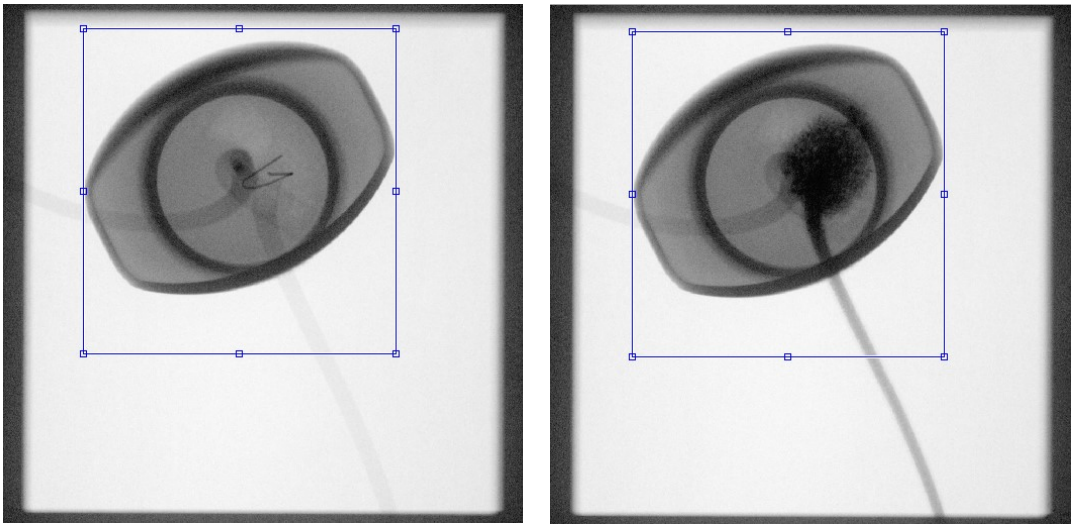

**Figure A 4: Images showing the glass jar with a sponge that was used as the reservoir mimicking microvascular system in experiment 2.** The left image mages show the jar before the injection of contrast and the right image shows it during contrast injection as the sponge is opacified.

**Results**

The actual flow rates measured manually during the different resistance settings are shown in table A 6. It is interesting to note that Pd/Pa increases as the microvascular resistance is introduced and even normalises to 1 when the lesion resistance is removed. This is seen during clinical use of FFR.

The X-ray calibration image files for setting A were corrupted during transfer and therefore could not be analysed. The X-ray flow rate was calculated for settings B, C, and D. The results of XBF measured flow rates and the actual flow rates are shown in table A 6 and graphically presented in figure A 5.

The correlation between the XBF measured flow rates and actual flow rates were poor.

The thermodilution flow data were only obtained for settings A and D due to equipment malfunction. The results are presented in table A 8.

**Table A 6: Resistance settings for experiment 2 and comparison between Pd/Pa and actual measured flow rate**

| Setting | Lesion Resistance | Microvascular resistance | Pd/Pa | Actual measured flow ml/s |
|---|---|---|---|---|
| A | 0 | 0 | 1 | 5.40 |
| B | + | 0 | 0.61 | 3.40 |
| C | + | + | 0.85 | 2.44 |
| D | 0 | + | 1 | 2.91 |

Pd/Pa – ratio of pressure distal to lesion resistance to the pressure in the proximal tubing. In setting A there was no additional resistance giving maximum flow. In setting B lesion resistance was added reflecting reduction in flow and Pd/Pa. As the MVR was introduced in setting C, flow reduced even further but Pd/Pa increased. In setting D lesion resistance is removed with some increase in flow but normalisation of Pd/Pa

**Table A 7: Results from experiment 2 – Comparison of XBF flow rate compared to actual flow rate.**

| Setting | Actual flow ml/s | XBF flow rate ml/s |
|---|---|---|
| B | 3.40 | 1.75 |
| C | 2.44 | 1.16 |
| D | 2.91 | 1.20 |

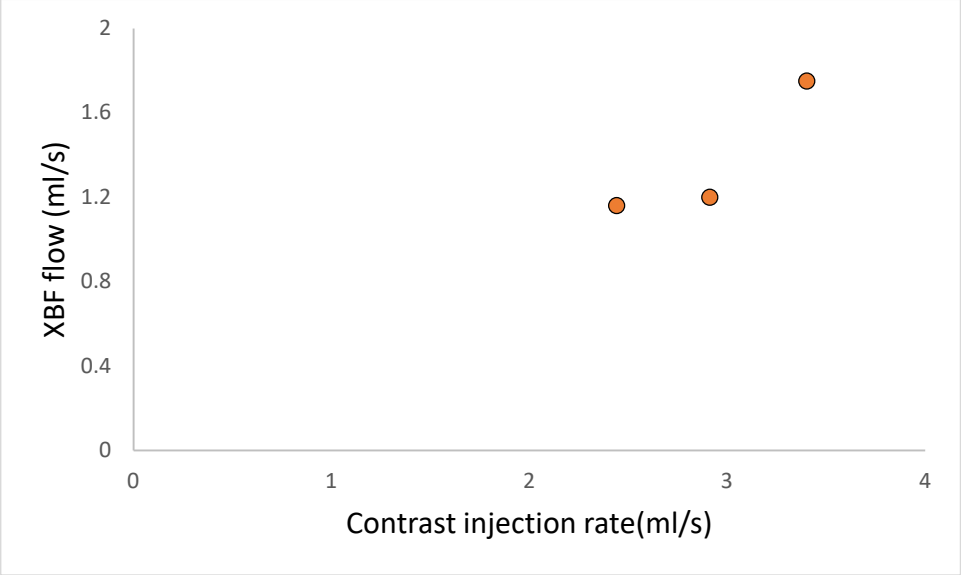


**Figure A 5: Experiment 2 results- XBF flow rates the actual measured flow rates.**

**Table A 8: Thermodilution study results from experiment 2- Actual flow compared to and Thermodilution measured flow rate.**

| Setting | Pd/Pa | Actual flow ml/s | Thermodilution flow ml/s |
|---|---|---|---|
| A | 1 | 5.40 | 6.80 |
| B | 0.61 | 3.40 | NA |
| C | 0.85 | 2.44 | NA |
| D | 1 | 2.91 | 2.87 |

Pd/Pa- ratio of pressure distal to lesion resistance to the pressure in the proximal tubing.

**Discussion**

There were insufficient data to draw any meaningful conclusion from this study. Although we tried to solve the performance issues with the phantom, we realised that the model was not performing reliably especially once contrast was introduced. The problems were mainly related to the submersible pump

(GP1652, high flow submersible pump, Whale pumps, Bangor, Northern Ireland) used to circulate the fluid through the tubing and the heart model. Once contrast was introduced into the system, there was a difference in the pump output. This was most likely due to the contrast being a more viscous solution as compared to water. There were further issues with air accumulation within the system. The micro air bubbles created during the turbulence of the water returning to the water bath were being aspirated into the pump and the small air bubbles would coalesce to form large air bubbles which caused a reduction in flow. In order, to overcome these difficulties, the phantom underwent further iterative changes.

# Appendix 2- Ethical approval

NHS
Health Research Authority
NRES Committee Yorkshire & The Humber - Leeds Bradford
North East REC Centre
Room 002
TEDCO Business Centre
Viking Industrial Park
Rolling Mill Road
Jarrow
NE32 3DT

Telephone: 0191 4283645

14 October 2013

Professor Mohan U Sivananthan
Consultant in Cardiac Imaging and Intervention
Leeds Teaching Hospitals NHS Trust
The Leeds General Infirmary,
Great George Street,
Leeds
LS1 3EX

Dear Professor Sivananthan

| | |
|---|---|
| **Study title:** | **Absolute quantification of coronary & myocardial blood flow from coronary angiographic Xray image acquisitions - A comparison with Fractional Flow Reserve and Thermodilution Coronary Flow measurements.** |
| **REC reference:** | **13/YH/0265** |
| **Protocol number:** | **1** |
| **IRAS project ID:** | **117142** |

Thank you for your letter of 16 September 2013, responding to the Committee's request for further information on the above research and submitting revised documentation.

The further information has been considered on behalf of the Committee by the Chair.

We plan to publish your research summary wording for the above study on the NRES website, together with your contact details, unless you expressly withhold permission to do so. Publication will be no earlier than three months from the date of this favourable opinion letter. Should you wish to provide a substitute contact point, require further information, or wish to withhold permission to publish, please contact the REC Manager Hayley Jeffries, nrescommittee.yorkandhumber-leedsbradford@nhs.net

**Confirmation of ethical opinion**
On behalf of the Committee, I am pleased to confirm a favourable ethical opinion for the above research on the basis described in the application form, protocol and supporting documentation as revised, subject to the conditions specified below.

**Ethical review of research sites**
NHS sites

The favourable opinion applies to all NHS sites taking part in the study, subject to management permission being obtained from the NHS/HSC R&D office prior to the start of the study (see "Conditions of the favourable opinion" below).

**Conditions of the favourable opinion**
The favourable opinion is subject to the following conditions being met prior to the start of the study.

Management permission or approval must be obtained from each host organisation prior to the start of the study at the site concerned.

*Management permission ("R&D approval") should be sought from all NHS organisations involved in the study in accordance with NHS research governance arrangements.*

Guidance on applying for NHS permission for research is available in the Integrated Research Application System or at http://www.rdforum.nhs.uk.

*Where a NHS organisation's role in the study is limited to identifying and referring potential participants to research sites ("participant identification centre"), guidance should be sought from the R&D office on the information it requires to give permission for this activity.*

Registration of Clinical Trials

All clinical trials (defined as the first four categories on the IRAS filter page) must be registered on a publically accessible database within 6 weeks of recruitment of the first participant (for medical device studies, within the timeline determined by the current registration and publication trees).

There is no requirement to separately notify the REC but you should do so at the earliest opportunity e.g when submitting an amendment. We will audit the registration details as part of the annual progress reporting process.

To ensure transparency in research, we strongly recommend that all research is registered but for non clinical trials this is not currently mandatory.

If a sponsor wishes to contest the need for registration they should contact Catherine Blewett (catherineblewett@nhs.net), the HRA does not, however, expect exceptions to be made. Guidance on where to register is provided within IRAS.

# Appendix 3 - Patient information leaflet

The Leeds Teaching Hospitals NHS
NHS Trust

UNIVERSITY OF LEEDS

## QUANTITATIVE CORONARY ANGIOGRAPHY IN CORONARY HEART DISEASE

**(CHIEF INVESTIGATOR: PROFESSOR U M. SIVANANTHAN)**

**PATIENT INFORMATION SHEET**

**Dear Patient,**
You are invited to take part in a research study. Before you decide whether to take part, it is important for you to understand why the research is being done and what is involved. Please take the time to read the following information carefully and discuss it with others if you wish. Please ask if there is anything that is not clear, or if you would like further information. Please take time to decide whether or not you wish to take part.

**Purpose of the study**
As you know you are going to have a coronary angiogram, and possibly angioplasty as part of your treatment for your heart condition. During your procedure the doctor sees the vessels of the heart by using X-rays. In The Leeds Teaching Hospitals NHS Trust we are testing a new X-ray technique. The new technique has been designed to allow the measurement of blood flow to the heart through the coronary arteries and in the heart muscle itself. We hope the new technique will help improve the treatment for future patients with heart disease. This study aims to assess how accurately the new technique is when compared with measurements taken using standardized medical equipment required in many angioplasty and stenting procedures.

**Why have you been chosen?**
You have been invited to take part in this study because you are due to have a coronary angiogram and / or coronary angioplasty and stenting procedure to widen the blood vessels supplying your heart.

**Do you have to take part?**
No. Your participation in this study is completely voluntary. If you decide to take part you are still free to withdraw at any time and without giving a reason. This

**What will happen to you if you take part?**
If you agree to take part in this study, your procedure will begin as normal. It may be that once the doctor sees the X-ray pictures of your heart, he or she may decide that it is not appropriate to include you in the study. If this happens he or she will tell you immediately and your treatment will proceed as normal. Otherwise, we would plan to perform a small part of your whole clinical procedure using the new X-ray technique. To perform this technique we will need you to remain as still as possible on the procedure table and at a number of times we would need you to hold your breath for up to 15 seconds. To assess the technique we would plan to use a special guide wire that allows measurements of vessel pressure and blood flow whilst performing your angioplasty and stenting procedure. This guide wire has the same safety features as other standard guide wires which are used to position stents during such procedures. Making these research measurements would involve the injection of a medication called Adenosine to improve blood flow to the heart. Following your clinical procedure we would aim to repeat the X-ray technique and guide wire measurements as part of the research, in order to assess the difference in blood flow.

**Is there any risk or discomfort associated with participation?**
Coronary angioplasty and stenting procedures are associated with certain small risks and you will be fully informed about these risks as part of the standard clinical consent process. Undertaking your clinical procedure will require the insertion of a tube (sheath) either into the artery in your wrist or if this proves impossible or is unsuitable this sheath will need to be placed in the large artery in you groin. This sheath is required in order to perform the coronary angioplasty and stenting procedure. Taking part in this study will not change this requirement or any small risks related to this sheath.

If you take part in this study, there will be a small increase in the amount of contrast dye and X-ray radiation exposure you receive. We would also need to insert an additional catheter through a large vein into your heart and administer a medication called Adenosine in order to acquire pressure measurements.

Contrast dye is used to highlight the disease present within your coronary arteries. The kidneys remove this contrast dye from your bloodstream. The dose of contrast required to undertake your clinical procedure and this research study will be kept to a minimum level according to recognized clinical guidelines. This increase in contrast dose may be associated with a very small increased risk of an adverse reaction such as an allergic reaction or short-lived mild kidney impairment. If you receive a large dose of contrast dye then we will arrange follow up blood tests to ensure that you do not develop any kidney problems.

Ionizing radiation is present within our living environment such that we are all exposed to a background level of radiation continuously. All X-ray related procedures require exposure to a specific dose of radiation which is kept as low as practicable according to internationally recognized policies. A detailed assessment as to the longer term risk of the additional radiation exposure required for this study has been conducted. We anticipate at the very most a 50% increase in the total radiation dose should you agree to take part. To

put this in context, the clinical procedure without the additional radiation dose is associated with a 1 in 2400 (0.04%) risk of lifetime fatal cancer. The longer term risk related specifically to the additional exposure is negligible with an increased risk (over

and above the clinical procedure risk) of associated lifetime fatal cancer of less than 1 in 4800 (0.02%).
Many cardiac investigations require the insertion of catheters through veins and into the heart. Such catheters are routinely used in certain clinical situations and add negligible additional risk to your procedure. To do this will require placing a tube (sheath) into a large vein in the groin under local anaesthetic. This tube will be removed very shortly after the clinical procedure and will not delay your recovery. The main risks of this extra research procedure is some discomfort during insertion of the sheath which will be minimized by using local anaesthetic, mild discomfort in the groin when the sheath is removed, and the development of at most mild bruising at the groin site following removal of the sheath at the end of the procedure. These types of sheaths are very frequently used in a range of cardiac procedures and are required in order to measure the pressure of blood within the heart.

The administration of Adenosine medication which increases blood flow to the heart is also very frequently used in cardiac procedures and is extremely safe. Giving Adenosine is recognized to frequently cause a brief slowing or irregularity of the heartbeat and often causes flushing, mild breathlessness, and chest discomfort. All these effects are short-lived and will completely resolve usually within 20-30 seconds after the medication is stopped. You will be informed when to anticipate these side effects and will be fully monitored throughout the whole procedure.

**Are there any benefits to you?**

Occasionally when measuring pressures within the heart and coronary arteries during Adenosine administration, we identify patients who do not actually need or will not benefit from coronary angioplasty and stenting even though the clinical coronary angiogram pictures suggest that they will. Taking part in this study would accurately identify if this applied in your case. In addition, if you take part in the study you will have more contact with us, which offers more opportunity to ask questions about your health, which some patients find helpful. Beyond this, we cannot promise the study will directly benefit you, but the information we get from this study may help the treatment of future patients.

**What happens to the information that is collected, and how is your confidentiality protected?**

Taking part in the study will require us to review your medical records. This is necessary to fully confirm your suitability for the study. Should you be considered unsuitable due to specific selection requirements, no information about you will be recorded. All personal information collected about you, should you agree to take part, will be kept strictly confidential. This information will be securely stored according to the provisions of the 1998 Data Protection Act. Any information about you which leaves the hospital will have your personal details removed so that you cannot be identified. Images and other data recorded will be sent to The University of Leeds or Philips Healthcare (a manufacturer of X-ray equipment), but only after personal details

have been removed. Your personal identity will not be revealed in any report or publication that may result from this research.

Your data may also provide a resource for future studies. If any information from this study is used to develop new research, data protection regulations will be observed and strict confidentiality maintained.

If you withdraw consent from the study, or if you were to become incapacitated during the study, any data collected about you up to that point will remain on file and will be included in the final study analysis.

**What will happen to the results of the research study?**

When the study is complete, the results will be published in a medical journal, but individual patients will not be personally identified. Details regarding the research study and its results will be available for public viewing on the Leeds X-ray Imaging website (lxi.leeds.ac.uk). In addition to this, we will inform you as to the results of the study as soon as possible after its completion.

**Indemnity / Compensation**

If you are harmed as a direct result of taking part in this study, there are no special compensation arrangements. If you are harmed due to medical negligence, then you may have grounds for legal action. Regardless of this, if you have any cause to complain about any aspect of the way you have been approached or treated during the course of this study, the normal National Health Service complaints mechanisms are available to you. If you have private medical insurance, please ensure that participation in the study will not affect your cover.

**Who is organising and funding this research?**

This study has been organised by The Leeds Teaching Hospitals NHS Trust and the University of Leeds in collaboration with Philips Healthcare. The study has been fully evaluated through a standard ethical review process.
The study is funded by The Leeds Teaching Hospitals Charitable Foundation. No payments are made to your doctor should you participate in this study.

**For further information please contact:**

Prof. U. M. Sivananthan
Leeds General Infirmary
Leeds LS1 3EX
Tel.: 0113 3925735

or

Dr Seth Vijayan
Interventional Fellow
Leeds General Infirmary
0113 3925735
sethvijayan@nhs.net

# Appendix 4- Patient consent form

The Leeds Teaching Hospitals NHS
NHS Trust

UNIVERSITY OF LEEDS

Study Number: **13/YH/0265**
Patient Identification Number for this trial:

## CONSENT FORM

**Title of Project**: Quantitative Coronary Angiography in Coronary Heart Disease
**Name of Researcher**: Professor U M Sivananthan

Please initial all boxes

1. I confirm that I have read and understand the information sheet dated 11th Sept 2013 (version 2) for the above study. I have had the opportunity to consider the information, ask questions and have had these answered satisfactorily. ☐

2. I understand that my participation is voluntary and that I am free to withdraw at any time without giving any reason, without my medical care or legal rights being affected. ☐

3. I understand that relevant sections of my medical notes and data collected during the study, may be looked at by individuals from regulatory authorities or from the Leeds Teaching Hospitals NHS Trust, where it is relevant to my taking part in this research. I give permission for these individuals to have access to my records. ☐

4. I agree to my GP being informed of my participation in the study. ☐

5. I agree to take part in the above study. ☐

| Name of Participant | Date | Signature |
|---|---|---|
| Name of Person taking consent. | Date | Signature |

## Appendix 5 - GP information leaflet

# QUANTITATIVE CORONARY ANGIOGRAPHY IN CORONARY HEART DISEASE

**(CHIEF INVESTIGATOR: PROFESSOR U M. SIVANANTHAN)**

General Practitioner Information sheet

Version 1.0 June 2013.

10/06/2013

Dr

**Re:**

Dear colleague,

Your patient has agreed to participate in a study evaluating a new X-ray Coronary Angiography technique. We would like to give you some relevant information about this study.

**Purpose of the study:**

In the Leeds Teaching Hospitals NHS trust, we are testing a new X-ray technique applicable to the many patients coming forward for coronary angiography. The new technique has been designed to potentially enable the measurement of absolute blood flow to the heart through the coronary arteries and in the heart muscle itself. We are primarily assessing the accuracy of this technique against widely available but specific guide-wire equipment, which provides reference quantifiable measurements of absolute blood flow and the severity of a coronary stenosis, at the time of coronary intervention including, either pressure wire assessment and/or angioplasty and stenting. Additional aims of the study include assessing whether we can measure the severity of a coronary stenosis using the X-ray coronary angiography images, quantify cardiac muscle blood flow in terms of millilitres / amount of tissue / minute, quantify resistance to cardiac muscle blood flow when blood flow measurements are combined with coronary pressure measurements, measure these indices in the heart arteries and cardiac muscle at different times within the cardiac cycle, produce tomographic images of myocardial perfusion at the time of coronary angiography and assess to what extent the quality of the image and radiation exposure dose to the patient affect the quantitative measures taken.

**Recruitment:** 50 patients will be recruited to this initial pilot study, which is being conducted at The Leeds Teaching Hospitals NHS Trust.

**What will happen to your patient?**

A small part of their clinically indicated X-ray coronary interventional procedure will be allocated to acquiring extra X-ray images using the new technique. Reference measurements will be taken from the pressure / flow guide-wire used at the time of their procedure. Patient's going on to have coronary angioplasty and stenting will have repeat X-ray and guide-wire related measurements after the artery has been widened.

Participation in this study will result in a marginal increase in radiation exposure to your patient and also a moderate increase in X-ray contrast dose administration. These aspects have been considered carefully in order to minimise risks in respect of your patient's participation into this study. Standard clinical protocols exist to ensure review of a patient should they receive radiation exposures or contrast doses above specific levels. We will enact these protocols and inform you accordingly should this occur.

The study protocol has been thoroughly evaluated by a Radiation Protection Adviser within The Medical Physics Department, and The Department of Radiology at Leeds Teaching Hospitals Trust, and also reviewed extensively through the National Research Ethics Service.

No formal follow up will be required given the context of the study aims. All patients however, will be reviewed from a clinical perspective through routine cardiology outpatient attendance with their Cardiologist.

**Confidentiality:**

All information, which is collected about your patient during the course of the research, will be kept strictly confidential. Patients will not be identified in any publication that may result from this research. We will inform you of any problems arising directly from the research. This information will be included within routine clinical documentation forwarded following your patient's procedure.

Indemnity/Compensation: If patients are harmed as a direct result of taking part in this study, there are no special compensation arrangements. If patients have any cause to complain about any aspect of the way they have been approached or treated during the course of this study, the normal National Health Service complaints mechanisms are available to them.

**The research organisation:**

This study is organized by The Leeds Teaching Hospitals NHS Trust in collaboration with The Leeds Medical X-ray Imaging Group at the University of Leeds with support from Philips Healthcare. The study is funded by The Leeds Teaching Hospitals Charitable Foundation.

For further information please contact:

Dr Seth Vijayan

Interventional Fellow

Department of Cardiology

Great George Street

Leeds General Infirmary

LS1 3EX

Tel 07810350780

sethvijayan@nhs.net

or

Mr Andrew Davies

Lecturer & Research Officer

Division of Medical Physics

Level 8, Worsley Building

Clarendon Way

The University of Leeds

LS2 9JT

Tel: 0113 3438313

a.g.davies@leeds.ac.uk

# Appendix 6 – Ethical amendment

NHS
Health Research Authority
Yorkshire & The Humber - Bradford Leeds Research Ethics Committee

Room 001
Jarrow Business Centre
Viking Industrial Park
Rolling Mill Road
Jarrow
NE32 3DT

Tel: 0207 1048 088

15 April 2016

Professor Mohan Sivananthan
Consultant in Cardiac Imaging and Intervention
Leeds Teaching Hospitals NHS Trust
The Leeds General Infirmary,
Great George Street,
Leeds
LS1 3EX

Dear Professor Sivananthan

| | |
|---|---|
| **Study title:** | **Absolute quantification of coronary & myocardial blood flow from coronary angiographic Xray image acquisitions - A comparison with Fractional Flow Reserve and Thermodilution Coronary Flow measurements.** |
| **REC reference:** | **13/YH/0265** |
| **Protocol number:** | **1** |
| **Amendment number:** | **Substantial Amendment 1, 01/03/16** |
| **Amendment date:** | **22 March 2016** |
| **IRAS project ID:** | **117142** |

The above amendment was reviewed at the meeting of the Sub-Committee held by correspondence.

**Summary of amendment**

This amendment was submitted to recruit patients of all cohorts of acute coronary syndrome (to include patients presenting with ST segment elevation ACS), and increase the total number of recruited patients to 110.

**Ethical opinion**

The members of the Committee taking part in the review gave a **favourable** ethical opinion of the amendment on the basis described in the notice of amendment form and supporting documentation.

**Approved documents**

The documents reviewed and approved at the meeting were:

| *Document* | *Version* | *Date* |
|---|---|---|
| Notice of Substantial Amendment (non-CTIMP) | Substantial Amendment 1, 01/03/16 | 22 March 2016 |
| Participant information sheet (PIS) | 3 | 01 March 2016 |

**Membership of the Committee**

The members of the Committee who took part in the review are listed on the attached sheet.

**R&D approval**

All investigators and research collaborators in the NHS should notify the R&D office for the relevant NHS care organisation of this amendment and check whether it affects R&D approval of the research.

**Statement of compliance**

The Committee is constituted in accordance with the Governance Arrangements for Research Ethics Committees and complies fully with the Standard Operating Procedures for Research Ethics Committees in the UK.

We are pleased to welcome researchers and R & D staff at our NRES committee members' training days – see details at http://www.hra.nhs.uk/hra-training/

**13/YH/0265: Please quote this number on all correspondence**

Yours sincerely
pp

Sarah Prothero

**Dr Janet Holt**
**Chair**

E-mail: nrescommittee.yorkandhumber-bradfordleeds@nhs.net

*Enclosures: List of names and professions of members who took part in the review*

# Appendix 7- Abridged patient information leaflet

Version 2. February 2016

The Leeds Teaching Hospitals NHS
NHS Trust

UNIVERSITY OF LEEDS

## QUANTITATIVE CORONARY ANGIOGRAPHY IN CORONARY HEART DISEASE

(CHIEF INVESTIGATOR: PROFESSOR U M. SIVANANTHAN)

### PATIENT INFORMATION SHEET

**Dear Patient,**

- You are invited to take part in a research study testing a new X-ray technique to measure the blood flow through the heart arteries which will improve treatment in future.
- You are being approached as you are about to have an X-ray angiography and most likely coronary angioplasty procedure.
- Your participation in this study is completely voluntary. You are free to withdraw at any time and without giving a reason. This will not affect the standard of care that you receive from the NHS.
- The research study will start only after your treatment has been completed.
- If you are suitable to take part, we will perform a small part of your coronary angiography using the new X-ray technique.
- You will need to remain as still as possible on the procedure table and hold your breath for up to 15 seconds on three or four occasions
- We will use a special guide wire that allows measurements of blood pressure and temperature from within the blood vessels. This guide wire has the same safety features as other standard guide wires used during angioplasty
- A drug called Adenosine can improve the blood flow through the heart muscle and is often used in the treatment of patients with heart attack. Adenosine or similar drugs will be give through a cannula placed in one of your veins.
- Adenosine can sometimes cause a brief irregularity of the heartbeat, flushing, mild breathlessness and chest discomfort. All these effects are short-lived and will completely resolve usually within 20-30 seconds after the medication is stopped.
- Taking part in the study does not alter the risks associated with the procedure.
- In addition, there will be a small increase in the amount of contrast dye and X-ray radiation exposure you receive.
- Large increase in contrast dye can cause kidney impairment. If you are deemed to be at high risk for kidney impairment, we will monitor your kidney function with blood tests and take necessary protective precautions.

- The longer term risk related specifically to the additional X-ray exposure is negligible with an estimated increased risk of associated lifetime fatal cancer of less than 1 in 4800 (<0.02%).
- All the data collected will be kept strictly confidential in accordance with the 1998 Data Protection Act.
- Any information about you which leaves the hospital will have your personal details removed so that you cannot be identified.
- Your General Practitioner will be informed of your taking part in the study.
- If you are harmed as a direct result of taking part in this study, there are no special compensation arrangements. If you have any cause to complain about any aspect of the way you have been approached or treated during the course of this study, the normal National Health Service complaints mechanisms are available to you.
- This study has been organised by The Leeds Teaching Hospitals NHS Trust and the University of Leeds in collaboration with Philips Healthcare. The study is funded by The Leeds Teaching Hospitals Charitable Foundation.

**For further information please contact:**

Prof. U. M. Sivananthan
Leeds General Infirmary
Leeds LS1 3EX
Tel.: 0113 3925735

or

Dr Seth Vijayan
Interventional Fellow
Leeds General Infirmary
0113 3925735
sethvijayan@nhs.net